Development of a Real-Time Physics-Based Spinal Fusion Training Simulator for Lumbar Discectomy

Trevor Robert Cotter

McGill

Department of Mechanical Engineering

McGill University, Montreal

April 2022

A thesis submitted to McGill University in partial fulfillment of the requirements of the degree of Doctor of Philosophy in Mechanical Engineering

Dedication

This thesis is dedicated to my parents, Anne and Rob, for their ongoing support and endless patience. Without their encouragement for my entire life, I would not be the man I am today. I thank them for always helping me in whatever way they can.

I also dedicate it to my brother, Anthony, for his incredible example and unshakeable faith in me. I hope that I can be as inspiring to you as you have been to me.

I finally would like to dedicate this to the rest of my family, especially those I lost throughout this work who have always inspired me to continue learning. I thank them for their encouragement and love.

Table of Contents

Table of Tables

Table of Figures

Table of Equations

Glossary, Symbols, and Abbreviations

3D	Existing in 3 dimensions
3D Printing	An additive manufacturing technique
American Wire Gauge (AWG)	Wire size unit
Ampere (A)	SI unit of electrical current
Annulotomy	An incision into the annulus fibrosus of the IVD
Annulus Fibrosus	The fibrous exterior of the IVD
Augmented Reality (AR)	A system in which an artificial world is superimposed on the surroundings of the user
Axis	A line used for positional and rotational reference in space, can also be along or about which motion or loading occurs
Bill of Materials (BOM)	A list of the components of an assembly
Bur Tool	A surgical spinning and cutting tool used to remove tissue
Caudal	Anatomical direction towards the feet
Centimeter (cm)	SI unit of length
Central Processing Unit (CPU)	A computer component that performs a wide variety of operations
ChainMail	A computational method to model deformable bodies using element interference
Computer-Aided Design (CAD)	Computer-based modeling of objects
CONCORDE® Clear	A vacuum curette designed for lumbar discectomy
Cranial	Anatomical direction towards the head
Compute Unified Device Architecture (CUDA)	Software that allows CPU tasks to be performed on a GPU
Curette	A surgical scraping tool used to remove tissue
Current (I)	Electrical current
DCX	Maxon DC motor model line

Degree (°)	The angle of a joint
Degree of Freedom (DOF)	The number of independent dimensions along which an object can move
Direct Current (DC)	One-directional flow of electrical charge
Discectomy	Removal of the IVD
Electromagnetic Interference (EMI)	A disruption caused by and electromagnetic field
Encoder	An electromechanical device that tracks rotational position
Endplate	The cartilaginous part of the IVD that connects it to the adjacent vertebrae
ENX	Maxon encoder model line
Extended Finite Element Method (XFEM)	A computational method to simplify fracture propagation modeling
Facet Joint	A joint between adjacent vertebra bound by the SAP and IAP
Facetectomy	Removal of the facet joint
Finite Element Model (FEM)	A mechanical model that uses material constitutive properties to calculate deformation of a body under load
Fluoroscopy	A type of medical imaging that consists of continuous X-ray images to form a video
Force	A push or pull exerted on an object
Functional Spinal Unit (FSU)	A subcomponent of the spine consisting of two adjacent vertebrae and the IVD contained between them
GPX	Maxon planetary gearhead model line
Gram (g)	SI unit of mass
Graphical User Interface (GUI)	A visual display through which users interact with a device
Graphics Processing Unit (GPU)	A computer component that performs simple operations
Haptic	Technology that stimulates the sense of touch
Haptic Device	A device that provides haptic feedback
Haptic Torque Handle	A uniaxial haptic device to deliver torque
Hertz (Hz)	SI unit of frequency
High Torque (HT)	High torque configuration of the haptic torque handle
Hooke's Law	A strain deformation model
in silico	Testing that occurs on a computer or simulated environment
in vitro	Testing that occurs outside of the natural environment

in vivo	Testing that occurs in a living organism
Inferior Articular Process (IAP)	A part of the vertebra that faces downwards to form the SAP joint
Intervertebral Disc (IVD)	Soft tissue component of the spine that sits between the vertebrae
Just-Noticeable Difference (JND)	The minimum change in force perceptible by humans
Kambin's Triangle	A triangular anatomical feature made up of the exiting spinal nerve root, transverse process, SAP, and IAP
Kilogram (kg)	SI unit of mass
LabVIEW	A computer program often used for data acquisition
Load Encoder A/B (LEA/B)	Signal channels for the load-side encoder in the haptic torque handle
Low Torque (LT)	Low torque configuration of the haptic torque handle
Lua	A computer programming language
Lumbar	A section of the spine in the lower part of the back. Abbreviated L_x
Lumbar Interbody Fusion (LIF)	A surgical method where adjacent lumbar vertebrae are fused together to prevent movement
Magnetic Resonance Imaging (MRI)	A type of medical imaging that uses magnetic fields and radio waves
Mass Spring Model (MSM)	A mechanical model that uses Hooke's Law to calculate deformation of a body under load
MATLAB	A numerical programming language
MEDTEQ	Quebec Consortium for Industrial Research and Innovation in Medical Technology
Meshless Three-Parameter Viscoelastic Model (TPM)	A computational method to model deformable bodies using fixed-volume spheres connected with mechanical structures
Microsoft Visual Studio	A versatile computer program development program
Millimeter (mm)	SI unit of length
Minimally Invasive (MI)	A procedure that does little damage to tissue
Minimally Invasive Surgery (MIS)	Surgery that is performed through a small opening in the tissue
Motor Encoder A/B (MEA/B)	Signal channels for the motor-side encoder in the haptic torque handle
Newton (N)	SI unit of force
NSERC	Natural Sciences and Engineering Research Center

Nucleus Pulposus	The soft center of the IVD
Ohm (Ω)	SI unit of electrical resistance
Planetary Gearbox	A gear system of inner and outer gears used to modify speed and torque output
Kerrison	A surgical clamping tool used to remove tissue
Posterior Lumbar Interbody Fusion (PLIF)	A LIF procedure with an approach from the back
Printed Circuit Board (PCB)	An electrical subassembly used to build electrical circuits
Qt	A computer programming language for developing GUIs
Quick-Release Mechanism (QRM)	A mechanical component that connects the haptic device to tools in the surgical simulator
Sacral	A section of the spine connected to the pelvis. Abbreviated S_x
Slipring	An electromechanical device that conducts electrical signals across a rotating body
Stereolithography (SLA)	A type of 3D printing
Superior Articular Process (SAP)	A part of the vertebra that faces upwards to form the SAP joint
Système international d'unités (SI)	Standardized system of units
Thoracic	A section of the spine in the middle part of the back. Abbreviated T_x
Tissue Retractor	A surgical tool for displacing tissue
Total Lagrangian Explicit Dynamic Algorithm (TLED)	Computational method to improve speed for nonlinear FEM
Torque (τ)	Rotational equivalent to force
Torque Constant (k_t)	Motor torque constant
Transforaminal Lumbar Interbody Fusion (TLIF)	A LIF procedure with an approach slightly to the side of a PLIF
Vertebra	Individual bone of the spine
Virtual Instrument (VI)	A program in the LabVIEW programming language
Virtual Reality (VR)	A system in which an artificial world is entirely simulated
Volt (V)	SI unit of electrical potential
W3D	Entact Robotics W3D device, which has 6-DOF of position tracking and 3-DOF of haptic feedback
Watt (W)	SI unit of power
X-ray	A type of medical imaging that uses electromagnetic waves

Abstract

Simulation is an essential component in training, from animal models for surgeons to virtual reality flight simulators for pilots. New medical advances have increased the need for specialized training platforms. This thesis focused on one intervention for the treatment of the leading cause of disability worldwide: low back pain and lumbar interbody fusion. The removal of the intervertebral disc, or discectomy, is a key part of interbody fusion and is the focal point of this thesis. Surgeons use visual and haptic, or touch-based, indicators to operate. Thus, the global focus of this work was to develop a virtual reality simulator focused on delivering effective haptic feedback to teach surgeons the skills and techniques essential for performing minimally invasive lumbar discectomies.

This work encompassed three hypotheses aimed towards developing said simulator. The first hypothesis was that a functionally and geometrically accurate analogue tool could be developed to deliver realistic (≥3 on a 1-5 Likert scale questionnaire) and appropriate ([-800, 800] N·mm) haptic feedback to simulate a virtual discectomy, a need stemming from a clear gap in existing commercial devices. A novel tool to deliver torque was designed, constructed, and evaluated to augment a haptic device. Twenty-nine surgeons performed a discectomy via a simulator with the novel haptic tool. Questionnaire results (≥3) indicated that the physical appearance and maneuverability of the novel tool accurately simulated the procedure, but they found its response implemented in the simulator lacking (<3). Its torque capability met the established need, with a theoretical peak 830 N·mm.

A second hypothesis, executed in parallel to the first, was that discectomy linear and torsional responses would be dependent on spinal level and decrease as tissue was removed during repeated passes at a magnitude detectable to a surgeon (≥7% difference). A tool mounted on a mechanical testing system was used to characterize the linear (2.1±1.6 N/mm, 25.2±16.7 N at 11.5 mm) and torsional (5.6±4.3 N·mm/°, 146.6±90.0 at 20°) response when penetrating lumbar intervertebral discs in two cadavers. Significant differences ($p < 0.05$) were found between initial and later passes through the tissue, as well as among lumbar levels, tool depth, and speed. All differences exceeded the just-noticeable difference, the minimum detectable change between two responses, indicating a surgeon should be able to distinguish the shifts in haptic feedback.

The third hypothesis was that freehand biomechanical tests and traditional controlled tests would yield different linear resistances ($p < 0.05$) when measuring force during discectomy tool insertion. This was done to imitate surgical movements more closely during testing. A novel 6-degree-of-freedom freehand device was designed and produced to track a surgeon's position in space and monitor the resulting linear resistance during use. Linear resistance differences were measured among controlled testing of torso and spine (8% lower, not statistically significant) samples, as well as spine samples with controlled and freehand testing (70% lower, $p < 0.001$). Traditional biomechanical testing procedures and results may be modified to inform a surgical simulator using this method that better approximates surgical conditions.

The global focus of creating a virtual reality discectomy simulator to train surgeons was achieved through these three objectives. A novel tool, built to give torque feedback, was integrated into a surgical simulator. Cadaveric testing quantified linear and torsional responses encountered during surgery, which, in turn, informed the tool of the first objective. A new freehand testing device and sample comparisons further refined and augmented the traditional tissue testing performed. In parallel, additional work, such as meshing to give visual and haptic responses, was carried out to create the simulator. Gameplay developed with surgeons and industry partners ensured the simulator was relevant to the needs of all users. The three primary objectives used to build the simulator add to the existing body of knowledge in the world of spine biomechanics and more, specifically spine surgery. This work will inform the next generation of surgical simulators, lead to more effective surgical training solutions, and, hopefully, contribute to better outcomes for patients.

Résumé

La simulation est un élément essentiel de la formation de plus de professionnels chaque année. Les avancées médicales ont démontré le besoin de systèmes de formation spécialisées. Cette thèse s'est concentrée sur une intervention pour la principale cause d'invalidité dans le monde: la lombalgie et la fusion intervertébrale lombaire. L'enlèvement du disque, la discectomie, est un élément clé de fusion. Les chirurgiens utilisent des signes visuels et haptiques, ou tactiles, pour opérer. Par conséquent, l'objectif global de ce travail était de développer un simulateur de réalité virtuelle concentré sur l'obtention d'un retour haptique efficace pour enseigner aux chirurgiens les compétences essentielles pour effectuer des discectomies.

Le développement du simulateur a été divisé en trois hypothèses. Le premier était qu'un outil analogique pouvait être développé pour fournir un retour haptique réaliste (≥3 sur un questionnaire de Likert de 1 à 5) et approprié ([-800, 800] N·mm) pour simuler une discectomie. Un nouvel outil pour fournir un couple a été conçu, construit et évalué pour augmenter un dispositif haptique. Vingt-neuf chirurgiens ont effectué une discectomie sur un simulateur. Les scores (≥3) ont indiqué que l'apparence physique et la maniabilité du nouvel outil haptique a simulé avec précision la procédure, mais le couple était insuffisant (<3). Sa capacité de couple a répondu au besoin établi, avec un pic théorique de 830 N·mm.

Une deuxième hypothèse était que les réponses linéaires et de torsion de la discectomie dépendraient du niveau de la colonne vertébrale et diminueraient à mesure que le tissu était retiré au cours de passes répétées à une amplitude détectable par un chirurgien (≥7% de différence).

Un outil monté sur un système de test mécanique a caractérisé les réponses linéaires (2,1±1,6 N/mm, 25,2±16,7 N à 11,5 mm) et de torsion (5,6±4,3 N·mm/°, 146,6±90,0 à 20°) lors de la pénétration des disques intervertébraux lombaires sur deux cadavres. Des différences ($p < 0,05$) ont été trouvées entre les passages initiaux et ultérieurs à travers le tissu, ainsi qu'entre, les niveaux lombaires, la profondeur de l'outil et la vitesse. Toutes les différences dépassaient la différence juste perceptible, le changement minimum détectable entre deux réponses, ce qui indique qu'un chirurgien devrait être capable de détecter les changements dans la réponse haptique.

La troisième hypothèse était que les tests biomécaniques à main levée et les tests contrôlés traditionnels cela donnera des résistances linéaires différentes ($p < 0,05$) lors de la mesure de la force pendant l'insertion de l'outil de discectomie. Cela a été fait pour imiter de plus fidèlement les mouvements chirurgicaux pendant les tests. Un nouveau dispositif à main levée à 6 degrés de liberté a été créé et produit pour suivre la position d'un chirurgien dans l'espace et surveiller la résistance linéaire qui en résulte pendant l'utilisation. Des différences de résistances linéaires ont été mesurées entre les tests contrôlés de torse et de colonne vertébrale seule (8% inférieures, non statistiquement significatif), ainsi que de colonne vertébrale soumise à des tests contrôlés et à main levée (70% inférieures, $p < 0,001$). Les résultats des tests biomécaniques traditionnels peuvent être modifiés pour alimenter un simulateur chirurgical utilisant cette méthode qui se rapproche davantage des conditions chirurgicales.

L'objectif global de créer un simulateur de discectomie en réalité virtuelle pour former des chirurgiens a été atteint. Un nouvel outil, conçu pour fournir de couple, a été intégré dans un simulateur. Des tests cadavériques ont quantifié les réponses linéaires et de torsion rencontrés pendant la chirurgie, qui, à leur tour, ont été informés l'outil précédent. Un nouveau dispositif de test à main levée a augmenté les tests de tissus traditionnels effectués. Parallèlement, des travaux supplémentaires, comme le maillage pour donner des réponses visuelles et haptiques, ont été effectués. Le gameplay a développé avec des chirurgiens et des partenaires s'est assuré que le simulateur était adapté aux tous. Les trois objectifs utilisés pour construire le simulateur s'ajoutent au corpus de connaissances existant dans le monde de la biomécanique et de la chirurgie de la colonne vertébrale. Ces travaux éclaireront la prochaine génération de simulateurs, conduiront à des solutions de formation en chirurgie plus efficaces et pourraient contribueront à de meilleurs résultats pour les patients.

Acknowledgements

I would like first to thank my research supervisor and mentor, Professor Mark Driscoll for believing in me and providing continuous support and assistance throughout my doctoral work, as well as providing professional development opportunities over the last 3 years. Without his extraordinary patience and knowledge, I would be in a much different position today. He has met and exceeded all promises he gave before I joined his research team. He and my co-supervisor, Professor Rosaire Mongrain, were endless sources of academic and professional support. I would additionally like to thank the other advisory committee members, Professor Jozsef Kovecses and Professor Rolando Del Maestro for their help and guidance in the development of this work.

Within the Musculoskeletal Biomechanics Research Lab, Dr. Khaled El-Monajjed and Dr. Sneha Patel were incredible colleagues who supported and guided me through this work. Additional help from Brittany Stott, Michael Grizenko-Vida, Maxence Coulombe, and Dr. Rodrigo Navarro-Sanchez ensured the success of this work. Additional specific acknowledgements are described in each chapter.

This project could not have been completed without outside help. I would like to thank the Natural Science and Engineering Research Council of Canada (NSERC), the Quebec Consortium for Industrial Research and Innovation in Medical Technology (MEDTEQ), DePuy Synthes Companies, CAE Healthcare, Inc., and McGill University, which all supported this work under Grant CRDPJ 515768-17. Specifically, Dr. Clément Forest at CAE and Ryan Leslie at Entact Robotics both offered unending technical support through this work. Professor Yvan Petit, Professor Eric Wagnac, and Elisabeth Laroche at École de technologie supérieure (ÉTS) and the Laboratoire de Recherche en Imagerie et Orthopedie division de l'Hôpital du Sacré-Coeur de Montréal graciously helped guide our testing.

Finally, I would like to thank all those who helped support me outside of research during my doctorate. I cannot thank my parents, Anne and Robert, enough for encouraging and supporting me to follow my passions. My brother, Anthony, has always been available to help, engage, or distract me in whatever way necessary. Finally, I could not have made it to this point without an amazing community of friends here in Montréal and around the world who have helped me get to where I am today.

Contribution to Original Knowledge

The work presented in this thesis represents novel developments in the biomechanical, robotic, and surgical simulation communities. All contributions aligned to the global objective of creating a real-time physics-based lumbar discectomy training simulator. The contributions include:

1. The first engageable uniaxial self-contained robotic haptic torque handle for surgical simulation was designed and shown to be successful in conveying appropriate feedback and user experience.

2. Force and torque analyses of a cadaveric vacuum curette discectomy showed that discectomy resistive forces and torque differ between position within the number of passes that are employed to remove the disc matter.

3. A novel device with integrated 6-axis position and load measurement for mechanical testing was designed and compared to controlled testing techniques. Differences were observed between test methods as well as between cadaveric spine and cadaveric torso specimens.

Contribution of Author

I, Trevor Cotter, confirm that I am the primary author and contributor to all work contained within this thesis. This includes all chapters as well as the manuscripts contained within them. The beginning of each chapter contains specific acknowledgements to those that assisted in the work. All work was done under the supervision and co-authorship of Professors Mark Driscoll and Rosaire Mongrain. I designed, built, and tested the robotic haptic torque handle for orthopedic simulation. Additionally, I planned and executed the testing methods and analysis for the discectomy biomechanics study. The freehand testing device design, assembly, and testing were done by me. I built and programmed the gameplay to integrate all work into the simulator platform.

1 Introduction

The following work encompasses the rationale, conception, and development of the global objective: to develop a virtual reality simulator focused on effectively delivering haptic feedback to teach surgeons the skills and techniques essential for performing minimally invasive lumbar discectomies. It begins with a literature review that investigates the topics relevant to the simulator. This background research includes, but is not limited to, physiological conditions that lead to low back pain, surgical interventions, tissue mechanics, robotics, haptics, and simulation training in surgery. Next, three chapters encompass the three objectives of the research: development of a haptic torque handle, evaluation of discectomy biomechanics, and secondary freehand mechanical testing. Each of these chapters outline how the work was done, include a manuscript dedicated to the subject, and elaborate on additional studies that complement the work to further develop the objective. The final simulator design, implementation, and validation are then presented, followed by a general discussion of each of the key findings from the objectives and simulator. Finally, a brief conclusion ties the work back to the global objective of simulator development.

2
Literature Review

The rise of augmented and virtual reality (AR and VR) technology has progressed beyond the realm of science fiction and its applications in medicine are an emerging field with the potential to help millions of people. Effective AR/VR simulators, ranging from neurosurgery to childbirth, have already been developed, and shifting these devices into the field of spinal surgery has the potential to revolutionize the standard of care. About 3.4 million spinal fusions were expected to be performed in 2020, leading to a worldwide market of $3.8 billion USD [1]. Training devices make it easier for surgeons to improve skills or even prepare for difficult, patient-specific procedures in a low-stakes environment. Surgeons visualize a mock patient and surgical tools are mounted on haptic, or touch, robotic feedback arms to mimic the resistance of different parts of the patient's body. While there are multiple treatments for low back pain, spinal fusion is one surgical intervention that is commonly practiced.

2.1 Spinal Anatomy and Physiology

The spine is a stack of alternating vertebrae and intervertebral discs (IVDs). The vertebrae provide strength and rigidity while the IVDs connect them for articulation and shock absorption. In addition to the IVDs, support and alignment for the spine comes from the articular and transverse processes of the vertebrae. The spine can be considered a sum of multiple functional spinal units (FSUs), which contain two adjacent vertebral bodies, the IVD, and the ligaments that connect them [2].

The lumbar spine sits between the rig cage and the pelvis, which correspond to the thoracic (T_1-T_{12}) and sacral (S_1-S_5) sections, respectively. The number subscript indicates a particular vertebra in the section, where a lower number is further cranial and a higher number is further caudal. Each of the lumbar vertebra, L_1-L_5, and IVDs, L_1L_2-L_4L_5, bear the sum of the upper spinal loads and are consequently a source of many spinal disorders. Back pain affects millions of people each year, and low back pain, one of the most prevalent forms, is isolated to the lumbar region [1]. Even though the spine is capable of supporting loads above 1kN and is very resistant to fatigue, compression and degeneration can occur both acutely and chronically [3].

The IVD is composed of three distinct parts: the nucleus pulposus, annulus fibrosus, and the cartilaginous endplate, and can be seen in Figure 2.1 [2]. The annulus fibrosus encircles and contains the nucleus pulposus, and both are sandwiched by the two cartilaginous endplates. The endplates are bound on the outside to their respective vertebrae. They are made of 60% water and their dry components are a combination of collagen and proteoglycans. The endplates allow for transport of nutrients from the vertebrae to the avascular IVD, an effect that decreases with age [2,4–10]. The annulus fibrosus is mostly water (65-70%), but its dry components are primarily collagen (50-70%) and proteoglycan (20%), with a small amount of elastin (2%) [2,11–15]. Collagen fibers oriented ±25-45° from vertical, an angle that alternates in layers of fibers that are wrapped circumferentially [2,16,17]. The nucleus has a water content ranging from 70-90% [2,18,19]. The dry components are proteoglycan (35-65%) and collagen (5-20%) [2,12,19–21]. With support from the endplates, vertebrae, and annulus fibrosus, the nucleus pulposus acts as a fluid sac with pressures typically ranging from 91-1330 kPa, though higher *in vivo* pressures have been observed in weighted or lifting actions [2].

A healthy IVD connects the adjacent vertebrae and allows for torsion and compression of the spine. As the IVD ages, the annulus fibrosus stiffens in compression while the nucleus pulposus shrinks, loses water, and drops in pressure, transferring more compressive load to the annulus [12,13,22–26]. The disc height decreases, causing pinching of the exiting spinal nerve root, or radiculopathy, and causing lower back pain [27]. Bulging or herniated IVDs, wherein the nucleus pulposus pushes against and past a protruding annulus fibrosus, can also result in increased pressure. Spondylolisthesis, or the slippage of one vertebra relative to its neighbor, can also cause this pressure [3].

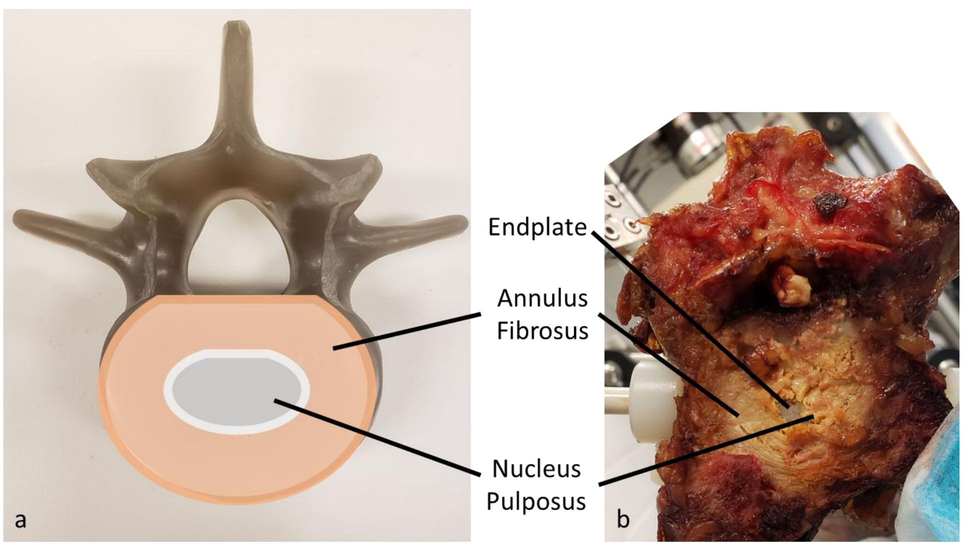

Figure 2.1: Intervertebral disc (IVD) geometry. a) shows an illustration of the disc, and b) shows a cadaveric disc.

2.2 Surgical Intervention for Low Back Pain

If non-surgical methods are unsuccessful in treating lower back pain resulting from disc compression or herniation, a lumbar interbody fusion (LIF) may be performed [20]. LIF aims to combine two adjacent vertebrae into a single vertebra. This prevents impingement on the exiting nerve root since the two vertebrae are fixed to each other. After access to the IVD is gained, a discectomy is performed. This is the removal of the nucleus pulposus with a specialized tool called a curette. After the discectomy, the cleared space is packed with a bone graft and a metal cage is inserted to achieve the desired vertebral separation. The vertebrae are further secured via rods attached to pedicle screws. Increased proficiency with the discectomy has been correlated with improved surgical recovery rates, and new tools have been developed to make the minimally invasive (MI) surgical (MIS) approach more efficient [20,28]. These include the CONCORDE® Clear MIS Discectomy Device, a vacuum curette from DePuy Synthes, Inc. (Johnson & Johnson; Boston, USA) (Figure 2.2) [29]. From this point forward, this tool is referred to as the Concorde Clear.

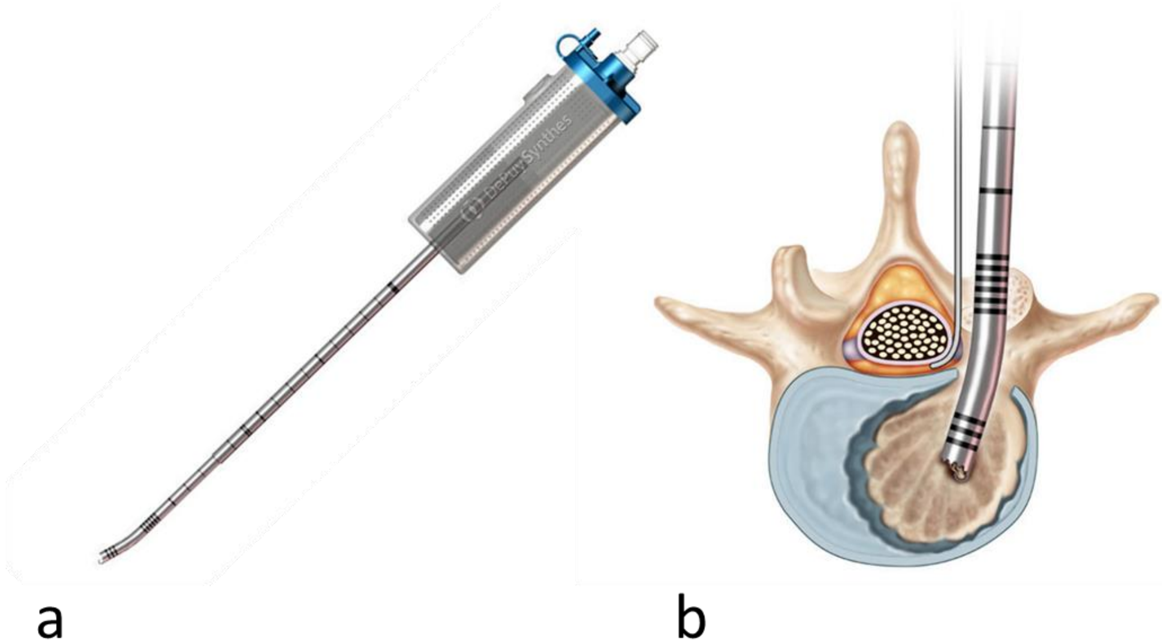

Figure 2.2: DePuy Synthes, Inc. CONCORDE® Clear device a) in its entirety and b) inside an IVD during use.

While various LIF access methods are preferred for different spinal regions and disease states, posterior (PLIF) and transforaminal (TLIF) are preferred for spondylolisthesis at the L_4L_5 IVD [20]. As technology has developed, MI approaches have grown in popularity [20]. These techniques use a smaller access point and specialized tools to minimize the amount of collateral damage incurred during surgery, which has been shown to reduce blood loss, and shorten hospital stay, minimize complications, and shorten healing times [20,30]. However, these new procedures require advanced training. Surgeons must learn how to use new tools as well as new anatomical references, such as Kambin's Triangle, an IVD access point bounded by the exiting spinal nerve root, transverse process, superior articular process (SAP), and inferior articular process (IAP), as shown in Figure 2.3 [31]. While this access has been associated with improved surgical results, it is only 60-108 mm^2 across the lumbar region, with larger areas at lower joints, and thus surgeries through this feature require very advanced training [31,32]. However, there is a current lack of adequate training systems and in the biomechanical understanding of the forces and moments involved with this step.

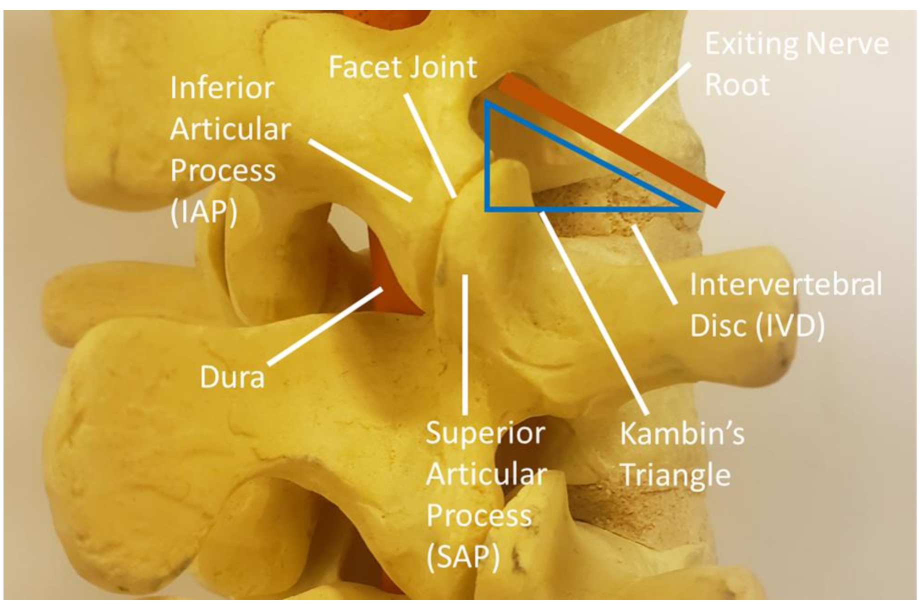

Figure 2.3: Spinal anatomy and location of Kambin's Triangle.

2.3 Training Methods

Many different approaches are used to adequately prepare surgeons for practice on new and existing procedures. Various training systems can be used, including artificial, animal, and cadaveric models. Additionally, surgeons in training will observe surgeries. Eventually, however, the surgeon will need to perform on their first patient, and the goal of training systems is to minimize the risk during this and subsequent procedures. Learning curves differ among surgeons and procedures, but studies have found that for an MI discectomy, there can be significant improvements in operation time, recovery time, and reoperation rates between patients 1-20 and 41-60 for some surgeons [33]. Surgical mistakes are considered a critical part of the training process [34]. This means that operations early in a surgeon's training have a higher chance for errors and complications than subsequent procedures.

New technologies have enabled the design of more realistic non-biological models. VR and AR can be combined with haptic feedback to create training systems that look and feel real without a physical model patient. In VR, a headset or screen displays the virtual world of the surgery. Haptics refer to any sort of touch sensation built into a system. In the case of passive haptic feedback, this can be as simple as a surgical tool with the same size and weight as the actual tool it is simulating. An active haptic could be a robotic device that provides an accurate sense of touch based on position in a virtual spine model. In surgical simulation, haptics are essential for maintaining the illusion of an actual procedure. Interchanging different haptic systems has been found to have minimal effects on some evaluation metrics, indicating that further investigation may be necessary to determine the effect of different haptic capabilities in training [35].

The use of VR simulators to train professionals is not unique to the medical industry. The path towards widespread adoption of training platforms has already been established in motorsports and aviation [36,37]. Professional pilots must meet established metrics to be certified to fly a given airplane, and this certification must be maintained with regular training sessions and updates [38]. Similar development in medicine has the potential to improve surgeon confidence and accommodate mistakes while minimizing risks for patients. Additionally, it offers an opportunity to accelerate the lengthy surgeon training process, giving surgeons more time to practice at higher proficiency.

Existing neurosurgery simulators have been shown to distinguish between surgeon proficiencies, but there are no established industry-wide benchmarks for proficiency [39]. One roadblock in the way of approval may be the use of physics-based haptics. Spinal surgery training platforms have been developed to simulate the feel of a real surgery, but the haptic feedback delivered in these platforms is not based on actual measured forces during the surgery but rather an estimate based on surgeon feedback [40]. One primary aim of future surgical simulator development is to make quantitative measurements of the forces present during a surgery so that these values can be used to inform the haptics in the simulator. Then the simulator will have metrics based on real-world data in addition to accurate feeling. This builds a stronger argument for the adoption of the simulator and its metrics.

2.4 Simulator Validation

Before a simulator can be used as a training tool, its validity as a training tool should be established [41–43]. While there is no universal method to validate a simulator, face, content, and construct validity are established techniques to support the use of simulators in training

[41,44]. Face validity evaluates the realism of the simulator [41]. Essentially, this test determines how well a given simulator component matches that used in a normal surgery. Content validity focuses on the appropriateness of the simulator by determining if the simulator teaches the desired concepts [41]. Finally, construct validity assesses whether the simulator can distinguish between novice and expert surgeons [41]. The combination of each of these have been used to determine the overall validity of various surgical simulators [45–48]. Other *in silico* models in healthcare, if testing a medical device, should adopt a risk-based credibility assessment which details validity in a different method to that specific for leveraging simulation for the sake of surgical training [49].

Testing to determine each of the simulator validations is also necessary. While construct validity can be delivered by patterns and results directly from the simulator, face and content validity require additional investigation. This is often done via a Likert scale questionnaire [45–48]. This questionnaire allows a user to rate a given aspect of the simulator on a numerical scale ranging from poor (low) to good (high). Questions can focus on a given aspect of validity and the answers indicate user satisfaction. For example, on a 1-5 face validity question regarding the realism of the simulator visuals, an answer >3 would indicate the visuals were valid. This style of questionnaire can be applied to multiple aspects of face and content validity [45–48].

2.5 Modeling Surgical Forces

To ensure the haptic forces in a simulator mimic the *in vivo* forces that surgeons encounter, both real and virtual models can be used. Multiple companies, such as The Chamberlain Group (Massachusetts, USA) create physical models that surgeons manipulate for procedures such as cardiac surgery. Others, such as CAE Healthcare (Quebec, CA) have tools mounted to robotic haptic devices that simulate the dimensions and textures of the virtual models of the anatomy [50]. These virtual systems have the advantage that they require less maintenance and do not need to be replaced after use, which is the case for many physical models. To develop virtual systems, a framework must be established to model both the dimensions and mechanical properties of the tissue.

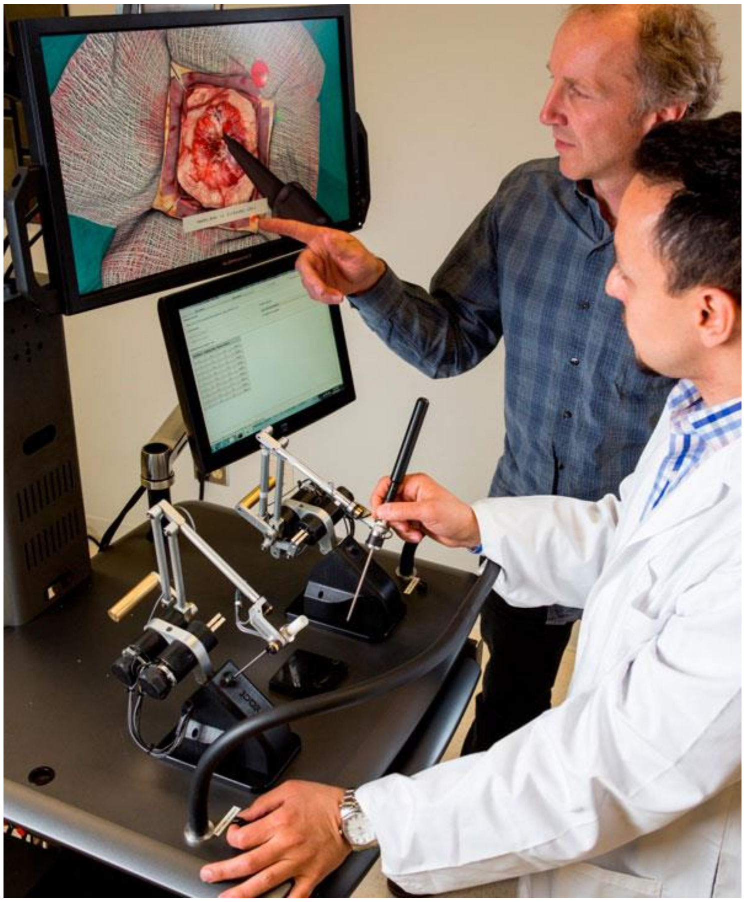

Figure 2.4: Example of a virtual reality (VR) haptic simulator [50].

Two primary methods, amongst many, that can be used to model deformations for robotic haptic feedback are mass-spring models (MSM) and finite element models (FEM). An MSM is built on the principle of dynamics and is a heuristic approach. Distinct points in the model, each with a given mass, are connected using one or more springs. The dynamics of deformation may be used to determine the resulting force of contacting a body. FEM, which is based on continuum mechanics, can similarly be used to calculate the forces present in the deformation of a body, but the approaches are very different. After conditions such as volume, mechanical properties, and input forces are set, the continuous system is discretized into a mesh made of small geometric elements bounded by vertices, called nodes. The deformation is defined by the movement of these nodes, which is solved numerically for each node. The FEM approach has the advantage that rather than individual MSM systems that must be independently tuned to give the desired forces, FEM can determine the necessary force based on material constitutive properties. A constitutive property determined by mechanical testing, such as elastic modulus, can be directly assigned to the material in FEM, and the particular geometry and loading of the model will be used to calculate the material response. These models, as well as hybrids of the two, have been used in simulation [51–53].

Additional computational methods to MSM and FEM exist to model biological tissues. The extended finite element method (XFEM) is one such approach. One drawback of FEM is that it is computationally expensive and difficult to rebuild a mesh, something that is necessary when material fracture causes discontinuities in the mesh. XFEM accommodates this by adding additional functions and meshing exclusively within the cracking region, allowing for localized modeling [54]. Another method, the ChainMail model, uses voxels, which are similar to tetrahedron but are units of a regular volumetric grid, rather than a volume of the necessary size to render a mesh. These voxels displace when pressed but do not affect their neighboring voxels until after a certain overlap threshold has been met [55]. After sufficient intersection, spring or other models are implemented to interact between voxels. A meshless three-parameter viscoelastic model (TPM) has been used to model soft tissue deformations differently [56]. In

TPM, a volume is filled with spheres connected by viscoelastic spring structures. Deformation of these structures is limited by the fixed volume of the spheres they connect, preventing overlap. The methods outlined here represent a subset of the many computational methods that have been employed for in surgical simulation [40,52].In MSM and FEM modeling methods, as well as many more, some form of Hooke's law is used to calculate linear elastic deformations. In an MSM, this is done on a bulk scale, while in FEM, this is done on the scale of individual elements/nodes. Uniaxial Hooke's law is shown in Equation 2.1, where f is force, k is stiffness, and u is the element's displacement from equilibrium. This can be further expanded and generalized for a multidimensional continuous material as shown in Equation 2.2, where $[\sigma]$, $[c]$, and $[\varepsilon]$ are multidimensional tensors of stress, stiffness, and strain, respectively.

$$f = ku$$

Equation 2.1: 1-D Hooke's Law.

$$[\sigma] = [c][\epsilon]$$

Equation 2.2: 3 D or generalized Hooke's Law.

A variety of FEM solvers can be used depending on the scenario being modeled. Implicit solvers often use a direct approach. After reducing the partial differential equations, the inverse of the stiffness matrix, $[c]$, is calculated and multiplied by stress to get the displacement, $[\varepsilon]$, of the nodes. This works for linear and some non-linear problems. However, for more complicated problems, such as non-linear time-dependent modeling, it may be necessary to use different methods. Explicit solvers may use an iterative approach to determine a solution. After beginning with an estimate for $[\varepsilon]$, they continue iterating until the change in $[\varepsilon]$ is below a set threshold, i.e. an optimal deformation is reached [57]. However, this comes at a cost, as FEM calculations have been found to be up to 10 times slower than MSM [58]. Unfortunately, these MSM objects have been found to have inaccurate deformations in soft materials with concentrated stresses [58].

FEM speed deficiencies can be remedied using advanced numerical methods. One such method is the total Lagrangian explicit dynamic (TLED) algorithm, which can accommodate nonlinear models [59]. This method precomputes offline shape function derivatives or matrix inverses for the models so that they can be referenced at each iteration, rather than recomputing them at each step. Additionally, soft tissues can also be computed with larger time steps, minimizing computational cost. For each step, loads and conditions must be applied to each node, the individual element forces and stresses are computed, and the resulting displacements are finally calculated [59].

Additionally, new technologies have been adopted to overcome these computational costs. The popularity of gaming and advanced graphics has pushed the development of a graphics processing unit (GPU). A computer's central processing unit (CPU) can perform a wide variety of operations, whereas a GPU can only compute simple operations. However, a CPU has fewer cores, meaning that it can't perform as many operations at the same time. Essentially, a CPU can do more advanced work in series, whereas a GPU does simpler work in parallel. In a medical simulator, a GPU presents a huge advantage over a traditional CPU. Methods such as the TLED solver can be parallelized and are therefore ideal for implementation on a GPU. This will result in faster computation time for simulator mechanics and deformation [59]. Free platforms, such as Compute Unified Device Architecture (CUDA), allow users to allocate tasks that would normally be computed on a CPU to the computer's GPU, and this framework has been used in FEM analysis [60].

FEM is the preferred choice for modeling soft biological tissues because they can be tuned to more accurately reflect the non-Hookean behavior of the native tissue using constitutive mechanical properties, in comparison to the empirical but more heuristic MSM [40]. Most tissues in the body are nonlinear and anisotropic while exhibiting time-dependent strain. This complexity indicates a discretized continuous model has the potential to be more effective than an MSM. Previous studies have modeled the IVD as hyperelastic and viscoelastic materials, both of which are nonlinear [61]. While Hooke's law strictly models two points' interaction as a spring, viscoelastic models include a dashpot, which effectively resists rapid displacement and enables relaxation of the tissue. Elastic and viscoelastic behaviors are shown in Figure 2.5. While the perfectly elastic behavior exhibited by Hooke's Law results in a straight line on the graph where a unique stress corresponds with each particular strain. Viscoelastic materials exhibit a hybrid of this and a viscous model, where the stress varies based on both time and strain. The hysteresis shown is an example of what one would expect from an experimental data set, where the area contained within the curve represents the energy lost to heat and deformation of the material [62].

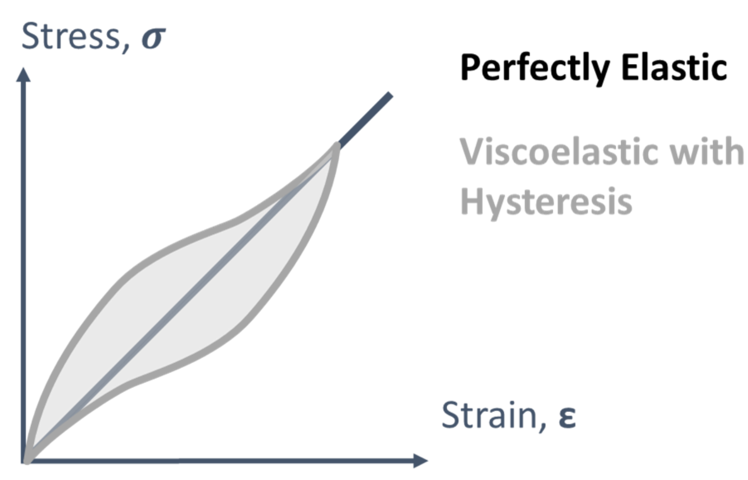

Figure 2.5: Stress-strain curve showing a comparison of elastic viscoelastic models. The shaded area represents the total range of potential stresses at a given strain.

Figure 2.6 shows two viscoelastic models, Maxwell and Kelvin-Voigt. These two represent the extremes of viscoelasticity using a spring-damper system, where Maxwell (Equation 2.3) uses the two subcomponents in series and Kelvin-Voigt (Equation 2.4) uses the two in parallel. For each model, σ is stress, E is the elastic modulus, ε is the strain, η is the viscosity, and t is the time, with m and v subscripts representing the Maxwell and Kelvin models, respectively [63].

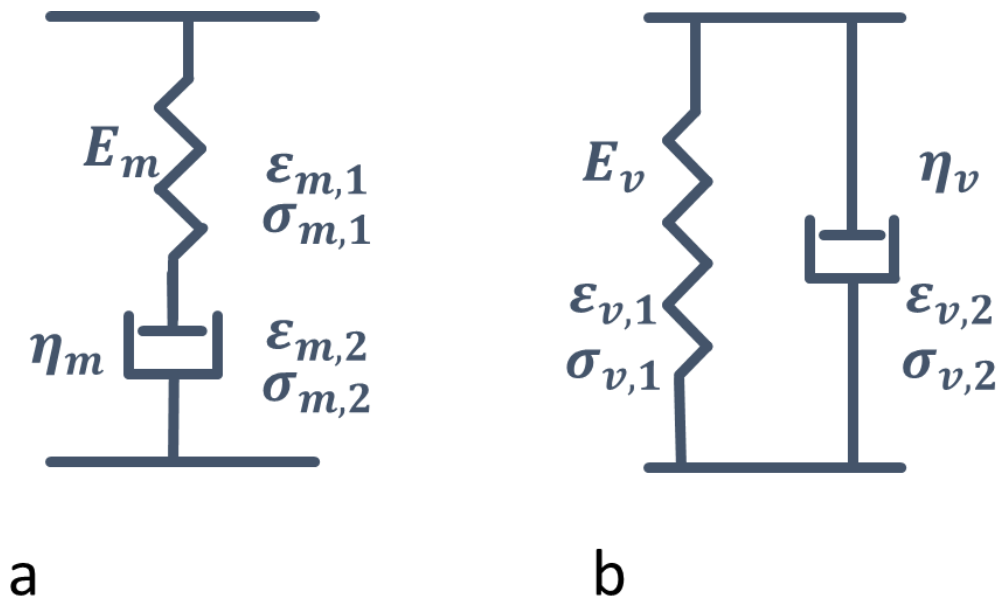

Figure 2.6: Two viscoelastic models. a) shows the Maxwell model and b) shows the Kelvin-Voigt model.

$$\sigma_m = \sigma_{m,1} = \sigma_{m,2}, \qquad \varepsilon_m = \varepsilon_{m,1} + \varepsilon_{m,2}, \qquad \frac{d\varepsilon_m(t)}{dt} = \frac{1}{E_m}\frac{d\sigma_{m,1}(t)}{dt} + \frac{\sigma_{m,1}(t)}{\eta_m}$$

Equation 2.3: Maxwell viscoelastic model.

$$\sigma_v = \sigma_{v,1} + \sigma_{v,2}, \qquad \varepsilon_v = \varepsilon_{v,1} = \varepsilon_{v,2}, \qquad \sigma_v(\mathrm{t}) = E_v\varepsilon_v(\mathrm{t}) + \eta_v\frac{d\varepsilon_v(t)}{dt}$$

Equation 2.4: Kelvin-Voigt viscoelastic model.

These models individually represent extreme implementations of a viscoelastic model, and real-world viscoelastic materials, such as tissues, can be represented by combinations of both models to varying degrees of complexity [63].

2.6 Haptic Torque

Haptics, in the context of a physics-based surgical simulator, are used to transform answers from numerical models into physical sensations observed by the user in VR. Advancements have enabled greater use of robotic haptic feedback with the use of FEM. The speed at which the haptics interact with the user differs greatly from the visual speed. While visual feedback refresh rates of 30 Hz are often sufficient to make a screen appear realistic to a user and haptic feedback for soft tissues can be performed at around 300 Hz, operating speeds of up to 1000 Hz are necessary to convince the user that a body is rigid [64]. Additionally, the ability of the user to distinguish between forces varies, but in general hands and fingers are extremely sensitive to the sense of touch [65]. The just-noticeable difference (JND) is a measure of this sensitivity, and it represents the minimum perceptible change in force by a person. A JND of [5,10]% change for [2,10] N loads between fingers or in elbow extension has been observed, but these measurements vary depending on individual fingers, training, and frequency [66–69]. They have also been a bit higher in haptic device studies, ranging from 23±13% for [0.4,8.8] N forces and 34±24% for [20,410] N·mm torques [70]. However, none of these studies represent tests on surgeons, and existing studies show that surgical skills improve with training [34,71]. In order to optimize the entire system so that the various visual and haptic components of the simulator can be run at a speed and sensitivity that provides accurate feedback in each medium, these human perceptual differences must be considered.

Haptic devices can be roughly broken into two categories. Devices that sense operator input force and then control the position are called admittance devices. Devices that sense operator position and then control the output force based on a virtual model are called impedance devices. Intrinsic mechanical resistance should be minimized in impedance devices, meaning that low friction, inertia, backlash, and torque ripple, or the steadiness of the torque output across the motor range, are desirable. Additionally, back-driveability can give a device the ability to reduce some of these effects. This makes impedance devices common choices for surgical simulators.

Before the user feels a response from an impedance device, the force must be calculated for a given position. The desired force, F, is input and the torque, τ, necessary to create it for the user is given by Equation 2.5, where J^T, with units of distance, is the transpose of the Jacobian matrix for a given haptic device [72]. The geometric Jacobian is a matrix that similarly converts the robot joint rates to the end-effector velocities and is dependent on the mechanical design of the device.

$$\tau = J^T F$$

Equation 2.5: Calculation of robot motor torque for a desired force output.

In an open-loop system, Equation 2.5 is used and the motors can be controlled to the desired torque. This works for idealized systems, but mechanical errors, inertia, and other real-world inaccuracies mean that the calculated and actual force outputs differ. Factors to accommodate these can be incorporated into the signal sent to the motors in an open-loop system, or a closed-loop system can be used, where the discrepancy between desired and actual outputs is calculated and used to inform future iterations of the control loop.

Haptic robotic devices are used for many applications, ranging from aviation to gaming [52,73–75]. They can be classified by their degrees of freedom (DOF). A 1-DOF device with track or control movement about a single axis, while a 3-DOF device will do the same for three axes, typically x, y, and z. A 6-DOF device will additionally control torque about those three axes. While many haptic devices provide 3 axes of force feedback, fewer control torque about those same axes [76]. However, torque at the user end is essential for the realistic feeling of tasks as simple as writing on different surfaces, so coupled or decoupled torque can be added to the forces calculated in Equation 2.5 [76]. In the field of orthopedic surgery, some procedures include steps with screwing or twisting motions. Robotic haptic torque devices have been designed for applications such as doorknobs, but currently, active haptic torque along the tool length is not often applied to surgical simulation [77]. Examples of existing commercial haptic devices for surgical simulation are shown in Table 2.1.

2.6.1 1-DOF Haptic Control

In general, as the number of DOF controlled increases, the complexity of the haptic device also increases. 1-DOF haptics can be used to control such mechanisms as screw knobs [78], remotely piloted aircraft throttles [79], and steering wheels in driving video games [75]. However, such devices may be insufficient to cover a surgeon's entire range of motion during a typical procedure.

2.6.2 3-DOF Haptic Control (Force Only)

Surgical simulation with 3-DOF haptic control is common. NeuroVR (CAE Healthcare; Montréal, Canada) uses the Phantom Desktop 3-DOF device (3D Systems (Formerly SensAble Technologies); Rock Hill, USA) or W3D (Entact Robotics; Toronto, Canada) [80]. Dental and other medical simulators have been designed with the Phantom Desktop (3D Systems) [81], Geomagic Touch (3D Systems) [82], Virtuose 3D Desktop (Haption; Soulgé-sur-Ouette, France) [83], and omega.3 and delta.3 (Force Dimension; Nyon, Switzerland) devices [84], as well as others.

Table 2.1: Commercial haptic devices for surgical simulation.

Manufacturer	Manufacturer Location	Haptic Device	Control/Track DOF	Peak Force	Peak Torque (Roll Axis)
3D Systems (Formerly Sensable Technologies) [82]	Rock Hill, USA	Premium 1.5	3/6	8.5 N	NA
		Premium 1.5/6DOF	6/6	8.5 N	170 N·mm
		Premium 1.5 High Force	3/6	37.5 N	NA
		Premium 1.5 High Force/6DOF	6/6	37.5 N	170 N·mm
		Premium 3.0/6DOF	6/6	22.0 N	170 N·mm
		Touch	3/6	3.3 N	NA
		Touch X	3/6	7.9 N	NA
Haption [83]	Soulgé-sur-Ouette, France	Virtuose 3D Desktop	3/6	10.0 N	NA
		Virtuose 6D Desktop	6/6	10.0 N	800 N·mm
		Virtuose 3D	3/6	34.0 N	NA
		Virtuose 6D	6/6	34.0 N	3100 N·mm
		Virtuose 6D TAO	6/6 + Grasping	42.0 N	5000 N·mm
Force Dimension [84]	Nyon, Switzerland	omega.3	3/6	12.0 N	NA
		delta.3	3/6	20.0 N	NA
		omega.6	3/3	12.0 N	NA
		omega.7	3/6	12.0 N	NA
MPB Technologies [85]	Montréal, Canada	Freedom 7S	6/6	2.5 N	150 N·mm
		Freedom 6S	6/6 + Grasping	2.5 N	150 N·mm
Entact Robotics	Guelph, Canada	W3D	3/6	15.0 N	NA
		W5D	5/6	-	NA
Quanser [86]	Toronto, Canada	HD² High-Definition Haptic Device	6/6	20.0 N	1720 N·mm
Butterfly Haptics [87]	Pittsburgh, USA	Maglev 200	6/6	40.0 N	3600 N·mm
Novint Technologies [85]	Albuquerque, USA	Falcon	3/3	~9.0 N	NA

2.6.3 >3-DOF Haptic Control

It is less common to control torque about the three force axes discussed [76]. Nevertheless, a variety of higher DOF devices have also been applied to surgical simulations [88,89]. As shown above, The NeuroTouch System (now NeuroVR) discussed earlier was also developed to be compatible with the Freedom 6S 6-DOF device (MPB Technologies; Montréal, Canada) [80,90]. The effect of adding torque to force control has been explored using the Phantom 1.5 (3D Systems), which has 6-DOF control [88]. The W5D (Entact Robotics) controls 5-DOF [91,92]. The omega.6 (Force Dimension) 6-DOF device builds on the omega.3, and the omega.7 (Force Dimension) adds a graspable DOF in the handle [84]. The Virtuose 6D Desktop (Haption) also has 6-DOF and replaceable handles, and the larger Virtuose 6D TAO (Haption) will also track the grasp position 7th DOF, but without haptic feedback [83].

2.6.4 Adjustable-DOF Haptics

Changing the DOF of a haptic device can be done simply by deactivating motors that would typically control a given DOF. Previous studies have investigated the necessity of torque during a procedure with a Phantom Premium 1.5. Operators used all 6-DOF (force and torque) control in some situations, and only 3-DOF (force only) control in others to find that increased DOF control improves user perception but may not affect performance [88]. Multiple 1-DOF haptic devices have been developed to augment the Phantom Omni for torque or grip force feedback [93,94]. Unfortunately, these may require external wiring and control systems. Additionally, the currently documented torque 1-DOF device is limited to 89 N·mm [94]. Future developments could improve the current state of adjustable-DOF haptic devices.

2.7 Tissue Testing

To properly inform simulator haptics for realistic feedback, the tissues in the procedure must be mechanically characterized. While many of the tissues in the spine have been tested *in vitro*, this data alone paints an incomplete picture of the forces and torques observed in a given procedure. This would preferably be done during the procedure itself, but that is unfeasible for a variety of ethical and practical reasons. Therefore, cadaveric or animal analogs are often used [95]. These models can remain intact or be dissected down to relevant parts as needed. So while it may seem unnecessary to use an entire cadaver to test a lumbar discectomy when the IVD is the only tissue being tested, studies have found that the spine is stiffer when tested with intact supporting muscles and ligaments [96–99]. The impact of additional tissue inclusion has been studied extensively in the spine, but to the author's knowledge, not in the context of the force required to perform a discectomy [96–100].

IVD mechanical studies are often focused on how the IVD performs under everyday compressive loading [101–104]. Tests of isolated annulus fibrosus tissue have been found the axial Young's modulus on the range [~0.1, 1.0] MPa [24,105–107]. The nucleus pulposus is approximately two orders of magnitude softer, at 6 kPa [107]. The IVD as a whole has been observed to be both non-linear and rate-dependent [108–110]. The non-linearity implies that pre-loading should be considered when attempting to replicate *in vivo* loading conditions, thus highlighting the importance of intact specimens [110]. While existing work shows a non-linear compressive loading response at higher frequencies, tests on the range [0.1, 10] Hz show a linear response [111,112].

It is less common to measure force as surgeons encounter in surgery [113]. Though spinal ligaments, muscles, and IVD components have all been characterized individually, these components cannot simply be summed up and put into a model that will operate in real-time. Many mechanical components will be ignored, and the computational costs of mimicking the individual tissues may be very high. Instead, the anatomy within the scope of the operator's view must be characterized while the other parts can be generalized based on tissue testing performed on a gross scale. Work has been done to characterize the gross forces associated with the insertion of certain instruments in various surgeries, but this has not yet been done for a discectomy [114]. Additionally, torque has been measured during some procedures, but not a discectomy [114].

Puncturing, such as that occurring during insertion of the Concorde Clear into the IVD during discectomy, is a complex process. Tool geometry, material, and testing conditions all impact how cracks form and propagate in a punctured material [115–117]. For a discectomy, the mechanical response to the surgeon's movements is not only due to the IVD, but the deflection of the spine and entire body of the patient. Additionally, this force changes as tissues are deformed or destroyed. Tool speed has been found to impact force due to tissue deformation and friction, but not a material fracture toughness [118]. Studies show that increased needle speed during tissue puncture results in decreased puncture force, but that this puncture force will stabilize at high speeds [113,119]. This is explained by the viscoelastic properties of tissue, whose stiffness response is delayed. In tests with faster needle punctures, the delay in tissue stiffness response allows the fracture limits of the tissue to be overcome earlier, resulting in lower puncture forces. Therefore, it is necessary to consider the sum of forces present when performing a gross tissue characterization. For needle insertion, existing studies have considered the total force (f_{needle}) to be the sum of all other forces of the tissue. This includes tissue deformation ($f_{stiffness}$), friction ($f_{friction}$), and cutting ($f_{cutting}$) forces, which are dependent on position, x, as shown in Equation 2.6 [120].

$$f_{needle}(x) = f_{stiffness}(x) + f_{friction}(x) + f_{cutting}(x)$$

Equation 2.6: Total force during needle insertion.

This is further illustrated in Figure 2.7, an example data set during multiple passes through the same tissue. After the initial pass through a given tissue, the tissue has been cut and $f_{cutting}$ will be zero. Then f_{needle} in subsequent passes will be lowered as it is only the sum of deformation and friction. Finally, f_{needle} during retraction of the tool is the same for all passes, as it is only the friction present between the tissue and the tool. For haptics in a simulator, it is helpful to know both the force at a given loading, and how that force changes during movement. For example, it may be helpful to know both the force, N, as well as the linear resistance, N/mm, to create haptic models to imitate a procedure.

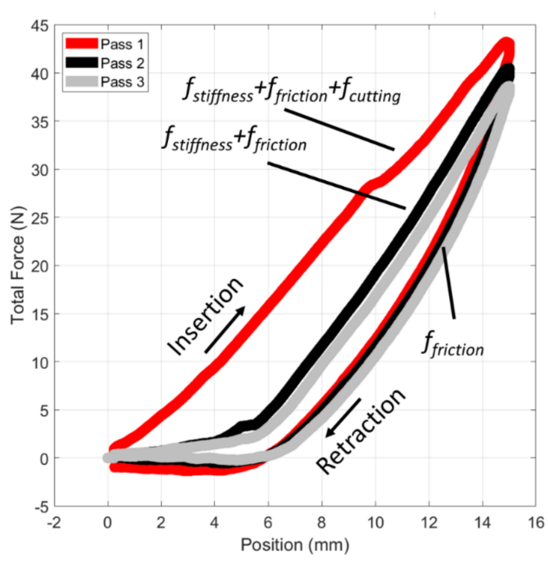

Figure 2.7: Example of the total forces present during multiple passes through a punctured tissue.

Tissue testing can be performed in various ways. Commonly, it is down with a mechanical testing system, such as an MTS (MTS Systems Corporation; Minneapolis, USA) [95,121,122]. This device can monitor position and loading while manipulating tissues. The testing system can uniaxially stretch a tissue and the resulting position and load data can be used to calculate material properties, such as elastic modulus [123]. This method can be used with isotropic samples, which have uniform mechanical properties in all directions. However, biological samples are often anisotropic, meaning they have unique mechanical properties in different directions. As a result, biological testing systems have been created to test multiple axes at the same time. The Instron (Boston, USA) Biaxial Cruciform system can move along two axes on a plane, and the MTS Bionix can perform parallel linear and torsional movements [124,125]. These tools can and have been used to characterize the anisotropic properties of biological tissues, such as IVDs [121,126].

A key aspect of surgery is missing from the mechanical characterizations already discussed: the flexibility of the surgeon. Surgeons do not operate along one or two axes of motion, they use infinite DOF in free space during a procedure. Therefore, the entire range of motion and loading should be considered when designing surgical haptic feedback. While freehand testing devices have been used to quantify orthopedic surgery, they do not appear to have not been compared to existing test methods to for discectomy [127–129]. Of the handheld testing techniques described in literature, many do not use position tracking [128,130]. Even when the position is being tracked during a real or simulated procedure, often only the force is reported [131]. Those that do include both electromagnetic and visual position sensing technologies [129]. To understand the movement of the surgeon during a procedure, it is essential to track position and orientation about 3-DOF (x, y, and z axes), creating a 6-DOF position tracking system. A complementary 6-

DOF load cell could monitor the force and torque on the same axes. Such load cells have been used to monitor surgical or robotic forces during procedures [128,129]. After combining the two 6-DOF technologies for simultaneous position and load tracking, natural surgical motions and tissue anisotropies could be evaluated using the same tool. A greater understanding of the motions of a surgeon as well as the forces applied during a procedure has the potential to revolutionize future tool design. In addition to the clear necessity of withstanding the demands of the surgery, smart tools are being designed to help surgeons during a procedure, with various levels of assistance [132]. Some of these tools prevent injury to the patient by physically preventing a surgeon from exerting too much force [133,134]. Many of these accommodate and stabilize the movement of the surgeon relative to the patient [135,136]. An even more advanced application of surgical biomechanics-informed tool design is a robotic surgical system. The da Vinci Surgical System (Intuitive Surgical; San Francisco, USA) and Mazor (Medtronic; Minneapolis, USA) are just two examples of established robotic systems for surgery, and there are many more in various stages of adoption [137–140]. These systems can be designed and enhanced using biomechanical data derived from the multiple types of mechanical measurement techniques described.

2.8 Project, Hypotheses, and Objectives

The global objective of this work is to develop a VR simulator focused on effectively delivering haptic feedback to teach surgeons the skills and techniques essential for performing minimally invasive lumbar discectomies. To do this, three primary hypotheses were proposed:

Hypothesis 1 A functionally and geometrically accurate analogue tool can be developed to deliver realistic (≥3 on a 1-5 Likert scale questionnaire) and appropriate ([-800, 800] N·mm) haptic feedback to simulate a virtual discectomy

Hypothesis 2 Lumbar discectomy force and torque will be dependent on spinal level and removed tissue at a magnitude detectable to a surgeon (≥7% difference)

Hypothesis 3 Freehand biomechanical tests and traditional controlled tests would yield different linear resistance measurements ($p < 0.05$) when testing lumbar cadaveric specimens

The three primary objectives outlined here address these hypotheses and present a combination of hardware design, biomechanical testing, and robotics necessary to accomplish the global objective. This simulator will then be brought to surgeons for their evaluation.

Objective 1 Development of a Haptic Torque Handle

A novel haptic torque device will be designed, evaluated, and implemented within a surgical simulator. While robotic haptic torque devices have been designed for other industries, there does not yet exist an easily detachable and self-contained device that can mimic the uniaxial torque along the tool axis necessary for mimicking screw insertion or scraping of the endplate during discectomy. Therefore, a haptic torque device that can be incorporated into existing haptic devices is necessary to mimic MI discectomy during surgical simulation.

Objective 2 Discectomy Biomechanics

Mechanical testing will be performed to inform the designed haptic torque device. Cadaveric lumbar IVDs will be tested with a Concorde Clear device on a mechanical tester to measure the linear and torsional resistance during discectomy. This data can then be used in the simulator to recreate the tissue mechanics.

Objective 3 Freehand Mechanical Testing

The design, construction, and testing of a freehand testing apparatus to track surgeon motion and load in 6-DOF will complement and contrast the work done in Objective 2. By providing the range of motion present during an actual procedure, this testing will have the potential to gain new insights into the mechanics present during lumbar discectomy.

2.9 Expected Contributions

Each of the 3 objectives outlined here are imperative to a larger interdisciplinary, multinational effort to create a real-time physics-based spinal fusion simulator. This project will be combined with other steps of the surgery to create an accurate simulator for the entire procedure. The simulator will be used to train surgeons around the world and has the potential to make efficient back pain care more widely available and safer.

Objective 1 Development of a Haptic Torque Handle

Beyond the general contributions outlined, this haptic torque handle will be the first of its kind. No existing detachable uniaxial self-contained robotic haptic torque handles capable of generating greater than 170 N·mm of torque are currently being used in orthopedic surgical simulation in conjunction with force-generating haptic devices. This has the potential to be used in a much larger variety of surgical simulators, with applications such as bone screws, catheter twisting, and more.

Objective 2 Discectomy Biomechanics

The quantitative mechanical loading on the spine and tool are currently uncharacterized for the Concorde Clear device. Understanding these mechanics, including the various components of the

IVD, has the potential to improve future curette designs as well as create a better simulator so that surgeons have a more thorough understanding of the limits of the tool and tissue.

Objective 3 Freehand Mechanical Testing

While mechanical testing is commonly performed using similar methods to those used in Objective 2, testing rarely mimics the range of motion of a surgeon during a procedure. This testing will shed light on the data lost during traditional testing, including the off-axis forces present and the specific forces experienced by the surgeon. This will also illustrate how traditional testing techniques could be adapted to inform haptic simulators.

3

Haptic Torque Handle

3.1 Context

This chapter focuses on Objective 1, which was performed to answer Hypothesis 1. This includes the conception, manufacturing, and testing of a new detachable uniaxial robotic haptic device to be implemented on the surgical simulator. The aim of the work was to take an existing haptic device, the Entact Robotics W3D, which has 6-degree of freedom (DOF) tracking and 3-DOF control, and turn it into a 4-DOF control device. This was done to accommodate simulator needs for torsional haptic response, which is outlined further in later chapters. The haptic torque handle can deliver torque and be connected via a custom quick-release mechanism (QRM), allowing for rapid, tool-free adaptation of the haptic device during use. To the author's knowledge, no such detachable uniaxial robotic haptic device exists for surgical simulation. After the manuscript text, additional relevant work describes complementary parts of the development that could not be contained in the manuscript. Ethical approvals for the surgeon studies are shown in Appendix II.

The work presented in this chapter was assisted by numerous collaborators. Technical assistance came from Ryan Leslie at Entact Robotics for all aspects of the project. Within the Musculoskeletal Biomechanics Research Lab at McGill, Michael Grizenko-Vida assisted with the design, manufacturing, and testing of the haptic torque handle, and Brittany Stott designed the QRM. An engineering capstone group consisting of Michael Grizenko-Vida, Nicholas Vaillancourt, Luyi Zheng, and Ghulam Murtaza helped develop the first prototype. Dr. Brahim Brahmi designed the control system for the robot.

A subset of this work was presented at the 8th International Conference on Mechanics and Materials in Design (M2D) in Bologna, Italy in September 2019, under the name "Design of a Robotic Torque Handle for Orthopedic Haptic Simulation," in addition to the peer-reviewed abstract publication for this conference. The following manuscript, Design Synthesis of a Robotic Uniaxial Torque Device for Orthopedic Haptic Simulation, was accepted for publication in the Journal of Medical Devices in March 2022 [141]. The contribution of the first author was 75%, which included supervision, mechanical design, testing, analysis, and writing. The second author contributed 10% for review, and the third author contributed 15% for research guidance and review.

3.2 Article 1: Design Synthesis of a Robotic Uniaxial Torque Device for Orthopedic Haptic Simulation

Trevor Cotter, Ph.D
Department of Mechanical Engineering
McGill University
Montréal, Quebec H3A 0G4
Canada
Orthopaedic Research Laboratory
Montréal General Hospital
Montréal, Quebec H3G 1A4
Canada
e-mail: trevor.cotter@mail.mcgill.ca

Rosaire Mongrain, P.Eng, Ph.D
Professor
Department of Mechanical Engineering
McGill University
Montréal, Quebec H3A 0G4
Canada
e-mail: rosaire.mongrain@mcgill.ca

Mark Driscoll, P.Eng, Ph.D
Professor
Department of Mechanical Engineering
McGill University
Montréal, Quebec H3A 0G4
Canada
Orthopaedic Research Laboratory
Montréal General Hospital
Montréal, Quebec H3G 1A4
Canada
e-mail: mark.driscoll@mcgill.ca

[1]Corresponding author.

3.2.1 Abstract

3.2.1.1 Introduction

Robotic devices are commonly used in surgical simulators to provide tactile, or haptic, feedback. They can provide customized feedback that can be rapidly modified with minimal hardware changes in comparison to non-robotic systems. This work describes the design, development, and evaluation of one such tool: a novel uniaxial torque haptic device for a surgical training simulator. The objective of the work was to design a single connection haptic device that could augment an existing six degree of freedom haptic device to mimic a Concorde Clear vacuum curette.

3.2.1.2 Materials and Methods

Design and evaluations focused on the tool's ability to deliver adequate torque, imitate a surgical tool, and be integrated into the haptic device. Twenty-nine surgeons tested the tool in the simulator and evaluated it via a questionnaire.

3.2.1.3 Results

The device was found to deliver the 800 N·mm of torque necessary to mimic an orthopedic procedure. Surgeons found it accurately imitated surgical tool physical appearance and maneuverability, scoring them 3.9±1.0 and 3.3±1.2, respectively, on a 1-5 Likert scale. By virtue of the functionality necessary for testing and evaluation, the device could be connected to the haptic device for mechanical and electrical engagement

3.2.1.4 Discussion

This device is a step forward in the field of augmentable haptic devices for surgical simulation. By changing the number of robotically-controlled degrees of freedom of a haptic device, existing

devices can be tuned to meet the demands of a particular simulator, which has the potential to improve surgeon training standards

3.2.2 Introduction

Augmented and virtual reality (*AR* and *VR*) technologies have progressed beyond the realm of science fiction and its applications in medicine are an emerging field with the potential to help millions of people. Effective *AR* and *VR* simulators, ranging from neurosurgery to childbirth, have already been developed. Machine learning approaches have been found to be effective in identifying patterns and distinguishing surgeons based on expertise levels [1]. Training systems make it easier for surgeons to improve their skills or prepare for difficult patient-specific procedures in a low-stakes environment, but they must be validated for clinical relevance [2,3]. The research reported herein contributes to the growing field of surgical simulation by introducing a first of its kind robotic device that can be quickly removed or disengaged from a system to add torque feedback in orthopedic simulation. It has been tested for torque output and face validity when used to augment an existing device. The design focuses on the DePuy Synthes (Boston, USA) Concorde Clear vacuum curette used in spine discectomy procedures [4,5].

There are two essential components to a medical training simulator: visual and haptic feedback. The user must be immersed in an environment that mimics the appropriate visuals; screens [6], *AR* goggles [7], and mock patients such as mannequins have all been used to do this [8,9]. The tactile, or haptic, feedback must also realistically mimic the feel of different parts of the patient's body, and studies have shown that the integration of haptic feedback in such simulators has the potential to be a positive or negative training tool [10,11]. Simply interacting with a physical mock patient is a common and proven way to provide feedback [9,12], but for destructive surgical procedures that involve steps such as tissue cutting, it may be preferable to have a device that simulates tissue manipulation to limit replacement parts and simulator maintenance. Haptic robotic devices are used for various applications in the aviation industry [13], medical simulation [14], robotic surgery [15], and consumer gaming [16].

Graspable haptic devices often operate in many degrees of freedom (DOF), the minimum number of independent coordinates needed to indicate the overall configuration of the device, including position and orientation [17,18]. In this manuscript, 6-DOF refers to the x, y, z positions and the corresponding axial rotations around them which can be tracked. Active robotic devices can additionally provide haptic feedback to controlled DOF, which are a subset of all the measured DOF. In general, adding control to additional DOF makes a haptic device capable of simulating a more natural surgical environment where the surgeon is free to move in any direction. 1-DOF haptics for surgical simulation exist to mimic orthopedic procedures such as screwing motions, however, such devices may be insufficient to cover a surgeon's entire range of motion during a typical procedure [19,20]. 3-DOF haptic control has been used extensively in surgical simulation, such as the Phantom (3D Systems, (formerly Sensable Technologies); Rock Hill, SC, USA) Desktop 3-DOF device or W3D (Entact Robotics; Guelph, ON, Canada) device, both of which track 6-DOF position and output 3-DOF forces (Figure 3.1) [6].

While many haptic devices provide 3 axes of force feedback, fewer devices control torque about those same axes [21]. The necessity of additional DOFs during a procedure has been studied by using a Phantom Premium 1.5 (6-DOF) with all 6-DOF (force and torque) controlled in some situations, and only 3-DOF (force only) controlled in others [22]. Tests using higher-DOF configurations found surgeons have fewer errors and find the procedure easier when all controlled DOF are used, but these higher-DOF situations are more expensive and complex, and it is unclear whether these results translate to real-world surgical outcomes [22]. 1-DOF attachments have been developed to provide torque or grip feedback with the Phantom Omni, but they are externally wired, may use separate control systems, and are limited to 89 N·mm of torque [23,24]. While 1-DOF [20] and 3-DOF [22–25] robotic haptic torque devices have been used in surgical simulation, to the authors' knowledge, there remains a lack of robotic torque haptic devices that can be quickly added or removed from an existing haptic device in a surgical simulator.

Surgical torque can vary widely across procedures. Bone screwing operations have been shown to have a peak torque of approximately 3,000 N·mm [19,20], while studies have characterized much smaller catheter torques of 15 N·mm inside an in vitro vasculature model [26]. Work using the Concorde Clear vacuum curette shows much lower average torques of approximately 150 N·mm at 20° of rotation [27]. For a 1-DOF system with a single motor, a given motor torque, τ, is dependent on the current supplied to it, I, as well as a motor torque constant, k_T, as shown in Equation 3.1 [17].

$$\tau = k_t I$$

Equation 3.1: Torque equation for a DC motor.

If the desired torque and the motor torque constant are known, then Equation 3.1 can be rearranged to solve for the necessary current to provide the desired torque.

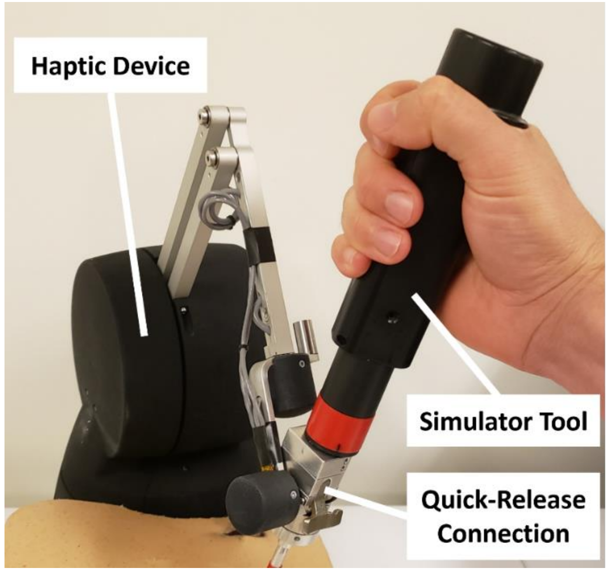

Figure 3.1: Entact Robotics W3D Device with the simulator tool attached via a quick-release mechanism for electrical and mechanical connections. An operator is holding the tool as they typically would during use.

3.2.2.1 Problem Description

It was thus hypothesized that this study could augment an existing haptic device by adding a detachable tool with an additional DOF to mimic an existing surgical tool. In the present disclosed design synthesis, the tool design and testing were informed by 3 primary categories of considerations: (1) 800 N·mm of active torque delivery to conservatively mimic the average Concorde Clear operating conditions, (2) physical imitation of the Concorde Clear by having a surgeon-based Likert score average greater than 3, and (3) integration with an existing haptic device confirmed through use of the tool in a simulated procedure during the testing of the above requirements. Two of the considerations focus on the mechanical design of the tool, and the surgeon survey ensures accurate simulation in the eyes of the end users. Henceforth, the term “surgical tool” refers to the Concorde Clear used during real surgery, whereas “simulator tool” refers to the uniaxial torque haptic device being designed for simulated surgery.

3.2.3 Materials and Methods

The final design of the simulator tool is shown in Figure 3.2. The following sections discuss the tool requirements as well as the materials and test methods designed to validate those requirements.

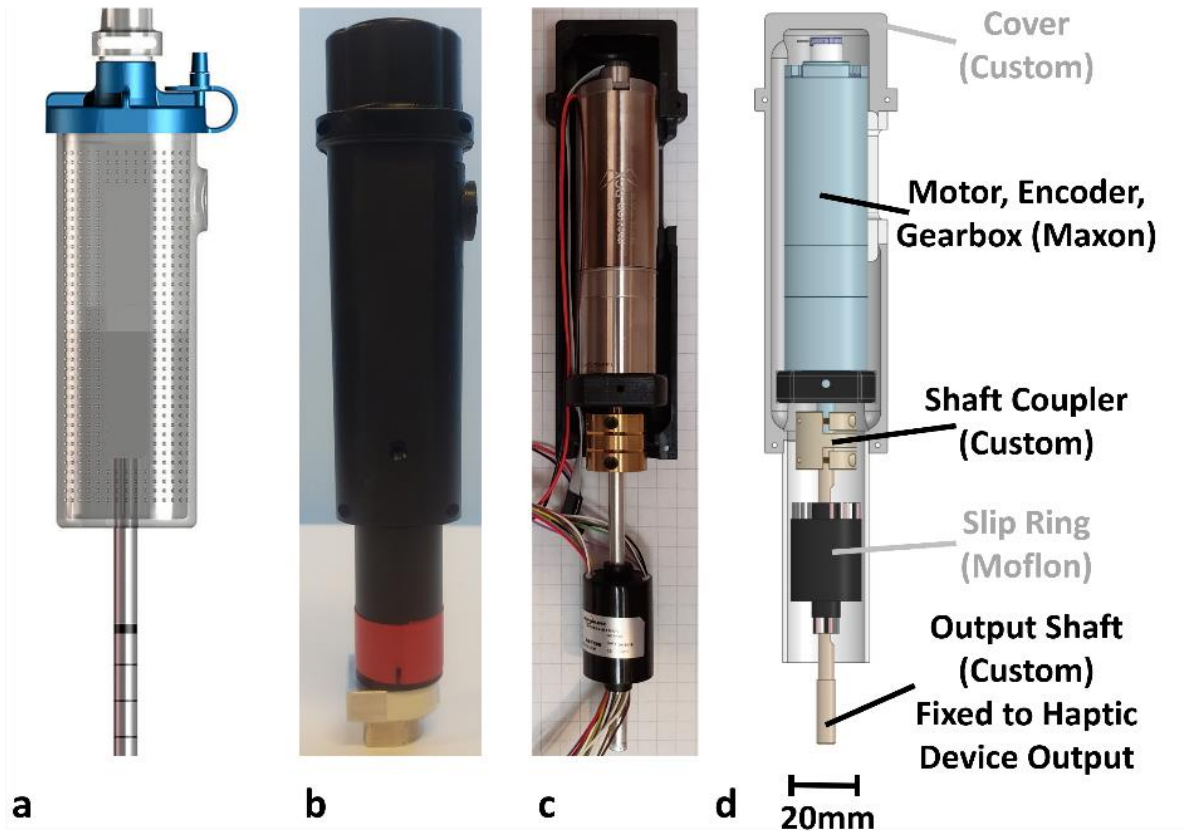

Figure 3.2: Layout of the surgical and simulator tools. a) shows the surgical tool [4], b) shows the final assembled simulator tool, c) shows the simulator tool with the covers removed, and d) shows the computer-aided design (CAD) model of the simulator tool. Manufacturer is noted in parentheses, where applicable. The cover hides the motor, encoder, and gearbox assembly. A shaft coupler connects the motor shaft to the device output shaft, and a slip ring allows for unrestricted rotation. The grey components are electrical or aesthetic, whereas the black components provide mechanical torque transmission.

3.2.3.1 Active Torque Delivery

As a haptic device, the primary goal of the simulator tool was to provide tactile feedback. The simulator tool must adjust its torque output based on the virtual surgical environment conditions. This means that under any loading scenario the simulator tool must be able to react appropriately to the simulated tissue as would the surgical tool to live tissue. For example, if the tool cuts through and destroys a piece of tissue in the virtual environment, the simulator tool should not generate torque when in this position later in the simulator. Thus, the position and orientation of the simulator tool must be tracked at all times so that the simulator tool feedback can be driven by the current conditions of the virtual environment.

An initial target peak torque specification of 3000 N·mm was set based on common orthopedic surgical torque profiles [19,20]. After the first iteration of the design process, surgical data were experimentally collected using cadavers under ethical approval (IRB A04-M13-18A) and were found to have a much lower peak torques, resulting in a conservative new peak torque specification of 800 N·mm, with a programmed torque limit of 300 N·mm [27]. This reduction allowed for the peak torque target to decrease, resulting in a second design iteration. A Maxon (Sachseln, OW, Switzerland) DC motor was chosen as the preferred method of torque generation. The motor configuration is a combination of a Maxon DCX series motor, Maxon GPX series planetary gearbox, and a Maxon ENX series encoder. The 22 W, 24 V motor is 26 mm in diameter in a precious metal brush, ball bearing, reduced backlash configuration. The motor output torque is amplified by a reduced backlash gearhead connected to the shaft. The first version of the motor assembly used a 62:1 reduction with a 3-stage gearbox, and the second used a 16:1 reduction with a 2-stage gearbox. These configurations are referred to, here, as high torque (HT) and low torque (LT), respectively. The change from HT to LT limited peak torque to a level consistent with the updated torque specification while reducing friction and resistance in the assembly. Finally, an ENX10 EASY encoder was used to monitor the position of the motor shaft during operation. The HT and LT configurations have encoder counts of 512 and 1024, respectively. There remained space to add another rotary encoder to track the position of the output shaft, should the backlash need to be accommodated. The simulator tool was mounted vertically (Figure 3.3) to test the torque output of the entire assembly. An adapter was used to connect the simulator tool to an Imada (Toyohashi, Aichi, Japan) GLK500E digital torque screwdriver, creating the torque measurement device shown in Figure 3.3. A given torque command was input and the screwdriver was held to measure the maximum delivered torque.

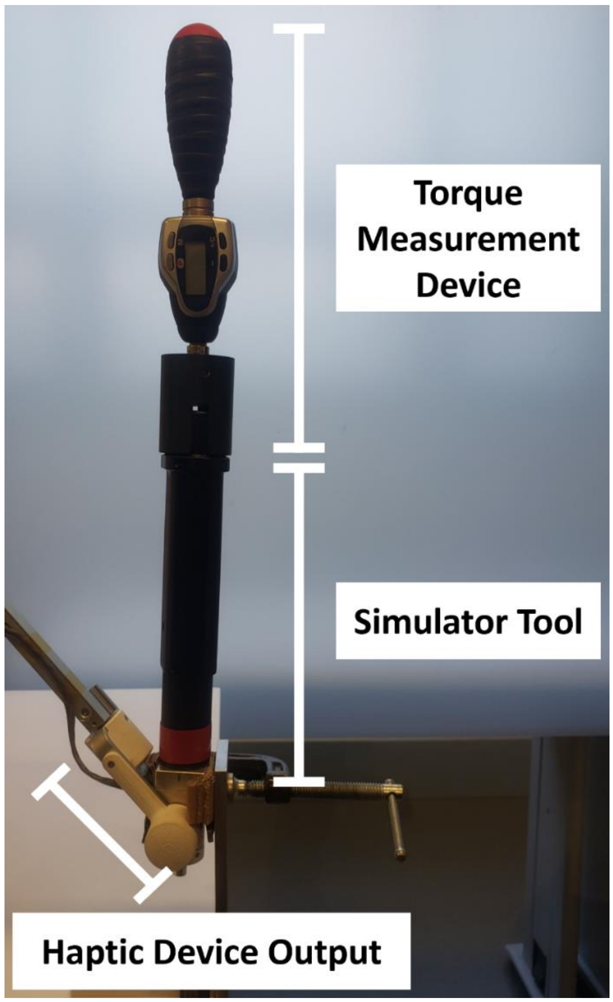

Figure 3.3: Layout of the torque measurement tests. The output of the haptic device was secured to isolate the simulator tool degree of freedom (DOF). The user can grasp the torque measurement device, which is made of a digital torque screwdriver and adapter, to measure torque generated by the simulator tool. The torque measurement device was removed for the torque activation and deactivation tests.

3.2.3.2 Surgical Tool Imitation

To create a high fidelity immersive simulator, the visual and physical components must both imitate a surgical environment. For the simulator tool, it is ideal that the physical appearance and weight match that of the surgical tool. Furthermore, the surgical tool must not be constrained in, nor should it have resistance in any axis. Additionally, the tool must be handheld and portable. Friction and other types of resistance are present in the simulator tool, whereas none exists in moving the surgical tool through space.

A custom machined Delrin® (DuPont; Wilmington, DE, USA) cover was bolted over the motor assembly to contain the motor and match surgical tool dimensions. Delrin® was chosen because it is durable, machinable, lightweight, and non-conductive. No post-processing was performed for surface treatment after machining. To test the aggregated friction and resistance of the assembly, the simulator tool was oriented upright as in Figure 3.3 with the adapter and digital torque screwdriver removed, and the programmed torque was increased until it began to move, overcoming the static resistance. Then the programmed torque was decreased until the simulator tool stopped from the kinetic resistance overcoming the inertia and motor torque. To confirm the face validity of the tool, its appearance was evaluated by twenty-nine orthopedic and neurosurgeons, similar to existing methods of evaluating surgical model validity [3,28]. They filled out (verbally or manually) a printed 1-5 Likert Scale questionnaire that asked how the simulator tool compared to the surgical tool in terms of its physical accuracy and maneuverability. Responses of 5 denoted strongly agree and 1 strongly disagree, so responses greater than 3 indicated the simulator tool accurately mimicked the surgical tool. Seven of the surgeons took the survey after performing both a cadaveric and simulated procedure with the surgical and simulator tools, respectively, and the remaining surgeons had a surgical tool handle on display to compare to the simulator tool.

3.2.3.3 Haptic Device Integration

Finally, the simulator tool must integrate with existing hardware and software. The haptic device used in the present design synthesis was the Entact W3D outlined earlier (Figure 3.1). The W3D device has an additional motor channel capable of providing 3 A constant and 6 A peak current, as well as two encoder channels wired for 5 V, ground, A, and B single-ended signals to track rotation in additional axes. The peak torque the end effector can withstand is 1200 N·mm, based on calculated overloading the gimbal bearings. Finally, the simulator tool must have mechanical and electrical quick connect and disconnect capability with the W3D device. The confirmation of these requirements was confirmed in the operations outlined earlier for the other requirements.

The motor assembly and covers moved independently from the W3D device output quick-release connection. A 6061 aluminum output shaft transmitted the motor shaft torque to the W3D device and was secured in place with a custom 360 brass coupler. A MOFLON (Shenzhen, GD, China) MT0522-S12 12-wire slip ring allowed unrestricted rotation of the motor. The output shaft ran through a hole in the slip ring to allow wires on the motor side to spin freely, while those on the W3D device side remained static. A black cylindrical Delrin® cover (not shown) hid the coupler, output shaft, and slip ring. The simulator tool could be connected by the output shaft to a custom quick-release mechanism to interface with the end effector of the W3D device, providing mechanical and electrical connections.

Design to avoid electromagnetic interference (EMI) in the encoder signal wires was a key consideration. This was anticipated due to the proximity of the encoder signal wires to both the motor and the motor power wires. The effects of EMI were tested by activating a torque response at a given angle during rotation. Then the tool was held at this angle so that torque was generated. The tool could then be twisted into this angle to create a rapid increase in torque and EMI. Expected EMI would cause drift in the encoder signal and therefore the angle at which the torque engaged. A given orientation angle was chosen to introduce a rapid increase in torque, and after repeatedly passing through this angle, the observed change in this orientation was used to determine drift. A schematic of the test setup and torque diagram are shown in Figure 3.4. Introducing an inline resistor in the encoder A and B signals was tested as a filter.

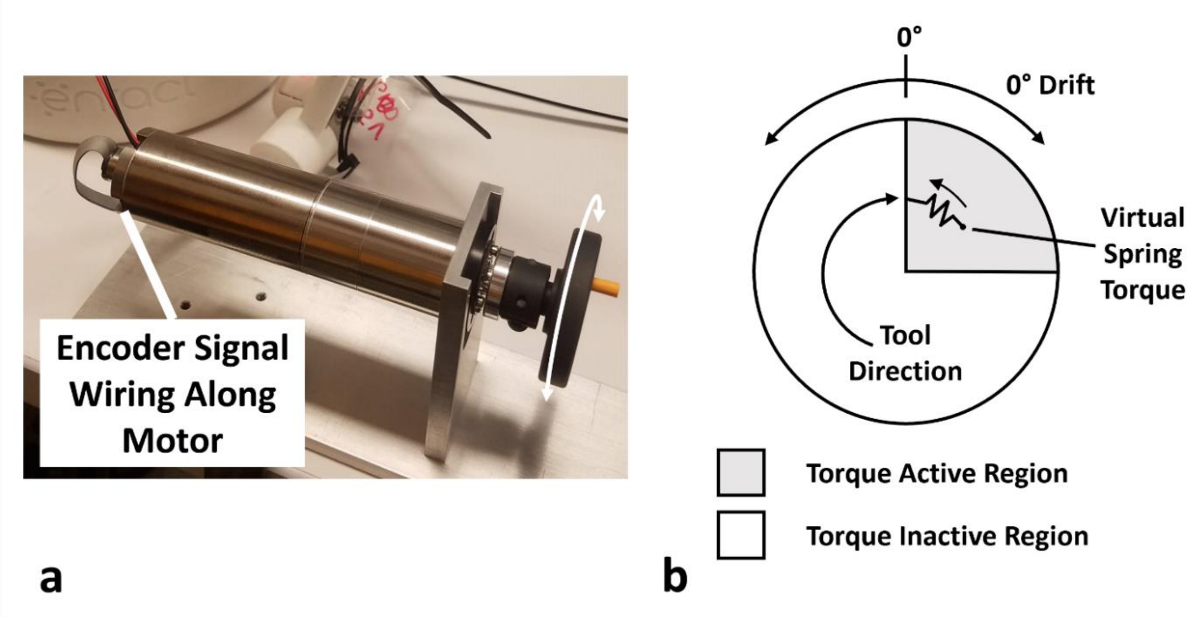

Figure 3.4: Layout of the electromagnetic interference (EMI) testing. a) shows the simulator tool motor testing setup and b) shows the range of motion and programmed torque profile.

3.2.4 Results

The simulator tool (Figure 3.1 and Figure 3.2) was integrated with the W3D device. A direct current (DC) motor, gearbox, and encoder assembly shaft connected to an output shaft with a custom coupler. This output shaft connected to the W3D device to transmit torque. The motor assembly was covered with custom machined parts to match the geometry of the represented surgical tool. A slip ring allowed for unconstrained rotation.

3.2.4.1 Active Torque Delivery

The programmed torque was compared to the observed torque in Figure 3.5. The x-axis shows the torque programmed to the simulator tool, and the y-axis shows the observed torque. A line above 45° indicates the torque is higher than expected, and a line below it indicates a torque below what was programmed. The grey and black boxes contextualize the output within the simulator.

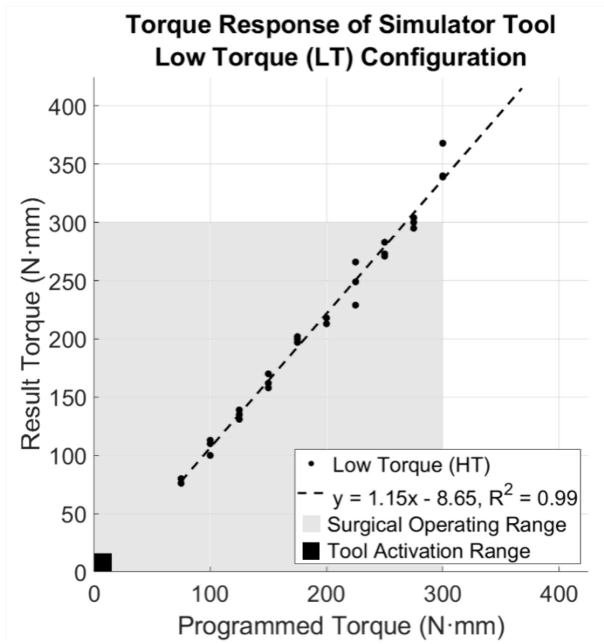

Figure 3.5: Comparison of programmed input and measured output torque for the low torque (LT) simulator tool configuration. The grey area shows the programmed operating torque range for the simulator, and the black area shows the torque necessary to activate or deactivate the torque, as shown in Figure 3.6.

The limits for the two motor configurations are shown in Table 3.1. A 1.25 A current limit was imposed to enable the use of braided 26 gauge wire for power transmission. The HT configuration, with its 512 count encoder, had a motor shaft resolution of 0.70°, which was 0.01° at the output shaft after passing through the 62:1 gearbox reduction. The equivalent resolutions of the LT configuration with a 1024 count encoder and 16:1 reduction was 0.35° and 0.02°, respectively. Both resolutions were below the manufacturer-specified average backlash of 0.9° in both configurations.

Table 3.1: Design comparison of the high torque (HT) and low torque (LT) simulator tool configurations. Peak torque was calculated using Equation 3.1.

Simulator Tool Configuration	High Torque (HT)	Low Torque (LT)
Gearbox Ratio (Number of Stages)	62:1 (3-stage)	16:1 (2-stage)
Resolution	0.01°	0.02°
Peak Torque at 1.25 A	3290 N·mm	830 N·mm
Mass (uncut wires, no connection)	430 g	410 g

3.2.4.2 Surgical Tool Imitation

The simulator tool imitated the handheld section of a surgical tool which served to perform a discectomy during a spine surgical procedure and was shaped like a rectangular prism with rounded corners. The surgical tool has a length and width of 38.1 mm x 28.4 mm and a height of 107.1 mm. Measurements of the handheld section of the simulator tool are within 1% of this, at 38.3 mm x 28.3 mm x 106.8 mm. On the 1-5 Likert Scale asking about the physical accuracy of the simulator tool with respect to the surgical tool, the average answer of the twenty-nine surgeons was 3.9±1.0.

The surgical tool has a mass of 73.6 g. The simulator tool weighed 430 g and 410 g in the HT and LT versions respectively, with all wires uncut and without the attachment mechanism to the W3D device. On the 1-5 Likert Scale survey asking about the maneuverability of the simulator tool with respect to the surgical tool, the average surgeon response was 3.3±1.2. Both activation and deactivation torque were measured for the LT configuration (Figure 3.6).

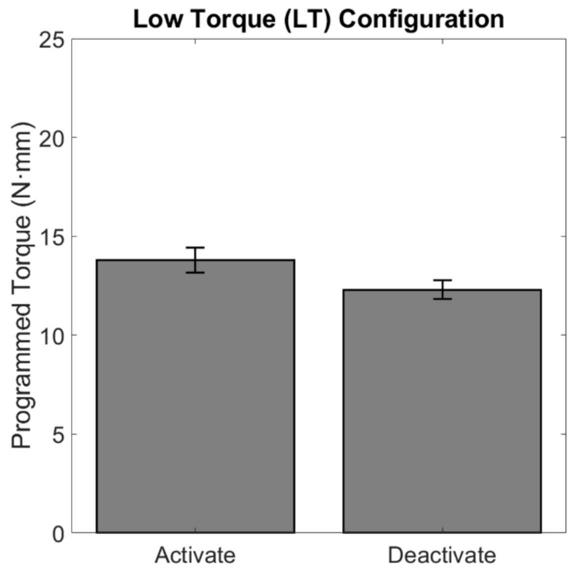

Figure 3.6: Comparison of programmed input torque thresholds to activate and deactivate (begin or end rotation) for the low torque (LT) configuration. N=10 for each data set and the standard deviation is shown.

3.2.4.3 Haptic Device Integration

The integration of the haptic device and simulator tool was evaluated via the testing outlined above. The mechanical and electrical connections of the quick-release mechanism, as shown in Figure 3.1 and Figure 3.2, enabled full use of the tool.

EMI was observed to have a maximum impact when the motor power cables were secured directly parallel to the motor and encoder wire bundles. Maintaining parallel wiring throughout the device and introducing inline resistors in the encoder A and B signals were observed to reduce noise and remedy any drift in the motor encoder signal.

3.2.5 Discussion

This study presented the design, development, and evaluation of a novel analog surgical tool to emulate feedback profiles experienced by surgeons. A new removable uniaxial active haptic device was created to add realism to the simulator and enhance the immersive experience via additional DOF, as has been shown previously [21,22]. This device demonstrates a new way to customize existing haptic devices for increased functionality [6,19,20]. The simulator tool may be able to be used in future studies that characterize surgical proficiency, as has been demonstrated in other works [1]. Based on the above reported assessments, the simulator tool accurately mimicked the surgical tool for each of the key design considerations, as detailed:

3.2.5.1 Active Torque Delivery

The simulator tool met and exceeded the torque requirements in both HT and LT configurations. Each version can deliver a variable torque output that can be synced to live updates in the virtual world of the simulator. The adaptability of the design was successfully evaluated after tissue testing resulted in a reduced peak torque specification and a new motor was swapped in without mechanical design updates [27]. Both configurations could continuously deliver the desired 800 N·mm necessary to encompass the range required in the simulator and remain below the limit of the W3D device, an additional DOF that was expected to improve the simulator similar to previous work [22,27]. The HT tool configuration can theoretically mimic bone screw procedures, as have been simulated previously without the additional 3-DOF of force feedback presented here [19,20]. The feedback given by the simulator tool was additionally characterized beyond the initial motor specifications. The simulator tool was tested for torque response to a programmed input torque and performed as expected (Figure 3.5). Software and firmware changes enable this output torque to be tuned appropriately for a given application, but this data indicates that the tool does indeed respond as expected.

3.2.5.2 Surgical Tool Imitation

The simulator tool additionally matched the relevant geometry of the surgical tool, the Concorde Clear vacuum curette. The simulator tool extended above and below the grip to allow for the motor and haptic device connection, but these sections were not touched by the surgeon during use. Therefore, this extra volume did not detract from the physical experience. The simulator tool lacked the surface features of the surgical tool, but it retained the overall dimensions, meaning that it felt similar when the user was visually immersed in the simulator. Though the black Delrin® did not match the tool color, the color was not relevant when the user was using the simulator visuals and was therefore acceptable. Additionally, this color was chosen to hide the enclosed electronic components. The surgeon survey further confirmed face validity, that the simulator tool did accurately resemble the surgical tool. Even for surgical simulators with multiple tools and steps, this face validity is not often done for individual tools and this work shows how a particular simulator subcomponent can be evaluated [28].

The simulator tool weight did not match that of the surgical tool. Because it was connected to the W3D device, however, there is the possibility of compensating for the extra mass via the force output and a gravity compensation program. Nevertheless, it was observed that the additional weight did not alter the simulated surgical experience in which the focus is on feedback and not tool weight. The most significant source of mass was the motor, gearbox, and encoder assembly, at 290 g (66% of the total mass) and 260 g (64%) for the HT and LT versions, respectively. This assembly was located in the palm of the user, which minimized moments caused by the mass and, as a result, the user's perception of that mass. The results from the surgeon survey regarding the maneuverability further indicated that the simulator tool did indeed match the usability of the surgical tool. This once again confirmed the face validity of the simulator tool, a departure from other face validations that often focus on the entire simulator and not individual tools [3,28].

3.2.5.3 Haptic Device Integration

All electrical connections were confirmed to be adequate to use the simulator tool. It could track position as well as generate torque. The chosen electrical and mechanical components were compatible with the hardware of the W3D device, evident by the testing performed by surgeons.

This integration represents a way to modify the DOF of a haptic device that complements findings in the value of DOF control as well as other augmentable haptic devices [22,24].

3.2.5.4 Limitations and Future Improvements

The design presented here, while meeting all the requirements presented above, does indeed have several limitations to its use. This custom design was created for use with the W3D device, and other haptic devices may lack the adaptability to allow for the augmentation presented here. Other devices may be unable to accommodate additional motor and encoder channels or be unable to withstand the torques generated by the simulator tool. Furthermore, while the LT configuration was designed to accommodate the specific needs of the surgical tool [27], and the HT configuration is theoretically capable of accommodating existing surgical torques [19,20], it was not tested above the torques shown here or for torque accuracy beyond the assessment shown in Figure 3.5. The covers and housing presented in this manuscript were designed specifically to imitate the surgical tool, and new versions would be necessary to mimic additional tools for other procedures. The validity questionnaire could be further improved as well. There are a variety of methodologies used evaluate surgical simulators, as well as implementations of higher-resolution Likert questionnaires, but the 5 point method shown here was chosen because it is an established and accepted validation method [2,3,28,29].

In the future, the simulator tool could be further developed. The torque DOF enabled by this device could be used to give haptic texture feedback as described previously [21]. Empty channels in the current slip ring could be used to add additional capabilities to the device such as lights, buttons, or other electrical components. Further, there was additional room to add an encoder at the output shaft so that errors resulting from backlash in the motor and gearbox could be accounted for. While the observable EMI reduction was realized, other filtering options could be used to reduce encoder signal noise [30]. As well, the dimensions and surface features could be modified to match other devices, mate with other tools, or make the tool lighter. It could be made more adaptable by incorporating a standardized connection that would allow for additional tools to be adapted on, much in the way the quick-release connection allows the simulator tool to be connected to the haptic device. This would enable the use of the simulator tool for other procedures with different tools that also require torque haptic feedback [20]. Each of these modifications could make the simulator tool adaptable to other user needs.

Finally, it will be necessary to test this tool more specifically. The face validity testing shown here is only a first test in simulator validity, as has been documented previously [2,3,28]. Future work should be done to assess the torque accuracy of the device, the content and construct validity of the tool within the simulator, as well as further advanced machine learning techniques to identify surgeon patterns during use [1,3,28].

3.2.6 Conclusions

The novel simulator tool reported herein achieved three primary categories of needs: (1) active torque delivery, (2) physical surgical tool imitation, and (3) integration with an off the shelf haptic device. This design could be used to inform future projects seeking to augment existing haptic device capabilities. Further, the methods and steps employed to independently evaluate the simulator tool, from the total construct or surgical simulator platform, provides value towards assessing the overall fidelity of a simulator via a component-based approach and may be adopted by others.

3.2.7 Acknowledgment

The authors thank Entact Robotics, CAE Healthcare, and DePuy Synthes Companies for their technical support. Michael Grizenko-Vida, Brahim Brahmi, PhD, and Lorne Beckman also assisted in design, manufacturing, and testing of the device.

3.2.8 Ethics

All appropriate ethical approvals and consent were obtained before the surgeon study under IRB A03-M15-20A / 20-03-019.

3.2.9 Funding

Financial support for this work came from the Natural Sciences and Engineering Research Center (NSERC), Quebec Consortium for Industrial Research and Innovation in Medical Technology (MEDTEQ), CAE Healthcare Inc., DePuy Synthes Companies, and McGill University through grant CRDPJ 515768-17.

3.2.10 Nomenclature

AR	Augmented Reality
VR	Virtual Reality
DOF	Degrees of freedom
τ	Motor torque
I	Current
kt	Motor torque constant
Hz	Hertz, SI unit of frequency
Surgical Tool	The tool being used during the surgical procedure
Simulator Tool	The tool meant to mimic the surgical tool in the simulator
N	Newton, SI unit of force
mm	Millimeter, SI unit of length
N·mm	Newton·millimeter, SI derived unit of torque
g	Gram, SI unit of mass
W3D	Entact Robotics W3D device, which has 6-DOF of position tracking and 3-DOF of haptic feedback
A	Ampere, SI unit of electrical current
V	Volt, SI unit of electrical potential
DC	Direct Current
CAD	Computer-aided design
DCX	Maxon DC motor model line
GPX	Maxon planetary gearhead model line
ENX	Maxon encoder model line
W	W, SI unit of power
HT	High torque configuration of the simulator tool
LT	Low torque configuration of the simulator tool
°	Degree
EMI	Electromagnetic interference
Ω	Ohm, SI unit of electrical resistance

3.2.11 References

[1] Winkler-Schwartz, A., Yilmaz, R., Mirchi, N., Bissonnette, V., Ledwos, N., Siyar, S., Azarnoush, H., Karlik, B., and Del Maestro, R., 2019, "Machine Learning Identification of Surgical and Operative Factors Associated With Surgical Expertise in Virtual Reality Simulation," JAMA Netw. Open, **2**(8), pp. e198363, 1–16.

[2] McDougall, E., 2007, "Validation of Surgical Simulators," J. Endourol, **21**(3), pp. 244–247.

[3] Oliveira, M., Araujo, A., Nicolato, A., Prosdocimi, A., Godinho, J., Valle, A., Santos, M., Reis, A., Ferreira, M., Sabbagh, A., Gusmao, S., and Del Maestro, R., 2016, "Face, Content, and Construct Validity of Brain Tumor Microsurgery Simulation Using a Human Placenta Model," Oper. Neurosurg., **12**(1), pp. 61–67.

[4] Depuy Synthes Inc, 2017, CONCORDE™ Clear MIS Discectomy Device.

[5] Mo, F., Yuan, P., Araghi, A., and Serhan, H., 2018, "Time Savings and Related Economic Benefits of Suction-Curette Device for Transforaminal Lumbar Interbody Fusion Discectomy," Int. J. Spine Surg., **12**(5), pp. 582–586.

[6] Delorme, S., Laroche, D., Diraddo, R., and Del Maestro, R., 2012, "NeuroTouch: A Physics-Based Virtual Simulator for Cranial Microneurosurgery Training," Neurosurgery, **71**(Suppl 1), pp. 32–42.

[7] CAE Healthcare Inc, 2020, "Vimedix Ultrasound Simulator" [Online]. Available: https://caehealthcare.com/ultrasound-simulation/vimedix/.

[8] Mahvi, D., and Zdeblick, T., 1996, "A Prospective Study of Laparoscopic Spinal Fusion: Technique and Operative Complications," Ann. Surg., **224**(1), pp. 85–90.

[9] Cooper, J., and Taqueti, V., 2004, "A Brief History of the Development of Mannequin Simulators for Clinical Education and Training.," Qual. Saf. Health Care, **13**(Suppl 1), pp. i11–i18.

[10] Chmarra, M., Dankelman, J., Van Den Dobbelsteen, J., and Jansen, F., 2008, "Force Feedback and Basic Laparoscopic Skills," Surg. Endosc., **22**(10), pp. 2140–2148.

[11] Kim, H., Rattner, D., and Srinivasan, M., 2003, "The Role of Simulation Fidelity in Laparoscopic Surgical Training," *Medical Image Computing and Computer-Assisted Intervention - MICCAI 2003. MICCAI 2003. Lecture Notes in Computer Science*, T.M. Peters, R.E. Ellis, G. Goos, J. Hartmanis, and J. van Leeuwen, eds., Springer, Montréal, Canada, pp. 1–8.

[12] Sweet, R., 2017, "The CREST Simulation Development Process: Training the Next Generation," J. Endourol., **31**(Suppl 1), pp. S69–S75.

[13] Mathieu, L., and Lee-Huu, P., 1998, "Seat for Motion Simulator and Method of Motion Simulation," pp. 1–3. US Patent Number US5980255A.

[14] Misra, S., Ramesh, K., and Okamura, A., 2008, "Modeling of Tool-Tissue Interactions for Computer-Based Surgical Simulation: A Literature Review," Presence: Teleoperators Virtual Environ., **17**(5), pp. 463–491.

[15] Okamura, A., 2009, "Haptic Feedback in Robot-Assisted Minimally Invasive Surgery," Curr. Opin. Urol., **19**(1), pp. 102–107.

[16] Behensky, M., Moncrief, R., Durfey, E., and Loper, M., 1991, “Control Device Such As A Steering Wheel For Video Vehicle Simulator With Realistic Feedback Forces,” pp. 1–13. US Patent Number US5044956A.

[17] Lynch, K., and Park, F., 2017, *Modern Robotics. Mechanics, Planning, and Control*, Cambridge University Press, New York City.

[18] Culbertson, H., Schorr, S., and Okamura, A., 2018, “Haptics: The Present and Future of Artificial Touch Sensation,” Annu. Rev. Control Robot. Auton., 1, pp. 385–409.

[19] Acker, W., Tai, B., Belmont, B., Shih, A., Irwin, T., and Holmes, J., 2016, “Two-Finger Tightness: What Is It? Measuring Torque and Reproducibility in a Simulated Model,” J. Orthop. Trauma, **30**(5), pp. 273–277.

[20] Majewicz, A., Glasser, J., Bauer, R., Belkoff, S., Mears, S., and Okamura, A., 2010, “Design of a Haptic Simulator for Osteosynthesis Screw Insertion,” *2010 IEEE Haptics Symposium, HAPTICS 2010*, Boston, USA, pp. 497–500.

[21] Pedram, S., Klatzky, R., and Berkelman, P., 2017, “Torque Contribution to Haptic Rendering of Virtual Textures,” IEEE Trans. Haptics, **10**(4), pp. 567–579.

[22] Forsslund, J., Selesnick, J., Salisbury, K., Silva, R., and Blevins, N., 2013, “The Effect of Haptic Degrees of Freedom on Task Performance in Virtual Surgical Environments,” *Studies in Health Technology and Informatics (Medicine Meets Virtual Reality 20: NextMed/MMVR20)*, J.D. Westwood, S.W. Westwood, L. Felländer-Tsai, R.S. Haluck, R.A. Robb, and K.G. SengeVosburgh, eds., IOS Press, San Diego, USA, pp. 129–135.

[23] Mortimer, M., Horan, B., and Stojcevski, A., 2014, “Design for Manufacture of a Low-Cost Haptic Degree-Of-Freedom,” Int. J. Electron. Electr. Eng., **2**(2), pp. 85–89.

[24] Turini, G., Moglia, A., Ferrari, V., Ferrari, M., and Mosca, F., 2012, “Patient-Specific Surgical Simulator for the Pre-Operative Planning of Single-Incision Laparoscopic Surgery with Bimanual Robots,” Comput. Aided Surg., **17**(3), pp. 103–112.

[25] Weller, R., and Zachmann, G., 2012, “User Performance in Complex Bi-Manual Haptic Manipulation with 3 DOFs vs. 6 DOFs,” *Haptics Symposium 2012, HAPTICS 2012 - Proceedings*.

[26] Thakur, Y., Holdsworth, D., and Drangova, M., 2009, “Characterization of Catheter Dynamics During Percutaneous Transluminal Catheter Procedures,” IEEE Trans. Biomed. Eng., **56**(8), pp. 2140–2143.

[27] Cotter, T., Mongrain, R., and Driscoll, M., 2022, “Vacuum Curette Lumbar Discectomy Mechanics for Use in Spine Surgical Training Simulators,” Med. Biol. Eng. Comput. Under Review.

[28] Ledwos, N., Mirchi, N., Bissonnette, V., Winkler-Schwartz, A., Yilmaz, R., and Del Maestro, R., 2021, “Virtual Reality Anterior Cervical Discectomy and Fusion Simulation on the Novel Sim-Ortho Platform: Validation Studies,” Oper. Neurosurg., **20**(1), pp. 74–82.

[29] Goldenberg, M., and Lee, J. Y., 2018, “Surgical Education, Simulation, and Simulators—Updating the Concept of Validity,” Curr. Urol. Rep., **19**(7).

[30] Kuphaldt, T., *Lessons in Electric Circuits*, All About Circuits.

3.3 Additional Studies

Numerous studies and design considerations were made in addition to those mentioned in Article 1: Design Synthesis of a Robotic Uniaxial Torque Device for Orthopedic Haptic Simulation. These updates and choices to adapt the tool to the simulator are discussed here. Figure 3.7 shows the surgical tool, the DePuy Synthes CONCORDE® Clear, as well as the final haptic torque handle assembly as it is used in the simulator. An exploded view is shown in Figure 3.8. The entire labeled tool assembly and bill of materials (BOM) can be seen in Figure I.1 and Table I.1 of 0.

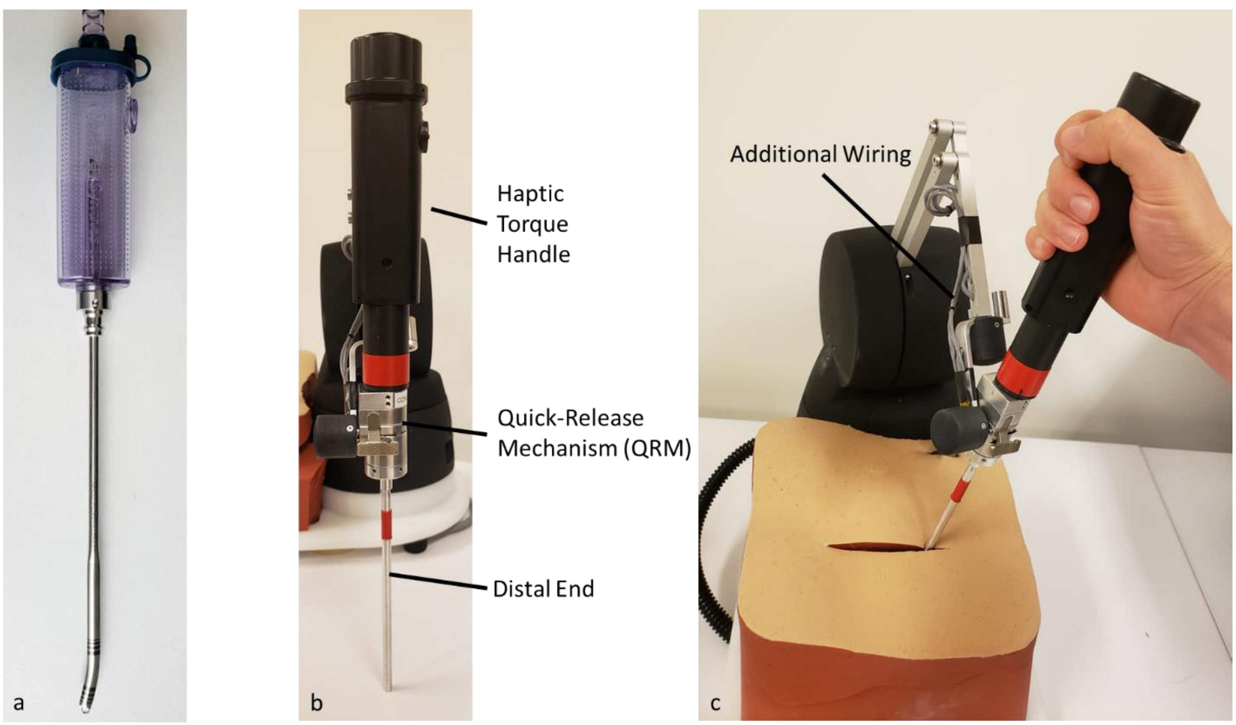

Figure 3.7: Multiple versions on the DePuy Synthes Concorde Clear MIS discectomy tool. a) shows the surgical tool, b) shows the haptic torque handle assembled onto the haptic device, and c) shows the haptic torque handle as it was used in the simulator.

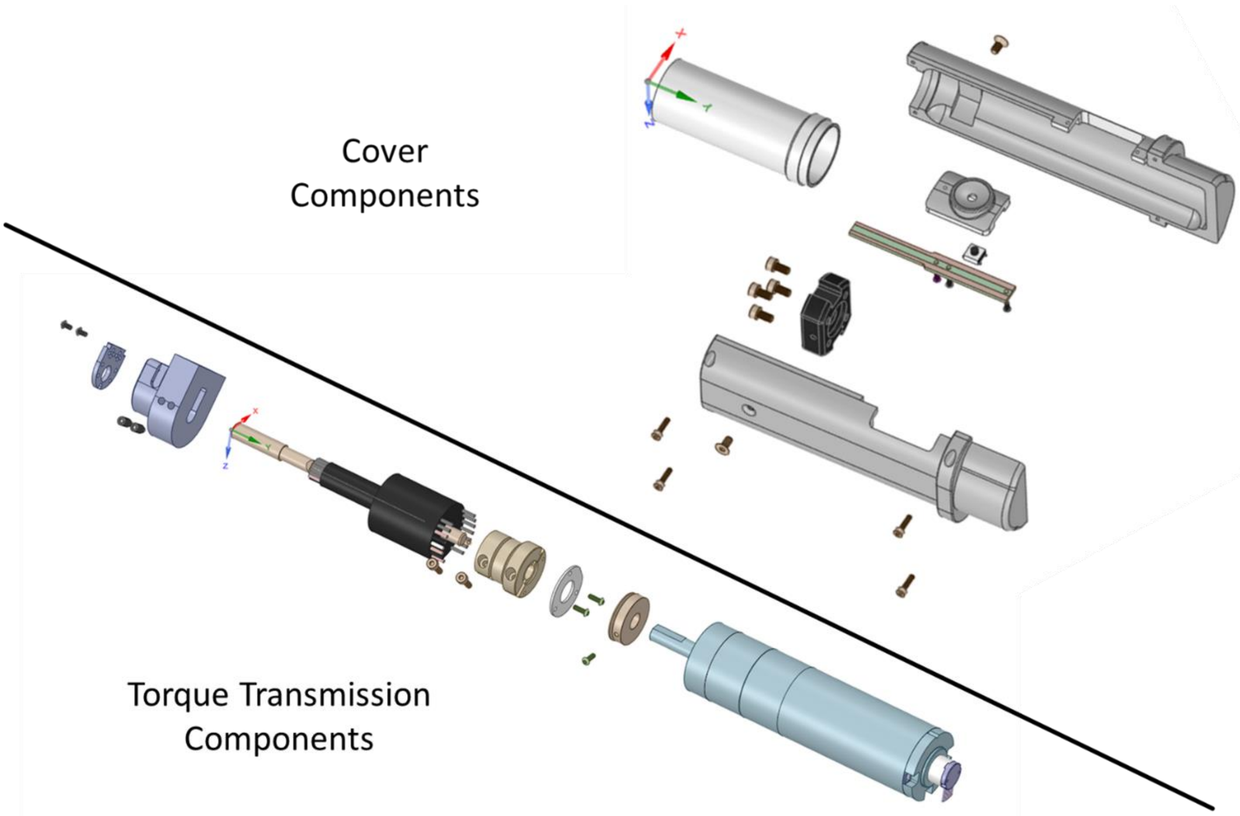

Figure 3.8: Entire haptic torque handle assembly split into the cover components as well as the motorized and torque transmission components.

3.3.1 Quick-Release Mechanism (QRM)

The QRM was essential for interfacing the Entact W3D haptic device and haptic torque handle. Figure 3.9 shows the mating surfaces and individual assemblies that make up the QRM. Figure 3.7b,c shows the final assembly. Once inserted into the QRM, the haptic torque handle is mechanically secured with a spring latch. The electrical connections in the QRM were made possible by two mating printed circuit boards (PCBs). The haptic device PCB had spring-loaded pin connectors and the haptic torque handle side had surface contacts.

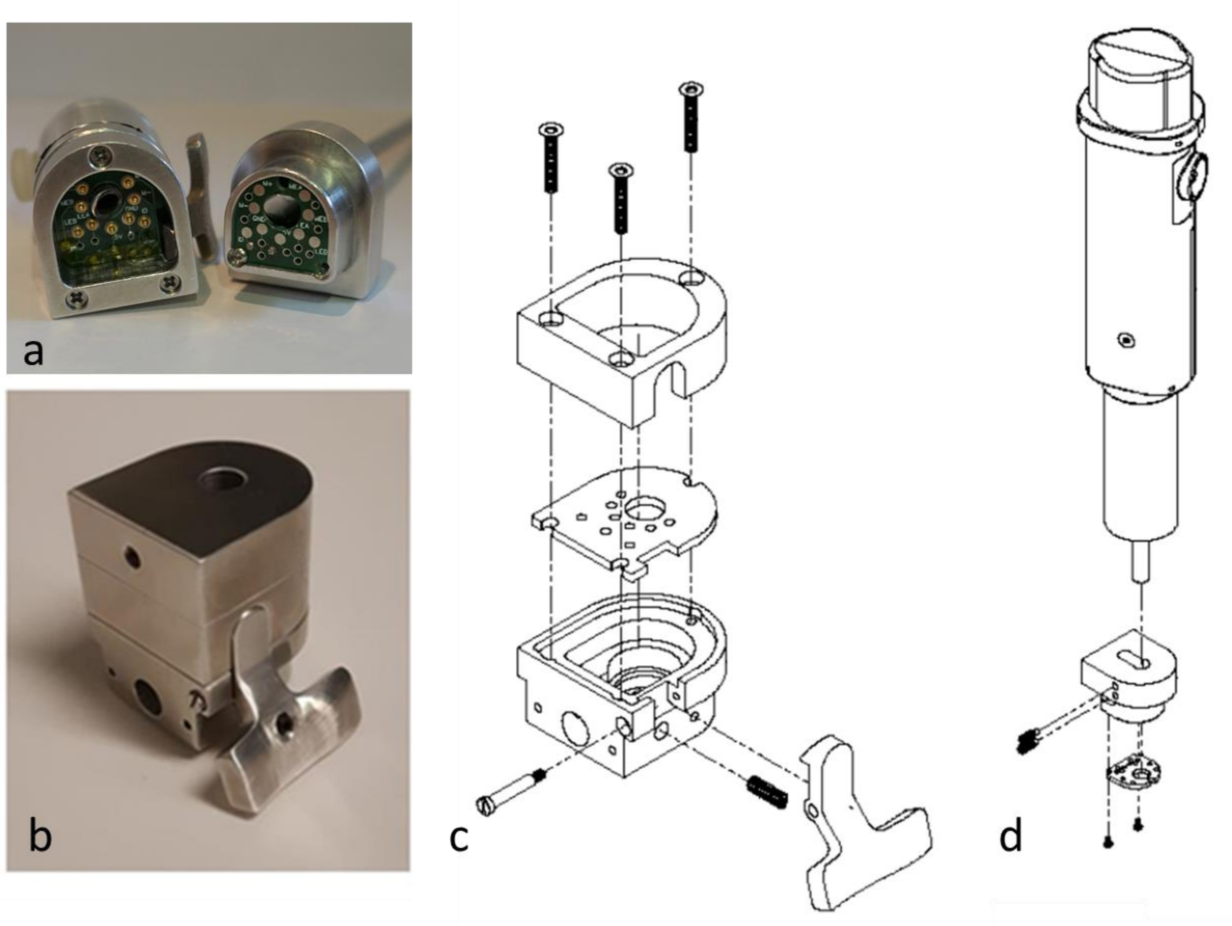

Figure 3.9: Essential components of the quick-release mechanism (QRM). a) shows the two mating electromechanical connections, b) shows the assembled QRM, c) shows the haptic device side of the QRM assembly, and d) shows the haptic torque handle side of the QRM assembly.

3.3.2 Electrical Design

The haptic torque handle needed to effectively receive and transmit electrical signals through the QRM to deliver torque, measure position, identify itself, and other necessary surgical tool functions. All connections are shown in Table I.2. To identify the haptic torque handle in the simulator gameplay, a Teensy 3.2 board (PJRC; Portland, USA) circuit was used. The 5V power supplied by the Entact W3D device was drawn through resistors that identified the connected haptic torque handle and then sent back to the Teensy board through the ID channel. The voltage measured by the Teensy board was used in the simulator gameplay to signal the tool was connected. The Concorde Clear device has a port for the surgeon to use to apply vacuum, and thus a button was incorporated into the design (Figure I.1). The button was placed in parallel to the ID channel, such that both voltages when the button was and was not pressed could be used to identify the tool. Sufficient voltage change was present such that the simulator gameplay could identify when the button was pressed, signifying the vacuum should be applied within the simulator.

Appropriate wiring size was also a design consideration. Since the haptic device must move with minimal resistance, it was necessary to choose the smallest and most flexible wiring that could deliver the necessary current to power the motor. A five-wire cable of 30 AWG (NMUF 5/30-4046 SJ) wire from Cooner (Los Angeles, USA) was used to match the rest of the haptic device for all but the motor wires, and a two-wire cable of 26 AWG (NMEF 2/26-6544 SJ) wire was chosen to power the motors with similar mechanical flexibility. The additional wiring is labeled in Figure 3.7. The motor is capable of producing 670 N·mm/A, and a solid core 26ga copper wire has an expected max current of 2.2 A [142]. The chosen wire has 65 40ga strands and it was decided that the 0.45 A necessary to generate the 300 N·mm simulator peak torque limit, elaborated in Chapter 4, would be a conservative estimate of the wire current capacity.

3.3.3 Electromagnetic Interference (EMI)

EMI testing was present throughout the design process, as outlined in Figure 3.4 in Article 1: Design Synthesis of a Robotic Uniaxial Torque Device for Orthopedic Haptic Simulation. Non-continuous positional readings or drift of the 0° point in the motor shaft were used to determine the presence of EMI. The haptic torque handle encoder A/B signal wires were determined to be the most likely point where EMI would appear, because of their small amplitudes and close proximity to the spinning motor. Therefore, testing was done to understand and correct the interference before assembly. The motor was mounted horizontally and a motor control program was built in Microsoft Visual Studio to imitate an artificial “wall,” as seen in Figure 3.4a. At [0, 90]° rotation, a rotational spring torque was calculated to push the motor shaft back towards 0°. The tool was spun from the [90, 360]° zone where torque was inactive into the [0, 90]° zone where torque was active as seen in Figure 3.4b. By increasing the virtual spring stiffness and changing the spin speed, it was possible to increase EMI spikes. Through this testing, it was found that laying the motor power cables and encoder signal wires next to each other along the side of the motor resulted in increased EMI. Introducing the slipring added to the EMI observed. To alleviate this, resistors were placed in series with the encoder signal wires to act as an RC filter.

Additionally, improving the QRM contacts was imperative in alleviating EMI. Any small misalignment between the QRM PCBs had the potential to introduce noise into the signal. The encoder wires were swapped from the motor encoder A and B (MEA/B) contacts to the load encoder A and B (LEA/B) contacts. The LEA/B contacts were originally placed to accommodate an optional load-side encoder that enabled monitoring on both sides of the motor, as shown in Figure I.1 and Table I.1. The LEA/B connection was more central to the QRM PCB, as shown in Figure 3.10. The two mounting points are located on one side of the PCB, and therefore any misalignment between the adjacent connecting PCBs in the QRM would be amplified more at the MEA/B locations than the LEA/B. Additionally, some damage was visible on the surface mounts of the MEA/B surface contacts, which would have also introduced poor signal conduction. After making this change, EMI manifested as irregular position readings in the simulator was eliminated.

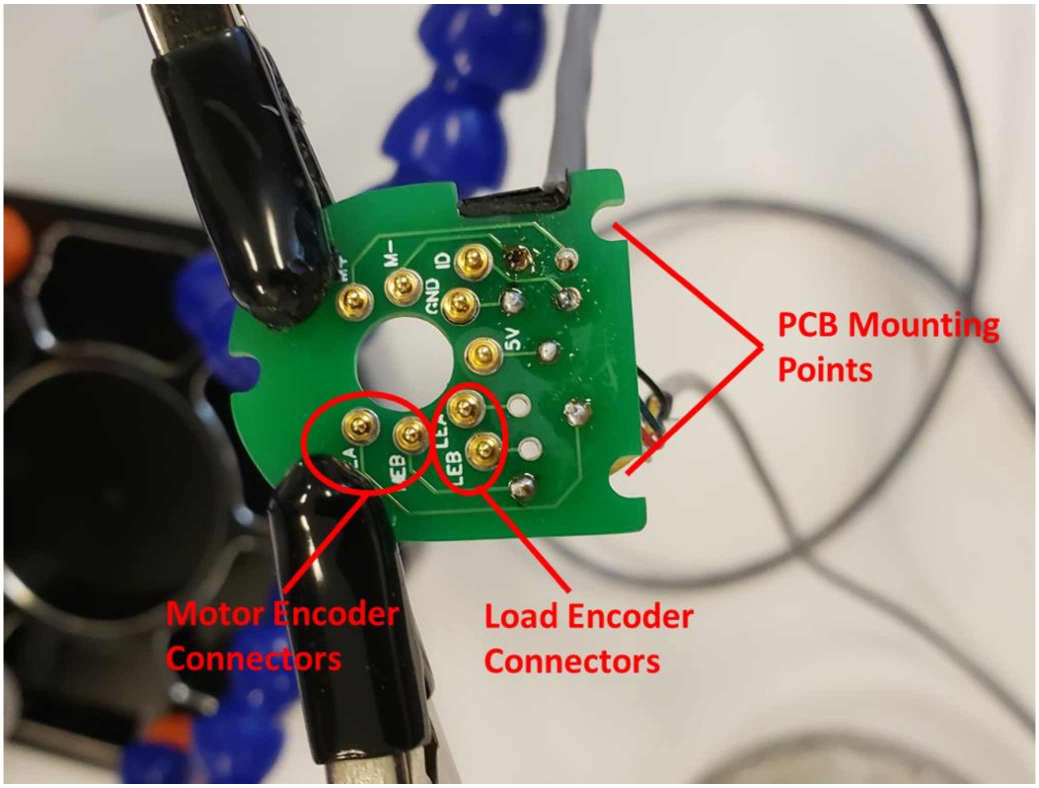

Figure 3.10: Quick-Release Mechanism (QRM) printed circuit board (PCB) with labeled encoder channels and mounting points.

3.3.4 Sources of Error

In addition to the mechanical testing and EMI investigation performed to understand potential errors in the haptic torque handle, there remain additional inaccuracies that could occur. Mechanically, the LT haptic torque handle configuration has 0.9° of backlash. While it would be impossible to mechanically bring this to 0°, future iterations could use both the second encoder to monitor this and accommodate any discrepancies. However, this was not noted by surgeons and was therefore not considered necessary. Both torque measurement tests, the quantification of the torque output as shown in Figure 3.5 and the activation and deactivation torque as shown in Figure 3.6, were performed using handheld or approximately vertical tests. These tests could be performed at multiple orientations and on a rigid test jig to ensure consistent results. Regardless, both results shown still indicate the haptic torque handle has an accurate response. Finally, it is essential to consider how the haptic torque handle interacts with the entire haptic system. The software used to determine the desired torque output, the control system of the robot to understand the electrical needs to deliver that output, and the ability of the haptic device to send appropriate electrical signals to the haptic torque handle all must work in harmony to generate a proper haptic response. Adjustment to any of these components could affect the haptic output, but the system as detailed in Article 1: Design Synthesis of a Robotic Uniaxial Torque Device for Orthopedic Haptic Simulation and used throughout the rest of this manuscript has proven to deliver the haptic torque response needed by the simulator.

3.3.5 Surgeon Evaluation

The number of surgeons who have evaluated the haptic torque handle in simulation has increased since the study outlined in Article 1: Design Synthesis of a Robotic Uniaxial Torque Device for Orthopedic Haptic Simulation. A total of 29 orthopedic and neurosurgeons have used the tool and completed the 5 point Likert scale questionnaire, as shown in Table IV.3. Seven of the surgeons completed the testing after performing a cadaveric procedure with the Concorde Clear tool, while the remaining surgeons performed it without cadaveric practice. The results show that the surgeons think the haptic torque handle accurately resembles the Concorde Clear tool in physical appearance (3.9±1.0) and maneuverability (3.3±1.2). Future studies could be enhanced by including the cadaveric practice component for all surgeons, ensuring they were all familiar with the Concorde Clear tool before simulation.

3.4 Conclusion

The haptic torque handle was designed, built, and implemented into the simulator successfully. Mechanical and electrical testing was performed to validate its response, as well as surgeon testing to confirm it is an accurate representation of the original Concorde Clear tool. It is capable of delivering the torque necessary to mimic the tissue response investigated in Chapter 4. This work represents a step forward in the field of augmentable active haptic robotics for surgical simulation.

4

Discectomy Mechanics

4.1 Context

This chapter discusses Objective 2, a biomechanical characterization of lumbar discectomy with the Concorde Clear tool in response to Hypothesis 2. The aim of this characterization was to use data acquired during cadaveric testing to program the simulator haptics and novel tool from Chapter 3for surgeon training. The work involved measuring force and torque profiles during insertion and torsion inside lumbar intervertebral discs (IVDs) during the act of a discectomy. These profiles were then compared with consideration of specimen, spinal level, and other conditions. The force and torque were averaged and programmed into the simulator where multiple surgeons tested and evaluated their haptic similarity to real procedures. No data has been published on such a study of the Concorde Clear tool force and torque during lumbar discectomy. After the manuscript text, additional relevant work describes other parts of the development that were not contained in the manuscript, including the force and torque models implemented in the simulator. Relevant ethical approvals are contained in Appendix II.

The work presented in this chapter was executed with additional collaborators. Dr. Khaled El-Monajjed and Dr. Sneha Patel assisted in all aspects of the test design and execution. Testing was performed at Laboratoire de Recherche en Imagerie et Orthopedie division of l'Hôpital du Sacré-Coeur de Montréal (Montréal, QC) under the supervision of Prof. Yvan Petit and Prof. Eric Wagnac of École de technologie supérieure (ÉTS) (Montréal, QC). Elisabeth Laroche assisted with the operation and design of the testing. Dr. Rodrigo Navarro-Ramirez helped prepare, dissect, and advise the cadaveric testing. The spine displacement study was performed with the assistance of Lorne Beckman at the Orthopedic Research Lab at the McGill General Hospital (Montréal, QC).

Portions of this work were presented at multiple conferences as well as their associated peer-reviewed abstract publications. To date, ePosters resulting from this research include: "Mechanics of Minimally Invasive Discectomy Using a New Curette" at the 2020 Global Spine Congress (canceled due to COVID-19), "Lumbar Discectomy Tool Torque Hysteresis for Application in a Surgical Simulator" at EUROSPINE 2020, "Mechanics of Lumbar Discectomy Tool Insertion for Application in a Surgical Simulator" at the 2021 Canadian Society of Biomechanics, "Discectomy Tool Mechanical Testing in Cadaveric Spine" at the 2021 Global Spine Congress, and "Combining Freehand and Controlled Movement for Calculating Surgical Simulator Forces" at the 2021 Simulation Summit [143–146]. The following manuscript, Vacuum Curette Lumbar Discectomy Mechanics for Use in Spine Surgical Training Simulators, was submitted for publication in Scientific Reports in April 2022 [147]. The contribution of the first author was 75%, which included test design and execution, analysis, and writing. The second and third authors contributed 10% and 15%, respectively, for research guidance and review.

4.2 Article 2: Vacuum Curette Lumbar Discectomy Mechanics for Use in Spine Surgical Training Simulators

Trevor Cotter[1,2], Rosaire Mongrain[1], P.Eng, PhD, Mark Driscoll[1,2], P.Eng, PhD

[1]Musculoskeletal Biomechanics Research Lab, Department of Mechanical Engineering, McGill University, Montreal H3A 0G4, Canada.

[2]Orthopedic Research Laboratory, Montreal General Hospital, Montreal QC H3H 1V8, Canada.

Correspondence should be addressed to:

Mark Driscoll

McGill University, Department of Mechanical Engineering

817 Sherbrooke Street West, Montreal, QC, H3A 0C3

Macdonald Eng. Bldg. office #153

T: 1.514.398.6299 F: +1.514.398.7365

mark.driscoll@mcgill.ca

This is an Original Article Submission to Scientific Reports

Main Text Word Count:3,761

Abstract Word Count: 198

Number of Figures: 5

Number of Tables: 3

4.2.1 Abstract

Simulation in surgical training is a growing field and this study aims to understand the force and torque experienced during lumbar spine surgery to design simulator haptic feedback. It was hypothesized that force and torque would differ among lumbar spine levels and the amount of tissue removed by ≥7%, which would be detectable to a user. Force and torque profiles were measured during vacuum curette insertion and torsion, respectively, in multiple spinal levels on two cadavers. Multiple tests per level were performed. Linear and torsional resistances of 2.1±1.6 N/mm and 5.6±4.3 N·mm/°, respectively, were quantified. Statistically significant differences were found in linear and torsional resistances between all passes through disc tissue (both $p = 0.001$). Tool depth ($p < 0.001$) and lumbar level ($p < 0.001$) impacted torsional resistance while tool speed affected linear resistance ($p = 0.022$). Average differences in these statistically significant comparisons were ≥7% and therefore detectable to a surgeon. The aforementioned factors should be considered when developing haptic force and torque feedback, as they will add to the simulated lumbar discectomy realism. These data can additionally be used inform next generation tool design. Advances in training and tools may help improve future surgeon training.

Keywords: Spine, Force Feedback, Torque Feedback, Medical Simulation, Surgical Instruments

4.2.2 Introduction

Virtual-reality (VR) simulation training is an essential tool in training techniques for fields ranging from aviation to driving and beyond [1–5]. Simulators have been able to identify operator skill levels and are required in some cases before professionals are allowed to perform their duties [6–8]. Recent computational and simulation advances have enabled these tools to reach more industries, each with unique challenges. In medicine, the complex nature of the human body, as well as the risks associated with surgery, mean simulators have the potential to revolutionize the way surgeons prepare for procedures [9, 10].

4.2.2.1 Surgical Simulation

Surgery carries many dangers, thus the importance of effective surgeon practice and training is evident. Traditionally, surgeons have undergone a combination of classroom, animal, and cadaveric surgical training before a living patient [2, 11, 12]. However, each of these training methods have limitations such as inaccurate anatomy or physiological response [2]. Alternatively, simulators with various degrees of complexity have been developed to train surgeons on a variety of procedures, from analog laparoscopic knot tying to full VR brain tumor resection [13, 14]. The addition of robotic haptic, or touch, devices has enabled these simulators to become more adaptable by removing disposable components such as synthetic tissues and using robotic components to communicate the feeling of them consistently with minimal maintenance [2]. The demand for this type of training is evident by the numerous simulators that have been developed for spine surgery alone [2, 15–18]. However, simulators using this technology may require tissue testing and an understanding of the biomechanics of the procedure.

Robotic haptic feedback must communicate the sensations a surgeon encounters during a procedure. This can be broken into two categories: the force and torque present in the procedure, and the force and torque felt by the surgeon.

4.2.2.2 Tissue Mechanics

Many techniques exist to mechanically characterize tissues. Properties such as elastic modulus and tensile strength can be derived from tests that measure force or torque and linear or angular displacement on a mechanical tester [19, 20]. While this equipment is often limited to one or two axes, multiple tests can be used to generate a multi-axial characterization of the tissue [21, 22]. Destructive tests often result in complex tissue mechanics. For needle insertion, existing studies have considered the total force f_{needle} to be the sum of the tissue deformation ($f_{stiffness}$), friction ($f_{friction}$), and cutting ($f_{cutting}$) forces, which are dependent on position, x [23]:

$$f_{needle}(x) = f_{stiffness}(x) + f_{friction}(x) + f_{cutting}(x)$$

Equation 4.1

4.2.2.3 Human Perception of Force

The mechanical understanding of biological tissues can be used to inform a robot to communicate the tissue force to a user. However, this communication must consider the boundaries of human perception. The just-noticeable difference (JND) is a measure of the minimum perceptible change in force. Hands and fingers are extremely sensitive to the sense of touch, and it has been found that intentional training can improve surgeon skills [24–26]. A JND of [5,10]% change has been observed during [2,10] N loads between fingers or in elbow extension, but can vary based on finger, training, and frequency [27–30]. Work on haptic devices has found higher JNDs, including 23±13% and 34±24% detectable changes for force and torque on the ranges of [0.4,8.8] N and [20,410] N·mm, respectively [31]. While existing literature shows a wide range of observed JNDs, it is necessary to consider this sensitivity when determining how users will interpret differences in simulated tissue.

4.2.2.4 Spinal Mechanics Studies

Spinal orthopedic procedures are of particular interest in new surgical simulators [2]. The spine is made up of alternating rigid vertebra and flexible intervertebral discs (IVDs) to create a flexible, supportive structure that protects the spinal cord and other anatomies. Over time or due to injury, IVDs can become compressed or deform, affecting the nerve root exiting from the spinal cord and causing intense pain [32–34]. Treatment of back pain is of immense importance, as it affects 80% of people at some point in their lives and is the leading cause of disability in the world [35, 36]. Many treatment options for this pain exist, but the present work focuses on one surgical intervention: lumbar interbody fusion (LIF) [37].

A LIF procedure aims to relieve pressure on the exiting nerve from the spinal cord. A surgeon performs a discectomy, or removal of the IVD. The surgeon then uses a curette to remove the nucleus pulposus and prepare the endplates of the IVD. With a gap now created, an interbody cage may be placed where the collapsed IVD had been. Bone graft is added at the interbody cage to fuse the two adjacent vertebrae at an appropriate spacing. Finally, pedicle screws and rods are placed to maintain the stability of the vertebrae during healing.

Like many other surgical procedures, modern developments have improved LIF, yielding minimally invasive (MI) procedures. MI surgeries have been found to decrease hospital stays and recovery times [37–39]. As such, a new vacuum curette was developed (Concorde Clear MIS Discectomy Device; DePuy Synthes; Boston, USA) to allow surgeons to perform discectomies with a single tool faster and safer than existing curettes [40]. The adoption of a novel tool requires training. In a surgical simulator context, this also requires the characterization of force and torque encountered when using this tool.

Biomechanical studies performed on the IVD have traditionally been focused on various loading scenarios a person may encounter [41–44]. Few studies deal with the force as surgeons encounter them during surgery [45]. While the known biomechanical properties of the IVD may predict spine behavior under loading, they may be inadequate in predicting mechanical interactions with surgical tools. The unique shape, cutting surfaces, and vacuuming effect of the Concorde Clear may yield unpredictable biomechanical responses. As a result, this work compares peak force and torque, which are the aggregate of stiffness, friction, cutting, and other factors during tool insertion as shown in Equation 4.1. Similarly, resistance for each of these quantities is defined by the change of each quantity during loading. Therefore, linear resistance is N/mm and torsional resistance is N·mm/°.

This manuscript hypothesizes that discectomy force and torque will be dependent on spinal level and removed tissue at a ≥7% difference, a magnitude detectable to a surgeon. This data can then be used to inform haptic feedback in relevant surgical simulators while drawing attention to the importance of such model selection in other biomechanical studies of the disc.

4.2.3 Materials and Methods

Mechanical testing was performed on human tissues to characterize linear and torsional movements. These data were then analyzed and compared to understand how they differ between anatomical and procedural conditions.

4.2.3.1 Sample Preparation

Two fresh frozen cadaveric torsos were acquired from Science Care, Inc. under ethical approval (IRB A04-M13-18A). Both samples had no history of radiation treatment or spinal surgery. X-rays were used to measure the height of each lumbar IVD. Specifications for the cadavers can be seen in Table 4.1. All IVD height measurements were taken from El-Monajjed et. al, who used the same specimens and methods for preparation [45]. Cadavers were stored at -20°C, thawed for 5 days at 2°C, and held at room temperature for 72-96 hours before testing. A 30x30 cm posterolateral window was removed from the skin, fascia, and muscle to expose the posterior lumbar spine. A 1x1 cm annulotomy was performed posterolaterally to gain access to the IVD as would be done in an MI LIF.

Table 4.1: Cadaveric torso properties. The cadaver measurements are from a previous work [45].

CADAVERIC TORSO PROPERTIES

Cadaver				C1	C2
Gender				M	M
Age				63	69
Height			cm	175	178
Weight			kg	73	86
Collapsed Disc				None	L_4/L_5
IVD Dimensions	L_1/L_2	Height	mm	10.0	5.2
		Width	mm	44.7	49.4
	L_2/L_3	Height	mm	10.3	7.6
		Width	mm	46.1	45.7
	L_3/L_4	Height	mm	11.6	5.7
		Width	mm	47.6	60.6
	L_4/L_5	Height	mm	10.3	3.1
		Width	mm	54.1	NA

Note: IVD width is the lateral width

4.2.3.2 Testing Setup

A custom jig supported the cadaveric torso. The torso was laid on its chest and rotated to allow a linear tester to penetrate at approximately 40° lateral to a fully posterior approach. Testing was performed with an MTS 858 Mini-Bionix II testing apparatus and a force and torque load cell of 2.5 kN and 25 N·m, respectively (662.20D-01, MTS Systems Corporation; Minneapolis, USA). Custom fixturing connected the tester to one of two tools (Figure 4.1).

(a) (b)

Figure 4.1: Concorde Clear tools used in the test. a) shows the straightened tool (left) used in the linear test as well as the normal bent tool (right) used in the torsional test. b) shows the test setup and motion, where the tool is inserted (1) into the intervertebral disc (IVD) and twisted (2). The linear test involved motions 1 and 2, while the torsional test was only motion 2. IVDs are marked.

4.2.3.3 Linear Testing

The first test was a linear insertion that mimicked a surgeon penetrating the IVD. The load cell was secured to a straightened version of the Concorde Clear shaft tip, shown in Figure 4.1a. The shaft tip was lowered to 5 mm inside the IVD space before beginning. The shaft tip was then inserted at a rate of 0.25 mm/s from [0,12-15] mm of tool travel, depending on disc size. Meanwhile, the tool was rotated [±20]° at 20°/s to prevent snagging and ensure penetration into the IVD. The tool was then withdrawn at the same rates until it returned to its starting position.

The tool path can be seen in Figure 4.1b, where motions 1 and 2 were performed. Time, position, force, angle, and torque were all recorded at 100 Hz. An example of the position and force results can be seen in Figure 4.2a. The test was performed 3 times on the left and right sides of lumbar IVDs between L1 and L5. Additional speed studies were also performed. Linear speeds of 0.25, 0.50, 0.75, and 1.00 mm/s were compared on the right side of C1 L3L4. Torsional speeds of 10, 20, 30, and 40°/s were compared on the right side of C1 L4L5. Test details are shown in Table 4.2.

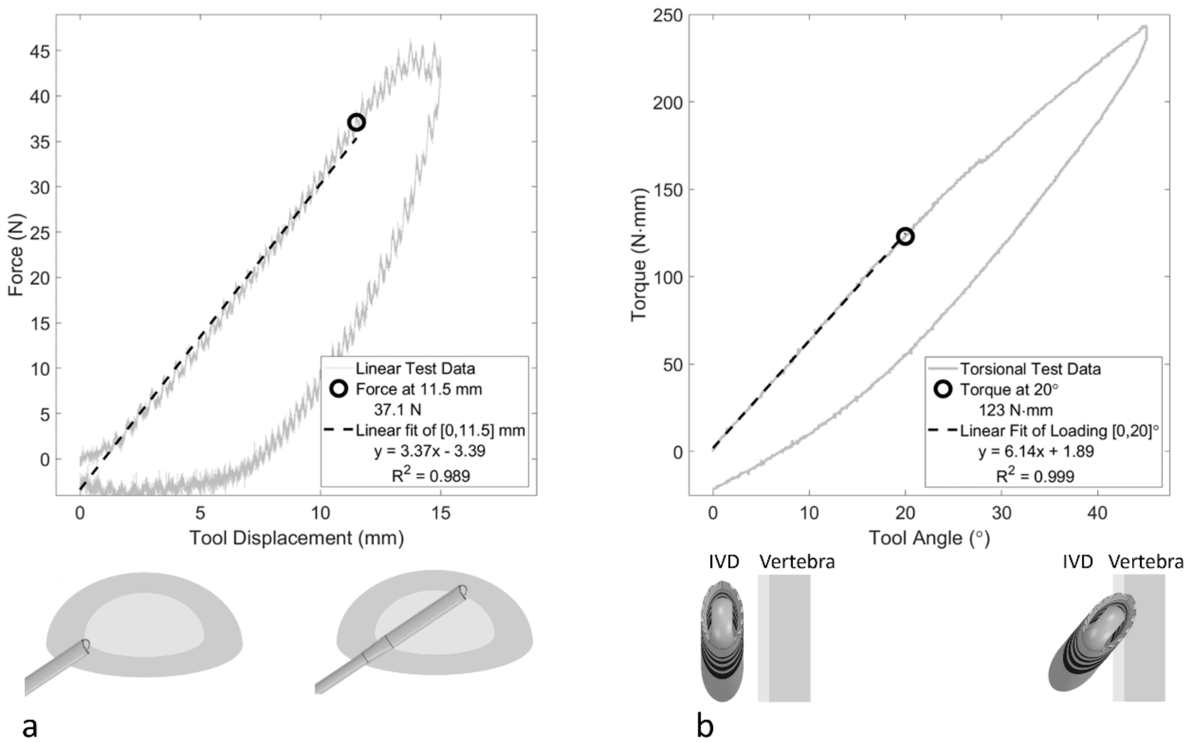

Figure 4.2: Examples of linear (a) and torsional (b) tests with extracted peak and resistance values for the first trial of the right side of C2 L_3L_4. The torsional test was performed at a 5 mm depth. Schematics of the tool orientation within the intervertebral disc (IVD) are shown.

Table 4.2: Testing parameters.

TESTING PARAMETERS

Test Name		Linear Test	Torsional Test
IVD Levels		L_1L_2 - L_4L_5	
Sides		Left and Right	
Linear Motion	Waveform	Triangle	NA
	Starting Position	5 mm inside IVD	NA
	Range	0-12/15 mm	NA
	Speed	0.25 mm/s	NA
	Additional Speed Tests	0.50, 0.75, 1.00 mm/s	NA
Torsional Motion	Waveform	Sinusoidal	Sinusoidal
	Starting Position	0°	0°
	Range	±20°	±45°
	Speed	40°/s	2°/s
	Additional Speed Tests	20, 60, 80°/s	3, 4, 6, 8°/s
Number of Trials		3	5

4.2.3.4 Torsion Testing

The second test was a torsional motion that mimicked a surgeon twisting inside the IVD space. The load cell was secured as for the linear test but with an angled Concorde Clear shaft tip, shown in Figure 4.1a. The shaft tip was lowered to 5 mm inside the IVD space and twisted at 2°/s to [±45]° for a total of 5 full cycles. One cycle represented a tool path that proceeded through angles of 0°, 45°, -45°, and finally 0°. The tool path can be seen in Figure 4.1b, where only motion 2 was performed. Data recording was the same as the linear testing. An example of the angle and torque results can be seen in Figure 4.2b. This test was repeated at a 20 mm penetration depth on the right and left sides of each lumbar IVD between L1 and L5. Torsional speeds of 2, 3, 4, 6, and 8°/s were compared on the right side of C1 L4L5. Test details are shown in Table 4.2.

4.2.3.5 Data Analysis

The data were then analyzed for comparison. Initial position, angle, force, and torque were normalized at the start of each test. This applied to all linear tests, but notably only the first torsional test. After extracting the relevant parameters, a variety of statistical comparisons were performed to determine the significance of differences between cadavers (C1, C2), lumbar levels (L1L2, L2L3, L3L4, L4L5), and tool passes (1, 2, 3, (4, 5)) of linear (0.25, 0.50, 0.75, 1.00 mm/s) and torsional speed (10, 20, 30, 40°/s). Additional comparisons of penetration depth (5, 20 mm) and torsional speed (2, 3, 4, 6, 8°/s) were performed on the torsional tests. A Mann-Whitney U test was used to compare two conditions, Kruskal-Wallis was used for tests with three or more conditions, and data were compared to IVD height using Spearman correlation after confirming they were not normally distributed using a Shapiro-Wilk normality test [46–49]. Comparisons are summarized in Table 4.3, where bold, italicized values have a significance of $\alpha \leq 0.05$.

For linear tests, 11.5 mm of tool travel after the initial set position of 5 mm inside the IVD was used. A linear fit was performed on force vs position for the range of [0,11.5] mm, and the peak force at 11.5±0.25 mm was extracted. A sample fit is shown in Figure 4.2a.

For torsional tests, the first ±20° of tool rotation was used. A linear fit was performed on torque vs angle for the range of [0,±20]° and the peak torque at ±20±0.2° (±10 data points at 100 Hz) was extracted. A sample fit is shown in Figure 4.2b.

Table 4.3: Statistical comparison of testing conditions.

STATISTICAL COMPARISON OF TESTING CONDITIONS

Linear Tests		Force Peak				
	Comparison	Cadavers	Lumbar Level	Pass Number	Linear Speed	Torsional Speed
	All Passes	1.46E-01	7.23E-02	***2.05E-03***	***1.56E-02***	***2.16E-02***
	Pass 1	5.74E-01	1.35E-01	-	-	-
	Pass 2-3	***2.05E-02***	1.52E-01	*3.00E-01	8.33E-02	1.04E-01
	Test Method	Mann-Whitney U	Kruskal-Wallis			
		Linear Resistance				
	Comparison	Cadavers	Lumbar Level	Pass Number	Linear Speed	Torsional Speed
	All Passes	2.36E-01	1.58E-01	***1.49E-03***	***2.16E-02***	***1.88E-02***
	Pass 1	4.42E-01	1.13E-01	-	-	-
	Pass 2-3	***3.32E-02***	2.49E-01	*3.76E-01	8.33E-02	8.33E-02
	Test Method	Mann-Whitney U	Kruskal-Wallis			
Torsional Tests		Torque Peak				
	Comparison	Cadavers	Depth	Lumbar Level	Pass Number	Torsional Speed
	All Passes	***1.17E-05***	***5.69E-15***	***2.11E-10***	***1.63E-02***	***1.19E-03***
	Pass 1	***2.13E-02***	***1.49E-05***	***4.71E-02***	-	2.12E-01
	Pass 2-5	***1.93E-04***	***2.24E-11***	***2.62E-09***	2.56E-01	***1.04E-02***
	Test Method	Mann-Whitney U		Kruskal-Wallis		
		Torsional Resistance				
	Comparison	Cadavers	Depth	Lumbar Level	Pass Number	Torsional Speed
	All Passes	***1.29E-04***	***8.78E-05***	***5.27E-09***	***1.42E-03***	5.79E-02
	Pass 1	9.20E-02	***2.69E-03***	***3.74E-02***	-	6.82E-01
	Pass 2-5	***2.09E-04***	***4.34E-03***	***1.04E-07***	6.42E-01	8.29E-02
	Test Method	Mann-Whitney U		Kruskal-Wallis		

Note: all bolded, italicized values have significance $p \leq 0.05$ and exceed the JND threshold of 7%

* Performed with Mann-Whitney U Test

4.2.4 Results

Data and overall comparisons were considered separately with force in the linear tests and torque in the torsional tests.

4.2.4.1 Force

4.2.4.1.1. Peak

Peak force samples can be seen for multiple conditions in Figure 4.3. Average peak force at 11.5 mm was 25.2±16.7 N. There was a statistically significant difference between passes (P1, P2, P3). However, after the initial pass (P1), later passes (P2, P3) were similar, indicating that the results stabilize after the initial destructive pass (P1). Additionally, after the initial pass (P1) there was a statistically significant difference between cadavers (C1, C2). There was a significant difference when performing the test at linear speeds (0.25, 0.50, 0.75, 1.00 mm/s) and torsional speeds (10, 20, 30, 40°/s) when considering all trials. Boxplots containing this information are contained in Figure 4.3, with corresponding p-values in Table 4.3.

4.2.4.1.2. Resistance

The linear resistance can be seen for multiple conditions in Figure 4.3. Average resistance over the range [0,11.5] mm was 2.1±1.6 N/mm. All statistical differences match those observed for peak values. Boxplots containing this information are contained in Figure 4.3, with corresponding p-values in Table 4.3.

4.2.4.1.1. Disc Height Correlations

IVD height appeared to have no statistically significant correlation with either the peak or linear resistance as seen in Figure 4.4a,b.

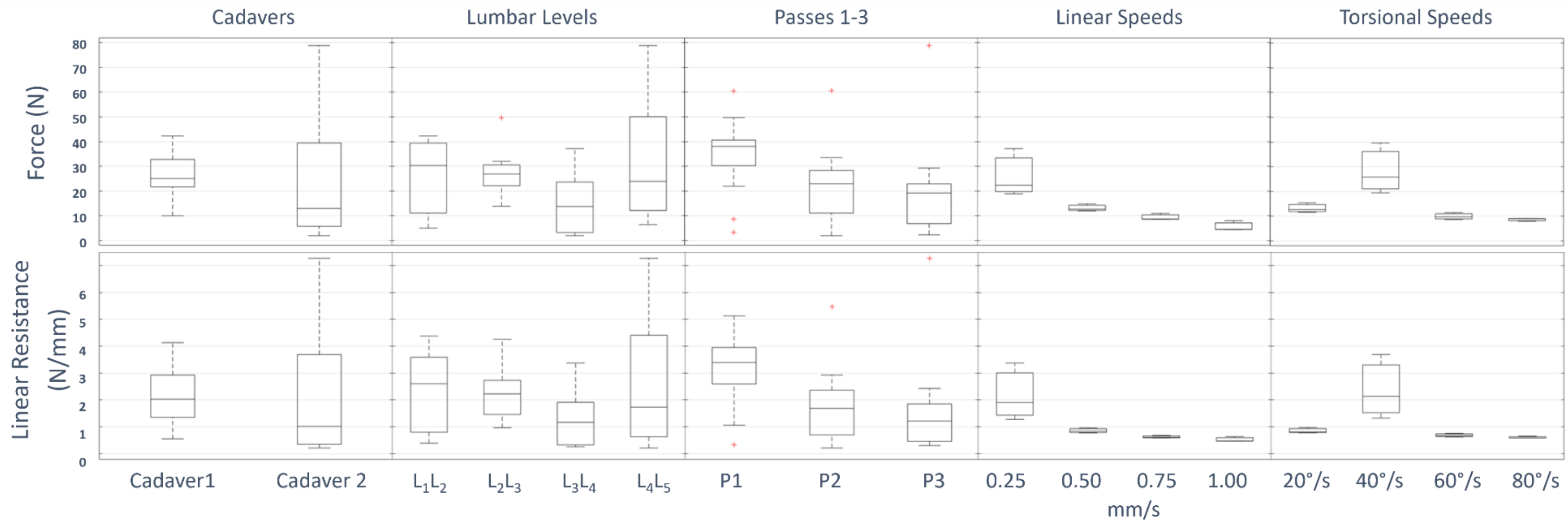

Figure 4.3: Force peak and linear resistance comparisons.

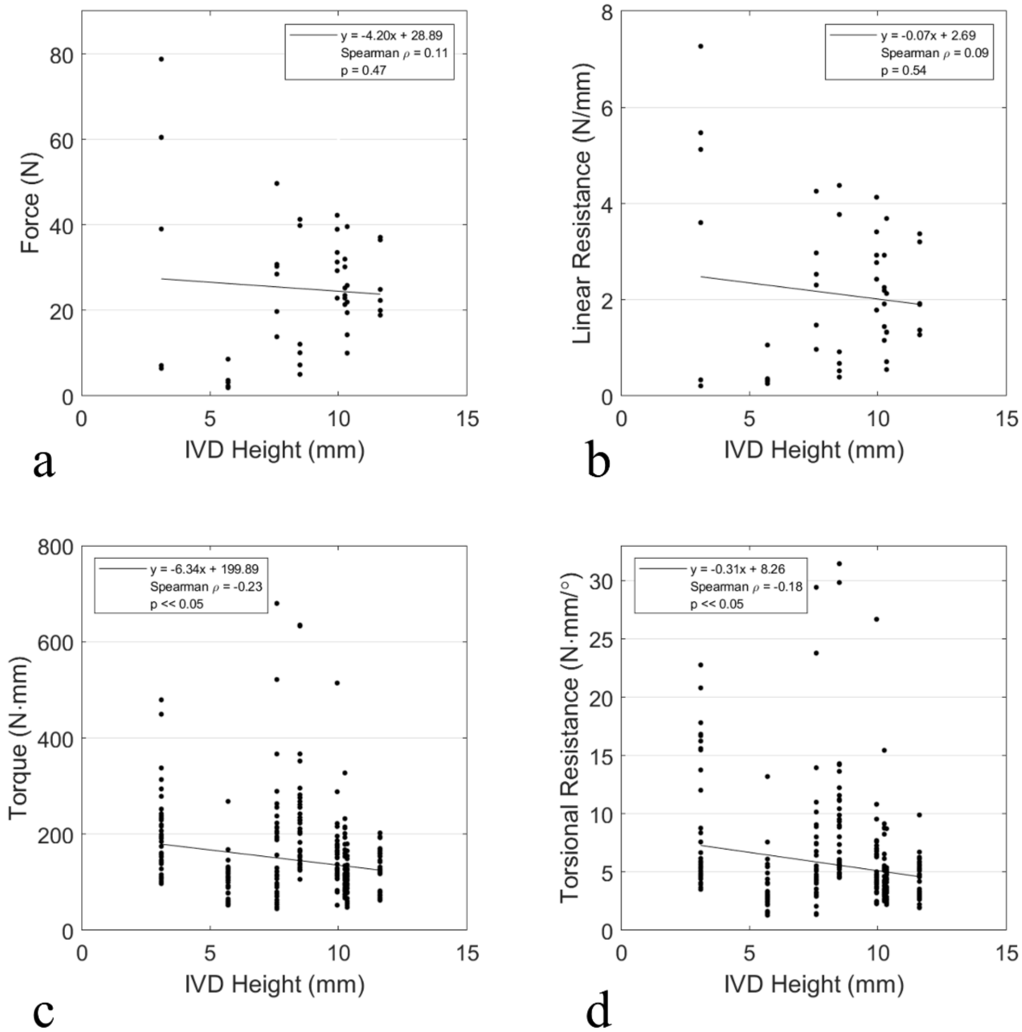

Figure 4.4: Linear (a, b) and torsional (c, d) peak and resistance values as correlated to intervertebral disc (IVD) height.

4.2.4.2 Torque

4.2.4.2.1. Peak

Peak torque samples can be seen in Figure 4.5. Average torque magnitude at ±20° was 146.6±90.0 N·mm. Statistically significant differences were observed between cadavers (C1, C2), depths (5, 20 mm), lumbar levels (L1L2, L2L3, L3L4, L4L5), and passes (P1, P2, P3, P4, P5). For torsional speeds (2, 3, 4, 6, 8°/s), a difference was observed across all passes and after the initial pass (P1), but not for the initial pass (P1). Boxplots containing this information are shown in Figure 4.5, with corresponding p-values in Table 4.3.

4.2.4.2.1. Resistance

The torsional resistance can be seen in Figure 4.5. The average resistance on the range [0,20]° was 5.6±4.3 N·mm/°. All statistical differences matched those observed for the peak values, with the exceptions that differences between torsional speeds (2, 3, 4, 6, 8°/s) for any pass combination and the initial pass (P1) between cadavers (C1, C2) were not significant. Boxplots containing this information are contained in Figure 4.5, with corresponding p-values in Table 4.3.

4.2.4.2.2. Disc Height Correlations

IVD height appeared to have no statistically significant correlation with either the peak or torsional resistance, as seen in Figure 4.4c,d.

4.2.1 Discussion

The data presented show the range of expected force and torque present during a lumbar discectomy using the Concorde Clear. The hypothesis that force and torque would be dependent on spinal level and removed tissue at a ≥7% difference was confirmed in most cases. The difference between peak force and torque, as well as linear and torsional resistance, differed by ≥7% between initial and later passes through the tissue. Similar differences were found between lumbar levels, except for the peak force comparisons that did not meet the 7% threshold. To create a simulator or inform next generation discectomy tools, it is essential to identify how these data can be used to replicate or facilitate the surgical experience. This discussion focuses on distinguishing between anatomies or procedural conditions during the discectomy with respect to the JND of the user.

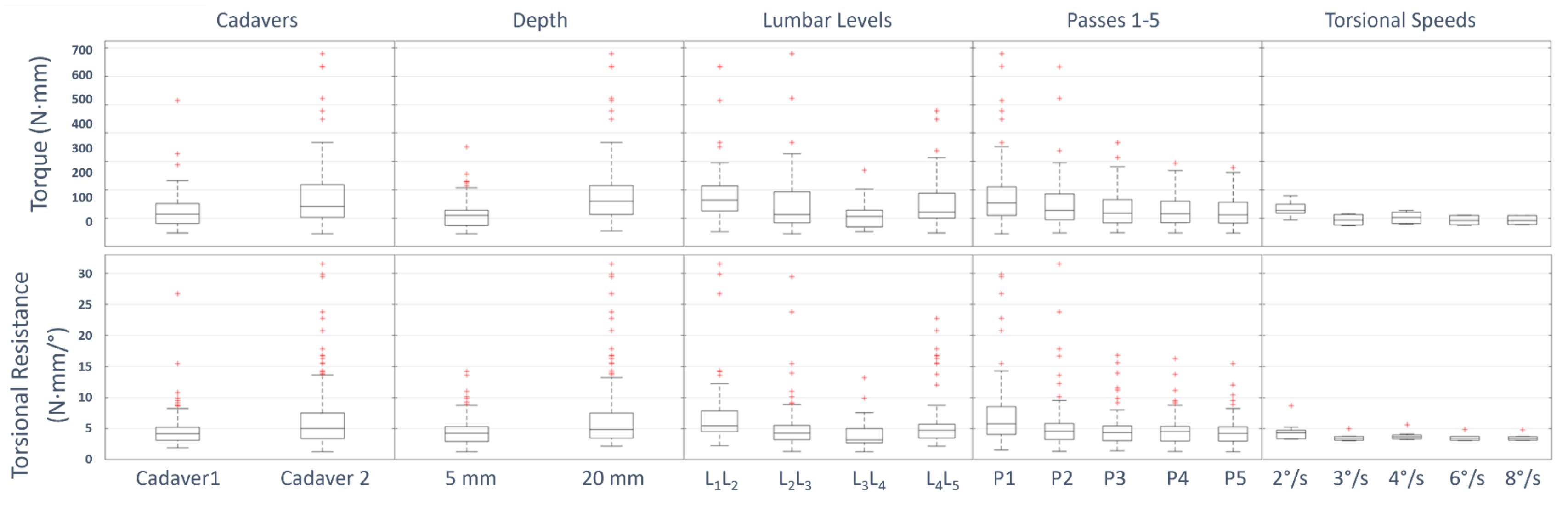

Figure 4.5: Torque peak and torsional resistance comparisons.

4.2.1.1 Force

Peak force at 11.5 mm and linear resistance over [0,11.5] mm followed the same statistical patterns. The largest statistically significant difference across all conditions was between all passes (P1, P2, P3), with peak force decreasing after the initial pass (P1). This change suggests that the removal of tissue, or $f_{cutting}$ in Equation 4.1), was an essential distinguishing element during the procedure. However, after the initial pass (P1), the measured force for later passes (P2, P3) was the same. Variability in the initial pass (P1) was large enough that the difference between cadavers (C1, C2) was insignificant. However, after this destructive initial pass (P1), the cadaveric variation (C1, C2) became visible. Additionally, both linear and torsional speeds significantly impacted the force of insertion. In contrast, IVD height did not show a correlation with a change in force or linear resistance. This disconnect may be attributed to anatomical geometry. IVD height inside the disc was larger than around its perimeter, meaning the tool did not need to separate adjacent vertebrae away to penetrate deeper tissue after it had already penetrated the disc. Therefore, it can be considered that the most important factors to consider when designing a simulator for insertion of the Concorde Clear are the number of times the tool has passed through the disc and the speed at which the device is being pushed and twisted.

4.2.1.2 Torque

Peak torque at ±20° and torsional resistance over [0,±20]° showed more statistical differences across comparisons than peak force and linear resistance. The peak torque was different between cadavers (C1, C2), penetration depths (5, 20 mm), and between all passes (P1, P2, P3, P4, P5), only being the same for the initial pass (P1) across the torsional speed (2, 3, 4, 6, 8°/s) tests. The torsional resistance was different across torsional speeds (2, 3, 4, 6, 8°/s) for all passes (P1, P2, P3, P4, P5), as well as the initial pass (P1) between cadavers (C1, C2). This suggests once again that the cutting torque, or other torque component only present in the initial pass, impacts the total torque significantly. Like the linear testing, both peak torque and torsional resistance were independent of IVD height. While the tool did not need to further spread the IVD when penetrating, as in the force test, it did abut the vertebral bodies during rotation. Adjacent IVDs may have accommodated this distraction by compressing and absorbing the torque, leading to similar results for all IVDs. However, the collapsed IVD (C2 L_4L_5), was included in this data set, and yet there was still no observed correlation. Greater variability between test conditions other than IVD height such as cadaver, pass number, and speed implies that more factors must be considered when designing torque output in a simulator than when designing the force output.

4.2.1.3 Simulator Application

The data shown could be used to determine the appropriate force and torque needed in a Concorde Clear discectomy simulator. However, it was still necessary to determine if a user could distinguish between the statistically different conditions outlined above and in Table 4.3. Using a JND of 7%, as previously suggested, all statistically significant differences in peak force, peak torque, linear resistance, and torsional resistance shown in Table 4.3 would be detected by the surgeon. This implies that cadaveric differences, pass number, linear speed, and torsional speed should all be considered when determining the robotic force output, while lumbar level should not. Furthermore, cadaveric differences, tool depth, lumbar level, pass number, and torsional speed in some circumstances should be accounted for when determining the robotic torque output.

4.2.1.4 Limitations

As with any study, there were limitations to its scope. One key shortcoming of this work was that only the tool travel was measured, not the displacement of the body. This means that for a given tool displacement, the actual penetration of the tool into the IVD was less. The cadaveric torso was intentionally allowed to move slightly within its jig to replicate the compression or movement a surgeon may experience during surgery. This setup introduced more variability into the study, as the specific orientation and support of the sample will have an impact on the test. This restricted the applicability of the study to determine material properties of the IVD but was necessary to replicate surgical conditions. This is why the peak and resistance values for both force and torque were used, as well as the aggregated subcomponents of each as shown in Equation 4.1 and previous work [23]. Another limitation was the impact of IVD height on beginning the discectomy. Both versions of the Concorde Clear were inserted 5 mm into the disc space before beginning the linear or torsional tests, meaning that the difficulty of entering the IVD before removing tissue was not measured. Because all data were normalized at 5 mm penetration for the linear test, differences in this initial force to penetrate the IVD, which may be more difficult for short IVDs, were not considered. Similarly, the torsional tests were only normalized at the beginning of the cyclical testing and the act of normalizing these data for each loading cycle for each pass and direction could have affected the results. Using more samples could have prevent wear and tissue destruction from impacting the results when performing multiple tests on the same IVD, however, this is why the total sum of forces was considered in the study. Finally, the assumptions used here, of a 7% JND, were based on existing work. However, studies have also found that providing feedback, training, and frequency changes can have an impact on JND [30]. Additionally, visual feedback has also been shown to impact user JND [50]. It is possible that surgeons, through their extensive training, have developed greater sensitivity. This could be tested in the future in a manner comparable to previous work that found surgeon forces differed based on experience level [51].

The force and torque profiles shown here can be used to inform a haptic robot to give feedback to a user or future tool design. Operator speed, number of passes, and patient differences should be considered when determining appropriate force and torque output. Lumbar level and tool depth should additionally be considered for proper torque output. By making these adjustments before and during the procedure, a simulator can be created to accurately mimic an MI LIF discectomy.

4.2.2 Conclusions and Future Work

This work presents the first biomechanical study of MI discectomy using the Concorde Clear. A framework is provided for the measured force and torque, how they vary over time and between multiple conditions. Improvements in these measurements could be made by quantifying the amount of tissue removed and correlating it to the measured mechanics. This would enable better modeling for the force output by allowing the simulator to respond to tissue removal as the user proceeds through a procedure. Following simulator development, studies must be performed with surgeons to evaluate how experts perceive the mechanics that have been measured and subsequently integrated. Perhaps surgeon JND differs from that of the normal population and therefore the simulator must be sensitive to minute differences between tissues in the procedure. This would validate the study results by showing how effective these data are in a simulator that is both biomechanically accurate and relevant for training. Overall, this study provides a better understanding of the force and torque encountered by a surgeon using a tool, such as the Concorde Clear, during a lumbar discectomy, and how these measures can be applied in a simulated environment.

4.2.1 Acknowledgment

The authors would like to thank Dr. Rodrigo Navarro-Ramirez, who helped with cadaveric preparation, dissection, and test method setup. Funding and guidance were provided by CAE Healthcare, Inc. (Montreal, Canada) and DePuy Synthes. Testing was performed at Laboratoire de Recherche en Imagerie et Orthopedie division de l'Hôpital du Sacré-Coeur de Montréal under Prof. Yvan Petit and Prof. Eric Wagnac, with assistance from Ms. Elisabeth Laroche. Dr. Khaled El-Monajjed and Ms. Sneha Patel also assisted in the test design and execution.

4.2.1 Additional Information

The work was supported in part by the Natural Sciences and Engineering Research Center (NSERC), the Quebec Consortium for Industrial Research and Innovation in Medical Technology (MEDTEQ), DePuy Synthes, CAE Healthcare, Inc., and McGill University under Grant CRDPJ 515768-17.

4.2.2 References

1. Sweet RM (2017) The CREST Simulation Development Process: Training the Next Generation. Journal of Endourology 31:S69–S75. https://doi.org/10.1089/end.2016.0613

2. Ruikar DD, Hegadi RS, Santosh KC (2018) A Systematic Review on Orthopedic Simulators for Psycho-Motor Skill and Surgical Procedure Training. Journal of Medical Systems 42:168: 1–21. https://doi.org/10.1007/s10916-018-1019-1

3. Cooper JB, Taqueti VR (2004) A brief history of the development of mannequin simulators for clinical education and training. Quality & Safety In Health Care 13:i11–i18. https://doi.org/10.1136/qshc.2004.009886

4. Go TH, Bürki-Cohen J, Soja NN (2000) The Effect of Simulator Motion on Pilot Training and Evaluation

5. Casutt G, Theill N, Martin M, et al (2014) The drive-wise project: Driving simulator training increases real driving performance in healthy older drivers. Frontiers in Aging Neuroscience 6:86: 1–14. https://doi.org/10.3389/fnagi.2014.00085

6. Alotaibi F, Del Maestro R, AlZhrani G, et al (2015) Utilizing NeuroTouch, a virtual reality simulator, to assess and monitor bimanual performance during brain tumor resection. Canadian Journal of Neurological Sciences / Journal Canadien des Sciences Neurologiques 42:S20. https://doi.org/10.1017/cjn.2015.108

7. Alotaibi FE, AlZhrani GA, Mullah MAS, et al (2015) Assessing Bimanual Performance in Brain Tumor Resection With NeuroTouch, a Virtual Reality Simulator. Neurosurgery 11:89–98. https://doi.org/10.1227/NEU.0000000000000631

8. Winkler-Schwartz A, Yilmaz R, Mirchi N, et al (2019) Machine Learning Identification of Surgical and Operative Factors Associated With Surgical Expertise in Virtual Reality Simulation. JAMA Network Open 2:e198363, 1–16. https://doi.org/10.1001/jamanetworkopen.2019.8363

9. Nikolaidis N, Marras I, Mikrogeorgis G, et al (2008) Virtual Dental Patient: A 3D Oral Cavity Model and its Use in Haptics-Based Virtual Reality Cavity Preparation in Endodontics. Dental Computing and Applications: Advanced Techniques for Clinical Dentistry 317–336. https://doi.org/10.4018/978-1-60566-292-3.ch018

10. Klein S, Whyne CM, Rush R, Ginsberg HJ (2009) CT-based Patient-specific Simulation Software for Pedicle Screw Insertion. Journal of Spinal Disorders and Techniques 22:502–506. https://doi.org/10.1097/BSD.0b013e31819877fd

11. Akhtar KSN, Chen A, Standfield NJ, Gupte CM (2014) The role of simulation in developing surgical skills. Current Reviews in Musculoskeletal Medicine 7:155–160. https://doi.org/10.1007/s12178-014-9209-z

12. Torkington J, Smith SGT, Rees BI, Darzi A (2000) The role of simulation in surgical training. Annals of the Royal College of Surgeons of England 82:88–94

13. Kurashima Y, Feldman L, Al-Sabah S, et al (2011) A Novel Low-Cost Simulator for Laparoscopic Inguinal Hernia Repair. Surgical Innovation 18:171–175. https://doi.org/10.1177/1553350610395949

14. Delorme S, Laroche D, Diraddo R, F. Del Maestro R (2012) NeuroTouch: A Physics-Based Virtual Simulator for Cranial Microneurosurgery Training. Neurosurgery 71:32–42. https://doi.org/10.1227/NEU.0b013e318249c744

15. Wang Q, Qin J, Wang W, et al (2015) Haptic Rendering of Drilling Process in Orthopedic Surgical Simulation Based on the Volumetric Object. In: Proceedings of the International Conference on Digital Signal Processing, DSP. Institute of Electrical and Electronics Engineers Inc., pp 1098–1101

16. Fuerst D, Hollensteiner M, Schrempf A (2015) Assessment Parameters for a Novel Simulator in Minimally Invasive Spine Surgery. In: Proceedings of the Annual International Conference of the IEEE Engineering in Medicine and Biology Society, EMBS. pp 5110–5113

17. Carfango J (2019) How Osso VR is Reshaping the Surgical Training Process - Docwire News. In: DocWire News. https://www.docwirenews.com/docwire-pick/future-of-medicine-picks/how-osso-vr-is-reshaping-the-surgical-training-process/. Accessed 10 Aug 2021

18. Luciano CJ, Banerjee PP, Sorenson JM, et al (2013) Percutaneous Spinal Fixation Simulation With Virtual Reality and Haptics. Neurosurgery 72:89–96. https://doi.org/10.1227/NEU.0b013e3182750a8d

19. Instron Modulus of Elasticity. https://www.instron.com/en/our-company/library/glossary/m/modulus-of-elasticity. Accessed 11 Aug 2021

20. Ben-Ur Z, Mijiritsky E, Gorfil C, Brosh T (1999) Stiffness of different designs and cross-sections of maxillary and mandibular major connectors of removable partial dentures. The Journal of Prosthetic Dentistry 81:526–532. https://doi.org/10.1016/S0022-3913(99)70206-4

21. Arruda EM, Boyce MC (1993) A Three-Dimensional Constitutive Model for the Large Stretch Behavior of Rubber Elastic Materials. Journal of the Mechanics and Physics of Solids 41:389–412. https://doi.org/10.1016/0022-5096(93)90013-6

22. Cardenas RJ, Javalkar V, Patil S, et al (2010) Comparison of Allograft Bone and Titanium Cages for Vertebral Body Replacement in the Thoracolumbar Spine: A Biomechanical Study. Neurosurgery 66:314–318. https://doi.org/10.1227/01.NEU.0000370200.74098.CC

23. Okamura AM, Simone C, O'Leary MD (2004) Force Modeling for Needle Insertion Into Soft Tissue. IEEE Transactions on Biomedical Engineering 51:1707–1716. https://doi.org/10.1109/TBME.2004.831542

24. Penfield W, Boldrey E (1937) Somatic Motor and Sensory Representation in the Cerebral Cortex of Mman as Studied by Electrical Stimulation. Brain 60:389–443. https://doi.org/10.1093/brain/60.4.389

25. Kopta JA (1971) The Development of Motor Skills in Orthopaedic Education. Clinical Orthopaedics and Related Research 75:80–85. https://doi.org/10.1097/00003086-197103000-00011

26. Sadideen H, Alvand A, Saadeddin M, Kneebone R (2013) Surgical experts: Born or made? International Journal of Surgery 11:773–778. https://doi.org/10.1016/j.ijsu.2013.07.001

27. Pang XD, Tan HZ, Durlach NI (1991) Manual discrimination of force using active finger motion. Perception & Psychophysics 49:531–540. https://doi.org/10.3758/BF03212187

28. Allin S, Matsuoka Y, Klatzky R (2002) Measuring Just Noticeable Differences For Haptic Force Feedback: Implications for Rehabilitation. In: Proceedings of the 10th Symposium on Haptic Interfaces for Virtual Environment and Teleoperator Systems, HAPTICS 2002. Orlando, US, pp 299–302

29. Zoeller AC, Drewing K (2020) A Systematic Comparison of Perceptual Performance in Softness Discrimination with Different Fingers. Attention, Perception, and Psychophysics 82:3696–3709. https://doi.org/10.3758/s13414-020-02100-4

30. Omrani M, Lak A, Diamond ME (2013) Learning not to feel: reshaping the resolution of tactile perception. Frontiers in Systems Neuroscience 7:29: 1–13. https://doi.org/10.3389/fnsys.2013.00029

31. Vicentini M, Botturi D (2010) Perceptual Issues Improve Haptic Systems Performance. In: Zadeh MH (ed) Advances in Haptics. InTech, pp 415–438

32. Corey DL, Comeau D (2014) Cervical Radiculopathy. The Medical Clinics of North America 98:791–799. https://doi.org/10.1055/a-0575-7066

33. Edelson JG, Nathan H (1986) Nerve Root Compression in Spondylolysis and Spondylolisthesis. The Journal of Bone and Joint Surgery 68:596–599

34. Takahashi K, Shima I, Porter RW (1999) Nerve Root Pressure in Lumbar Disc Herniation. Spine 24:2003–2006. https://doi.org/10.1097/00007632-199910010-00007

35. Rubin DI (2007) Epidemiology and Risk Factors for Spine Pain. Neurologic Clinics 25:353–371. https://doi.org/10.1016/j.ncl.2007.01.004

36. Hoy D, March L, Brooks P, et al (2014) The global burden of low back pain: Estimates from the Global Burden of Disease 2010 study. Annals of the Rheumatic Diseases 73:968–974. https://doi.org/10.1136/annrheumdis-2013-204428

37. Mobbs RJ, Phan K, Malham G, et al (2015) Lumbar Interbody Fusion: Techniques, Indications and Comparison of Interbody Fusion Options Including PLIF, TLIF, MI-TLIF, OLIF/ATP, LLIF and ALIF. Journal of Spine Surgery 1:2–18. https://doi.org/10.3978/j.issn.2414-469X.2015.10.05

38. Mobbs RJ, Sivabalan P, Li J, et al (2013) Hybrid Technique for Posterior Lumbar Interbody Fusion: A Combination of Open Decompression and Percutaneous Pedicle Screw Fixation. Orthopaedic surgery 5:135–141. https://doi.org/10.1111/os.12042

39. Regan JJ, Yuan H, McAfee PC (1999) Laparoscopic Fusion of the Lumbar Spine: Minimally Invasive Spine Surgery: A Prospective Multicenter Study Evaluating Open and Laparoscopic Lumbar Fusion. Spine 24:402–411. https://doi.org/10.1097/00007632-199902150-00023

40. Mo F, Yuan P, Araghi A, Serhan H (2018) Time Savings and Related Economic Benefits of Suction-Curette Device for Transforaminal Lumbar Interbody Fusion Discectomy. International Journal of Spine Surgery 12:582–586. https://doi.org/10.14444/5071

41. Patwardhan AG, Havey RM, Meade KP, et al (1999) A Follower Load Increases the Load-Carrying Capacity of the Lumbar Spine in Compression. Spine 24:1003–1009. https://doi.org/10.1097/00007632-199905150-00014

42. Shan Z, Li S, Liu J, et al (2015) Correlation between biomechanical properties of the annulus fibrosus and magnetic resonance imaging (MRI) findings. European Spine Journal 24:1909–1916. https://doi.org/10.1007/s00586-015-4061-4

43. Hirsch C, Nachemson A (1954) New Observations on the Mechanical Behavior of Lumbar Discs. Acta Orthopaedica Scandinavica 23:254–283. https://doi.org/10.3109/17453675408991217

44. La Barbera L, Wilke HJ, Ruspi ML, et al (2021) Load-sharing biomechanics of lumbar fixation and fusion with pedicle subtraction osteotomy. Scientific Reports 11:3595: 1–13. https://doi.org/10.1038/s41598-021-83251-8

45. El-Monajjed K, Driscoll M (2021) Analysis of Surgical Forces Required to Gain Access Using a Probe for Minimally Invasive Spine Surgery via Cadaveric-Based Experiments towards Use in Training Simulators. IEEE Transactions on Biomedical Engineering 68:330–339. https://doi.org/10.1109/TBME.2020.2996980

46. Mann HB, Whitney DR (1947) On a Test of Whether one of Two Random Variables is Stochastically Larger than the Other. The Annals of Mathematical Statistics 18:50–60. https://doi.org/10.1214/aoms/1177730491

47. Kruskal WH, Wallis WA (1952) Use of Ranks in One-Criterion Variance Analysis. Journal of the American Statistical Association 47:583–621. https://doi.org/10.1080/01621459.1952.10483441

48. Gibbons JD, Chakraborti S (2003) Spearman's Coefficient of Rank Correlation. In: Dekker M (ed) Nonparametric Statistical Inference, 4th ed. pp 422–432

49. BenSaïda A (2021) Shapiro-Wilk and Shapiro-Francia normality tests. In: MATLAB Central File Exchange. https://www.mathworks.com/matlabcentral/fileexchange/13964-shapiro-wilk-and-shapiro-francia-normality-tests. Accessed 11 Aug 2021

50. Matsuoka Y, Brewer BR, Klatzky RL (2007) Using visual feedback distortion to alter coordinated pinching patterns for robotic rehabilitation. Journal of NeuroEngineering and Rehabilitation 4:17: 1–9. https://doi.org/10.1186/1743-0003-4-17

51. Ledwos N, Mirchi N, Bissonnette V, et al (2021) Virtual Reality Anterior Cervical Discectomy and Fusion Simulation on the Novel Sim-Ortho Platform: Validation Studies. Operative Neurosurgery 20:74–82. https://doi.org/10.1093/ons/opaa269

4.2.1 Author Contributions

The contribution of the first author was 75%, which included test design and execution, analysis, and writing. The second and third authors contributed 10% and 15%, respectively, for research guidance and review.

4.2.2 Author Biography

Trevor Cotter is a PhD candidate in Mechanical Engineering at McGill University in Montreal. He received his MS in Applied Physics from Northern Arizona University and his BS in Biomedical Engineering from the University of Minnesota Twin Cities. His doctoral work centers around the development of a physics-based augmented reality spine surgical simulator that gives visual and haptic feedback to train surgeons. He is passionate about bringing together multidisciplinary and translational teams to develop solutions using concepts from design, engineering, and medicine.

Rosaire Mongrain is a professor and Chair of the Department of Mechanical Engineering at McGill University, as well as an NSERC Chair in Design Engineering for Interdisciplinary Innovation of Medical Technologies. His research interests include blood flow modeling in circulatory pathologies (stenoses, aneurysms) and the influence of the flow on these diseases, the study of the mechanical properties of vascular tissues (vascular wall and arterial plaques, erythrocytes membrane), the design, development and evaluation of cardiovascular devices (heart pumps, heart valves, stents, catheters) using numerical, experimental and animal models and image processing for medical diagnosis (motion analysis, tissue characterization).

Mark Driscoll is an assistant professor in Mechanical Engineering at McGill University. His global focus is improving the biomechanical understanding of the spine to enhance diagnostic and treatment methods associated with spinal disorders. His fundamental research focuses on the progression of back pain. He is researching new notions of how fascia, intra-muscular and intra-abdominal pressure play a role in spinal stability, from an engineering perspective, and is also looking into the role of physiological stress shielding in spinal disorders. His applied research involves developing and validating a novel home diagnostic device to assist in an objective physical assessment of back pain patients via the non-invasive measure of tissue modulus and their muscular and abdominal pressures. At the other end of the back pain treatment spectrum for the surgical treatment of spinal disorders, he is developing a physics-based augmented reality spine surgical simulator with visual, audible, and haptic feedback.

4.3 Additional Studies

More investigations were performed as well as those presented in Article 3: Comparing Controlled and Freehand Test Techniques of Lumbar Discectomy Force Measurement for Spinal Surgery Simulation. These include more comparisons to those already shown, as well as entirely new methods of analysis. Crucially, this also includes the final force and torque models programmed in the simulator, as well as surgeon feedback.

4.3.1 Additional Peak and Resistance Comparisons

The work shown in Article 3: Comparing Controlled and Freehand Test Techniques of Lumbar Discectomy Force Measurement for Spinal Surgery Simulation did not discuss comparisons between cadaver sides. This was investigated as a subset of the dataset in the article to see if the cadavers differed from the left or right (L/R) approaches as shown in Figure 4.6 and Table 4.4. Notably, one cadaver (C2) did have very mild lumbar scoliosis (left concavity of 10° Cobb angle between L2 and L4), as noted in Table 4.1 [148]. Statistically significant differences between L/R were not present for the linear insertion data but were apparent in torsion when considering all lumbar IVDs of both cadavers. Additionally, comparisons were made between the first and second sides (S1/S2) of the cadavers. S1 would refer to the first side tested, and S2 would refer to the second side tested. This was done to see if the tests may have damaged tissue or otherwise had an effect on the opposite side of the IVD. The side (L/R) that was tested first was alternated between cadavers. Interestingly, only the torque peak values exhibited statistically significant differences between sides S1/S2, whereas all the other comparisons did not, as shown in Figure 4.6 and Table 4.4. This indicates that tests could be performed on a given IVD from multiple sides. All statistically significant differences were once again of a magnitude detectable to a surgeon.

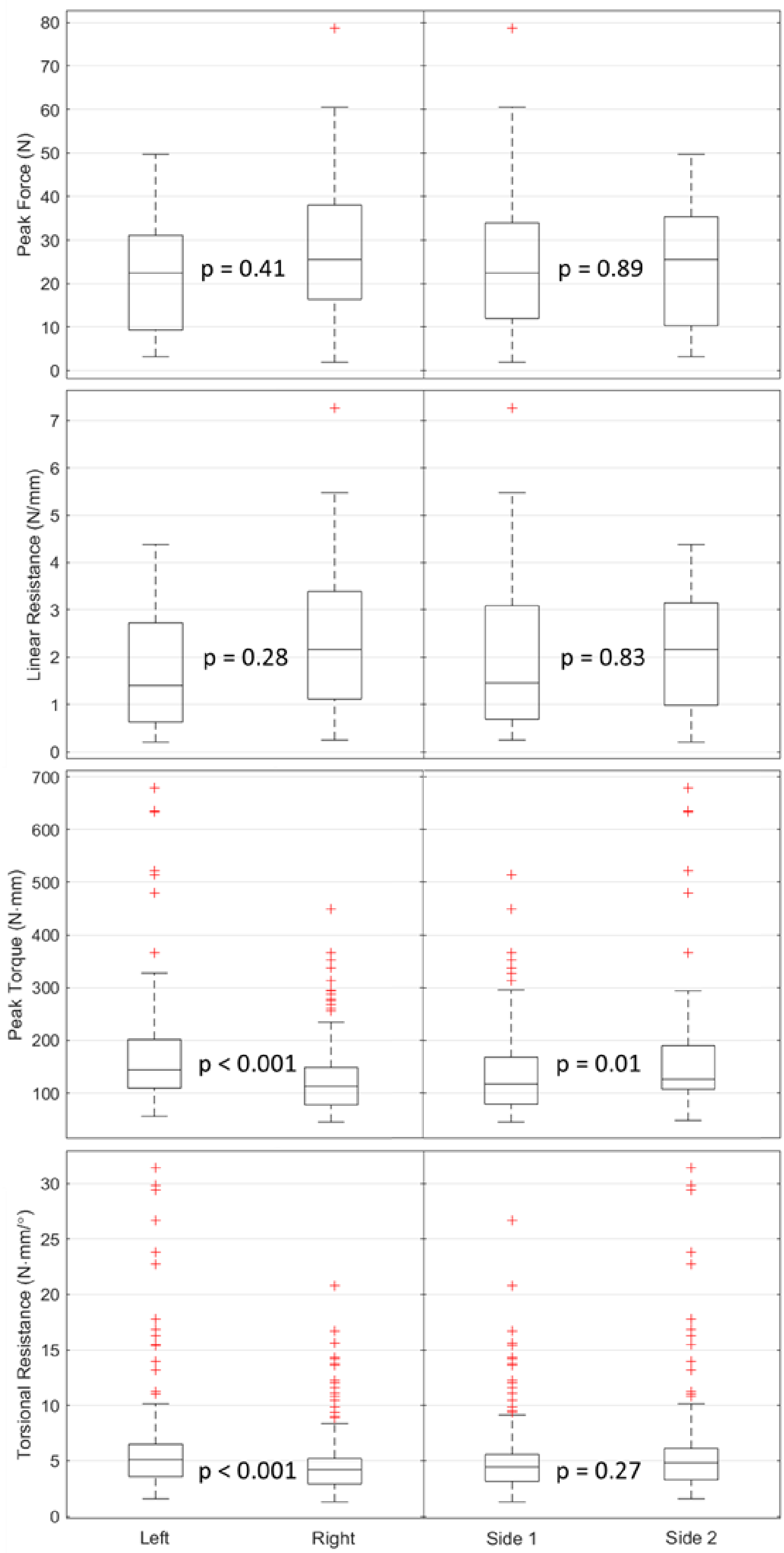

Figure 4.6: Force and torque peak and resistance comparisons between left and right sides of the cadavers, as well as the first and second sides tested.

Table 4.4: Statistical comparisons of cadaver testing left and right sides as well as first and second sides. The p-values are shown.

	Comparison	Force Peak		Linear Resistance	
		Left vs Right	Side 1 vs Side 2	Left vs Right	Side 1 vs Side 2
Linear Tests	All Passes	4.15E-01	8.93E-01	2.79E-01	8.29E-01
	Pass 1	-	-	-	-
	Pass 2-3	3.96E-01	9.85E-01	2.21E-01	8.95E-01
	Comparison	Torque Peak		Torsional Resistance	
		Left vs Right	Side 1 vs Side 2	Left vs Right	Side 1 vs Side 2
Torsional Tests	All Passes	***2.32E-07***	***1.50E-02***	***1.89E-05***	2.73E-01
	Pass 1	***2.45E-02***	3.51E-01	2.51E-01	6.53E-01
	Pass 2-5	***2.00E-06***	***2.07E-02***	***5.44E-06***	3.41E-01

All bolded, italicized values have significance $p \leq 0.05$ according to Mann-Whitney U Test

All significant values exceed the JND threshold of 7%

The collapsed L_4L_5 IVD in C2, as noted in Table 4.1, also could have affected the data, but excluding it for the force calculations resulted in few to the statistically significant differences outlined. Only the difference in force between C1/C2 for all tool passes became significant. The impact of the collapsed disc when comparing only C1/C2 for all tool passes shows the forces are relatively independent of IVD height. This could be due to the fact that once the Concorde Clear tool has already penetrated the IVD, as was done in these tests, the adjacent vertebrae are sufficiently spread apart to not impinge on the tool movement.

4.3.2 Analysis Limitations and Errors

A key factor in the linear and torsional resistance values reported is the quality of fit. A key assumption used throughout was that the total force and torque, as described in Equation 2.6, were considered for all tests. This did not capture the differences between initial passes with a cutting force and later passes without it. That is why the presented table comparisons in this chapter shows three different groups: All Data, Pass 1 Only, and Pass 2-3 (or 2-5 in the case of the torsional tests). These comparisons show how that cutting force and torque, while assumed to be present in all data, may have impacted the results. Linear fitting was used because it could capture much of the data while being simple to compare the slope as a resistance. While it does not necessarily describe each small change in force or torque, the linear approximation does reproduce the total data set. The testing reported had $R^2 = 0.796 \pm 0.213$ for the linear resistance results and $R^2 = 0.986 \pm 0.021$ for the torsional resistance results. However, to further improve this fit it was important to expand beyond the linear model to higher-order models, which was done for the simulator output and is discussed later.

The data shown used a single force and torque load cell to capture data, but it may have missed some aspects of the biomechanical response. After inserting the tool into the annulotomy, the contributions of individual anatomical components, such as the nucleus pulposus and annulus fibrosus, were not considered and the IVD was tested as a whole. This was done to simplify integration into the simulator haptics. Distinguishing these components would likely result in lower resistances when testing the nucleus pulposus and higher resistances when interacting with the annulus fibrosus [2]. Off-axis forces, or those that did not occur on the force and torque axes of the load cell, may have been present. Loads due to the tool catching on angled rigid tissues were minimized by rotation during all tests, but these forces may still have contributed significantly to the measured response. This is discussed further in Chapter 5. Using one tool per test type per cadaver, when the original Concorde Clear is intended to be a single-use tool, may have also impacted how the tool interacted with tissue as it dulled or acquired other wear during testing. Additionally, Coriolis forces were ignored due to the low tool speed and mass.

The impact of IVD height, a large source of expected variability in the patient population, was observed to have no impact on force and torque as shown in Figure 4.4. It is possible that other physiological conditions, such as herniation or tissue hydration, could impact the measured force and torque and therefore future studies should consider a wider range of potential conditions and variables in their study design to isolate the impact of each of these conditions.

Of further interest was torso deflection during testing. The motion of the cadaver, while essential in replicating real-world surgical conditions, nonetheless limits the data usefulness outside of this application. To analyze this, a study was conducted to measure the amount of displacement present at a given applied static force. C2 was thawed and supported at a similar angle as in the testing outlined earlier in 4.2.3.2 Testing Setup. A Shimpo (Nidec-Shimpo Corporation; Kyoto Japan) MF-20 mechanical force gauge was pressed onto a vertebral body while the displacement of the body was measured with a dial gauge as shown in Figure 4.7. The L_2 and L_4 vertebrae were tested, and the results are in Figure 4.8. Notably, this cadaver had already undergone extensive testing, including the testing outlined, as well as bone graft and intervertebral cage insertion. As a result, the visible side of L_2L_3 IVD was destroyed, meaning that the L_2 tests were likely the highest-deflection scenario possible. Similarly, the L_4L_5 IVD remained collapsed with little articulation, so the L_4 tests represent the lowest-deflection scenario. The average of the two data sets indicates that a compensation of 0.1 mm/N + 0.9 mm could be used to account for the error introduced by cadaveric deflection in the testing. This was implemented by scaling the measured tool movement for a given torque measurement in Chapter 5. However, this was found to be highly dependent on specific cadaveric torso angle and support. The relaxation deflection, also shown in Figure 4.8, measured the deflection in L_2 after the load was released. This was found to be very small for all applied loads. This deflection study was a noteworthy addition to the testing described earlier, however, it was not used to modify or reinterpret the tool penetration stated in the comparisons presented so far because the body deflection is present during a normal surgical procedure and therefore must be accounted for in the simulator.

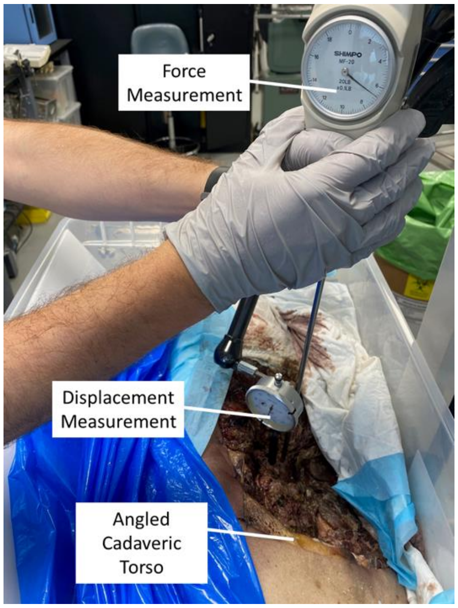

Figure 4.7: Setup for the cadaver deflection study.

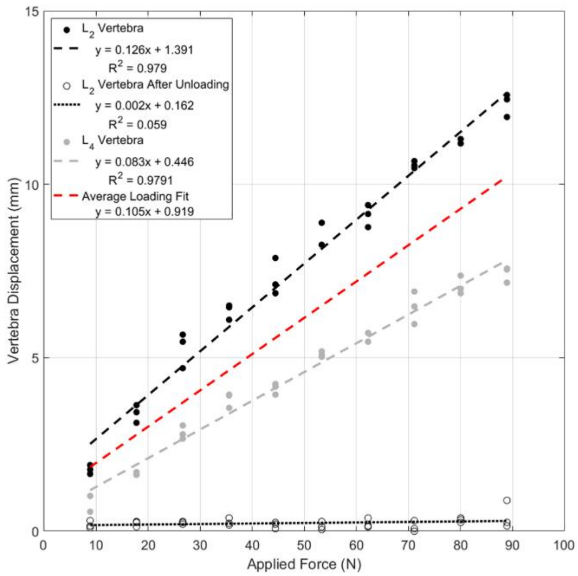

Figure 4.8: Cadaver deflection study results. The displacement after unloading was measured to ensure there was minimal cadaveric movement between tests.

4.3.3 Haptic Torque Handle Design Input

As described in Chapter 3, the haptics used to deliver the torque measured here were revised in multiple design iterations. The cadaveric testing described took place after the initial high torque (HT) design, as presented in Article 1: Design Synthesis of a Robotic Uniaxial Torque Device for Orthopedic Haptic Simulation, met the initial 3000 N·mm torque requirement. After discussions with a neurosurgical spine fellow, a ±20° range of motion was determined to be appropriate for normal use during surgery. Preliminary analysis at ±20° gave a torque of 800 N·mm. After collecting data from both cadavers, the peak torque during loading at ±20° occurred between the range [45, 680] N·mm, with an average of 150±90 N·mm. This confirmed that designing the low torque (LT) configuration with a peak torque capability 830 N·mm was appropriate to deliver the measured torque.

4.3.4 Energy Loss

Chapter 2discussed the nonlinear properties of biological tissues, including their viscoelasticity. This results in hysteresis during loading and unloading, displaying energy lost during movement. By fitting the data with an ellipse, the energy lost through heat and internal friction can be calculated from the area of the ellipse [62]. A study was conducted to see how this energy loss in torsion differed among testing conditions, similar to the linear and torsional comparisons made. This could shine a light on viscoelastic differences between samples not captured in the torque peak and torsional resistance comparisons. To start, a full testing cycle is shown in Figure 4.9a. This cycle was broken into positive and negative sections, representing each direction of torsion, one towards each vertebra. Then an elliptical fit was performed on the resulting data as seen in Figure 4.9b. This was done for comparisons C1/C2, L/R, 5/20 mm, $L_1L_2/L_2L_3/L_3L_4/L_4L_5$, and 2/3/4/6/8°/s. The comparisons can be seen in Figure 4.10, with the statistical results shown in

Table 4.5. Interestingly, statistically significant differences were seen for all cases except for the speed tests. This could be because these were the final tests performed and there may have been sufficient destructive testing performed earlier that torsion was interacting with less tissue. This tissue loss hypothesis is supported by the data in Table 4.3 showing that there is a difference in peak torque and torsional resistance between subsequent passes.

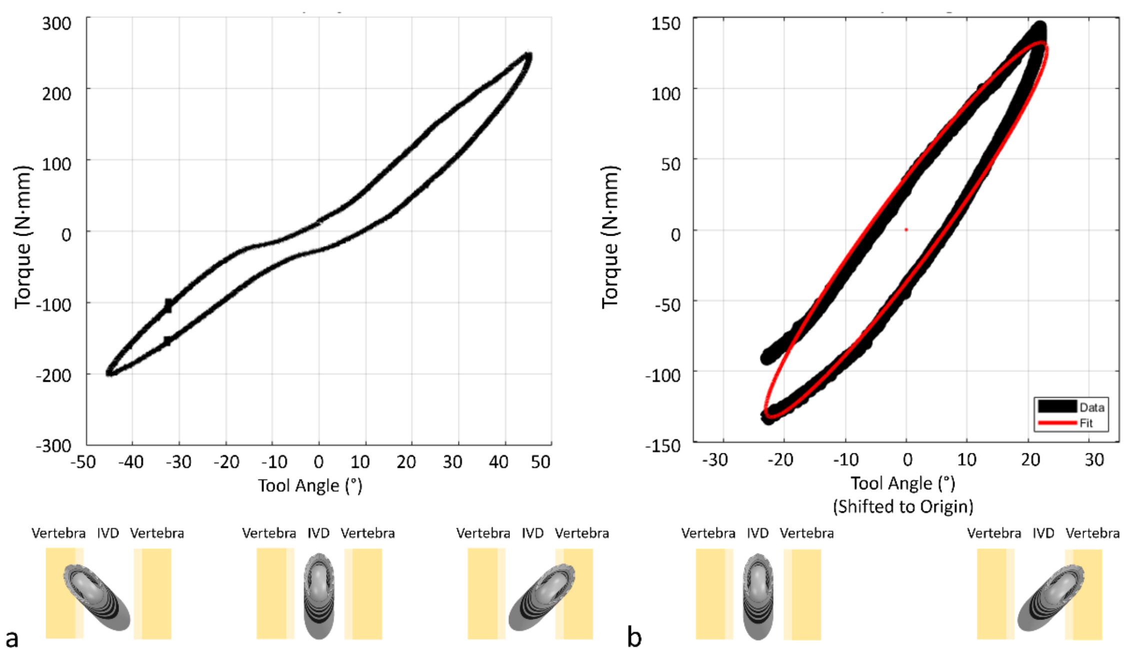

Figure 4.9: a) schematic of tool movement during testing and b) the ellipse fitting of a single cycle.

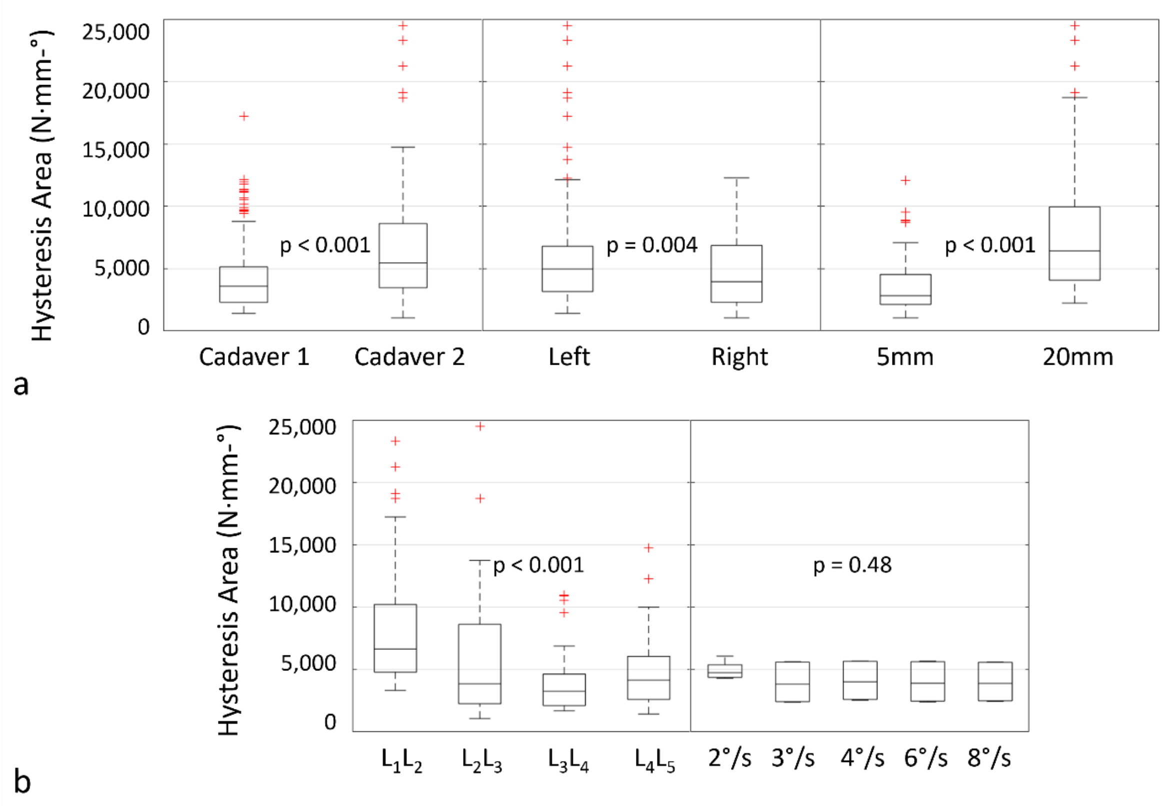

Figure 4.10: Boxplots of energy loss for multiple comparisons during torsional testing. a) shows comparisons among cadavers, sides, and penetration depths, while b) compares lumbar levels and tools speeds.

Table 4.5: Statistical comparisons of energy loss during torsion.

	Hysteresis Area				
	Cadaver 1 vs 2	Left vs Right	Tool Depth	Lumbar Level	Tool Speed
p-value	***7.14E-07***	***4.68E-03***	***4.89E-25***	***2.72E-13***	4.83E-01
Test Method	Mann-Whitney U			Kruskal-Wallis	

All bolded, italicized values have significance $p \leq 0.05$

4.3.5 Simulator Force and Torque Profiles

The linear fit data presented have been used to characterize discectomy with the Concorde Clear tool and compare cadaveric, lumbar level, and other differences. However, more advanced mathematical models were used in the final simulator. The models were chosen to accommodate the gameplay environment as well as haptic device capabilities. For example, Figure 4.11 shows the range of data present during tests on one cadaver. The maximum, normal, and minimum force profiles are shown, as well as an example quadratic fit that remains within the safe operating range of the Entact W3D haptic device. The "Benchtop Forces" label indicates that the interaction of the distal end of the tool. This illustrates the need for accommodating a wide range of data and limitations when designing the simulator.

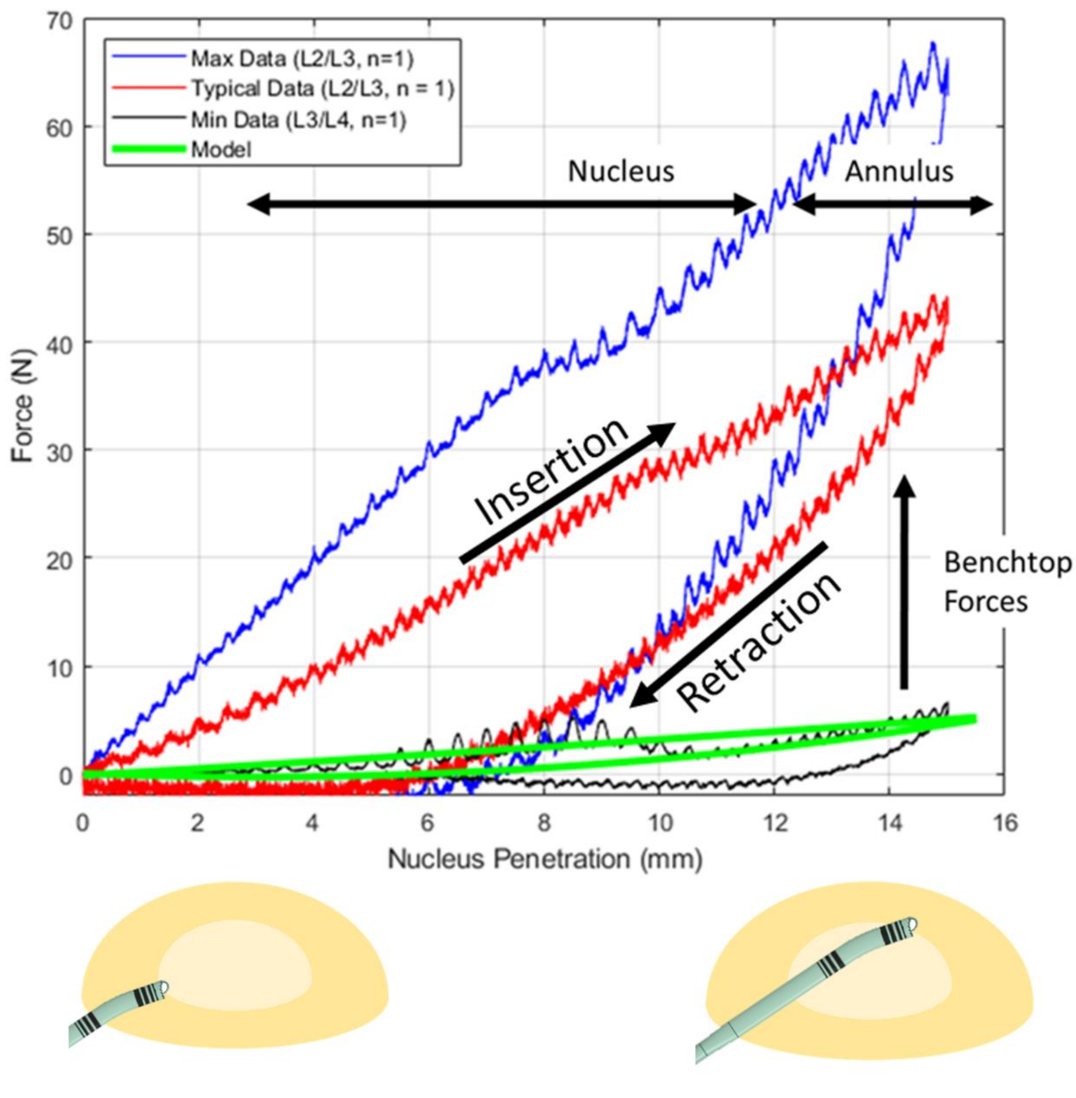

Figure 4.11: Example observed force and model profiles for the simulator.

Data from all tests, aside from speed tests, were averaged to create aggregate force profiles. These were then fit with quadratic functions as seen in Equation 4.2 and Equation 4.3, where d is the tool depth in mm. Linear fits from [0, 0.5] mm ensured stability at the initial penetration depth. This is shown graphically in Figure 4.12, with the same intended physical benchtop interaction forces. To accommodate the effect of tissue removal, an additional factor was added. The user experienced the lower retraction forces at a minimum. Additional force could be added depending on the amount of tissue in contact with the tool, eventually reaching a maximum of the upper insertion force. This ensured that the force felt by the user decreased as tissue was removed. The output of this tissue compensation model is shown in Figure 4.13.

$$F_{Insertion}\begin{cases} 0.49d & 0\ mm \leq d \leq 0.5\ mm \\ -0.01d^2 + 0.67d - 0.09 & 0.5\ mm < d \\ 4\ N & F_{x,y,z} > 4\ N \end{cases}$$

Equation 4.2: Simulator force profile during insertion of the Concorde Clear tool.

$$F_{Retraction}\begin{cases} 0.05d & 0\ mm \leq d \leq 0.5\ mm \\ 0.04d^2 + 0.25d - 0.11 & 0.5\ mm < d \\ 4\ N & F_{x,y,z} > 4\ N \end{cases}$$

Equation 4.3: Simulator force profile during retraction of the Concorde Clear tool.

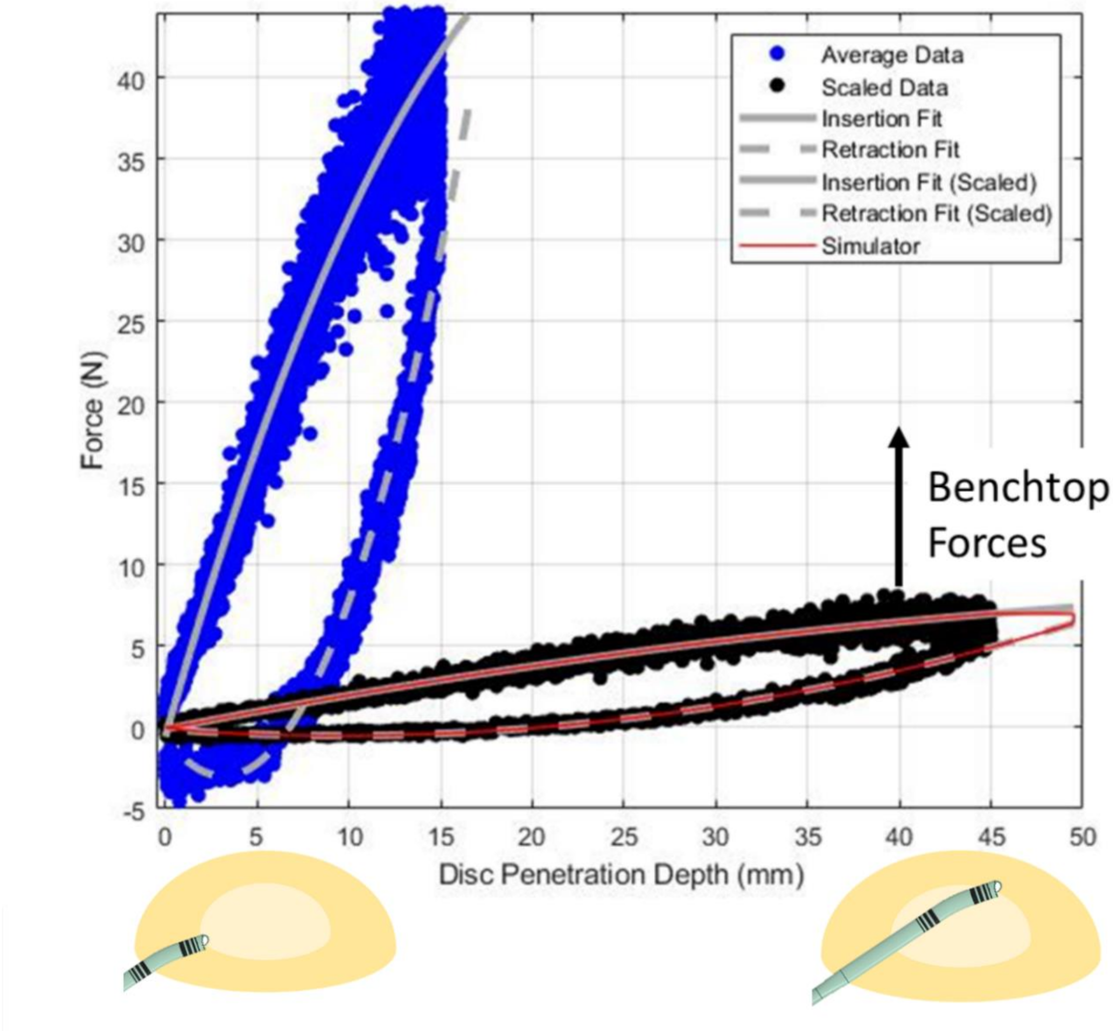

Figure 4.12: Insertion forces and quadratic fits during cadaveric testing. The blue data has been scaled linearly to the black data so that its line of fit matches the capabilities of the haptic device. The red data represents the equations programmed into the simulator.

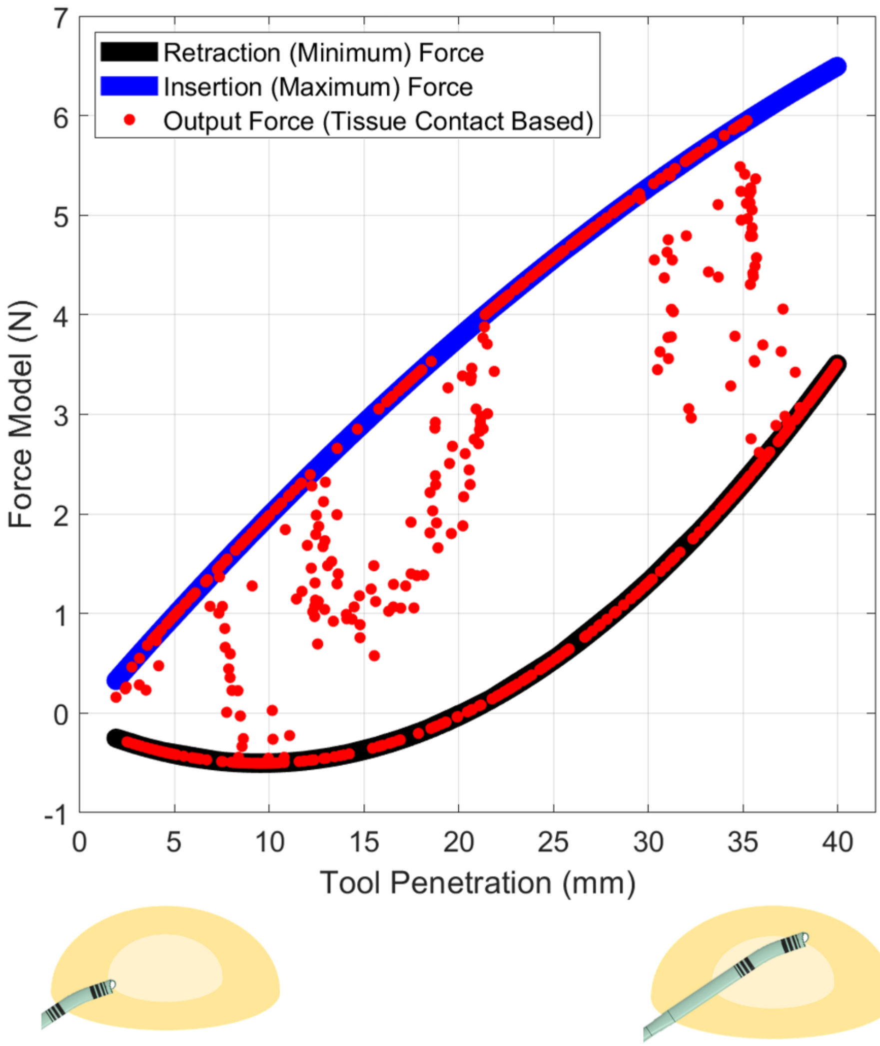

Figure 4.13: Force model with tissue compensation. The minimum retraction and maximum insertion force profiles (Equation 4.2 and Equation 4.3) are shown, as well as the output force based on the number of tissue contacts. This ensures that force decreases as tissue is removed.

Similarly, all torsion tests outside of the speed tests were averaged to create aggregate torque profiles. The quadratic fit functions during loading at multiple depths are shown in Equation 4.4 and Equation 4.5. Unloading functions at the same depths are shown in Equation 4.6 and Equation 4.7, where *a* is the tool angle. These equations were multiplied by a factor of ±1 to give the correct torque direction to push the tool back towards the neutral orientation, a = 0°. The direction, loading or unloading, was determined by the sign of the velocity of the tool. Linear fits from [-5, 5]° ensured stability about 0°, where the torque changed direction. An example of the fit equations is shown graphically in Figure 4.14. To accommodate the effect of tool depth, an additional factor was added. The 5 mm and 20 mm models were both calculated, and then the current tool depth was used to determine the appropriate torque. For example, torque magnitude at a tool depth between 5 and 20 mm would be between the 5 mm and 20 mm torque model. Similarly, tool depths <5 mm and >20 mm would result in torque magnitudes lower and higher than the 5 mm and 20 mm models, respectively. This is outlined in Figure 4.15.

$$\tau_{Loading,5\ mm\ Penetration}\begin{cases} 8.18a & 0° \le a \le 5° \\ 0.02a^2 + 4.30a + 18.93 & 5° < a \\ 300 & \tau > 300\ N \cdot mm \end{cases}$$

Equation 4.4: Simulator torque profile during loading torsion of the Concorde Clear tool into the intervertebral disc (IVD) at 5 mm penetration. Torque is then applied in the opposite direction to push the tool towards 0°.

$$\tau_{Loading,20\ mm\ Penetration}\begin{cases} 15.24a & 0° \le a \le 5° \\ 0.11a^2 + 4.20a + 52.40 & 5° < a \\ 300 & \tau > 300\ N \cdot mm \end{cases}$$

Equation 4.5: Simulator torque profile during loading torsion of the Concorde Clear tool into the intervertebral disc (IVD) at 20 mm penetration. Torque is then applied in the opposite direction to push the tool towards 0°.

$$\tau_{Unloading,5\ mm\ Penetration}\begin{cases} -1.85a & 0° \le a \le 5° \\ 0.10a^2 + 0.71a - 15.23 & 5° < a \\ 300 & \tau > 300\ N \cdot mm \end{cases}$$

Equation 4.6: Simulator torque profile during unloading torsion of the Concorde Clear tool away from the intervertebral disc (IVD) at 5 mm penetration. Torque is then applied in the opposite direction to push the tool towards 0°.

$$\tau_{Unloading,20\ mm\ Penetration}\begin{cases} -3.96a & 0° \le a \le 5° \\ 0.23a^2 - 1.06a - 20.27 & 5° < a \\ 300 & \tau > 300\ N \cdot mm \end{cases}$$

Equation 4.7: Simulator torque profile during unloading torsion of the Concorde Clear tool away from the intervertebral disc (IVD) at 20mm penetration. Torque is then applied in the opposite direction to push the tool towards 0°.

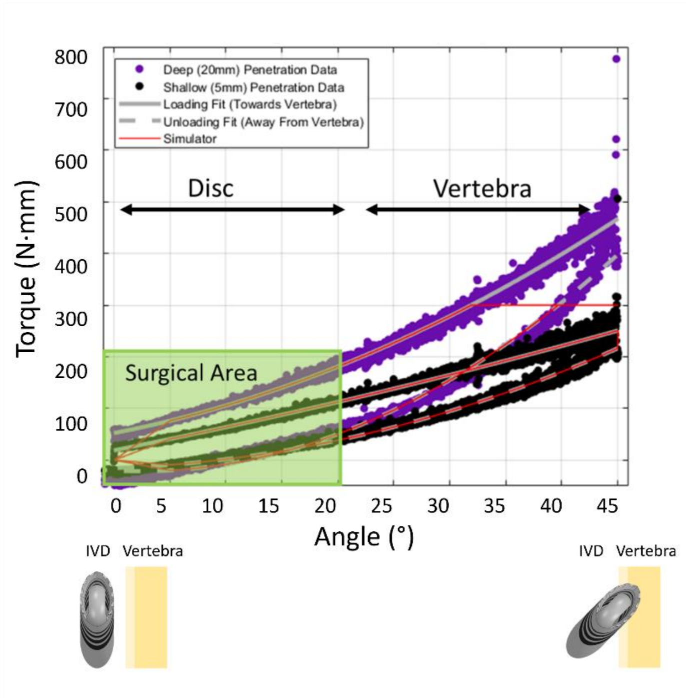

Figure 4.14: Example of the average, fitted, and programmed models of torque simulation. The typical surgical workspace is expected to be in the range of ±20°. Note: the torque orientation implemented is in the opposite direction to oppose motion.

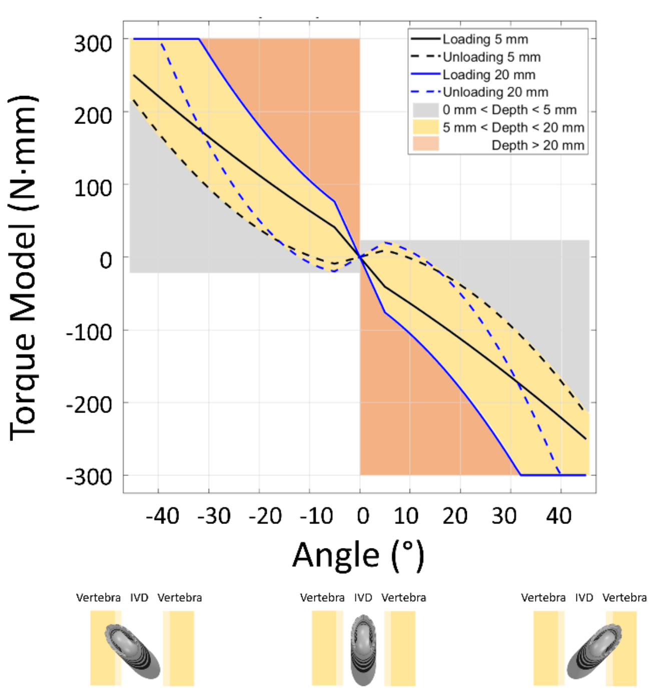

Figure 4.15: Torque model with depth factor. The minimum unloading and maximum loading torque profiles at the two reference depths are shown, as well as the torque modeled at a given tool depth. This ensures that torque magnitude increases as the tool is pushed deeper, as observed in the cadaveric trials.

4.3.6 Surgeon Evaluation

The same 5-point Likert scale survey as in Chapter 3 was used to evaluate surgeon impressions of the force and torque models in the simulator. A response of 1 indicated the simulator did not match the real procedure, and 5 indicated that it matched the procedure well. The seven surgeons who used the simulator directly following cadaveric procedures rated the force and torque present in the simulator to be 2.7±1.1 and 2.6±1.1, respectively. Out of the total 29 surgeons that evaluated the simulator with or without cadaveric procedures before, these responses were 2.8±1.1 and 2.9±1.1. These average values <3 indicate that the force and torque profiles, as implemented, did not accurately represent the procedure. However, the standard deviation range does cover an accurate haptic response. This indicates the testing and modeling used in the simulator may still be valid.

4.4 Conclusion

Cadaveric testing was performed to quantify the force and torque present during lumbar discectomy with the Concorde Clear tool. This data was analyzed to determine which factors were necessary to consider when designing the simulator mechanical models. Two key factors that were used were tissue removal and tool depth in the force and torque output, respectively. The force and torque models were output with the novel tool developed in Chapter 3and validated by surgeons. This work describes the novel characterization and implementation of lumbar discectomy in a surgical simulator.

5

Freehand Tissue Testing

5.1 Context

This chapter examines Objective 3 in order to confirm Hypothesis 3, that freehand and controlled biomechanical testing would yield different results. This work was done to complement the findings of Chapter 4. A novel freehand testing device was designed, built, and evaluated to allow for free range of motion during handheld mechanical testing. This work was necessary to understand how the controlled testing performed with an MTS machine compared to the freedom present during normal surgery. After the device was designed, additional testing was done to quantify the biomechanical differences between specimen types, either cadaveric torsos or spines. This was the first use of this tool, as well as the first published work on freehand testing of the biomechanics of lumbar discectomy. A manuscript is presented, followed by additional work describing other parts of the development of the freehand device. Relevant ethical approvals are contained in Appendix II.

This work was assisted by additional researchers. Advising on the design of the freehand device was received from Ryan Leslie of Entact Robotics. An engineering capstone group consisting of Alex Pieters, Nicholas Pinkerton, Marc-Olivier Van Dorpe, and Zachary Waldman helped design the initial prototype, including most hardware components and specifying the necessary load cell. The position tracking software was developed with CAE Healthcare with assistance from Dr. Clément Forest. The cadaveric testing was executed at the Orthopedic Research Lab with assistance from Lorne Beckman, Emily Newell, and Harriet Chorney. Lorne Beckman acquired spine samples and helped design the testing setup and test software. Dr. Rodrigo Navarro-Ramirez and Dr. Rakan Bokhari performed the freehand testing on the cadaveric spines.

Parts of this work was presented at the 2021 Simulation Summit and 2022 Canadian Spine Society as ePosters titled “Combining Freehand and Controlled Movement for Calculating Surgical Simulator Forces” and “Freehand Biomechanical Testing for Use in Lumbar Discectomy Training,” respectively [146,149]. It was also included in the peer-reviewed abstract publication for this conference. The following manuscript, “Comparing Controlled and Freehand Techniques of Lumbar Discectomy Force Measurement for Spinal Surgery Simulation,” was submitted for publication in Clinical Spine Surgery in February 2022 [150]. The contribution of the first author was 75%, which included mechanical design, testing, analysis, and writing. The second author contributed 15% for research guidance and review.

5.2 Article 3: Comparing Controlled and Freehand Test Techniques of Lumbar Discectomy Force Measurement for Spinal Surgery Simulation

Trevor Cotter[1,2], MS

Mark Driscoll[1,2], P.Eng., PhD

[1]Musculoskeletal Biomechanics Research Lab, Department of Mechanical Engineering, McGill University, Montreal QC H3A 0G4, Canada.

[2]Orthopedic Research Laboratory, Montreal General Hospital, Montreal QC H3H 1V8, Canada.

Correspondence should be addressed to:

Mark Driscoll

McGill University, Department of Mechanical Engineering

817 Sherbrooke Street West, Montreal, QC, H3A 0C3

Macdonald Eng. Bldg. office #153

T: 1.514.398.6299 F: +1.514.398.7365

mark.driscoll@mcgill.ca

Conflict of Interest and Source of Funding

The authors declare that there are no conflicts of interest regarding the publication of this paper.

Financial support for the submitted work came from the Natural Sciences and Engineering Research Center (NSERC), Quebec Consortium for Industrial Research and Innovation in Medical Technology (MEDTEQ), CAE Healthcare Inc., DePuy Synthes Companies, and McGill University (Grant CRDPJ 515768-17).

5.2.1 Structured Abstract

5.2.1.1 Study Design

Cadaveric biomechanical testing

5.2.1.2 Objective

The aim of this work was to compare resistance between traditional linear controlled biomechanical testing and freehand testing that more accurately imitates lumbar discectomy motion, with the hope of designing a haptic surgical simulator for physician training.

5.2.1.3 Summary of Background Data

Tissue testing is conventionally performed on a linear controlled tester. However, a surgeon operates freely and thus forces encountered during lumbar discectomy may differ from those measured in a controlled manner. A novel freehand testing device may accommodate the needs of tissue testing and surgical relevance when measuring forces for implementation in a haptic surgical simulator.

5.2.1.4 Methods

Vacuum curette discectomy was performed on two lumbar spine segments with a freehand device (13 mm/s, ≤24 tests per side) by two neurosurgical fellows. The same spines as well as two cadaveric torsos were tested using a linear controlled testing apparatus (0.25 mm/s, 3 tests per side) for comparison. Position and force along the tool axis (z) were measured, and the linear resistance was compared. The orthogonal forces (x, y) were also measured in the freehand testing.

5.2.1.5 Results

The controlled test resulted in lower (70%, $p < 0.001$) resistance than the freehand test. Spine specimens exhibited similar resistance to torso specimens using the controlled test. X and y

forces accounted for 18-67% of the force, which decreased by 7% per 10 N of force magnitude increase.

5.2.1.6 Conclusions

The freehand testing demonstrates a new data acquisition device for potential use in surgical simulation development that tracks position and has been compared to traditional techniques. This range of motion has a significant impact on linear resistance. As such, it is recommended to use either sample type with freehand testing so simulator haptics more accurately represent surgery.

5.2.2 Level of Evidence

NA

5.2.3 Key Words

Spine, simulation, haptics, training, force feedback, instruments, robotics, biomechanics

5.2.4 Introduction

Due to the extreme risk associated with surgery, the need for adequate surgeon training is evident, and training has been part of medical curricula for centuries.[1] Students learn anatomy and physiology before operating. However, the "see one, do one, teach one" strategy for training has been questioned.[2,3] Preparation for delicate procedures requires extensive practice, and studies show hands-on training is essential to develop appropriate motor skills.[4] New training strategies, such as simulation, could help surgeons acquire relevant abilities before operating.[3,4]

Robotic simulators are used in professional disciplines ranging from airplanes to cars.[5–8] Surgical simulators now have the same level of complex robotics as their non-medical counterparts.[9,10] They have evolved from analog devices to augmented and virtual reality systems coupled to robotic feedback.[8,9,11,12] Haptic, or touch, feedback replaces tissue mechanics experienced during surgery.[13–15] Improving haptics is a key focus are in refining surgical simulator realism.[13,15–17]

Biomechanical testing can inform haptics. Tissue specimens can be dissected to varying degrees before testing, ranging from individual tissues to entire cadavers. While studies have measured mechanical roles of lumbar spine components or the results of discectomy, there is a lack of literature on the necessity of additional tissues when testing the forces encountered during a discectomy.[18–21]

Cutting through tissue is a complex mechanical process that involves multiple forces. In Equation 1, the total force during a needle insertion (f_{needle}) is the sum of tissue deformation ($f_{stiffness}$), friction ($f_{friction}$), and cutting ($f_{cutting}$), which are all dependent on position(x):[22]

$$f_{needle}(x) = f_{stiffness}(x) + f_{friction}(x) + f_{cutting}(x)$$

Equation 5.1

This aggregated force simplifies the biomechanics underpinning the response of tissue during testing. In this manuscript, resistance is the force per distance a tool travels.

Biological specimens are typically tested on a system such as an MTS Bionix (MTS Systems Corporation; Minneapolis, USA).[23–25] Force is applied along an axis to calculate mechanical properties. However, testing becomes more complicated for biological specimens, such as intervertebral discs (IVDs), which have properties dependent on direction. Additionally, studies have modeled the viscoelastic time-dependent response of IVDs and other tissues, which means the speed at which they are tested can impact testing results.[24,26–30] These results could be used to program IVD response, as has been done with other tissues in haptic and visual simulators.[31–33]

However, these studies may not capture the time-dependent mechanical response of an entire cadaveric specimen during loading such as that found during a discectomy procedure.

Despite the popularity of controlled mechanical testing, one key aspect of surgery is missing from many biomechanical characterizations: the flexibility of the surgeon. To capture and recreate the unrestricted surgical environment in a simulator, the entire range of motion and resulting forces must be understood. This could be accomplished with testing devices that allow surgeons to operate freely. To fully characterize the motion, the positions and angular orientations about 3-axes (x, y, and z) can be tracked. Combined, this creates a 6-axis position tracking system. Similarly, a 6-axis load characterization would monitor the forces and torques about the same axes. The combination of these data during a procedure would give a complete understanding of the movement and forces experienced naturally by the surgeon. Freehand testing devices in orthopedic surgery exist, but, to the authors' knowledge, they have not been directly compared to existing test methods to recreate surgical motion in lumbar discectomy.[30,34–36]

This manuscript focuses on the resistive forces surgeons encounter during a discectomy, or IVD removal, during a minimally-invasive lumbar interbody fusion (MI-LIF) with a CONCORDE® Clear vacuum curette (DePuy Synthes; Boston, USA). The hypothesis is that freehand biomechanical tests and traditional controlled tests will yield different resistance measurements ($p < 0.05$) when testing lumbar cadaveric specimens. The intended outcome is to understand how each of these models and methods can be understood within the context of designing a surgical simulator or guide future tool design.

5.2.5 Materials and Methods

5.2.5.1 Test Specimens

Specimens are shown in Table 5.1. Two cadaveric torsos and two lumbar spine segments were acquired with ethical approval (IRB A04-M13-18A). All specimens were fresh-frozen to -20°C and had no history of spinal surgery. X-ray images were used for IVD measurements. The torso specimens were the same as El-Monajjed et. al and thus the measurements and preparation were the same.[29,(37)] Concisely, torsos were thawed for 5 days at 2°C. They were held at room temperature for 72-96 hours before testing to finish thawing, resulting in a single freeze-thaw cycle which should have minimal impact on the IVD mechanical properties.[38] A posterolateral 30x30 cm access through the skin, fascia, and muscle exposed the posterior lumbar spine. Access to the IVD was through a 1x1 cm posterolateral annulotomy, as in a typical MI-LIF procedure. Spine segments were thawed overnight at room temperature. Excess muscles and ligaments were removed to allow the same annulotomy as the torso specimens. Torsos were subjected to controlled tests only, while the spine segments were subjected to controlled and freehand tests (Table 5.1). The test order was reversed between spine segments to provide consistent results. All lumbar IVDs were tested on the left and right sides from each specimen.

Table 5.1: Properties of the cadaveric samples tested.

Cadaveric Specimen Properties						
Cadaver (C#)			C1	C2	C3	C4
Specimen Type			Torso	Torso	Lumbar Spine Only	Lumbar Spine Only
Test Methods (in order)			Controlled	Controlled	Freehand Controlled	Controlled Freehand
Gender			M	M	M	M
Age			63	69	74	71
Height		cm	175	178	175	185
Weight		kg	73	86	64	102
Collapsed Disc			None	L_4L_5	L_5S_1	None
Notes			None	Scoliosis (10° Cobb angle L_2-L_4, concave left)[38]	None	Osteocytes on Peripheral IVD
IVD Height	L_1L_2	mm	10.0	5.2	12.0	10.4
	L_2L_3	mm	10.3	7.6	13.6	9.8
	L_3L_4	mm	11.6	5.7	13.3	10.5
	L_4L_5	mm	10.3	3.1	8.2	10.8

5.2.5.2 Tissue Testing

The torsos (C1 and C2) were put into a custom jig that allowed an MTS 858 Mini-Bionix II tester with a force and torque load cell (model 662.20D-01) to penetrate at approximately 40° lateral to a fully posterior approach. The spines (C3 and C4) were mounted on a different jig and tested on an MTS 858 Mini-Bionix at the same orientation with a different force and torque load cell (model 662.20D-03). Fiberglass rods passed through the lumbar-adjacent vertebra (T_{12} and S_1) to secure them (Figure 5.1a). All testing was performed on lumbar IVDs (L_1L_2-L_4L_5). All controlled tests used a straightened CONCORDE® Clear (Figure 5.1b) and were performed according to the parameters shown in Table 5.2. The tool was positioned at 5 mm penetration into the IVD before beginning. The tool was then inserted at 0.25 mm/s to 12-15 mm penetration (disc size permitting) while rotating at 40°/s over the range ±20°. Tool movement can be seen in Figure 5.1a. After insertion, the tool was withdrawn at the same rates. This test was repeated for a total of three trials, as seen in Table 5.2. Time, position, force, angle, and torque were recorded at 100 Hz. After an additional freeze-thaw cycle, one torso was tested for deflection under loading. The resulting positional changes in a vertebra under a range of loads was used to create a linear normalization. This was used to adjust the tool position to give a modified tool penetration distance that accounted for deflection of the torso.

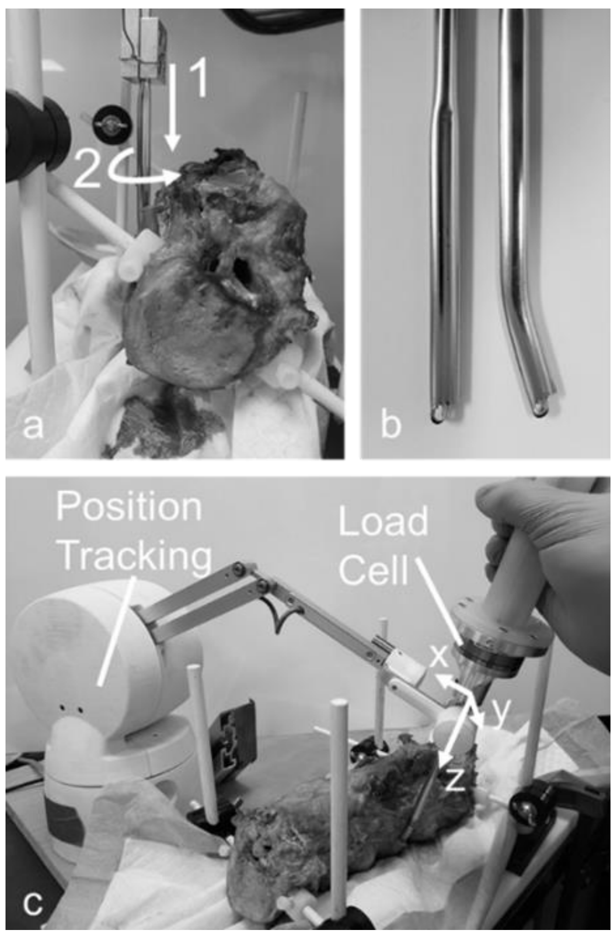

Figure 5.1: Tested tools and experimental setup. a) controlled test setup for spine specimens with linear (1) and rotational (2) movements, which were performed at the same time. T_{12} and S_1 were secured. b) The straight tool (left) was used in the controlled testing and the normal CONCORDE® Clear tool (right) was used in the freehand testing (c) in conjunction with the load cell and position tracker.

Table 5.2: Testing details for all cadaveric tests.

Testing Parameters			
Test Name		Controlled	Freehand
IVD Levels		L_1L_2 - L_4L_5	
Sides		Left and Right	
Linear Motion	Waveform	Triangle	NA
	Starting Position	5 mm inside IVD	5 mm inside IVD
	Range	0 - 15 mm	0 - 56 mm
	Range Used	0 - 11.5 mm	*0 - 14 mm
	Speed	0.25 mm/s	*13 ± 13 mm/s
Torsional Motion	Waveform	Sinusoidal	NA
	Starting Position	0°	0°
	Range	±20°	*-34 - 29°
	Speed	40°/s	*2 ± 14°/s
Number of Trials		3	≤24

*Outliers were removed for these ranges

Freehand testing was performed with a custom device (Figure 5.1c). A 3D printed handle designed to mimic the CONCORDE® Clear grip was attached to a Mini45 6-axis load cell (ATI Industrial Automation; Raleigh, USA) for force and torque tracking (≤1.5% resolution in all axes) with custom aluminum adapters. The CONCORDE® Clear shaft was secured to the output of a W3D 6-axis haptic device (Entact Robotics; Toronto, Canada) for position and orientation tracking (0.03 mm and 0.25° resolution). Position and force were monitored by custom LabVIEW (National Instruments; Austin, USA) and game engine (CAE Healthcare; Montreal, Canada) software at approximately 10 and 170 Hz, respectively. Tests were performed by neurosurgical fellows, one for each specimen. Each surgeon performed multiple passes through the IVDs and against the vertebral endplates as they would in a typical procedure.

5.2.5.3 *Data Processing*

Data were analyzed to compare specimens and test methods. Initial position, angle and force were normalized at the start of each controlled test. A linear fit of each controlled test on a range of [0, 11.5] mm was calculated to accommodate all data sets, with the slope equal to the linear resistance. In the case of the freehand testing, the lower frequency force and torque data were aligned to the position and orientation data. To perform a direct single axis comparison to the controlled data, position was calculated relative to the initial insertion point and magnitude of the x-, y-, and z-axis forces were used (Figure 5.1c). Additionally, the z-axis (insertion direction and parallel to the longitudinal axis of the inserted shaft) of the force was compared to the magnitude at different force magnitudes to quantify x- and y-axis, or off-axis, forces. Due to the inherent variability in freehand tool movement, data that passed through the range [9, 14] mm with at least 2.5 mm of forward motion were used to calculate the linear fit to compare with the controlled testing data from [0, 11.5] mm. Freehand tests did not always pass directly through the target penetration of 11.5 mm, but because force is dependent on position as shown in Equation 5.1, it was still necessary to take data from a range close to 11.5 mm. The threshold for forward motion was chosen to be half of that range, ensuring that the tissue would be loaded correctly. Additionally, measurements of the torso displacement per unit force was used to compare it to the more rigidly supported spine segment.

After extracting the relevant parameters and removing outliers exceeding three scaled median absolute deviations, Mann-Whitney U tests[39] were performed to determine the significance of differences between specimen types (torso/spine) and test methods (controlled/freehand). Only C4, the spine subjected to the controlled test before the freehand test, was compared to the torsos, so that new, untested samples could be evaluated (Table 5.2). A Spearman correlation was performed to determine the relationship between tool speed and resistance after checking data normality using a Shapiro-Wilk test.[40,41] A Kruskal-Wallis test was performed for comparisons of off-axis force contribution to multiple force magnitudes.[42]

5.2.6 Results

All studies were executed as described above. The left L_1L_2 and right L_3L_4 IVDs of C4 were excluded based on sample movement observed during testing and data analysis. An example of the controlled and freehand testing results can be seen in Figure 5.2.

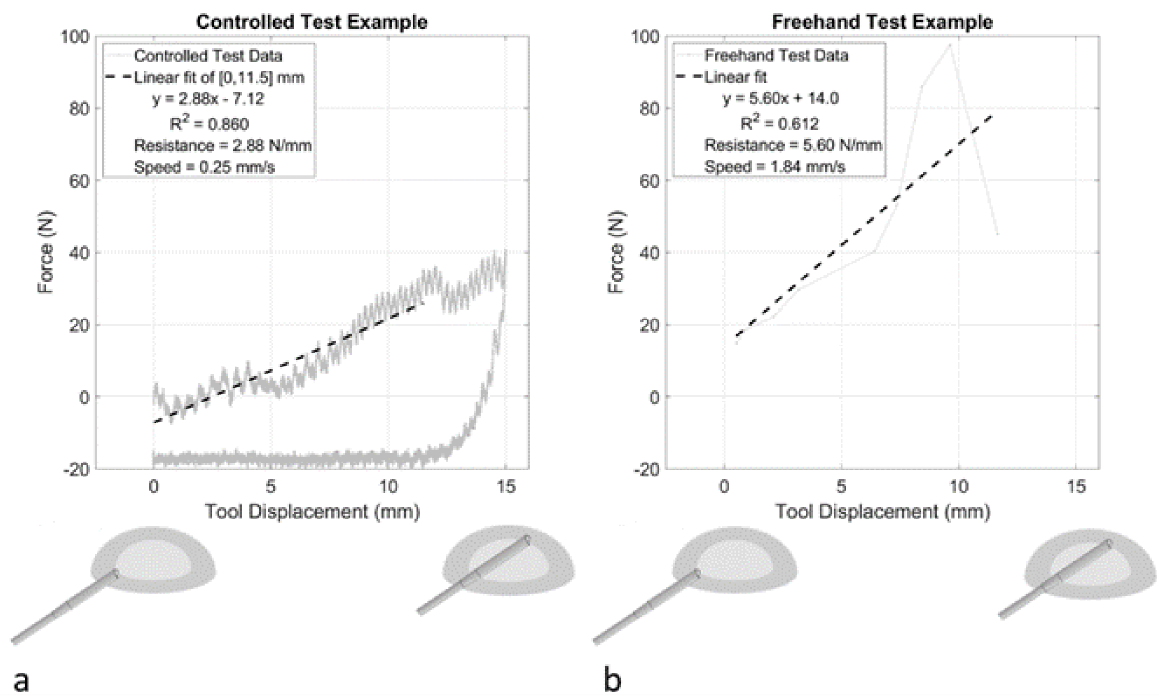

Figure 5.2: Example comparison of a) controlled and b) freehand test methods for the same specimen (C3 L_1L_2 left side trials 1 and 6, respectively). The relevant fit data and resistance values are shown.

5.2.6.1 Resistance

Figure 5.3 shows multiple resistance comparisons. The mean resistance (1.8±1.6 N/mm) in the spine was 8% less (not statistically significant) than that of the torso (2.0±1.4 N/mm) when using the controlled test, as shown in Figure 5.3a. This became a 27% difference (not statistically significant) when the torso specimen resistance was normalized for deflection (Figure 5.3b).

Figure 5.3c shows that the mean resistance measured, irrespective of tool speed, using the controlled test (1.2±0.9 N/mm) was 70% less ($p < 0.001$) than the freehand test (3.9±4.1 N/mm). Figure 5.3d displays the relationship between tool speed and resistance for all spine tests. The resistance distribution was not normally distributed and there was no statistically significant correlation with tool speed.

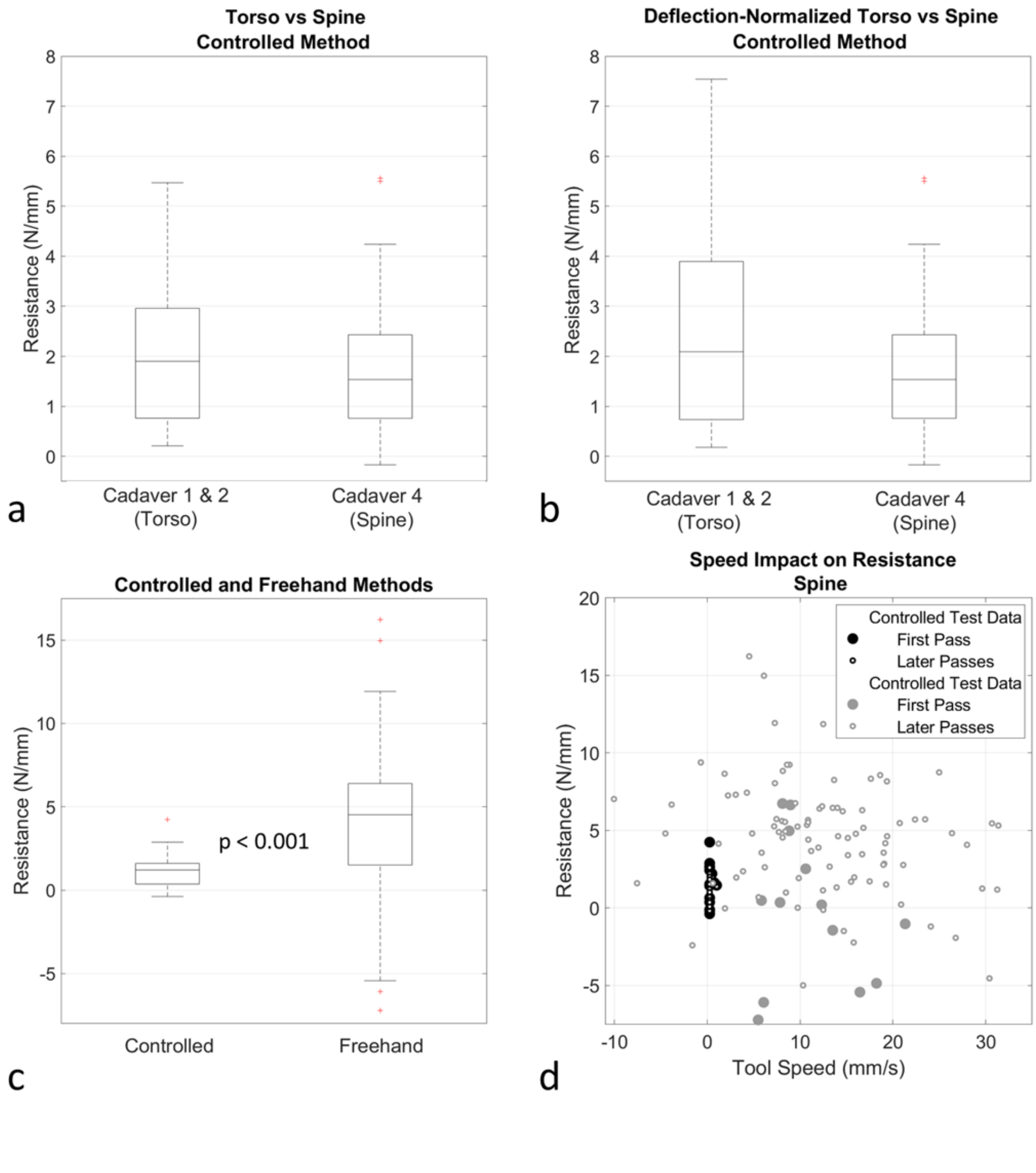

Figure 5.3: Box and whisker plot comparison of resistance encountered during testing scenarios. Differences between a) specimen types, b) specimen types after accounting for torso deflection, and c) test methods are shown. d) displays the relationship between resistance and tool speed for the spine tests.

5.2.6.2 Off-Axis Forces

Many forces were not along the z-axis, defined as the tool longitudinal or insertion axis, during freehand testing, as shown in Figure 5.4. The off-axis force, or x-y force, dropped by an average of 7.0±8.2% per 10 N of force magnitude increase for all trials. At higher forces, this contribution becomes less significant. The off-axis force decrease was found to be statistically significant ($p < 0.001$) for all trials.

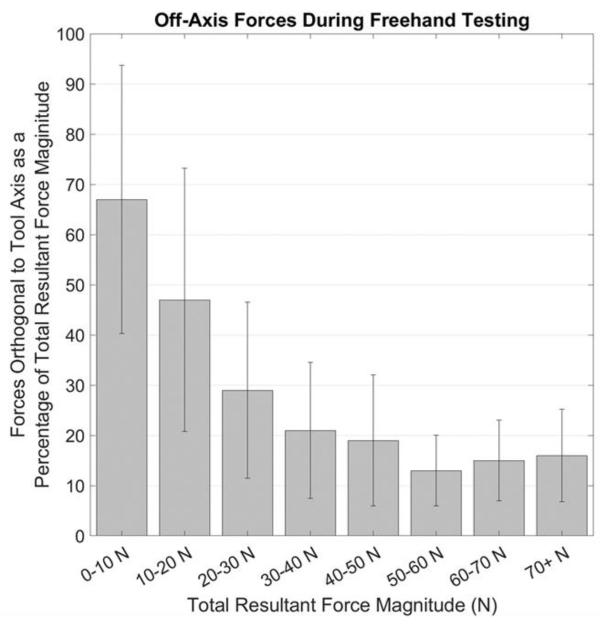

Figure 5.4: Forces orthogonal to tool longitudinal axis as a percentage of total resultant force magnitude for all freehand tests.

5.2.7 Discussion

This work represents a development in tissue testing used for haptic feedback in surgical simulation. A novel freehand testing apparatus was used to mimic the natural movement of a surgeon during a procedure. It allowed for more freedom when testing as it accommodated and measured off-axis forces present during discectomy. Data compared across test methods and specimen types helped show how these factors may have influenced observed linear resistance in terms of both magnitudes and directions. Understanding these differences was essential to characterize discectomy forces when designing haptic feedback.

The comparison between spine and torso specimens showed that while torsos had 8% higher resistances, there was no statistically significant difference between them. Despite studies documenting the role of soft tissues supporting lumbar spine and therefore increasing the overall rigidity of the more intact spine, it is possible that other factors contributed to the similarity.[19,20,43] Deflection may have occurred in other anatomies during torso testing, something that would not have happened in the spine segment mounted onto a rigid test fixture. After normalizing for deflection, the torso samples exhibited higher, but still not statistically significant, relative resistances (Figure 5.3b). While sample sizes could have been larger (48 torso tests, 24 spine tests before outlier removal), their size combined with the large standard deviation for each data set likely resulted in the statistical insignificance of this comparison. This divergence from literature data, which shows the inclusion of additional tissues result in increased stiffness, could be because studies documenting the impact of additional tissues on spine stiffness are typically done on spine segments rather than the entire torso.[19–21,43] The use of the torso here was important to mimic the entire body response during a surgical procedure, and this study showed how linear resistances acquired during testing on an excised spine differ compared to a torso when set up similar to a surgical procedure. The similarity between results show that it may be possible to use both dissected spine and intact torsos to generate linear resistance measurements for simulator haptics.

The use of the freehand tool and controlled testing on the same spine segment presented the opportunity to understand traditional testing technique limitations. Resistance was higher during the freehand testing, indicating that controlled testing missed some mechanical information.

Notably, the force often decreased at deeper penetrations (Figure 5.2b), sometimes to the extent of leading to a negative resistance (Figure 5.3a-c). Some decrease occurs after puncturing a tissue, but the final decrease may be caused by surgeon reducing pressure when approaching the distal side of the IVD, where an annular puncture could lead to surgical complications.[44] Off-axis forces, or those orthogonal to the line of action, likely accounted for a portion of that increase, but their relative contribution decreased at higher force magnitudes (Figure 5.4). Z-axis friction resulting from these x-y forces remains present throughout the testing, but tissue stiffness and cutting contribute more at higher total resultant force magnitudes (Equation 5.1). Tool speed appeared to have little impact on resistance, despite existing literature.[29,30] The freehand resistances show a slight but statistically insignificant negative correlation with tool speed (Figure 5.3d) which is in line with previous work analyzing needle punctures into tissue.[29,30] Physiological material elasticity and strength is well known to be strain rate dependent. However, the phenomenon of discectomy resistance, as explored herein, further comprises a potential combination of material fracture propagation, debris collection and subsequent displacement, and friction against adjacent tissues, in addition to material deformation. Thus, under this multifactorial combination, it is less clear if a distinct increase in the defined measure of resistance would correspond with tool speed. Another reason freehand resistance was higher than torso resistance may have been because the actual tool tip was used in the freehand testing instead of a straightened version for the controlled system, which was used to protect the load cell from bending torques (Figure 5.1b). Perhaps a combination of the surgeon flexibility and the actual tool being used were the cause of the increased resistance observed during freehand testing This suggests that established single axis tissue testing techniques, which have been used to inform haptic feedback in the past, may not capture the entire tissue response.[31–33] Therefore, freehand testing is recommended to advise future haptic feedback in surgical simulators because it is functionally more similar to surgical procedures and results in statistically different resistance measurements to traditional controlled testing.

Several limitations to this work exist. The freehand position tracking was much faster than the force, so it was necessary to only use the relevant position data at each time point. Tracking both at the same speed could have given different results with less data loss. By leaving the testing in the hands of the surgeon, the tool passes through the tissue were less consistent than the controlled test (Figure 5.2). Longer and smoother surgeon movements could have resulted in more similar freehand and controlled testing results, as previous studies have shown a decrease in puncture force with increased tool speed.[29,30] However, this force has been found to stabilize at higher needle puncture speeds, in a similar range of test speeds as those performed here.[30] The purpose of the testing was to imitate a surgeon movement, and therefore, the variety in speeds was expected and acknowledged. Torso deflection during controlled testing reduced tool penetration during testing, but, like the surgeon movements, this error was expected and compensated for in the comparison, and relevant in the context of imitating a real procedure. Finally, while use of fresh frozen samples is an established process in which a single freeze-thaw cycle has been found to minimally impact IVD mechanical properties, it is possible the subsequent cycle in the torso deflection study could have led to slightly lowered observed resistances.[38,45]

The devices and techniques presented helped characterize discectomy in MI-LIF procedures. Comparing torso and spine specimens gave a better understanding to the similarity between them, especially in the context of a surgical simulator. The freehand testing device showed clear differences between forces measured with traditional controlled tests and those present when surgeons operate naturally. Not only were forces in other directions present, but the force magnitude observed was larger. Given this knowledge, it is recommended to complete testing on either torso or spine samples with a freehand test to mimic a surgical environment more accurately, which will result in data and haptics that better represent a surgical discectomy. Testing this way will give surgeons better training simulators, which will hopefully lead to better surgical outcomes for patients.

5.2.8 Acknowledgments

All spine testing was performed at the Orthopedic Research Lab at the Montréal General Hospital with the assistance of Dr. Rodrigo Navarro-Ramirez, Dr. Rakan Bokhari, and Lorne Beckman. Cadaver testing was done at the Laboratoire de Recherche en Imagerie et Orthopedie division de l’Hôpital du Sacré-Coeur de Montréal under Prof. Yvan Petit and Prof. Eric Wagnac, with assistance from Elisabeth Laroche, Dr. Khaled El-Monajjed, and Sneha Patel. Funding and guidance were provided by the Natural Sciences and Engineering Research Center (NSERC), the Quebec Consortium for Industrial Research and Innovation in Medical Technology (MEDTEQ), DePuy Synthes, CAE Healthcare, Inc., and McGill University under Grant CRDPJ 515768-17. All data contained in the submitted work was collected under appropriate ethical approval (IRB A04-M13-18A).

5.2.9 References

1. Custers E, Cate O. The History of Medical Education in Europe and the United States, With Respect to Time and Proficiency. Academic Medicine. 2018;93:S49-S54.

2. Bergamaschi R. Farewell to see one, do one, teach one? Surgical Endoscopy. 2001;15:637.

3. Akhtar K, Chen A, Standfield N, Gupte C. The role of simulation in developing surgical skills. Current Reviews in Musculoskeletal Medicine. 2014;7:155-160.

4. Sadideen H, Alvand A, Saadeddin M, Kneebone R. Surgical experts: Born or made? International Journal of Surgery. 2013;11:773-778.

5. The Canadian Museum of Flight. Link Trainer.

6. Reid L. The Design of a Facility for the Measure of Human Pilot Dynamics.; 1965.

7. Federal Aviation Administration. National Simulator Program (NSP).

8. F1 Chronicle. How Does A Formula 1 Simulator Work?

9. Delorme S, Laroche D, Diraddo R, Del Maestro R. NeuroTouch: A Physics-Based Virtual Simulator for Cranial Microneurosurgery Training. Neurosurgery. 2012;71:32-42.

10. Cooper J, Taqueti V. A brief history of the development of mannequin simulators for clinical education and training. Quality & Safety In Health Care. 2004;13:i11-i18.

11. Weiss H, Ortmaier T, Maass H, Hirzinger G, Kuehnapfel U. A Virtual-Reality-Based Haptic Surgical Training System. Computer Aided Surgery. 2003;8:269-272.

12. Zhou M, Tse S, Derevianko A, Jones D, Schwaitzberg S, Cao C. Effect of Haptic Feedback in Laparoscopic Surgery Skill Acquisition. Surgical Endoscopy. 2012;26:1128-1134.

13. Moody L, Baber C, Arvanitis T. The Role of Haptic Feedback in the Training and Assessment of Surgeons using a Virtual Environment. Proceedings of EuroHaptics 2001. Published online 2001:170-173.

14. Bugdadi A, Sawaya R, Bajunaid K, et al. Is Virtual Reality Surgical Performance Influenced by Force Feedback Device Utilized? Journal of Surgical Education. 2019;76:262-273.

15. Ruikar D, Hegadi R, Santosh K. A Systematic Review on Orthopedic Simulators for Psycho-Motor Skill and Surgical Procedure Training. Journal of Medical Systems. 2018;42:168: 1-21.

16. Forsslund J, Selesnick J, Salisbury K, Silva R, Blevins N. The Effect of Haptic Degrees of Freedom on Task Performance in Virtual Surgical Environments. In: Westwood JD, Westwood SW, Felländer-Tsai L, Haluck RS, Robb RA, SengeVosburgh KG, eds. Stu*dies in Health Technology and Informatics (Medicine Meets Virtual Reality 20: NextMed/MMVR20)*. Vol 184. IOS Press; 2013:129-135.

17. Chmarra M, Dankelman J, Van Den Dobbelsteen J, Jansen F. Force feedback and basic laparoscopic skills. Surgical Endoscopy and Other Interventional Techniques. 2008;22:2140-2148.

18. Costi J, Ledet E, O'Connell G. Spine biomechanical testing methodologies: The controversy of consensus vs scientific evidence. JOR Spine. 2021;4:e1138.

19. Goel VK, Winterbottom JM, Weinstein JN, Kim YE. Load Sharing Among Spinal Elements of a Motion Segment in Extension and Lateral Bending. Journal of Biomechanical Engineering. 1987;109:291-297.

20. Schendel M, Wood K, Buttermann G, Lewis J, Ogilvie J. Experimental Measurement of Ligament Force, Facet Force, and Segment Motion in the Human Lumbar Spine. Journal of Biomechanics. 1993;26:427-438.

21. Goel V, Goyal S, Clark C, Nishiyama K, Nye T. Kinematics of the Whole Lumbar Spine: Effect of Discectomy. Spine. 1985;10:543-554.

22. Okamura A, Simone C, O'Leary M. Force Modeling for Needle Insertion Into Soft Tissue. IEEE Transactions on Biomedical Engineering. 2004;51:1707-1716.

23. Griffin M, Premakumar Y, Seifalian A, Butler P, Szarko M. Biomechanical Characterization of Human Soft Tissues Using Indentation and Tensile Testing. Journal of Visualized Experiments. 2016;118:e54872: 1-8.

24. Lee C, Langrana N. Lumbosacral Spinal Fusion: A Biomechanical Study. Spine. 1984;9:574-581.

25. MTS Systems. MTS Systems.

26. Instron. Instron Biaxial Cruciform - Instron.

27. MTS Systems. Bionix® Tabletop Test Systems.

28. Chen J, Li Y, Wen J, Li Z, Yu B, Huang Y. Annular Defects Impair the Mechanical Stability of the Intervertebral Disc. Global Spine Journal. 2021;2192568221.

29. El-Monajjed K, Driscoll M. Analysis of Surgical Forces Required to Gain Access Using a Probe for Minimally Invasive Spine Surgery via Cadaveric-Based Experiments towards Use in Training Simulators. IEEE Transactions on Biomedical Engineering. 2021;68:330-339.

30. Jiang S, Li P, Yu Y, Liu J, Yang Z. Experimental study of needle-tissue interaction forces: Effect of needle geometries, insertion methods and tissue characteristics. Journal of Biomechanics. 2014;47:3344-3353.

31. Cheng Q, Liu P, Lai P, Xu S, Zou Y. A Novel Haptic Interactive Approach to Simulation of Surgery Cutting Based on Mesh and Meshless Models. Journal of Healthcare Engineering. 2018;2018:9204949: 1-16.

32. Zou Y, Liu P, Cheng Q, Lai P, Li C. A New Deformation Model of Biological Tissue for Surgery Simulation. IEEE Transactions on Cybernetics. 2017;47:3494-3503.

33. Liu X, Xu S, Zhang H, Hu L. A New Hybrid Soft Tissue Model for Visio-Haptic Simulation. IEEE Transactions on Instrumentation and Measurement. 2011;60:3570-3581.

34. Nillahoot N, Suthakorn J. Development of Veress Needle Insertion Robotic System and its experimental study for force acquisition in soft tissue. In: *2013 IEEE International Conference on Robotics and Biomimetics (ROBIO).* ; 2013:645-650.

35. Georgilas I, Dagnino G, Tarassoli P, Atkins R, Dogramadzi S. Preliminary Analysis of Force-Torque Measurements for Robot-Assisted Fracture Surgery. In: *Proceedings of the Annual International Conference of the IEEE Engineering in Medicine and Biology Society.* ; 2015:4902-4905.

36. Georgilas I, Dagnino G, Alves Martins B, et al. Design and Evaluation of a Percutaneous Fragment Manipulation Device for Minimally Invasive Fracture Surgery. Frontiers in Robotics and AI. 2019;6:103: 1-9.

37. Cotter T, Mongrain R, Driscoll M. Under Review - Vacuum Curette Lumbar Discectomy Mechanics for Use in Spine Surgical Training Simulators. Scientific Reports. Published online 2022.

38. Newell N, Little J, Christou A, Adams M, Adam C, Masouros S. Biomechanics of the Human Intervertebral Disc: A Review of Testing Techniques and Results. Journal of the Mechanical Behavior of Biomedical Materials. 2017;69:420-434.

39. Mann H, Whitney D. On a Test of Whether One of Two Random Variables is Stochastically Larger Than the Other. The Annals of Mathematical Statistics. 1947;18:50-60.

40. Gibbons J, Chakraborti S. Spearman's Coefficient of Rank Correlation. In: Dekker M, ed. *Nonparametric Statistical Inference. 4th ed.* ; 2003:422-432.

41. BenSaïda A. Shapiro-Wilk and Shapiro-Francia normality tests. MATLAB Central File Exchange.

42. Kruskal W, Wallis W. Use of Ranks in One-Criterion Variance Analysis. Journal of the American Statistical Association. 1952;47:583-621.

43. Heuer F, Schmidt H, Klezl Z, Claes L, Wilke H. Stepwise reduction of functional spinal structures increase range of motion and change lordosis angle. Journal of Biomechanics. 2007;40:271-280.

44. Aichmair A, Fantini G, Garvin S, Beckman J, Girardi F. Aortic Perforation During Lateral Lumbar Interbody Fusion. Journal of Spinal Disorders and Techniques. 2015;28:71-75.

45. Tan J, Uppuganti S. Cumulative Multiple Freeze-Thaw Cycles and Testing Does Not Affect Subsequent Within-Day Variation in Intervertebral Flexibility of Human Cadaveric Lumbosacral Spine. Spine. 2012;37:e1238-e1242.

5.3 Additional Studies

Article 3: Comparing Controlled and Freehand Test Techniques of Lumbar Discectomy Force Measurement for Spinal Surgery Simulation described use for the freehand device. However, there was a lengthy design process encompassing both hardware and software that was necessary before tissue testing could be performed. This process, as well as additional tissue testing, is described hereunder.

5.3.1 Hardware Design

A comparison of the original Concorde Clear tool, haptic torque handle, and freehand testing device is shown in Figure 5.5, which also includes an exploded view of the freehand testing device components. Both novel tools designed and described in this manuscript, the haptic torque handle and freehand device, were made to imitate the Concorde Clear for simulator and testing contexts. The grip of the freehand device matched the dimensions of the original tool. This enabled the user to hold it while performing mechanical testing, as shown in Figure 5.6. The freehand device tracked the tool position and orientation, as well as force and torque, during testing. The assembly and bill of materials (BOMs) are available in 0.

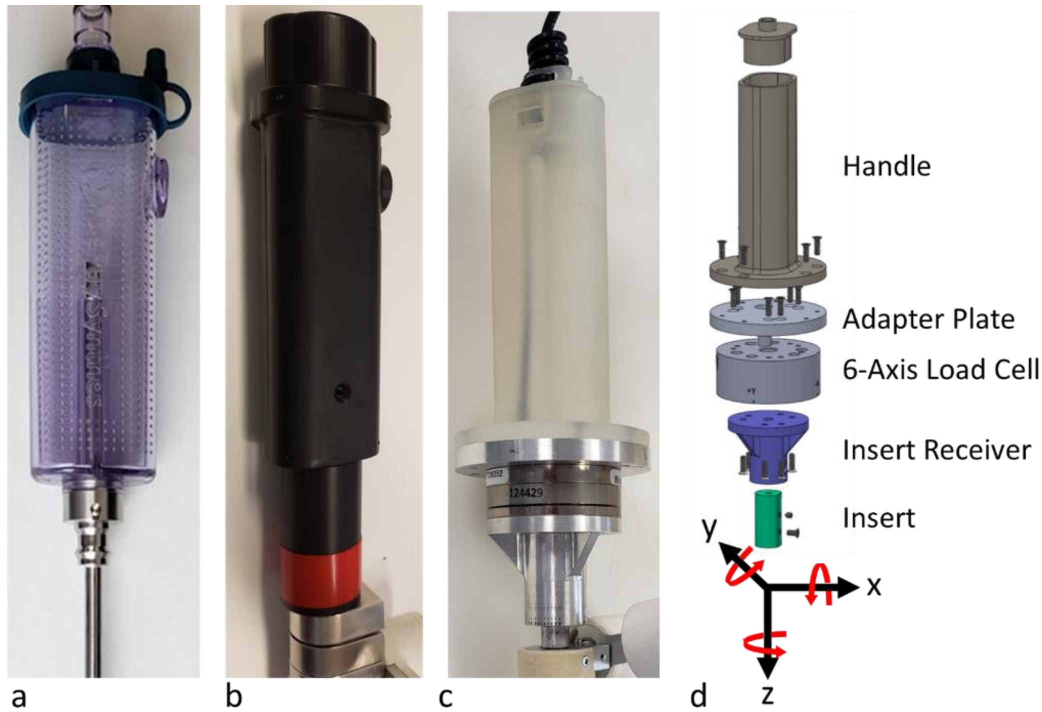

Figure 5.5: Multiple versions of the Concorde Clear tool and versions for simulation and testing. a) is the surgical tool, b) is the haptic torque handle used in the simulator, c) is the freehand testing apparatus version, and d) is an exploded view of the freehand testing apparatus with a coordinate system that is used in Table 5.3.

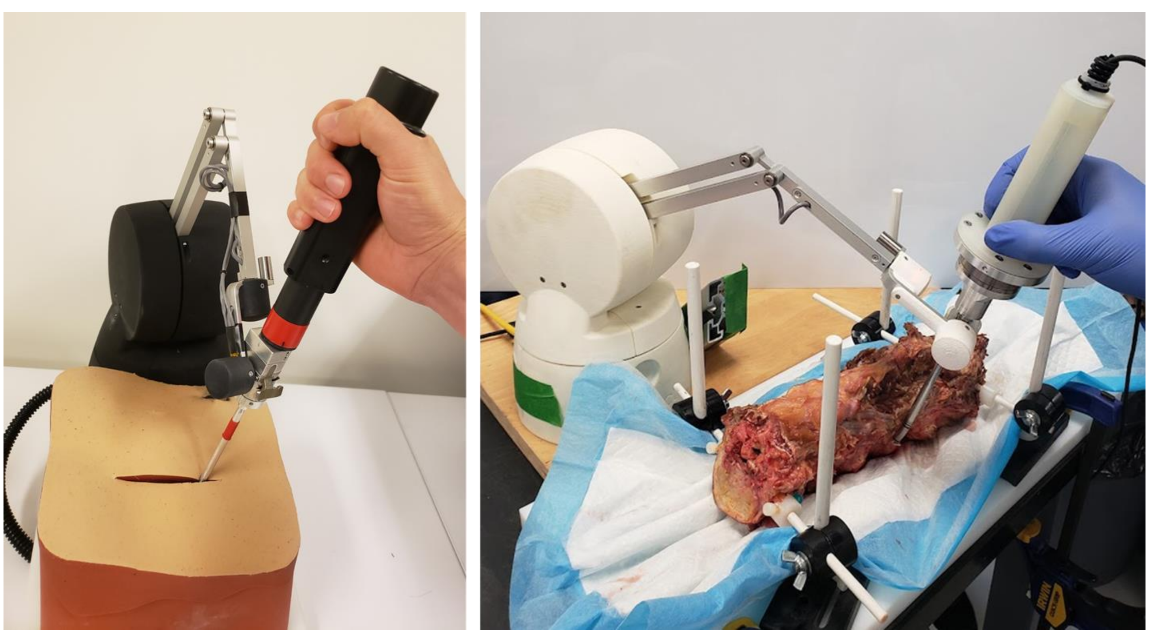

Figure 5.6: The two simulated versions of the Concorde Clear. The image on the left shows the haptic torque handle as used in the simulator, and the right shows the freehand apparatus that allows the surgeon to test forces with surgical freedom.

The position and orientation of the tool were tracked by the Entact W3D haptic device. The motors were deactivated but the encoders remained activated to track the position and orientation of the end effector. The final gimbal shaft of the W3D device, which tracked the rotation of the tool, was swapped with a Concorde Clear distal shaft so that the surgeon could perform testing. The insert, shown in Figure 5.7, was attached to the back of the Concorde Clear distal shaft so the rest of the assembly could be connected. This insert design was chosen so that the rest of the assembly could be used with distal tool shafts of multiple diameters. This would require only the design of a new insert, rather than the more complex insert receiver. It should be noted that this design was created with the intention of using a different position and orientation device that would have been more adaptable to tool distal shaft options.

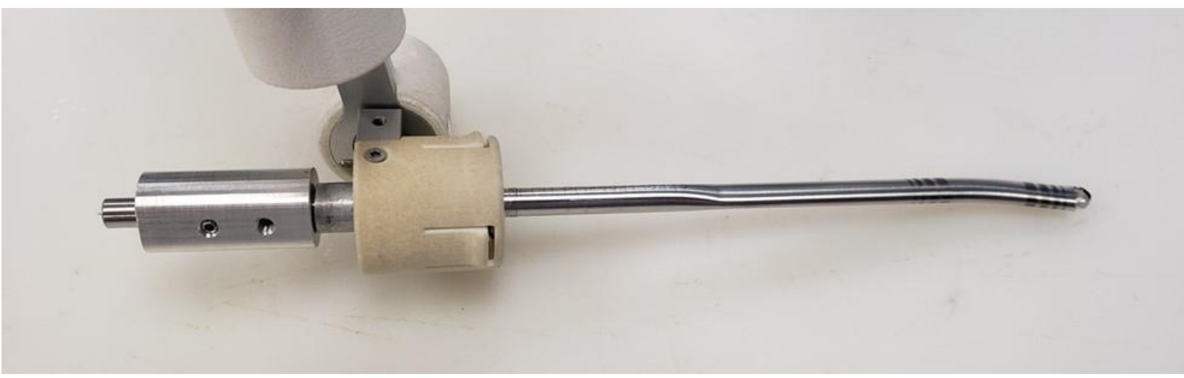

Figure 5.7: Insert mounted on to the Entact W3D device via a Concorde Clear shaft used in place of the normal final gimbal shaft. The rest of the freehand apparatus attaches onto the insert.

Additionally, it was necessary to measure the force and torque produced during testing. A Mini45 6-axis load cell (ATI Industrial Automation; Raleigh, USA) was used to do this. Force and torque capabilities of the Mini45 load cell are detailed in Table 5.3, where the axis directions correspond to those in Figure 5.5. These limits encompass the range of forces and torques measured in Chapter 4, meaning that this load cell was adequate for similar testing.

Table 5.3: Force and torque calibration specification of the Mini45 load cell.

	Force (N)			Torque (N·mm)		
Axis	x	y	z	x	y	z
Peak (±)	145	145	290	5000	5000	5000
Uncertainty (±)	1.25%	1.00%	0.75%	1.25%	1.50%	1.25%

Similar to the haptic torque handle from Chapter 3, it was necessary to match the original Concorde Clear tool as accurately as possible. While the freehand testing device was used for biomechanical measurements to inform the simulator haptics, the haptic torque handle was the only component that was included in the simulator. The Concorde Clear handle dimensions were replicated for the freehand device, but the weight could not be. The handle was 3D printed out of durable resin using a stereolithography (SLA) printer to minimize weight. The other components were made of machined 6061 aluminum to reduce weight compared to other metals. The aluminum parts allowed for a safety factor over 6 for the expected forces during the freehand testing. This gave an approximate freehand device weight of 280 g. To note, this number does not include weight from the W3D device, cables, or minor design modifications, though it remains significantly heavier than the original 74 g tool weight. However, the 92 g contribution of the Mini45 load cell alone meant that there would be a necessary weight increase over the original surgical tool. A waterproof load cell would have added additional weight, so a plastic sleeve was chosen to cover and protect the device.

The initial design for the freehand testing device involved a separate position tracking method. A PATRIOT™ electromagnetic motion tracker (Polhemus; Burlington, USA) was a lightweight option. However, electromagnetic interference (EMI) was observed during testing of the device. The various metallic components of the assembly, including the load cell, were believed to have interfered with the electromagnetic field used by the sensor to track position. This resulted in significant position and orientation errors. Once observed and measured, the decision was made to use the W3D device for motion tracking. This limited the tracking about the z-axis of the tool as the final gimbal shaft is shared by the W3D device and the tool tip that interfaces with the tissue.

5.3.2 Software Design and Analysis

Two programs were used to capture data during freehand testing. Both data acquisition hardware components, the load cell and the haptic device, required an ethernet connection. Therefore, two computers were used. The first program was a custom program developed within a virtual reality (VR) gameplay environment from CAE Healthcare. This software ecosystem is discussed further in Chapter 6. The program allowed for the user to make calibration timestamps and track the tip of the tool in space through the haptic device motions. The orientation of the tool about the z-axis was also tracked. The data was recorded at approximately 170 Hz.

The second data acquisition program was a virtual instrument (VI) built with LabVIEW. It used subVIs provided by ATI Industrial Automation to interface with the load cell. The VI built here, shown in Figure 5.8, added calibration timestamps, measured value displays, and recording to a data (DAT) file. The data was recorded at approximately 10 Hz.

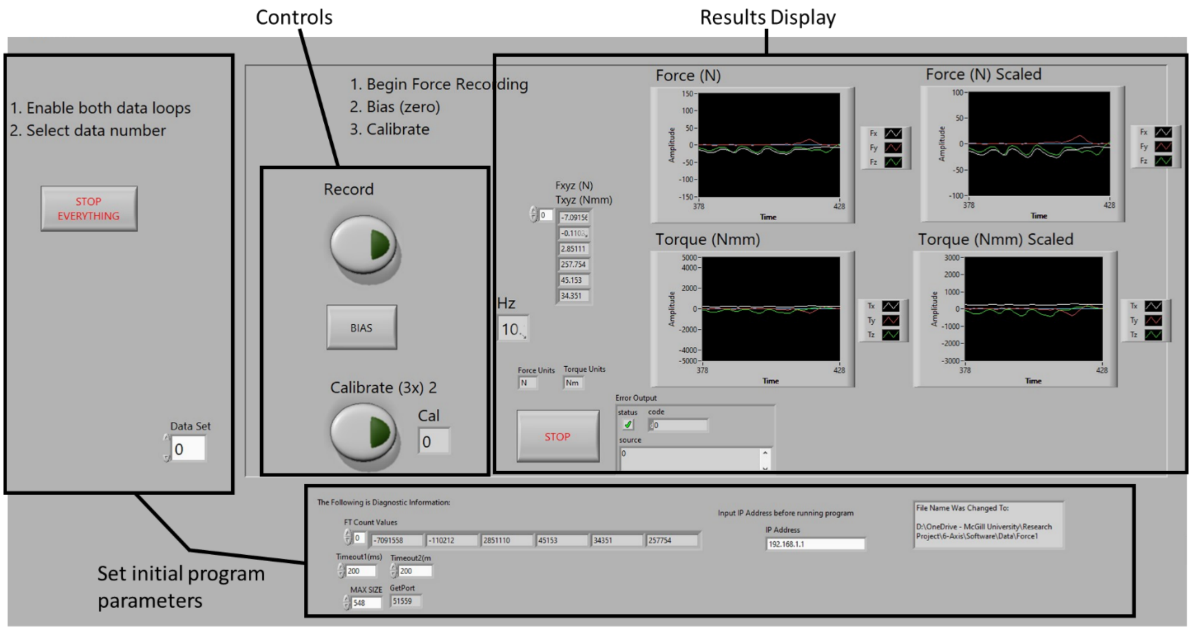

Figure 5.8: Front panel of the force and torque tracking Virtual Instrument (VI).

After testing, MATLAB (MathWorks; Boston, USA) was used to analyze the data. Calibration timestamps were input to both data recordings so the position and orientation could be synced with the force and torque. As stated in Article 3: Comparing Controlled and Freehand Techniques of Lumbar Discectomy Force Measurement for Spinal Surgery Simulation, the extra data recorded in the faster position and orientation software was removed. This was justified by a study of one IVD test with 13 trials. Data was collected using only the best-aligned data point while removing the excess points. Additionally, the same data set was analyzed by taking an average of ±5 data points to reduce the data loss. The calculated linear resistance resulted in a change of 1.7±10.4% between the two analysis methods, which was within an acceptable tolerance for this study. After aligning the data, the distance from the calibration point over time was plotted, as shown in Figure 5.9. Each trial was selected if it reached the range 11.5±2.5 mm during penetrating motion. Linear resistance of the IVD was then calculated as described in

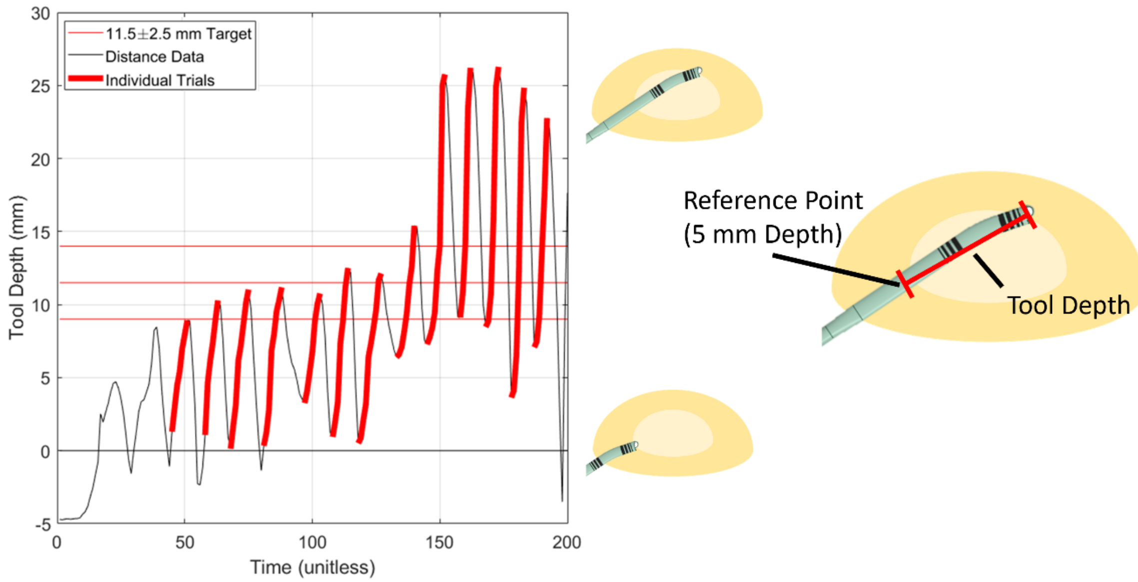

Figure 5.9: Freehand data over testing, with individual trials highlighted. Each individual trial was considered the equivalent of an MTS trial from Chapter 4. A schematic showing the tool depth is shown.

The angle and torque about the z-axis were also recorded to provide an additional comparison between the controlled and freehand test results. However, the torsional motion was less consistent than the linear motion analyzed for the force data. Additionally, the torque did not appear to always oppose the angle of the tool as expected and outlined in Figure 5.10. The observed torque was sometimes in the expected direction, but often it was not. Perhaps increasing the data collection rate or further investigation of the load cell could lead to better results, but as a result, the torque about the z-axis was not included in this study. The controlled test method from Chapter 4 can capture this, and because this torque only occurs and is delivered along a single axis, it was less likely to show the same level of change between controlled and freehand test methods as the multi-axis force data. In the simulator, torque can only be delivered along the z-axis, and therefore x- and y-axis torques were not considered.

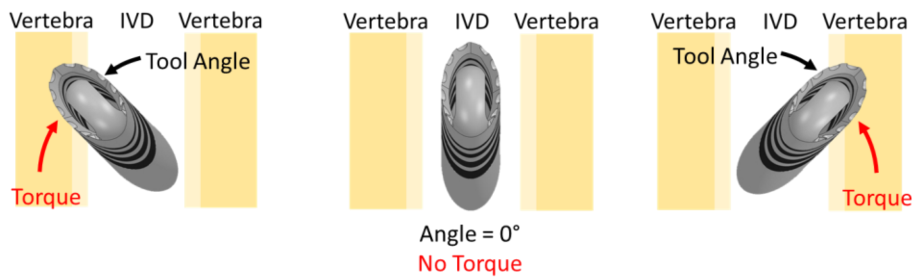

Figure 5.10: Expected torque response for tool twisting within the intervertebral disc (IVD).

5.3.3 Testing Considerations

The freehand testing was performed on an excised spine sample in a different test jig than that outlined in Chapter 4. Tool penetration into the spine IVDs was measured to be at least 12 mm during all 15 mm displacement tests using the controlled test method, indicating that little deflection occurred during the testing. This was likely due to the rigid support of the lumbar-adjacent vertebrae (T_{12} and S_1) as well as the support underneath L_3. The linear resistances between the directly supported IVDS (L_2L_3, L_3L_4) and fixed IVDs (L_1L_2, L_4L_5) were not statistically significant for the controlled and freehand test methods, as evidenced by Figure 5.11. The difference between test fixtures must be acknowledged when comparing the testing here to other samples, such as the cadaveric torsos that exhibited deflection under load.

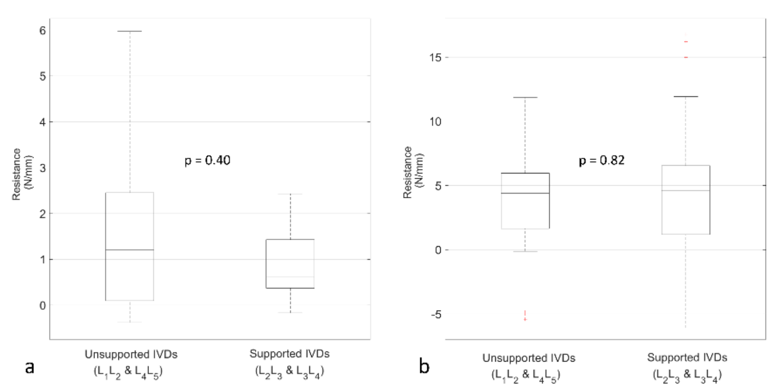

Figure 5.11: Comparing unsupported and supported intervertebral discs (IVDs) in the freehand test jig for both a) controlled tests and b) freehand tests.

The IVD height measurement briefly mentioned in Article 3: Comparing Controlled and Freehand Techniques of Lumbar Discectomy Force Measurement for Spinal Surgery Simulation, is shown in Figure 5.12. Five measurements across the IVD were made using ImageJ (National Institutes of Health; Washington, USA) and the average was used, with a reference, to calculate the IVD height.

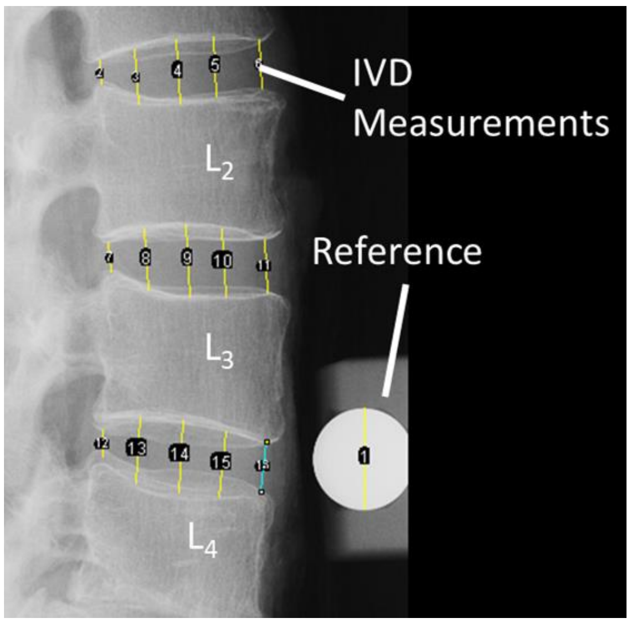

Figure 5.12: Intervertebral disc (IVD) measurement example for the spine samples.

The test order was shuffled between controlled and freehand tests. One specimen was tested using the controlled method and then the freehand method, and vice versa. The results of comparing the specimens and surgeons from Article 3: Comparing Controlled and Freehand Techniques of Lumbar Discectomy Force Measurement for Spinal Surgery Simulation are shown in Figure 5.13. However, because two spines were used, it cannot be determined if the statistically significant differences are caused by the surgeon or the specimen condition. Further testing on additional specimens would be needed to determine the cause of the differences.

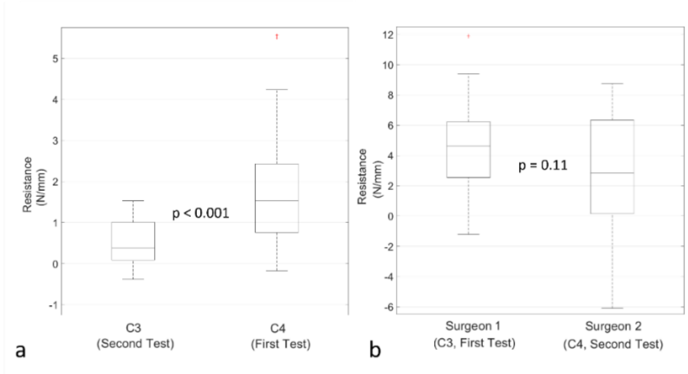

Figure 5.13: Comparison between a) spine specimens and b) surgeons. First and Second Test indicate when the given test method (controlled or freehand) was performed relative to the other test method.

As noted in Article 3: Comparing Controlled and Freehand Test Techniques of Lumbar Discectomy Force Measurement for Spinal Surgery Simulation, forces not along the z-axis made a significant and variable contribution to the total resultant force magnitude. While Figure 5.4 showed the x-y forces as a percentage of the total force magnitude, Figure 5.14 shows the magnitude of those off-axis forces. They increased statistically significantly ($p < 0.001$) with total resultant force magnitude. These off-axis forces, which are normal to the tool, will impact the frictional force encountered by the tool during insertion. Therefore, according to Equation 2.6, an increase in these off-axis forces will increase the frictional force and therefore the total z-axis force encountered during the procedure.

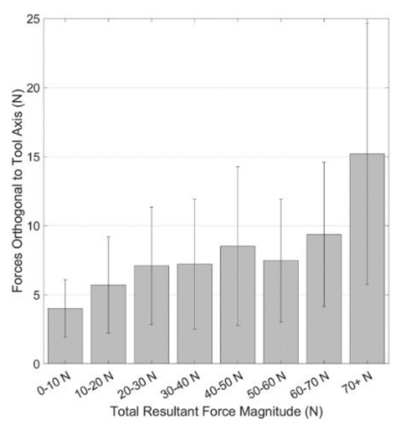

Figure 5.14: Magnitude of the off-axis forces present during freehand testing.

5.3.4 Sources of Error

In addition to the several sources of error acknowledged in Article 3: Comparing Controlled and Freehand Test Techniques of Lumbar Discectomy Force Measurement for Spinal Surgery Simulation, there remain more factors that should be considered. The studies presented here only considered the tool position relative to the annulotomy used to access the disc, while the force was measured along the tool axis. This means the tool travel direction may not have been the same as the tool axis. Deformation of the sample and test fixture were also not considered, and this could have also played a factor in the position measurements. Any tests where the specimens were observed sliding relative to the test fixture were discarded, but there was still some level of bending and deformation of the test specimen and fixture. This should be investigated in future studies.

The data sets, by nature of the testing methods compared, differed in length. The surgeons performed more shorter and faster movements for the freehand tests, and therefore more but shorter freehand data sets had to be used than the controlled tests. While speed normalization was used to accommodate some of this discrepancy, only a true viscoelastic model would be able to fully capture the natural tissue response. This was not done because the data captured and presented here represented only force and position, rather than the stress and strain necessary for a viscoelastic model. The tool penetration distance would be needed, and additionally, the composite makeup of the spine specimen would have meant only a gross approximation of the viscoelastic properties would have been possible. While viscoelastic studies of composite tissues have been performed, the analysis as shown here was determined to be sufficient within the context of developing a surgical simulator [151,152]. The observed trend seen in Figure 5.3d does show a slight, but not statistically significant, decrease in resistance as speed increases.

Existing studies have found similar behavior in tissue puncture using needles [113,119]. However, as the data collected here did not show the same trends, it is possible that the tool reached the speed at which puncture force stabilizes, or that the resistance is mostly caused by friction and deformation, rather than puncturing as described in Equation 2.6 [119].

The freehand and controlled tests were performed repeatedly. Table 5.2 shows the number of trials performed on each side of each lumbar IVD, which enabled the use of statistical comparisons. As shown in Table 4.3, after a single pass through the tissue the measured force profiles stabilized. This indicates that of the 6-27 tests performed on each IVD side in the freehand and controlled tests, the majority, 5-26, of them would fall within this stabilized range. To characterize the tissues and methods in the initial passes, future tests could use additional samples, which would add cost and complexity to the study. Future studies should consider using larger sample sizes to increase the statistical power of observed comparison and how confidently they can be extended to the general cadaveric or patient population.

As stated in Article 3: Comparing Controlled and Freehand Test Techniques of Lumbar Discectomy Force Measurement for Spinal Surgery Simulation, outliers were removed during the freehand studies. These outliers were likely due to surgeon variability and different loading profiles in terms of tissue depth and penetration speed as mentioned earlier. Additionally, some of the data showed negative forces during loading, which does not make physical sense and may have been caused by delays from the lower force measurement sampling rate compared to the position sampling rate. For each of the reasons listed, outliers exceeding three scaled median absolute deviations were removed.

5.3.5 Simulator Application

The work shown here indicated that there was a difference between the force observed during controlled testing in comparison to freehand testing. This testing could have been considered in designing the feedback for a surgical simulator. However, the surgeon studies of the force profiles in Chapter 4 indicated that surgeons perceived the established force response to be inadequate, future studies could be done to find if incorporating this data would improve surgeon impressions of the feedback.

5.3.6 Conclusions

A new tool for the freehand measurement of surgical forces was conceived, built, and tested. It was found to be a reliable method for tracking the natural movement of a surgeon during discectomy, while also monitoring the load applied by the surgeon. Freehand testing resulted in significantly higher forces than those measured with traditional mechanical testing. Additionally, the contribution of off-axis forces was also quantified. The data gathered could be used to further refine the haptic feedback of the surgical simulator, as well as be used to advance the development of future surgical tools. This work represents an additional step forward in the field of biomechanical testing, especially in making it relevant to the operating room.

6
Virtual Reality Simulator

6.1 Context

The three manuscripts presented were used to inform and help build the final simulator. Having already answered each hypothesis in Chapters 3, 4, and 5, this chapter investigates how the various tools and studies shown were incorporated in the design. The author was responsible for the successful development and deployment of the discectomy part of the simulator. The work was executed in parallel to additional surgical steps developed by Dr. Khaled El-Monajjed and Dr. Sneha Patel, who additionally gave input on all parts of the simulator. All surgical steps and procedural advising were given by DePuy Synthes, specifically Eric Buehlmann, Alicia McDermott, Eric Sheridan. The technical development of the simulator hardware and virtual reality (VR) environment was done with CAE Healthcare, specifically Dr. Clément Forest, Edouard Poutot, and Alex Mykris. Haptic device integration was assisted by Ryan Leslie at Entact Robotics and Dr. Brahim Brahmi developed a control system. Maxence Coulombe assisted with the development of the graphic user interface (GUI) and tool calibration. The additional tools used with the haptic device were designed by Brittany Stott. Michael Grizenko-Vida designed the benchtop assembly. Finally, Dr. Rodrigo Navarro-Sanchez provided advising from a surgical perspective during simulator development.

6.2 Transforaminal Lumbar Interbody Fusion (TLIF) Surgery

The simulator is made for training of a transforaminal lumbar interbody fusion (TLIF) procedure, as outlined in 2.2 Surgical Intervention. This procedure was broken into multiple sections, as shown in Table 6.1. The three sections of the simulator were Access Gaining, Discectomy, and Cage Insertion, which were developed by Dr. Khaled El-Monajjed, the author, and Dr. Sneha Patel, respectively. This work focuses on the Discectomy section of the simulator. This section occurs entirely within a minimally invasive (MI) port.

6.1 Simulator Design Overview

The basic components of the surgical simulator are shown in Figure 6.1. The entire simulator is run on a laptop that gives visual displays augmented by an additional screen. The surgeon uses multiple tools to interact with the haptic device and physical tissue model throughout the procedure. Deeper discussions of each of the hardware and software components follow.

Table 6.1: Individual steps of the transforaminal lumbar interbody fusion (TLIF) procedure.

Surgical Step	Substeps	Description	Unique Metrics
All Surgical Steps			Time Tool Position, Velocity, and Acceleration Proximity to Nerve Root and Dura Force Torque Tissue Volume Removed
Access Gaining	Locate and Access IVD	Use a multitool probe to locate Kambin's Triangle and the underlying IVD	Tool Orientation Intervertebral Disc Puncture
	Dilate for Port and Instrument	Expand access to IVD through dilation port, and instrument placement	No Unique Metrics
Discectomy	Facetectomy	Use a Bur and Kerrison to remove SAP Joint to expand access to IVD	% L_4 IAP Removed % L_5 SAP Removed
	Tissue Retractor	Use tissue retractor to displace and protect nerve if necessary	Duration of nerve displacement
	Annulotomy	Remove soft tissue and annulus fibrosus for access into the IVD	Size of annulotomy
	Discectomy	Remove nucleus pulposus in the IVD	% Nucleus Pulposus Removed % Annulus Fibrosus Removed % L_4 and L_5 Endplates Removed
Cage Insertion	Insert Bone Graft	Fill the emptied IVD space with bone graft	Volume of Graft Placed
	Insert Interbody Cage	Place interbody cage to maintain adequate vertebral spacing	No Unique Metrics
Pedicle Screw and Rod Placement	Not included in the simulator		

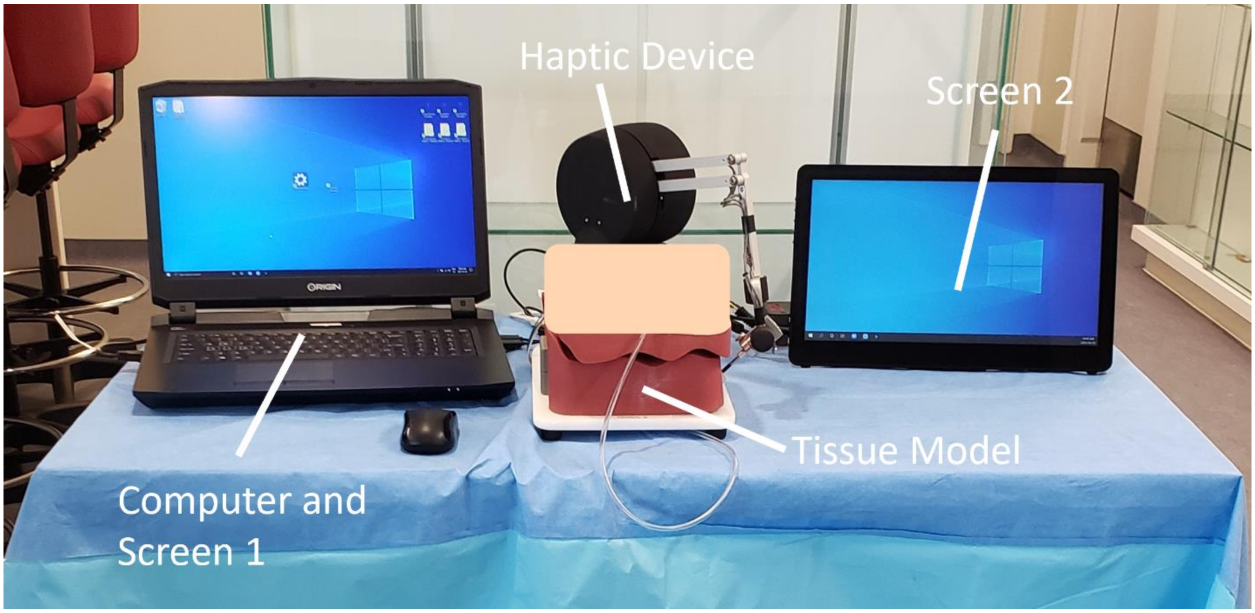

Figure 6.1: Overview of the basic surgical simulator components.

6.2 Simulator Hardware

6.2.1 Laptop and Display

The simulator was developed on an MSI (Taipei City, Taiwan) GT75 Titan laptop and an Origin (Miami, USA) EON17-X was used in the final version. It provided the primary display for the VR simulation. A GeChic (Taichung City, Taiwan) On-Lap 1503I touchscreen monitor was used as a secondary display. These gave the surgeon instrumentation views that they would receive in the operating room. The screens also provided additional details during the surgery, as outlined in 6.3.1 Graphic User Interface (GUI).

6.2.1 Haptic Device

An Entact Robotics W3D haptic device was used to track tool position as well as deliver force and torque feedback. It was customized as described in 3.3.1 Quick-Release Mechanism. It was mounted rigidly to a base that also supported the benchtop tissue model. This allowed for consistent alignment of the virtual and physical environments contained within the simulator.

6.2.2 Benchtop Tissue Model

The benchtop assembly can be seen in Figure 6.2. All components are mounted to a rigid base. The haptic device is placed next to a stereolithography (SLA) 3D printed durable resin L_4L_5 functional spinal unit (FSU). The FSU superior articular process (SAP) joint and intervertebral disc (IVD) are removed, and the haptic response is used to simulate the virtual presence of the missing tissues. The FSU additionally has a calibration port that is used during the procedure. The Polhemus Source, which is essential for the function of the port, is located next to the FSU.

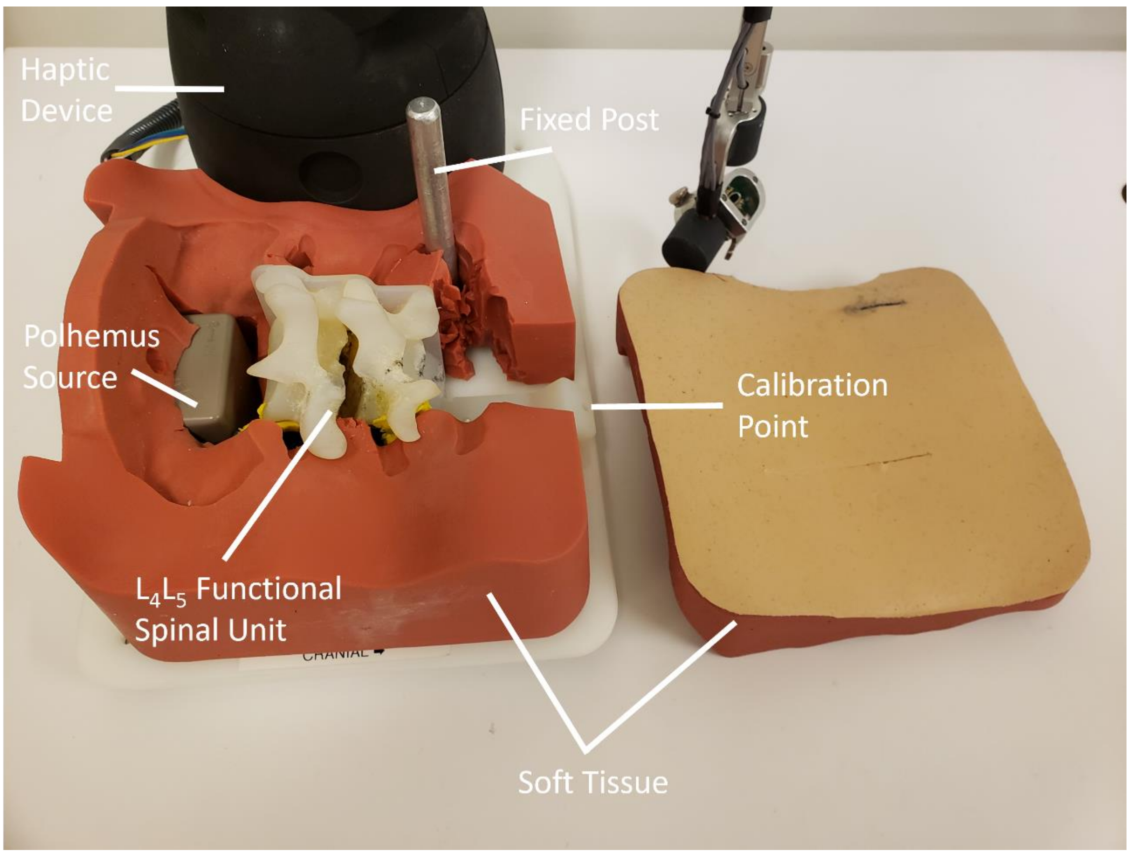

Figure 6.2: Benchtop assembly.

After the Access Gaining step of the procedure, the rest of the surgery was performed through a secured port, similar to that shown in Figure 6.3a. The surgeon could then visualize the procedure using a longitudinally and rotationally adjustable instrument. The position tracking of the port and instrument were both done via a Polhemus PATRIOT™ electromagnetic motion tracker, allowing for live positional updates of the position and orientation during the procedure. A Micro Sensor 1.8™ was embedded within the durable resin SLA 3D printed instrument, as seen Figure 6.3b. The use of metal tools had the potential to cause electromagnetic interference (EMI) during the procedure, but this was not observed for most surgeon trials. Additionally, any EMI distortion would have only caused discrepancies between the physical and virtual components of the simulator where they interfered. With the SAP joint and IVD removed in the physical model, the small amounts of EMI distortion would not be observed until the surgeon contacted the physical FSU, and this was generally not observed.

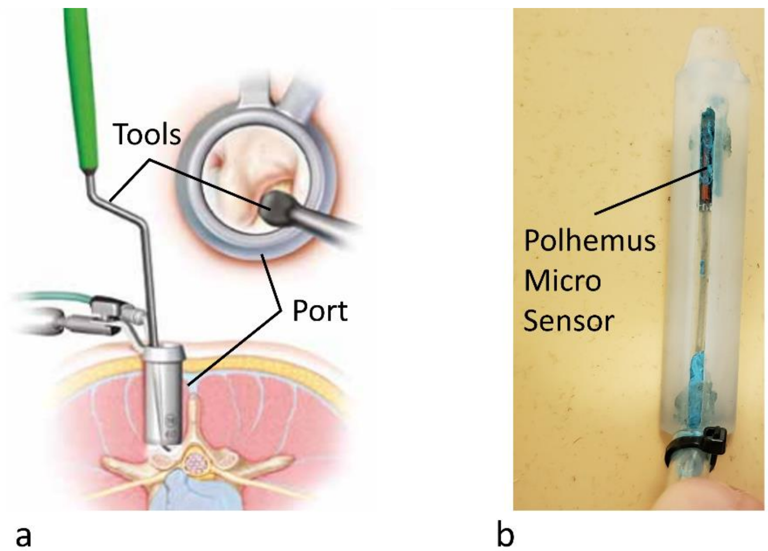

Figure 6.3: Access schematic. a) shows how the port may create the access area for the surgeon [153] *and b) shows the way the Polhemus Micro Sensor was embedded in the adjustable instrument.*

6.2.3 Physical Tools

Multiple tools were used in the simulator, which identified them via the same Teensy board connection style as the haptic torque handle in Chapter 3. The burr tool and an example kerrison are shown in Figure 6.4. They shared a distal shaft to interact with the physical tissue model. The cutting action of the burr tool is controlled by a foot pedal. When the pedal is pressed, a small vibration motor in the tool is activated, causing a buzzing sensation as would normally be experienced during a procedure. They connected to the haptic device via the same quick-release mechanism (QRM) assembly as the Concorde Clear tool, as shown in Figure 3.7 and Figure 3.9. An example tissue retractor is also shown in Figure 6.4.

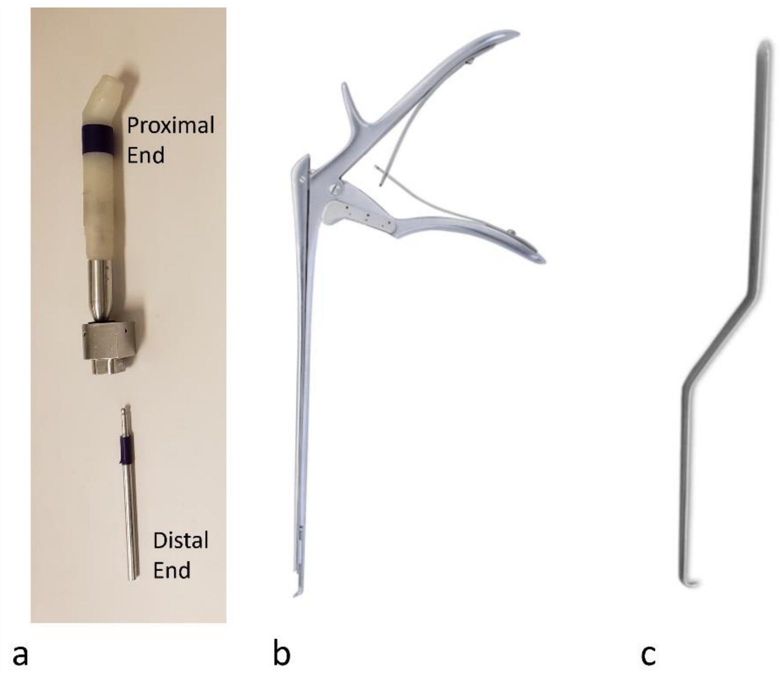

Figure 6.4: Additional tools used in the simulator, including a) the burr tool, b) an example of a kerrison [154], *and c) and example of a retractor* [155].

6.3 Simulator Software

The simulator was run within a custom VR gameplay program from CAE Healthcare. It was modified to the needs of this simulator, including the hardware interactions and gameplay. The software components are discussed here:

6.3.1 Graphic User Interface (GUI)

The GUI enabled the surgeon to interact with the simulator, as shown in Figure 6.5. It was displayed on the two screens in Figure 6.1 and used Qt (Qt Group; Helsinki, Finland) to turn the simulator gameplay into a convenient GUI. The step-specific controls such as view adjustment and calibration were displayed on the left side of screen 1. This screen also contained the VR port view as well as the relevant displayed metrics. If necessary, a tab allowed the surgeon to see instructions on how to perform the surgical step. Screen 2 showed multiple fluoroscopic views for guidance during the surgery, a 3D projected view, surgical step timeline, and general controls. Port views of each of the specific parts of the simulator are in Figure 6.6. The GUI was designed to be adaptable for all surgical steps, therefore the step-specific controls and metrics changed as appropriate for each section of the surgery. To change the difficulty of the simulator, fluoroscopic and 3D views could be removed. Additional troubleshooting and safety limits were also built into the GUI.

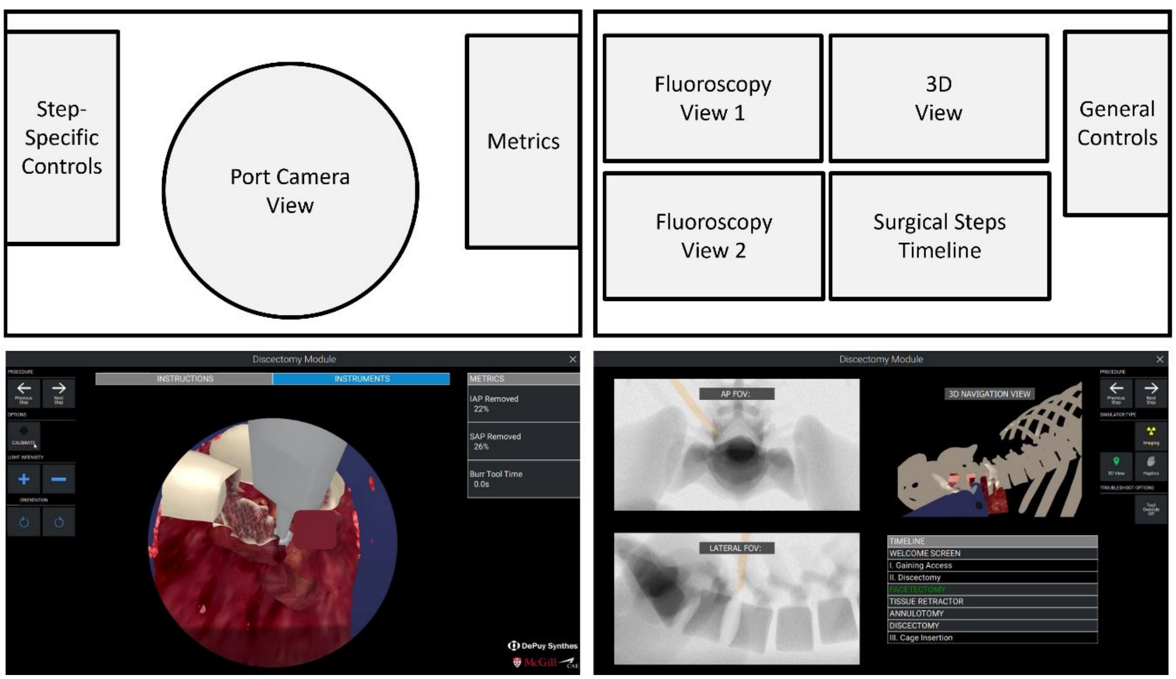

Figure 6.5: Graphic User Interface (GUI) components outlined and displayed on the two screens.

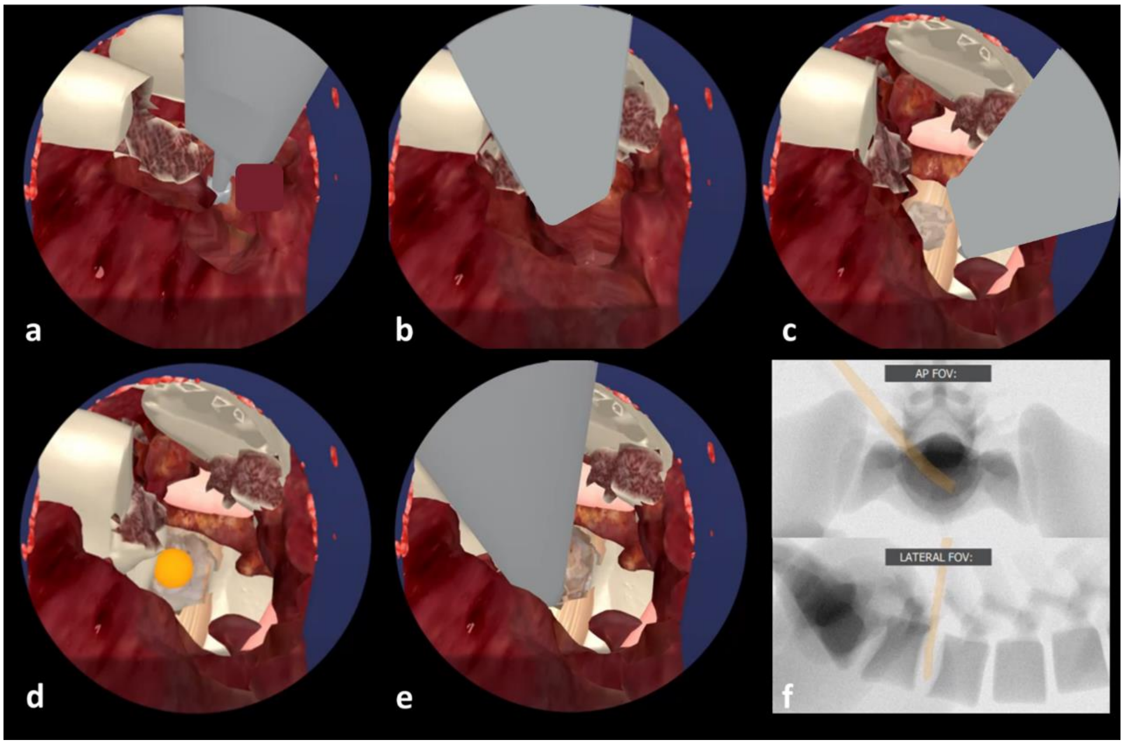

Figure 6.6: Each of the steps of the discectomy in order. a) facetectomy (burr tool), b) facetectomy (kerrison), c) tissue retractor, d) annulotomy (orange ball indicating annulotomy size), e) discectomy (Concorde Clear) and f) Discectomy (fluoroscopy view).

6.3.2 Virtual Tools

It was necessary to create VR models (Figure 6.7) to match the physical ones shown in Figure 3.7 and Figure 6.4. These models were adapted from computer-aided design (CAD) models provided by DePuy Synthes. They were integrated into the VR simulator and linked to the motion of the haptic device. Sound present during the procedure was adapted from different sources. The burr tool sounds were taken from the use of an actual burr tool cutting through tissue. The Concorde Clear sound was adapted from a dental suction recording. To enable interactions in the gameplay, contact collision objects were added to each of the tools, as shown in Figure 6.8. The interactions are discussed further in the following section.

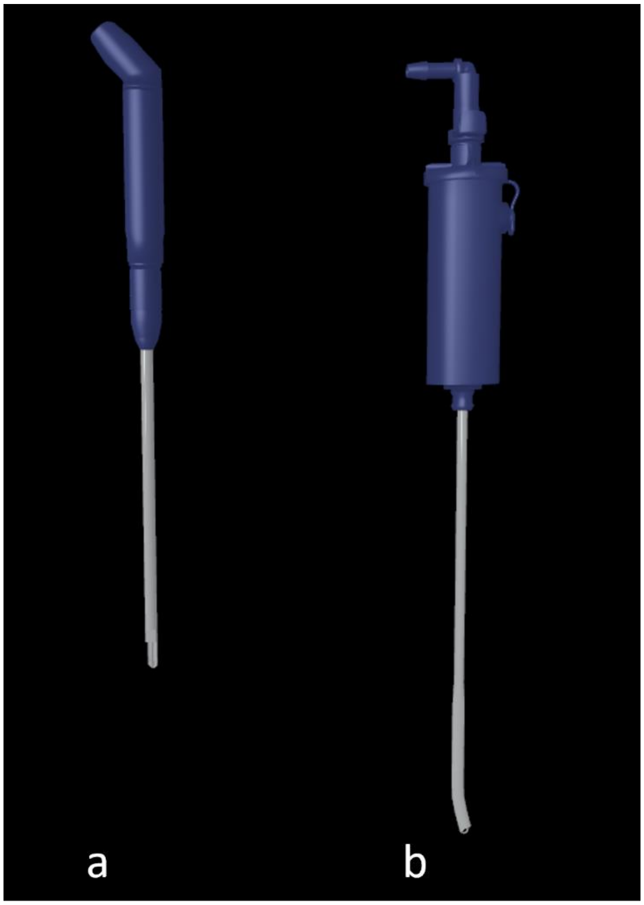

Figure 6.7: Virtual reality (VR) computer-aided design (CAD) models of the a) burr tool and b) Concorde Clear discectomy surgical tools.

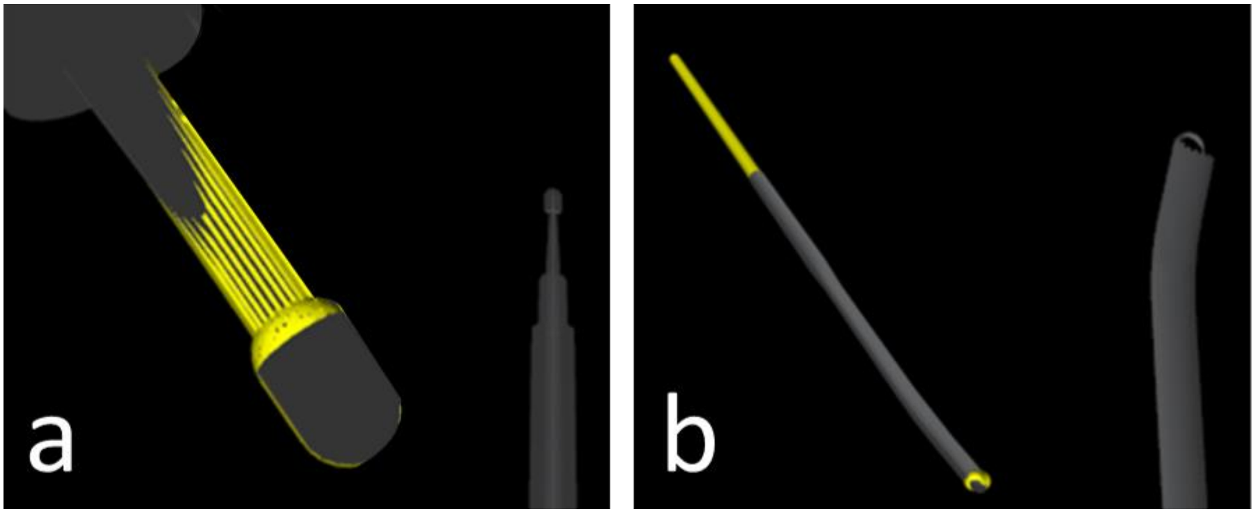

Figure 6.8: Discectomy tool tips with collision objects and side profiles shown in the order that they appear: a) burr tool and d) Concorde Clear.

6.3.3 Tissue Mesh and Interactions

Mimicking the soft-tissue interactions in the body was a key point of research in the simulator. The anatomical features and dimensions were based on magnetic resonance images (MRI) of a 22-year-old Japanese male with a weight of 65 kg and height of 173 cm. acquired from 3DBodyParts. They were adapted slightly for the simulator as discussed in previous work [156]. While the benchtop tissue model shown in Figure 6.2 provided physical interactions with the distal ends of the surgical tools, they were augmented with the haptic device. The IVD components, L_4 inferior articular process (IAP), L_5 SAP, and overlying muscles were not included in the benchtop tissue model and therefore were simulated. The final version of the simulated tissues is shown in Figure 6.9. The underlying meshing can be seen in Figure 6.9b. The effect of mesh tetrahedral size and visual texture changes can be seen in Figure 6.10. The finite element model (FEM) with a total Lagrangian explicit dynamic (TLED) algorithm solver was used with the computer graphics processing unit (GPU) via CUDA to provide real-time feedback. The meshes were made as fine as possible to still deliver live updates. One example of the simulator data indicated a visual operating frequency of 23±4 Hz. The haptics were run in parallel to give faster feedback, at 950±180 Hz for the same section of the simulator. The gameplay speed was adequate for all testing.

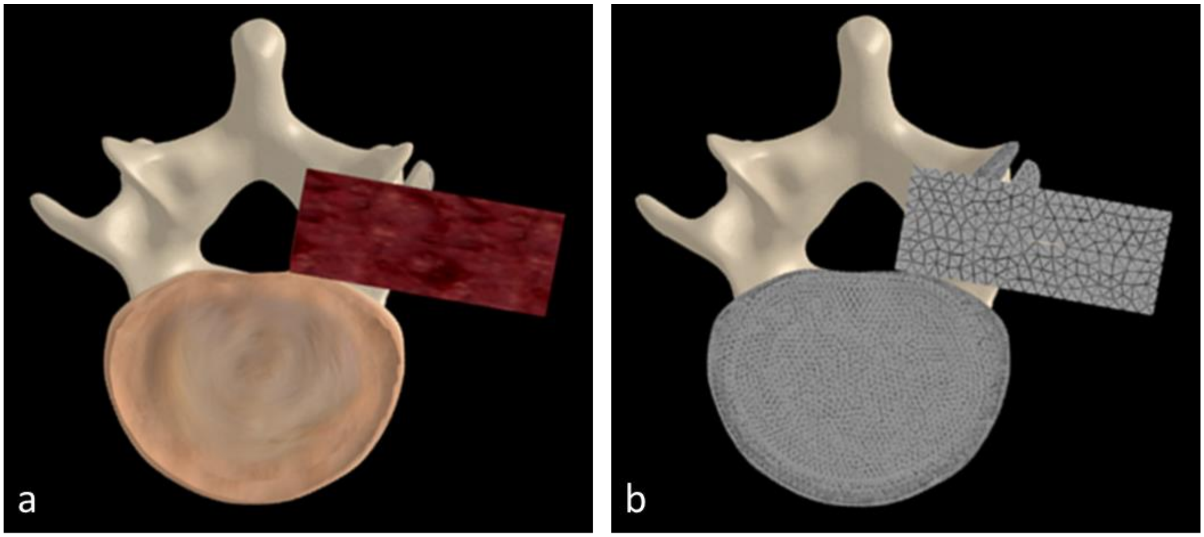

Figure 6.9: Final version of the soft tissues and L_4 vertebra is visible in a), and the simulated tissue meshes are shown in b).

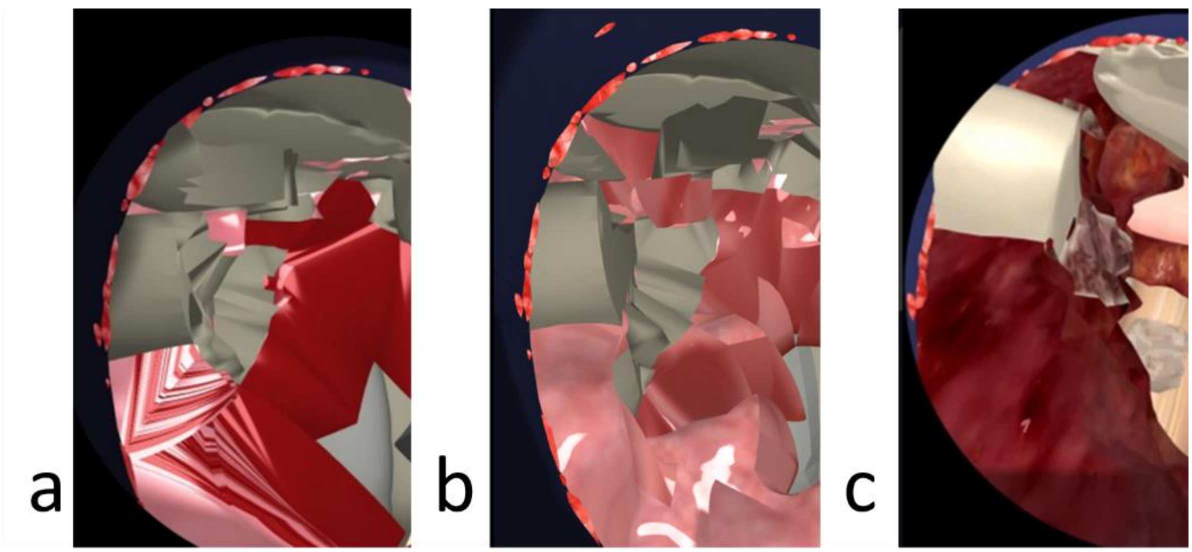

Figure 6.10: Mesh updates throughout development. a) shows a larger mesh size with less refined textures, b) shows the final mesh with 1 mm bone and 2 mm muscle tetrahedron sizes but an incomplete texture, and c) shows the final mesh size and texture.

6.3.4 Gameplay

To make all the surgical steps work together, the simulator operation was broken into many scripts, programmed in Lua. Each of them and their functions are shown in Table 6.2. The surgeon is then able to proceed through the simulator with the GUI described.

Table 6.2: Scripts used in the virtual reality (VR) simulator.

Lua Scripts Common to All Scenes	
Data	Generates all variables and metrics
Gameplay	Controls triggers and events
GUI	Controls feedback to the GUI, updates visuals for each scene, and performs tool identification
Metrics	Tracks metrics
REDACTED	REDACTED
Port	Gives port parameters
Serialize	Communication for ComputeForce to EntactComponent
GlobalFunctions	Contains functions used my other scripts (such as tissue identification and removal tracking)
SendMusclePunctures	Records tissue killed so it can be applied in subsequent scene volumetric mesh for continuity
Lua Scripts Unique to Discectomy	
BurrTool	Controls simulator logic and flow particular to the Burr Tool operation
ConcordeTool	Controls simulator logic and flow particular to the Concorde Clear Tool operation
REDACTED	Controls simulator logic and flow particular to the kerrison operation
computeForce	Controls and records the haptic force/torque output of the scene. This is currently separate for each scene.

6.4 Simulator Haptic Feedback

The haptic feedback for the Concorde Clear tool was outlined in 4.3.5 Simulator Force and Torque Profiles. However, the haptic device was unable to deliver the peak force output measured in cadaveric testing and was scaled down. Increasing the force experienced by the surgeon was originally intended to be accomplished by attaching a rubberized tip to the Concorde Clear distal shaft. This would increase friction between the tool and the benchtop tissue model. This was not used in the final simulator version, but it would be possible in the future to use the freehand tools from Chapter 5 to measure the force during procedures with and without various distal tips. This could augment the haptic device capabilities to give the simulator increased force output.

The burr tool and kerrison tools did not have cadaveric testing to inform the haptic response. Contact-based methods were used to generate forces from the FEM tissue. When the collision objects in Figure 6.8 interacted with the FEM tissue, the number of contacts, average contact depth, and average normal contact direction were calculated for both bone and soft tissue contacts. Then these parameters were used to create a haptic force output, using Hooke’s law as outlined in Equation 2.2, that increased as total penetration and contact area increased. The haptic output was scaled to provide adequate differentiation between tissue and bone contact. Coriolis forces were not considered due to the small mass of the oscillating tool components.

Some small modifications still had to be made to accomplish stability in the haptic device. A new closed-loop control system was developed. Haptics were run in parallel to the simulator visuals to help increase the frame rate. They were updated as often as possible by the slower gameplay. When updated, a force and torque smoothing algorithm was used to prevent large changes in force and torque. This resulted in a smooth, controlled force and torque profile. An example of this is shown in Figure 6.11, where the time is approximate and assumes that each data point is collected at 1000 Hz.

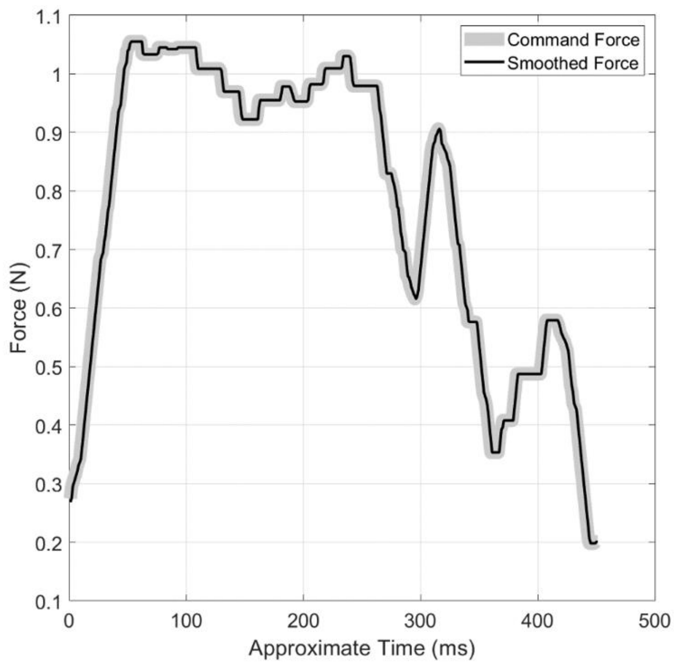

Figure 6.11: Smoothed force profile. The time is estimated for a refresh rate of 1000 Hz.

6.5 Surgeon Study

The simulator was finally brought to surgeons for their evaluation. All testing was done according to the ethical approvals laid out in IRB A03-M15-20A, which can be found in Appendix II. A preliminary trial of seven experienced spine surgeons was performed first. These surgeons performed the exact procedure on a cadaver and then used the simulator. Afterward, they filled out the same 1-5 Likert scale questionnaire in Chapters 3 and 5. Later, 22 additional orthopedic and neurosurgeons used the simulator without a cadaveric trial. The full list of questions and results relevant to the discectomy steps and general simulator are shown in Table IV.1 to Table IV.4. All but one of the general questions had average responses greater than 3. The answers from the discectomy and annulotomy steps are similar. Only the facetectomy step forces, maneuverability, and tools were considered inadequate, in addition to the sections of the study discussed earlier in the manuscript. Interestingly, soft tissue and bone forces for the burr tool (2.3±1.1 and 2.4±1.1, respectively) and kerrison (1.6±0.5 and 1.8±0.8, respectively) received scores under 3. The haptic torque handle forces and torques, while higher, were rated 2.8±1.1 and 2.9±1.1, respectively.

6.6 Discussion

The work presented in this chapter outline the full integration of the tested data. The surgeon questionnaire validated the simulator was a successful representation of the surgery. The fact that all but one of the general questions had responses greater than 3 indicated the overall functionality and use of the simulator were accurate. The burr tool and kerrison haptics were ranked lower than the haptic torque handle (Concorde Clear), the only component in the discectomy portion of the simulator that was informed by cadaveric testing. This indicated that even though all haptic feedback was rated as inadequate, physics-based cadaveric testing may have contributed to the more highly rated haptic feedback. Therefore, cadaveric testing should be considered in developing future haptic simulators.

6.7 Conclusion

This chapter explored the final integration of Chapters 3, 4, and 5as well as new components into the final surgical simulator. The cadaveric testing and novel haptic torque handle informed and delivered haptic feedback, respectively. Additional physical and virtual models were used to create the VR environment to run in real-time. Finally, surgeons evaluated the simulator and found it to be a good representation of the minimally invasive transforaminal lumbar interbody fusion (MI-TLIF) procedure. The use of physics-based haptic models appeared to be essential in developing the simulator haptics. The full simulator represents a new and exciting platform to train new spine surgeons.

7
General Discussion

The work presented here was all done within the context of developing a virtual reality (VR) simulator. Each objective had a particular relevance to this end goal. The work from each objective further contributed to the body of knowledge in its given field.

In Objective 1, a new haptic torque handle design was conceived and created. It was discovered that a direct current (DC) motor was an appropriate torque delivery method, as evidenced in its ability to match the biomechanical models. It delivers greater torque in a more self-contained package than comparable devices [82,85,94]. The reason for inadequate results in terms of torque feedback from the surgeon questionnaire could be due to the haptic rendering itself, not the capability of the haptic torque handle to match the model. Torque dissatisfaction may have been coupled with the surgeons' association of the force and torque in the same device. The torque modeled matched the cadaveric data, but the force was scaled down significantly to match the capabilities of the haptic device. While it is established that adding additional degrees of freedom (DOF) can improve simulation, perhaps this implementation was hindered by using a limited force model [88]. Using torque intentionally to augment force by rendering surface textures, as has been shown previously, could be a way to improve feedback while accommodating force limitations [76]. Developing the haptic torque handle to augment existing haptic devices also enhances the knowledge base on adaptable haptic interfaces, something that software seeks to accommodate as well [93]. Despite the work that went into determining the appropriate motor and torque for the device, electromagnetic interference (EMI) proved to be a major concern. Designing robust systems with reliable electrical connections and appropriate EMI shielding should be considered when creating future haptics, or more advanced established filtering systems could be used [157]. Though the final haptic torque handle looked and weighed differently than the Concorde Clear tool it imitated, those two factors did not appear to detract from the immersiveness of the simulator. It was imperative to keep the dimensions similar, so it felt like the surgeon was grasping the Concorde Clear tool, but the looks were less important. In general, it appears that replicating the dimensions and torque response of the real surgical tool are adequate when designing a simulator tool. The evaluation of an individual tool within a complex multi-tool simulator represents a step forward in detail from established validation that focuses on face, content, and construct validity of the overall simulator [45,46]. This objective generally addressed and confirmed Hypothesis 1. While the specific programmed feedback of the haptic torque handle, informed by cadaveric testing, was considered insufficient by the surgeons studied (<3 on the questionnaire), the overall size, functionality, and maneuverability were adequate (≥3). Additionally, the device was able to accommodate and exceed the necessary torque range needed for the procedure. Future refinements to feedback modeling with the current haptic torque handle may be sufficient to fully support Hypothesis 1.

For Objective 2, a few key factors appeared that would impact force and torque present during lumbar discectomy. The aggregated quadratic models of linear and torsional resistance integrated into the simulator considered tool depth and the amount of tissue removed when updating feedback over the course of a discectomy. These factors had an impact that surpassed the just-noticeable difference (JND) of 7%. However, the surgeons still rated the haptics as inadequate, likely due to the significant downscaling of the force output. Allowing the cadaveric torsos to compress during testing as they would during a real surgery was a key differentiator from many traditional biomechanical studies. This reduced the understanding of the specific intervertebral disc (IVD) mechanics but provided data that more closely mimicked the conditions found in an operating room, which was the intent of the testing and entire simulator. Additionally, this data, especially the peak force and torque values, can now be to aid in the design of future discectomy tools. The study used an aggregated force and torque assumption to simplify measurement for haptic feedback based on established modeling [120]. The 7% JND, taken from existing literature, may not reflect the reality of surgeons. Training and the addition of visual feedback have both been found to impact JND, which is supported by studies that found surgeon forces are dependent on training level [46,69,158]. Future iterations of the simulator should consider tool speed as well as physiological and lumbar level differences, as these were also determined to have a significant impact on resistance while also exceeding the JND. This objective successfully addressed Hypothesis 2. The spinal level was found not to impact force or linear resistance, but it did affect torque and torsional resistance. The amount of tissue removed, as evidenced by comparing initial and later passes through the tissue, was confirmed for all measurements. The later passes through the tissue were not statistically different, indicating that the initial cutting force or torque, as shown in Equation 2.6 does play a significant role in the evolution of the test specimen.

Objective 3 further expanded on the results presented with a novel freehand tissue testing device. While cadaveric compression was previously allowed in order to mimic the operating conditions, this objective added surgeon flexibility to extend the surgical relevance. The haptic device and haptic torque handle combined could deliver 4-DOF output, and therefore it was important to measure force in a similarly multiaxial way, with a tool modeled after the Concorde Clear tool geometry. The results showed the necessity of considering off-axis forces, as they made a large contribution to the total force measurement. The inclusion of multiple specimen types also showed that excised spine and intact torsos had similar resistances when subjected to the controlled method. This is significant because while it has long been established that the inclusion of adjacent tissues in testing increases spine stiffness, the inclusion of the entire torso to mimic the movement and compression of a patient in the operating room may negate this effect [97,159]. Therefore, testing done with the intent of building haptic feedback modeling can be performed on both a fully excised spine with most of the tissue removed or an intact torso, with statistically similar resistance results. This supports the work performed in Objective 2, where the entire torso was used for testing and generation of force and torque haptic feedback profiles. While it was statistically insignificant, the observed trend of decreasing resistance with increasing tool speed supports existing tool puncture studies [113,119]. It is possible that in the work presented here, the Concorde Clear tip, being less pointed than a needle often used in similar studies, forced much of the resistance to be caused by tissue stiffness and friction, rather than cutting [113,119,120]. The off-axis forces measured during testing provide more insight. These x-y forces impact the frictional force in the z-axis, and their increased magnitude at increased total resultant force magnitudes may be a significant contributing factor to the higher total force. Additionally, the variability between surgeons as measured with the freehand testing device could be further studied to gain insights into how different surgeons operate and the resulting forces they impart on a patient. The decrease in force at the end of penetration could be an intentional movement to reduce the likelihood of a dangerous distal annular puncture.

Comparisons between surgeon behaviors, such as total force application or this protective movement, could be done in a similar way to existing simulator construct validity tests to determine surgeon proficiency [39,41]. The testing of the device here shows how it can be used in the future to measure other biomechanical properties. It could be used to understand how surgeons contact the physical parts of the simulator, knowledge that could perhaps influence haptic device design to tune the physical distal tip interactions. This same information could be used to inform the next generation of smart tools designed to help surgeons and protect patients [133,134]. Critically, Hypothesis 3 was confirmed by this objective. A new testing device was built and tested to find a significant difference between freehand and controlled biomechanical test methods. The final simulator incorporated the objective results with additional developments. Interestingly, many of the low scoring aspects of the surgeon survey were from haptics that were not informed by cadaveric testing. While surgeons found much of the simulator to be an accurate representation of surgery, haptics were generally inadequate. However, the haptics informed by cadaveric testing were rated higher than other modeling, indicating the necessity of using testing to build haptic feedback models. Crucially, the results of the survey showed that this benchtop simulator as a whole was an accurate way to train surgeons.

While this work encompassed a broad range of topics associated with developing a haptic surgical simulator, there were nonetheless limitations to its scope. The haptic torque handle was found to accurately mimic the Concorde Clear, but there are limitations to their resemblance. The haptic torque handle has more mass and therefore increased inertia when moving the device. Even when connected to the Entact W3D haptic device, it cannot robotically replicate bending moments that may occur during the procedure. The distal tip of the tool was built to help alleviate this issue by providing physical contact with the simulator. This has improved the realism of the haptic torque handle in simulation, but it is still short of the full procedural experience. The biomechanical testing also had some shortcomings. The tool speeds required to safely use the mechanical tester were much slower than those observed in the freehand study. This could be improved by testing smaller, better characterized samples that would allow for safer mechanical tester operating speeds, but the decision to use intact torsos was done to ensure operating room similarity. More testing at various speeds could result in better characterization of the time-dependent viscoelastic properties of the IVD during puncturing, similar to what has been done in the past [113,119]. Additional investigations into the response of the entire torso mechanical response at different speeds could better quantify its viscoelastic properties during discectomy. The inherent variability in biological samples also likely played a critical role in all biomechanical tests. Preservation, age, and general health all have known impacts on IVDs [2,160,161]. Increasing the number of specimens tested or finding more similar specimens could have improved the statistical power of the studies. This would have further helped quantify the force required during initial versus later passes through the tissue, which could have helped build more detailed models for haptic response to repeated tissue removal. Tailoring the testing to the specific demographic targeted by the simulator is another logical next step. Testing exclusively on specimens with degenerated discs would focus the haptic modeling on those most likely to receive a minimally invasive lumbar interbody fusion (MI-LIF) procedure for low back pain [20]. The freehand testing performed would similarly benefit from larger samples, presenting an interesting way to compare surgeons. Increased sampling rates could also improve the data collected by the device during testing, in turn improving future haptic feedback or tool design.

Finally, improved surgeon study design through the inclusion of more cadaveric or preliminary training could impact the questionnaire results.

The combination of the three objectives in building the simulator has resulted in a realistic, but not perfect simulator. Size and technological limitations prevent the simulator from delivering an experience as immersive as the operating room. The surgeons still understand they are using a simulator based on the small benchtop model, haptic device, and screens used to display metrics. Improvements such as incorporating the tissue models into a finite element model (FEM) for haptic response rather than using resistance should be a key focus in future development. This would help sync visual and haptic realism, as well as enable rapid tuning of the model to different tissue parameters as needed. This work nonetheless presents a step forward in the field of haptic surgical simulation.

In summary, the objectives and work presented here accomplished the goal of creating a physics-based simulator for training surgeons. The haptic device, coupled to the haptic torque handle with a DC motor, was informed by cadaveric testing and was evaluated more favorably than haptics not based on tissue testing. The haptic response was normalized for tool depth and the amount of tissue removed, while future iterations should consider tool speed and off-axis forces, informed by freehand testing on cadaveric torso or spine samples, during the procedure. Each objective was combined with extensive development of the FEM visuals, gameplay, and hardware integration to give an immersive experience. Future testing will be done to evaluate the efficacy of the simulator in surgical training of a TLIF procedure. Hopefully, training on this simulator will enable surgeons around the world to learn or improve their skills so they are prepared to enter the operating room, resulting in improved patient outcomes.

8
Conclusion

The global objective of designing a virtual reality (VR) simulator to deliver haptic feedback to teach surgeons discectomy was accomplished. The three objectives each contributed to the simulator in addition to augmenting the body of knowledge in haptic robotics, surgery biomechanics, and mechanical testing.

Objective 1 detailed the conception, construction, and testing of a novel tool. The haptic torque handle was successfully built and used in the VR simulator to mimic the Concorde Clear tool during lumbar discectomy. Surgeons found that it delivered appropriate force and torque to replicate the procedure. It is the first tool-free engageable uniaxial self-contained robotic haptic torque handle for surgical simulation and is an exciting new step in the field of augmentable haptic devices.

Objective 2 outlined the cadaveric testing performed to imitate lumbar discectomy with the Concorde Clear tool. This data was used to build appropriate force and torque profiles for the VR simulator that could vary based on multiple factors. The accuracy of loading profiles was validated by surgeons who tested the VR simulator. This is the first biomechanical characterization and simulator implementation of lumbar discectomy with the Concorde Clear tool. The techniques shown here can be applied in other contexts to understand the biomechanics that surgeons encounter during a procedure.

Objective 3 incorporated robotics and tissue testing components of the first two objectives into a novel piece of equipment for the testing of tissues in a surgically relevant matter. This apparatus allowed the surgeon to perform a procedure as they normally would while monitoring the position and load of the tool. Data acquired during testing of this device was then compared and contrasted with that of Objective 2, to understand how traditional and novel tissue testing techniques could be used to build surgical simulators. This is the first example of a 6-degree of freedom (DOF) position and load measuring device used in biomechanical testing for discectomy. This work bridges the gap between biomechanists and surgeons. Often, it is difficult or impossible to perform biomechanical tasting in a way that is relevant to surgery, but this work shows how this can successfully be done.

Finally, aspects of each of the objectives outlined were incorporated to create the VR surgical simulator. This simulator contained additional hardware and software features to replicate a full surgical procedure. This included gameplay, user interfaces, soft tissue finite element model (FEM) visuals, additional tools, and extra surgical steps. Surgeons operating on the simulator generally found it to be an accurate representation of discectomy during a transforaminal lumbar interbody fusion (TLIF) procedure. The enormous complexity of the simulator and the substantial work put in by a dedicated team of talented interdisciplinary researchers, engineers, educators, and surgeons shows the current state of the art in haptic surgical simulation.

The three objectives combined to create a novel physics-based surgical simulator capable of accurately replicating lumbar discectomy. Twenty-nine surgeons have already used the simulator, and with time it will hopefully be used to train surgeons around the world to perform safer, more effective surgeries. The true end goal of this work is to improve the surgical outcomes and lives of patients. Between the work presented here and further progress that will inevitably develop and refine it, patient care around the world will continue to improve.

References

[1] GlobalData MediPoint, 2014, *Spinal Fusion - Global Analysis and Market Forecasts*, London.

[2] Newell, N., Little, J., Christou, A., Adams, M., Adam, C., and Masouros, S., 2017, "Biomechanics of the Human Intervertebral Disc: A Review of Testing Techniques and Results," Journal of the Mechanical Behavior of Biomedical Materials, **69**, pp. 420–434 DOI: 10.1016/j.jmbbm.2017.01.037.

[3] Denard, P., Holton, K., Miller, J., Fink, H., Kado, D., Yoo, J., and Marshall, L., 2010, "Lumbar Spondylolisthesis among Elderly Men: Prevalence, Correlates and Progression," Spine, **35**(10), pp. 1072–1078 DOI: 10.1097/BRS.0b013e3181bd9e19.

[4] Giers, M., Munter, B., Eyster, K., Ide, G., Newcomb, A., Lehrman, J., Belykh, E., Byvaltsev, V., Kelly, B., Preul, M., and Theodore, N., 2017, "Biomechanical and Endplate Effects on Nutrient Transport in the Intervertebral Disc," World Neurosurgery, **99**, pp. 395–402 DOI: 10.1016/j.wneu.2016.12.041.

[5] Soukane, D., Shirazi-Adl, A., and Urban, J., 2005, "Analysis of Nonlinear Coupled Diffusion of Oxygen and Lactic Acid in Intervertebral Discs," Journal of Biomechanical Engineering, **127**(7), pp. 1121–1126 DOI: 10.1115/1.2073674.

[6] Jackson, A., Huang, C., Brown, M., and Yong Gu, W., 2011, "3D Finite Element Analysis of Nutrient Distributions and Cell Viability in the Intervertebral Disc: Effects of Deformation and Degeneration," Journal of Biomechanical Engineering, **133**(9), p. 091006 DOI: 10.1115/1.4004944.

[7] Roberts, S., Menage, J., and Urban, J., 1989, "Biochemical and Structural Properties of the Cartilage End-Plate and Its Relation to the Intervertebral Disc," Spine, **14**(2), pp. 166–174 DOI: 10.1097/00007632-198902000-00005.

[8] Dowdell, J., Erwin, M., Choma, T., Vaccaro, A., Iatridis, J., and Cho, S., 2017, "Intervertebral Disk Degeneration and Repair," Clinical Neurosurgery, **80**(Suppl 3), pp. S46-54 DOI: 10.1093/neuros/nyw078.

[9] Bernick, S., and Cailliet, R., 1982, "Vertebral End-Plate Changes With Aging of Human Vertebrae," Spine, **7**(2), pp. 97–102 DOI: 10.1097/00007632-198203000-00002.

[10] Gullbrand, S., Peterson, J., Ahlborn, J., Mastropolo, R., Fricker, A., Roberts, T., Abousayed, M., Lawrence, J., Glennon, J., and Ledet, E., 2015, "Dynamic Loading–Induced Convective Transport Enhances Intervertebral Disc Nutrition," Spine, **40**(15), pp. 1158–1164 DOI: 10.1097/BRS.0000000000001012.

[11] Adams, P., Eyre, D., and Muir, H., 1977, "Biochemical Aspects of Development and Ageing of Human Lumbar Intervertebral Discs," Rheumatology, **16**(1), pp. 22–29 DOI: 10.1093/rheumatology/16.1.22.

[12] Antoniou, J., Steffen, T., Nelson, F., Winterbottom, N., Hollander, A., Poole, R., Aebi, M., and Alini, M., 1996, "The Human Lumbar Intervertebral Disc: Evidence for Changes in the Biosynthesis and Denaturation of the Extracellular Matrix with Growth, Maturation, Ageing, and Degeneration," Journal of Clinical Investigation, **98**(4), pp. 996–1003 DOI: 10.1172/JCI118884.

[13] Buckwalter, J., 1995, "Aging and Degeneration of the Human Intervertebral Disc," Spine, **20**(11), pp. 1307–1314 DOI: 10.1097/00007632-199506000-00022.

[14] Mikawa, Y., Hamagami, H., Shikata, J., and Yamamuro, T., 1986, "Elastin in the Human Intervertebral Disk: A Histological and Biochemical Study Comparing It with Elastin in the Human Yellow Ligament," Archives of Orthopaedic and Traumatic Surgery, **105**(6), pp. 343–349 DOI: 10.1007/BF00449940.

[15] Yu, J., Fairbank, J., Roberts, S., and Urban, J., 2005, "The Elastic Fiber Network of the Anulus Fibrosus of the Normal and Scoliotic Human Intervertebral Disc," Spine, **30**(16), pp. 1815–1820 DOI: 10.1097/01.brs.0000173899.97415.5b.

[16] Cassidy, J., Hiltner, A., and Baer, E., 1989, "Hierarchical Structure of the Intervertebral Disc," Connective Tissue Research, **23**(1), pp. 75–88 DOI: 10.3109/03008208909103905.

[17] Pooni, J., Hukins, D., Harris, P., Hilton, R., and Davies, K., 1986, “Comparison of the Structure of Human Intervertebral Discs in the Cervical, Thoracic and Lumbar Regions of the Spine,” Surgical and Radiologic Anatomy, **8**(3), pp. 175–182 DOI: 10.1007/BF02427846.

[18] McNally, D., and Adams, M., 1992, “Internal Intervertebral Disc Mechanics as Revealed by Stress Profilometry,” Spine, **17**(1), pp. 66–73 DOI: 10.1097/00007632-199201000-00011.

[19] Iatridis, J., Weidenbaum, M., Setton, L., and Mow, C., 1996, “Is the Nucleus Pulposus a Solid or a Fluid? Mechanical Behaviors of the Nucleus Pulposus of the Human Intervertebral Disc,” Spine, **21**(10), pp. 1174–1184 DOI: 10.1097/00007632-199605150-00009.

[20] Mobbs, R., Phan, K., Malham, G., Seex, K., and Rao, P., 2015, “Lumbar Interbody Fusion: Techniques, Indications and Comparison of Interbody Fusion Options Including PLIF, TLIF, MI-TLIF, OLIF/ATP, LLIF and ALIF.,” Journal of Spine Surgery, **1**(1), pp. 2–18 DOI: 10.3978/j.issn.2414-469X.2015.10.05. ISBN: 2414-469X (Print) 2414-4630.

[21] Dickson, I., Happey, F., Pearson, C., Naylor, A., and Turner, R., 1967, “Variations in the Protein Components of Human Intervertebral Disk with Age,” Nature, **215**, pp. 52–53 DOI: 10.1038/215052a0.

[22] Sato, K., Kikuchi, S., and Yonezawa, T., 1999, “In Vivo Intradiscal Pressure Measurement in Healthy Individuals and in Patients With Ongoing Back Problems,” Spine, **24**(23), pp. 2468–2474 DOI: 10.1097/00007632-199912010-00008.

[23] Kraemer, J., Kolditz, D., and Gowin, R., 1985, “Water and Electrolyte Content of Human Intervertebral Discs Under Variable Load,” Spine, **10**(1), pp. 69–71 DOI: 10.1097/00007632-198501000-00011.

[24] Iatridis, J., Setton, L., Foster, R., Rawlins, B., Weidenbaum, M., and Mow, V., 1998, “Degeneration Affects the Anisotropic and Nonlinear Behaviors of Human Anulus Fibrosus in Compression,” Journal of Biomechanics, **31**(6), pp. 535–544 DOI: 10.1016/S0021-9290(98)00046-3.

[25] O’Connell, G., Guerin, H., and Elliott, D., 2010, “Theoretical and Uniaxial Experimental Evaluation of Human Annulus Fibrosus Degeneration,” Journal of Biomechanical Engineering, **131**(11), pp. 111007: 1–7 DOI: 10.1115/1.3212104.

[26] Nachemson, A., 1965, “The Effect of Forward Leaning on Lumbar Intradiscal Pressure,” Acta Orthopaedica Scandinavica, **35**(1–4), pp. 314–328 DOI: 10.3109/17453676508989362.

[27] Cheung, K., Karppinen, J., Chan, D., Ho, D., Song, Y., Sham, P., Cheah, K., Leong, J., and Luk, K., 2009, “Prevalence and Pattern of Lumbar Magnetic Resonance Imaging Changes in a Population Study of One Thousand Forty-Three Individuals,” Spine, **34**(9), pp. 934–940 DOI: 10.1097/BRS.0b013e3181a01b3f.

[28] Mo, F., Yuan, P., Araghi, A., and Serhan, H., 2018, “Time Savings and Related Economic Benefits of Suction-Curette Device for Transforaminal Lumbar Interbody Fusion Discectomy,” International Journal of Spine Surgery, **12**(5), pp. 582–586 DOI: 10.14444/5071.

[29] Depuy Synthes Inc, 2017, *CONCORDE^TM Clear MIS Discectomy Device*.

[30] Wang, M., Lerner, J., Lesko, J., and McGirt, M., 2012, “Acute Hospital Costs after Minimally Invasive Versus Open Lumbar Interbody Fusion: Data From a US National Database With 6106 Patients,” Journal of Spinal Disorders and Techniques, **25**(6), pp. 324–328 DOI: 10.1097/BSD.0b013e318220be32.

[31] Kambin, P., and Sampson, S., 1986, “Posterolateral Percutaneous Suction-Excision of Herniated Lumbar Intervertebral Discs: Report of Interim Results,” Clinical Orthopaedics and Related Research, **207**, pp. 37–43.

[32] Hoshide, R., Feldman, E., and Taylor, W., 2016, “Cadaveric Analysis of the Kambin’s Triangle,” Cureus, **8**(2), p. e475: 1-8 DOI: 10.7759/cureus.475.

[33] Wang, H., Huang, B., Li, C., Zhang, Z., Wang, J., Zheng, W., and Zhou, Y., 2013, “Learning Curve for Percutaneous Endoscopic Lumbar Discectomy Depending on the Surgeon’s Training Level of Minimally Invasive Spine Surgery,” Clinical Neurology and Neurosurgery, **115**(10), pp. 1987–1991 DOI: 10.1016/j.clineuro.2013.06.008. ISBN: 1872-6968 (Electronic)r0303-8467 (Linking).

[34] Kopta, J., 1971, “The Development of Motor Skills in Orthopaedic Education,” Clinical Orthopaedics and Related Research, **75**, pp. 80–85 DOI: 10.1097/00003086-197103000-00011.

[35] Bugdadi, A., Sawaya, R., Bajunaid, K., Olwi, D., Winkler-Schwartz, A., Ledwos, N., Marwa, I., Alsideiri, G., Sabbagh, A., Alotaibi, F., Al-Zhrani, G., and Del Maestro, R., 2019, "Is Virtual Reality Surgical Performance Influenced by Force Feedback Device Utilized?," Journal of Surgical Education, **76**(1), pp. 262–273 DOI: 10.1016/j.jsurg.2018.06.012.

[36] Reid, L., 1965, *The Design of a Facility for the Measure of Human Pilot Dynamics*.

[37] F1 Chronicle, "How Does A Formula 1 Simulator Work?" [Online]. Available: https://f1chronicle.com/how-does-a-formula-1-simulator-work-f1-technology/. [Accessed: 08-Sep-2021].

[38] Federal Aviation Administration, "National Simulator Program (NSP)" [Online]. Available: https://www.faa.gov/about/initiatives/nsp/. [Accessed: 08-Sep-2021].

[39] Winkler-Schwartz, A., Yilmaz, R., Mirchi, N., Bissonnette, V., Ledwos, N., Siyar, S., Azarnoush, H., Karlik, B., and Del Maestro, R., 2019, "Machine Learning Identification of Surgical and Operative Factors Associated With Surgical Expertise in Virtual Reality Simulation," JAMA Network Open, **2**(8), pp. e198363, 1–16 DOI: 10.1001/jamanetworkopen.2019.8363.

[40] Cueto, E., and Chinesta, F., 2014, "Real Time Simulation for Computational Surgery: A Review," Advanced Modeling and Simulation in Engineering Sciences, **1**(11), pp. 1–18 DOI: 10.1186/2213-7467-1-11.

[41] McDougall, E., 2007, "Validation of Surgical Simulators," Journal of Endourology, **21**(3), pp. 244–247 DOI: 10.1089/end.2007.9985.

[42] Kneebone, R., 2003, "Simulation in Surgical Training: Educational Issues and Practical Implications," Medical Education, **37**(3), pp. 267–277 DOI: 10.1046/j.1365-2923.2003.01440.x.

[43] Issenberg, S., McGaghie, W., Petrusa, E., Gordon, D., and Scalese, R., 2005, "Features and Uses of High-Fidelity Medical Simulations That Lead to Effective Learning: A BEME Systematic Review," Medical Teacher, **27**(1), pp. 10–28 DOI: 10.1080/01421590500046924.

[44] Carter, F., Schijven, M., Aggarwal, R., Grantcharov, T., Francis, N., Hanna, G., and Jakimowicz, J., 2005, "Consensus Guidelines for Validation of Virtual Reality Surgical Simulators," Surgical Endoscopy and Other Interventional Techniques, **19**(12), pp. 1523–1532 DOI: 10.1007/s00464-005-0384-2.

[45] Oliveira, M., Araujo, A., Nicolato, A., Prosdocimi, A., Godinho, J., Valle, A., Santos, M., Reis, A., Ferreira, M., Sabbagh, A., Gusmao, S., and Del Maestro, R., 2016, "Face, Content, and Construct Validity of Brain Tumor Microsurgery Simulation Using a Human Placenta Model," Operative Neurosurgery, **12**(1), pp. 61–67 DOI: 10.1227/NEU.0000000000001030.

[46] Ledwos, N., Mirchi, N., Bissonnette, V., Winkler-Schwartz, A., Yilmaz, R., and Del Maestro, R., 2021, "Virtual Reality Anterior Cervical Discectomy and Fusion Simulation on the Novel Sim-Ortho Platform: Validation Studies," Operative Neurosurgery, **20**(1), pp. 74–82 DOI: 10.1093/ons/opaa269.

[47] Gavazzi, A., Bahsoun, A., Haute, W., Ahmed, K., Elhage, O., Jaye, P., Khan, M., and Dasgupta, P., 2011, "Face, Content and Construct Validity of a Virtual Reality Simulator for Robotic Surgery (SEP Robot)," Annals of the Royal College of Surgeons of England, **93**(2), pp. 152–156 DOI: 10.1308/003588411X12851639108358.

[48] Brewin, J., Nedas, T., Challacombe, B., Elhage, O., Keisu, J., and Dasgupta, P., 2010, "Face, Content and Construct Validation of the First Virtual Reality Laparoscopic Nephrectomy Simulator," BJU International, **106**(6), pp. 850–854 DOI: 10.1111/j.1464-410X.2009.09193.x.

[49] 2018, *V&V 40: Assessing Credibility of Computational Modeling through Verification and Validation: Application to Medical Devices*, The American Society of Mechanical Engineers. ISBN: 9780791872048.

[50] Government of Canada / Gouvernement du Canada, 2016, "CAE Healthcare Launches World-Class Neurosurgery Simulator in Partnership with the National Research Council of Canada" [Online]. Available: https://www.canada.ca/en/national-research-council/news/2016/01/cae-healthcare-launches-world-class-neurosurgery-simulator-in-partnership-with-the-national-research-council-of-canada.html. [Accessed: 04-Oct-2021].

[51] Ren, D., Chen, Y., Lin, B., Zeng, F., Huang, J., and Wang, J., 2017, "Modelling and Simulation of Vessel Surgery Based on Mass-Spring," *MATEC Web of Conferences*, EDP Sciences, p. 13004 DOI:

10.1051/matecconf/201710813004.

[52] Misra, S., Ramesh, K., and Okamura, A., 2008, “Modeling of Tool-Tissue Interactions for Computer-Based Surgical Simulation: A Literature Review,” Presence: Teleoperators and Virtual Environments, **17**(5), pp. 463–491 DOI: 10.1162/pres.17.5.463.

[53] Cotin, S., Delingette, H., and Ayache, N., 2000, “A Hybrid Elastic Model Allowing Real-Time Cutting, Deformations and Force-Feedback for Surgery Training and Simulation,” Visual Computer, **16**(8), pp. 437–452 DOI: 10.1007/PL00007215.

[54] Vigneron, L., Verly, J., and Warfield, S., 2004, “On Extended Finite Element Method (XFEM) for Modelling of Organ Deformations Associated with Surgical Cuts,” *Proceedings on the Internatinoal Symposium on Medical Simulation, ISMS 2004, Lecture Notes in Computer Science*, pp. 134–143 DOI: 10.1007/978-3-540-25968-8_15.

[55] Wang, X., and Fenster, A., 2004, “A Virtual Reality Based 3D Real-Time Interactive Brachytherapy Simulation of Needle Insertion and Seed Implantation,” *Proceedings of 2nd IEEE International Symposium on Biomedical Imaging: Macro to Nano, 2004*, pp. 280–283 DOI: 10.1109/isbi.2004.1398529.

[56] Bao, Y., Wu, D., Yan, Z., and Du, Z., 2013, “A New Hybrid Viscoelastic Soft Tissue Model Based on Meshless Method for Haptic Surgical Simulation,” The Open Biomedical Engineering Journal, **7**, pp. 116–124 DOI: 10.2174/1874120701307010116.

[57] Harish, A., 2019, “How to Choose a Solver for FEM Problems: Direct or Iterative?,” SimScale [Online]. Available: https://www.simscale.com/blog/2016/08/how-to-choose-solvers-for-fem/. [Accessed: 30-Apr-2019].

[58] Hammer, P., Sacks, M., Del Nido, P., and Howe, R., 2011, “Mass-Spring Model for Simulation of Heart Valve Tissue Mechanical Behavior,” Annals of Biomedical Engineering, **39**(6), pp. 1668–1679 DOI: 10.1007/s10439-011-0278-5.

[59] Miller, K., Joldes, G., Lance, D., and Wittek, A., 2007, “Total Lagrangian Explicit Dynamics Finite Element Algorithm for Computing Soft Tissue Deformation,” Communications in Numerical Methods in Engineering, **23**(2), pp. 121–134 DOI: 10.1002/cnm.887.

[60] Johnsen, S., Taylor, Z., Clarkson, M., Hipwell, J., Modat, M., Eiben, B., Han, L., Hu, Y., Mertzanidou, T., Hawkes, D., and Ourselin, S., 2015, “NiftySim: A GPU-Based Nonlinear Finite Element Package for Simulation of Soft Tissue Biomechanics,” International Journal of Computer Assisted Radiology and Surgery, **10**(7), pp. 1077–1095 DOI: https://dx.doi.org/10.1007/s11548-014-1118-5.

[61] Campana, S., Charpail, E., de Guise, J., Rillardon, L., Skalli, W., and Mitton, D., 2011, “Relationships Between Viscoelastic Properties of Lumbar Intervertebral Disc and Degeneration Grade Assessed by MRI,” Journal of the Mechanical Behavior of Biomedical Materials, **4**(4), pp. 593–599 DOI: 10.1016/j.jmbbm.2011.01.007.

[62] Kelly, P., “Chapter 10.6 Oscillatory Stress, Dynamic Loading and Vibrations,” *Solid Mechanics Part I: An Introduction to Solid Mechanics*, p. 330.

[63] Vincent, J., 1982, “Structural Biomaterials,” *Structural Biomaterials: Basic Theory of Elasticity and Viscoelasticity*, Th MacMillan Press Ltd, pp. 1–33. ISBN: 978-1-349-16673-2.

[64] Basdogan, C., Laycock, S., Day, A., Patoglu, V., and Gillespie, R., 2008, *Haptic Rendering: Foundations, Algorithms, and Applications*, A K Peters, Ltd., New York City, USA. ISBN: 978-1-4398-6514-9 (eBook - PDF).

[65] Penfield, W., and Boldrey, E., 1937, “Somatic Motor and Sensory Representation in the Cerebral Cortex of Mman as Studied by Electrical Stimulation,” Brain, **60**(4), pp. 389–443 DOI: 10.1093/brain/60.4.389.

[66] Pang, X., Tan, H., and Durlach, N., 1991, “Manual Discrimination of Force Using Active Finger Motion,” Perception & Psychophysics, **49**(6), pp. 531–540 DOI: 10.3758/BF03212187.

[67] Allin, S., Matsuoka, Y., and Klatzky, R., 2002, “Measuring Just Noticeable Differences For Haptic Force Feedback: Implications for Rehabilitation,” *Proceedings of the 10th Symposium on Haptic Interfaces for Virtual Environment and Teleoperator Systems, HAPTICS 2002*, Orlando, US, pp. 299–302 DOI: 10.1109/HAPTIC.2002.998972.

[68] Zoeller, A., and Drewing, K., 2020, “A Systematic Comparison of Perceptual Performance in Softness Discrimination with Different Fingers,” Attention, Perception, and Psychophysics, **82**(7), pp. 3696–3709 DOI: 10.3758/s13414-020-02100-4.

[69] Omrani, M., Lak, A., and Diamond, M., 2013, “Learning Not to Feel: Reshaping the Resolution of Tactile Perception,” Frontiers in Systems Neuroscience, **7**, pp. 29: 1–13 DOI: 10.3389/fnsys.2013.00029.

[70] Vicentini, M., and Botturi, D., 2010, “Perceptual Issues Improve Haptic Systems Performance,” *Advances in Haptics*, M.H. Zadeh, ed., InTech, pp. 415–438 DOI: 10.5772/8711.

[71] Sadideen, H., Alvand, A., Saadeddin, M., and Kneebone, R., 2013, “Surgical Experts: Born or Made?,” International Journal of Surgery, **11**(9), pp. 773–778 DOI: 10.1016/j.ijsu.2013.07.001.

[72] Jarillo-Silva, A., Domínguez-Ramírez, O., Parra-Vega, V., and Ordaz-Oliver, J., 2009, “PHANToM OMNI Haptic Device: Kinematic and Manipulability,” *Electronics Robotics and Automotive Mechanics Conference (CERMA)*, Cuernavaca, México, pp. 193–198 DOI: 10.1109/CERMA.2009.55. ISBN: 9780769537993.

[73] Mathieu, L., and Lee-Huu, P., 1998, “Seat for Motion Simulator and Method of Motion Simulation,” pp. 1–3. US Patent Number US5980255A.

[74] Okamura, A., 2009, “Haptic Feedback in Robot-Assisted Minimally Invasive Surgery,” Current Opinion in Urology, **19**(1), pp. 102–107 DOI: 10.1097/MOU.0b013e32831a478c.

[75] Behensky, M., Moncrief, R., Durfey, E., and Loper, M., 1991, “Control Device Such As A Steering Wheel For Video Vehicle Simulator With Realistic Feedback Forces,” pp. 1–13. US Patent Number US5044956A.

[76] Pedram, S., Klatzky, R., and Berkelman, P., 2017, “Torque Contribution to Haptic Rendering of Virtual Textures,” IEEE Transactions on Haptics, **10**(4), pp. 567–579 DOI: 10.1109/TOH.2017.2679000.

[77] MaClean, K., and Roderick, J., 1999, “Smart Tangible Displays in the Everyday World: A Haptic Door Knob,” *IEEE/ASME International Conference on Advanced Intelligent Mechatronics*, Atlanta, USA, pp. 203–208 DOI: 10.1109/aim.1999.803167.

[78] Badescu, M., Wampler, C., and Mavroidis, C., 2002, “Rotary Haptic Knob for Vehicular Instrument Controls,” *Proceedings on the 10th Symposium on Haptic Interfaces for Virtual Environment and Teleoperator Systems, HAPTICS 2002*, Orlando, USA, pp. 342–343 DOI: 10.1109/HAPTIC.2002.998978. ISBN: 0-7695-1489-8.

[79] Alaimo, S., Pollini, L., Magazzù, A., Bresciani, J., Robuffo Giordano, P., Innocenti, M., and Bülthoff, H., 2010, “Preliminary Evaluation of a Haptic Aiding Concept for Remotely Piloted Vehicles,” *EuroHaptics 2010: Haptics: Generating and Perceiving Tangible Sensations*, A.M.. Kappers, J.B.F. van Erp, W.M. Bergmann tiest, and F.C.. van der Helm, eds., Springer, Amsterdam, Netherlands, pp. 418–425 DOI: 10.1007/978-3-642-14075-4_62. ISBN: 978-3-642-14074-7.

[80] Delorme, S., Laroche, D., Diraddo, R., and Del Maestro, R., 2012, “NeuroTouch: A Physics-Based Virtual Simulator for Cranial Microneurosurgery Training,” Neurosurgery, **71**(Suppl 1), pp. 32–42 DOI: 10.1227/NEU.0b013e318249c744.

[81] Nikolaidis, N., Marras, I., Mikrogeorgis, G., Lyroudia, K., and Pitas, I., 2008, “Virtual Dental Patient: A 3D Oral Cavity Model and Its Use in Haptics-Based Virtual Reality Cavity Preparation in Endodontics,” Dental Computing and Applications: Advanced Techniques for Clinical Dentistry, pp. 317–336 DOI: 10.4018/978-1-60566-292-3.ch018.

[82] 3D Systems, 2020, “3D Systems” [Online]. Available: https://www.3dsystems.com/.

[83] Haption, 2020, “Haption” [Online]. Available: https://www.haption.com/. [Accessed: 04-Jun-2020].

[84] Force Dimension, “Force Dimension” [Online]. Available: https://www.forcedimension.com/.

[85] Saad, E., 2016, “A Virtual-Reality System for Interacting with Three-Dimensional Models Using a Haptic Device and a Head-Mounted Display,” McGill University.

[86] Quanser, “HD^2 High Definition Haptic Device” [Online]. Available: https://www.quanser.com/products/hd2-high-definition-haptic-device/. [Accessed: 03-Dec-2021].

[87] Butterfly Haptics LLC, “Maglev 200” [Online]. Available: https://butterflyhaptics.com/. [Accessed: 03-Dec-2021].

[88] Forsslund, J., Selesnick, J., Salisbury, K., Silva, R., and Blevins, N., 2013, "The Effect of Haptic Degrees of Freedom on Task Performance in Virtual Surgical Environments," *Studies in Health Technology and Informatics (Medicine Meets Virtual Reality 20: NextMed/MMVR20)*, J.D. Westwood, S.W. Westwood, L. Felländer-Tsai, R.S. Haluck, R.A. Robb, and K.G. SengeVosburgh, eds., IOS Press, San Diego, USA, pp. 129–135 DOI: 10.3233/978-1-61499-209-7-129.

[89] Baumann, R., Maeder, W., Glauser, D., and Clavel, R., 1997, "The Pantoscope: A Spherical Remote-Center-of-Motion Parallel Manipulator for Force Reflection," *Proceedings of International Conference on Robotics and Automation*, IEEE, Albuquerque, USA, pp. 718–723 DOI: 10.1109/robot.1997.620120.

[90] Demers, J., Boelen, J., and Sinclair, I., 1998, "Freedom 6S Force Feedback Hand Controller," *Proceedings of IFAC Workshop on Space Robotics (SPRO'98)*, S. Rondeau, ed., Pergamon, St-Hubert, Canada, pp. 115–120 DOI: 10.1016/s1474-6670(17)38396-9.

[91] Ruikar, D., Hegadi, R., and Santosh, K., 2018, "A Systematic Review on Orthopedic Simulators for Psycho-Motor Skill and Surgical Procedure Training," Journal of Medical Systems, **42**(9), pp. 168: 1–21 DOI: 10.1007/s10916-018-1019-1.

[92] Gallacher, C., Harrison, J., and Kövecses, J., 2015, "Characterizing Device Dynamics for Haptic Manipulation and Navigation," *IEEE International Conference on Robotics and Automation (ICRA)*, pp. 3689–3695 DOI: 10.1109/ICRA.2015.7139711.

[93] Turini, G., Moglia, A., Ferrari, V., Ferrari, M., and Mosca, F., 2012, "Patient-Specific Surgical Simulator for the Pre-Operative Planning of Single-Incision Laparoscopic Surgery with Bimanual Robots," Computer Aided Surgery, **17**(3), pp. 103–112 DOI: 10.3109/10929088.2012.672595.

[94] Mortimer, M., Horan, B., and Stojcevski, A., 2014, "Design for Manufacture of a Low-Cost Haptic Degree-Of-Freedom," International Journal of Electronics and Electrical Engineering, **2**(2), pp. 85–89 DOI: 10.12720/ijeee.2.2.85-89.

[95] Griffin, M., Premakumar, Y., Seifalian, A., Butler, P., and Szarko, M., 2016, "Biomechanical Characterization of Human Soft Tissues Using Indentation and Tensile Testing," Journal of Visualized Experiments, **118**, p. e54872: 1-8 DOI: 10.3791/54872. ISBN: 1940-087X (Electronic) 1940-087X (Linking).

[96] Costi, J., Ledet, E., and O'Connell, G., 2021, "Spine Biomechanical Testing Methodologies: The Controversy of Consensus vs Scientific Evidence," JOR Spine, **4**(1), p. e1138 DOI: 10.1002/jsp2.1138.

[97] Goel, V. K., Winterbottom, J. M., Weinstein, J. N., and Kim, Y. E., 1987, "Load Sharing Among Spinal Elements of a Motion Segment in Extension and Lateral Bending," Journal of Biomechanical Engineering, **109**(4), pp. 291–297 DOI: 10.1115/1.3138683.

[98] Schendel, M., Wood, K., Buttermann, G., Lewis, J., and Ogilvie, J., 1993, "Experimental Measurement of Ligament Force, Facet Force, and Segment Motion in the Human Lumbar Spine," Journal of Biomechanics, **26**(4–5), pp. 427–438 DOI: 10.1016/0021-9290(93)90006-Z.

[99] Goel, V., Goyal, S., Clark, C., Nishiyama, K., and Nye, T., 1985, "Kinematics of the Whole Lumbar Spine: Effect of Discectomy," Spine, **10**(6), pp. 543–554 DOI: 10.1097/00007632-198507000-00008. ISBN: 0362-2436 (Print).

[100] Bailey, S., and Vashishth, D., 2018, "Mechanical Characterization of Bone: State of the Art in Experimental Approaches-What Types of Experiments Do People Do and How Does One Interpret the Results?," Current Osteoporosis Reports, **16**(4), pp. 423–433 DOI: 10.1007/s11914-018-0454-8.

[101] Patwardhan, A., Havey, R., Meade, K., Lee, B., and Dunlap, B., 1999, "A Follower Load Increases the Load-Carrying Capacity of the Lumbar Spine in Compression," Spine, **24**(10), pp. 1003–1009 DOI: 10.1097/00007632-199905150-00014.

[102] Shan, Z., Li, S., Liu, J., Mamuti, M., Wang, C., and Zhao, F., 2015, "Correlation between Biomechanical Properties of the Annulus Fibrosus and Magnetic Resonance Imaging (MRI) Findings," European Spine Journal, **24**(9), pp. 1909–1916 DOI: 10.1007/s00586-015-4061-4.

[103] Hirsch, C., and Nachemson, A., 1954, "New Observations on the Mechanical Behavior of Lumbar Discs," Acta Orthopaedica Scandinavica, **23**(4), pp. 254–283 DOI: 10.3109/17453675408991217.

[104] La Barbera, L., Wilke, H., Ruspi, M., Palanca, M., Liebsch, C., Luca, A., Brayda-Bruno, M., Galbusera, F., and Cristofolini, L., 2021, “Load-Sharing Biomechanics of Lumbar Fixation and Fusion with Pedicle Subtraction Osteotomy,” Scientific Reports, **11**, pp. 3595: 1–13 DOI: 10.1038/s41598-021-83251-8.

[105] Elliott, D., and Setton, L., 2001, “Anisotropic and Inhomogeneous Tensile Behavior of the Human Anulus Fibrosus: Experimental Measurement and Material Model Predictions,” Journal of Biomechanical Engineering, **123**(3), pp. 256–263 DOI: 10.1115/1.1374202.

[106] Iatridis, J., Kumar, S., Foster, R., Weidenbaum, M., and Mow, V., 1999, “Shear Mechanical Properties of Human Lumbar Annulus Fibrosus,” Journal of Orthopaedic Research, **17**(5), pp. 732–737 DOI: 10.1002/jor.1100170517.

[107] Umehara, S., Tadano, S., Abumi, K., Katagiri, K., Kaneda, K., and Ukai, T., 1996, “Effects of Degeneration on the Elastic Modulus Distribution in the Lumbar Intervertebral Disc,” Spine, **21**(7), pp. 811–819 DOI: 10.1097/00007632-199604010-00007.

[108] Costi, J., Stokes, I., Gardner-Morse, M., and Iatridis, J., 2008, “Frequency-Dependent Behavior of the Intervertebral Disc in Response to Each of Six Degree of Freedom Dynamic Loading,” Spine, **33**(16), pp. 1731–1738 DOI: 10.1097/BRS.0b013e31817bb116.

[109] Smeathers, J., and Joanes, D., 1988, “Dynamic Compressive Properties of Human Lumbar Intervertebral Joints: A Comparison Between Fresh and Thawed Specimens,” Journal of Biomechanics, **21**(5), pp. 425–433 DOI: 10.1016/0021-9290(88)90148-0.

[110] Janevic, J., Ashton-Miller, J., and Schultz, A., 1991, “Large Compressive Preloads Decrease Lumbar Motion Segment Flexibility,” Journal of Orthopaedic Research, **9**(2), pp. 228–236 DOI: 10.1002/jor.1100090211.

[111] Marini, G., Huber, G., Püschel, K., and Ferguson, S., 2015, “Nonlinear Dynamics of the Human Lumbar Intervertebral Disc,” Journal of Biomechanics, **48**(3), pp. 479–88 DOI: 10.1016/j.jbiomech.2014.12.006.

[112] Kemper, A., McNally, C., and Duma, S., 2007, “The Influence of Strain Rate on the Compressive Stiffness Properties of Human Lumbar Intervertebral Discs,” Biomedical Sciences Instrumentation, **43**, pp. 176–181.

[113] El-Monajjed, K., and Driscoll, M., 2021, “Analysis of Surgical Forces Required to Gain Access Using a Probe for Minimally Invasive Spine Surgery via Cadaveric-Based Experiments towards Use in Training Simulators,” IEEE Transactions on Biomedical Engineering, **68**(1), pp. 330–339 DOI: 10.1109/TBME.2020.2996980.

[114] MacAvelia, T., Ghasempoor, A., and Janabi-Sharifi, F., 2014, “Force and Torque Modelling of Drilling Simulation for Orthopaedic Surgery,” Computer Methods in Biomechanics and Biomedical Engineering, **17**(12), pp. 1285–1294 DOI: 10.1080/10255842.2012.739163.

[115] Nguyen, C., and Vu-Khanh, T., 2009, “Mechanics and Mechanisms of Puncture by Medical Needles,” Procedia Engineering, **1**(1), pp. 139–142 DOI: 10.1016/j.proeng.2009.06.032.

[116] Rivlin, R., and Thomas, A., 1953, “Rupture of Rubber. I. Characteristic Energy for Tearing,” Journal of Polymer Science, **10**(3), pp. 291–318 DOI: 10.1002/pol.1953.120100303.

[117] Khadem, M., Rossa, C., Sloboda, R., Usmani, N., and Tavakoli, M., 2016, “Mechanics of Tissue Cutting during Needle Insertion in Biological Tissue,” IEEE Robotics and Automation Letters, **1**(2), pp. 800–807 DOI: 10.1109/LRA.2016.2528301.

[118] Barnett, A., Lee, Y., and Moore, J., 2016, “Fracture Mechanics Model of Needle Cutting Tissue,” Journal of Manufacturing Science and Engineering, Transactions of the ASME, **138**(1), pp. 1–8 DOI: 10.1115/1.4030374.

[119] Jiang, S., Li, P., Yu, Y., Liu, J., and Yang, Z., 2014, “Experimental Study of Needle-Tissue Interaction Forces: Effect of Needle Geometries, Insertion Methods and Tissue Characteristics,” Journal of Biomechanics, **47**(13), pp. 3344–3353 DOI: 10.1016/j.jbiomech.2014.08.007.

[120] Okamura, A., Simone, C., and O’Leary, M., 2004, “Force Modeling for Needle Insertion Into Soft Tissue,” IEEE Transactions on Biomedical Engineering, **51**(10), pp. 1707–1716 DOI: 10.1109/TBME.2004.831542.

[121] Lee, C., and Langrana, N., 1984, “Lumbosacral Spinal Fusion: A Biomechanical Study,” Spine, **9**(6), pp.

574–581. ISBN: 0362-2436; 0362-2436.

[122] MTS Systems, “MTS Systems” [Online]. Available: www.mts.com. [Accessed: 09-Sep-2021].

[123] Moebs, W., Ling, S., and Sanny, J., 2016, *University Physics*, OpenStax, Houston, TX. ISBN: 978-1947172203.

[124] Instron, “Instron Biaxial Cruciform - Instron” [Online]. Available: https://www.instron.com/en-us/products/testing-systems/dynamic-and-fatigue-systems/8800-cruciform. [Accessed: 09-Sep-2021].

[125] MTS Systems, “Bionix® Tabletop Test Systems” [Online]. Available: https://www.mts.com/en/products/biomedical/biomaterial-test-systems/bionix-tabletop. [Accessed: 09-Sep-2021].

[126] Chen, J., Li, Y., Wen, J., Li, Z., Yu, B., and Huang, Y., 2021, “Annular Defects Impair the Mechanical Stability of the Intervertebral Disc,” Global Spine Journal, **2192568221** DOI: 10.1177/21925682211006061.

[127] Nillahoot, N., and Suthakorn, J., 2013, “Development of Veress Needle Insertion Robotic System and Its Experimental Study for Force Acquisition in Soft Tissue,” *2013 IEEE International Conference on Robotics and Biomimetics (ROBIO)*, pp. 645–650 DOI: 10.1109/ROBIO.2013.6739532.

[128] Georgilas, I., Dagnino, G., Tarassoli, P., Atkins, R., and Dogramadzi, S., 2015, “Preliminary Analysis of Force-Torque Measurements for Robot-Assisted Fracture Surgery,” *Proceedings of the Annual International Conference of the IEEE Engineering in Medicine and Biology Society*, pp. 4902–4905 DOI: 10.1109/EMBC.2015.7319491. ISBN: 9781424492718.

[129] Georgilas, I., Dagnino, G., Alves Martins, B., Tarassoli, P., Morad, S., Georgilas, K., Koehler, P., Atkins, R., and Dogramadzi, S., 2019, “Design and Evaluation of a Percutaneous Fragment Manipulation Device for Minimally Invasive Fracture Surgery,” Frontiers in Robotics and AI, **6**, pp. 103: 1–9 DOI: 10.3389/frobt.2019.00103.

[130] Jagtap, A., and Riviere, C., 2004, “Applied Force during Vitreoretinal Microsurgery with Handheld Instruments,” *Proceedings of the IEEE Engineering in Medicine and Biology*, pp. 2771–2773 DOI: 10.1109/iembs.2004.1403792.

[131] Marcus, H., Zareinia, K., Gan, L., Yang, F., Lama, S., Yang, G., and Sutherland, G., 2014, “Forces Exerted during Microneurosurgery: A Cadaver Study,” International Journal of Medical Robotics and Computer Assisted Surgery, **10**(2), pp. 251–256 DOI: 10.1002/rcs.1568.

[132] Dario, P., Hannaford, B., and Menciassi, A., 2003, “Smart Surgical Tools and Augmenting Devices,” IEEE Transactions on Robotics and Automation, **19**(5), pp. 782–792 DOI: 10.1109/TRA.2003.817071.

[133] Sakaguchi, Y., Sato, T., Yutaka, Y., Muranishi, Y., Komatsu, T., Yoshizawa, A., Nakajima, N., Nakamura, T., and Date, H., 2018, “Development of Novel Force-Limiting Grasping Forceps with a Simple Mechanism,” European Journal of Cardio-thoracic Surgery, **54**(6), pp. 1004–1012 DOI: 10.1093/ejcts/ezy216.

[134] Horeman, T., Meijer, E., Harlaar, J., Lange, J., Van Den Dobbelsteen, J., and Dankelman, J., 2013, “Force Sensing in Surgical Sutures,” PLoS ONE, **8**(12), p. e84466: 1-12 DOI: 10.1371/journal.pone.0084466.

[135] Schwarz, M., Wagner, A., El-Shenawy, A., Gundling, R., Köpfle, A., Handel, H., Badreddin, E., Männer, R., Scharf, H., Götz, M., Schill, M., and Pott, P., 2009, “A Handheld Robot for Orthopedic Surgery - ITD,” *World Congress on Medical Physics and Biomedical Engineering*, pp. 99–102 DOI: 10.1007/978-3-642-03906-5_27.

[136] Yuen, S., Perrin, D., Vasilyev, N., Nido, P., and Howe, R., 2010, “Force Tracking With Feed-Forward Motion Estimation for Beating Heart Surgery,” IEEE Transactions on Robotics, **26**(5), pp. 888–896 DOI: 10.1109/TRO.2010.2053734.

[137] Intuitive Surgical Inc, “Da Vinci Surgery - Robotic Assisted Surgery for Patients” [Online]. Available: https://www.davincisurgery.com/. [Accessed: 26-Nov-2021].

[138] Medtronic, “Spine & Orthopaedic Products - Mazor” [Online]. Available: https://www.medtronic.com/ca-en/healthcare-professionals/products/spinal-orthopaedic/spine-robotics/mazor-x-stealth-edition.html. [Accessed: 26-Nov-2021].

[139] Peters, B., Armijo, P., Krause, C., Choudhury, S., and Oleynikov, D., 2018, "Review of Emerging Surgical Robotic Technology," Surgical Endoscopy, **32**(4), pp. 1636–1655 DOI: 10.1007/s00464-018-6079-2.

[140] Sayari, A., Pardo, C., Basques, B., and Colman, M., 2019, "Review of Robotic-Assisted Surgery: What the Future Looks like through a Spine Oncology Lens," Annals of Translational Medicine, **7**(10), pp. 224: 1–10 DOI: 10.21037/atm.2019.04.69.

[141] Cotter, T., Mongrain, R., and Driscoll, M., 2022, "Accepted - Design Synthesis of a Robotic Uniaxial Torque Device for Orthopedic Haptic Simulation," Journal of Medical Devices.

[142] PowerStream Technology, "American Wire Gauge Chart and AWG Electrical Current Load Limits Table" [Online]. Available: https://www.powerstream.com/Wire_Size.htm. [Accessed: 15-Sep-2021].

[143] Cotter, T., Driscoll, M., Mongrain, R., and Ouellet, J., 2020, "Lumbar Discectomy Tool Torque Hysteresis for Application in a Surgical Simulator - EPoster," *EUROSPINE*, Vienna, Austria (Online).

[144] Cotter, T., Driscoll, M., and Mongrain, R., 2021, "Mechanics of Lumbar Discectomy Tool Insertion for a Surgical Simulator - EPoster," *Canadian Society for Biomechanics*, Montréal, Canada (Online).

[145] Cotter, T., Driscoll, M., and Mongrain, R., 2021, "Discectomy Tool Mechanical Testing in Cadaveric Spine - EPoster," *Global Spine Congress*, Paris, France (Online).

[146] Cotter, T., Driscoll, M., and Mongrain, R., 2021, "Combining Freehand and Controlled Movement for Calculating Surgical Simulator Forces - EPoster," *Simulation Summit*, Canada (Online).

[147] Cotter, T., Mongrain, R., and Driscoll, M., 2022, "Under Review - Vacuum Curette Lumbar Discectomy Mechanics for Use in Spine Surgical Training Simulators," Scientific Reports.

[148] 2020, "Cobb Angle And Scoliosis," Core Concepts [Online]. Available: https://www.coreconcepts.com.sg/article/cobb-angle-and-scoliosis/. [Accessed: 22-Nov-2021].

[149] Cotter, T., Mongrain, R., Ouellet, J., and Driscoll, M., 2022, "Freehand Biomechanical Testing for Use in Lumbar Discectomy Training - EPoster," *Canadian Spine Society*, (Online).

[150] Cotter, T., Mongrain, R., and Driscoll, M., 2022, "Under Review - Comparing Controlled and Freehand Test Techniques of Lumbar Discectomy Force Measurement for Spinal Surgery Simulation," Clinical Spine Surgery.

[151] Wang, K., McCarter, R., Wright, J., Beverly, J., and Ramirez-Mitchell, R., 1993, "Viscoelasticity of the Sarcomere Matrix of Skeletal Muscles. The Titin-Myosin Composite Filament Is a Dual-Stage Molecular Spring," Biophysical Journal, **64**(4), pp. 1161–1177 DOI: 10.1016/S0006-3495(93)81482-6.

[152] Kocen, R., Gasik, M., Gantar, A., and Novak, S., 2017, "Viscoelastic Behaviour of Hydrogel-Based Composites for Tissue Engineering under Mechanical Load," Biomedical Materials (Bristol), **12**(2), pp. 025004: 1–11 DOI: 10.1088/1748-605X/aa5b00.

[153] Depuy Synthes Inc, 2011, *Spotlight™ MIS Access System*.

[154] BD, 2022, "Kerrison Ronguer - NL4291-71 | BD" [Online]. Available: https://www.bd.com/en-us/products-and-solutions/products/product-page.nl4291-71. [Accessed: 05-Apr-2022].

[155] IntegraLife, 2022, "Love Nerve Root Retractor" [Online]. Available: https://www.integralife.com/love-nerve-root-retractor/product/surgical-instruments-hospitals-surgery-centers-tissue-banks-ruggles-redmond-retractors-love-nerve-root-retractor. [Accessed: 05-Apr-2022].

[156] El-Monajjed, K., 2020, "Implementation of a Virtual Reality Module for Gaining Surgical Access via Planned Oblique Lateral Lumbar Interbody Fusion," McGill University.

[157] Kuphaldt, T., *Lessons in Electric Circuits*, All About Circuits.

[158] Matsuoka, Y., Brewer, B., and Klatzky, R., 2007, "Using Visual Feedback Distortion to Alter Coordinated Pinching Patterns for Robotic Rehabilitation," Journal of NeuroEngineering and Rehabilitation, **4**, pp. 17: 1–9 DOI: 10.1186/1743-0003-4-17.

[159] Heuer, F., Schmidt, H., Klezl, Z., Claes, L., and Wilke, H., 2007, "Stepwise Reduction of Functional Spinal Structures Increase Range of Motion and Change Lordosis Angle," Journal of Biomechanics, **40**(2), pp. 271–280 DOI: 10.1016/j.jbiomech.2006.01.007.

[160] Azarnoosh, M., Stoffel, M., Quack, V., Betsch, M., Rath, B., Tingart, M., and Markert, B., 2017, "A Comparative Study of Mechanical Properties of Fresh and Frozen-Thawed Porcine Intervertebral Discs in a Bioreactor Environment," Journal of the Mechanical Behavior of Biomedical Materials, **69**, pp. 169–177 DOI: 10.1016/j.jmbbm.2016.12.010.

[161] Ferguson, S., and Steffen, T., 2003, "Biomechanics of the Aging Spine," European Spine Journal, **12**(Suppl 2), pp. S97–S103 DOI: 10.1007/s00586-003-0621-0.

Appendix I

This appendix contains the part details for the haptic torque handle. A drawing of all parts can be seen in Figure I.1 and the bill of materials (BOM) is in Table I.1. All the electrical connections in the haptic torque handle can be seen in Table I.2.

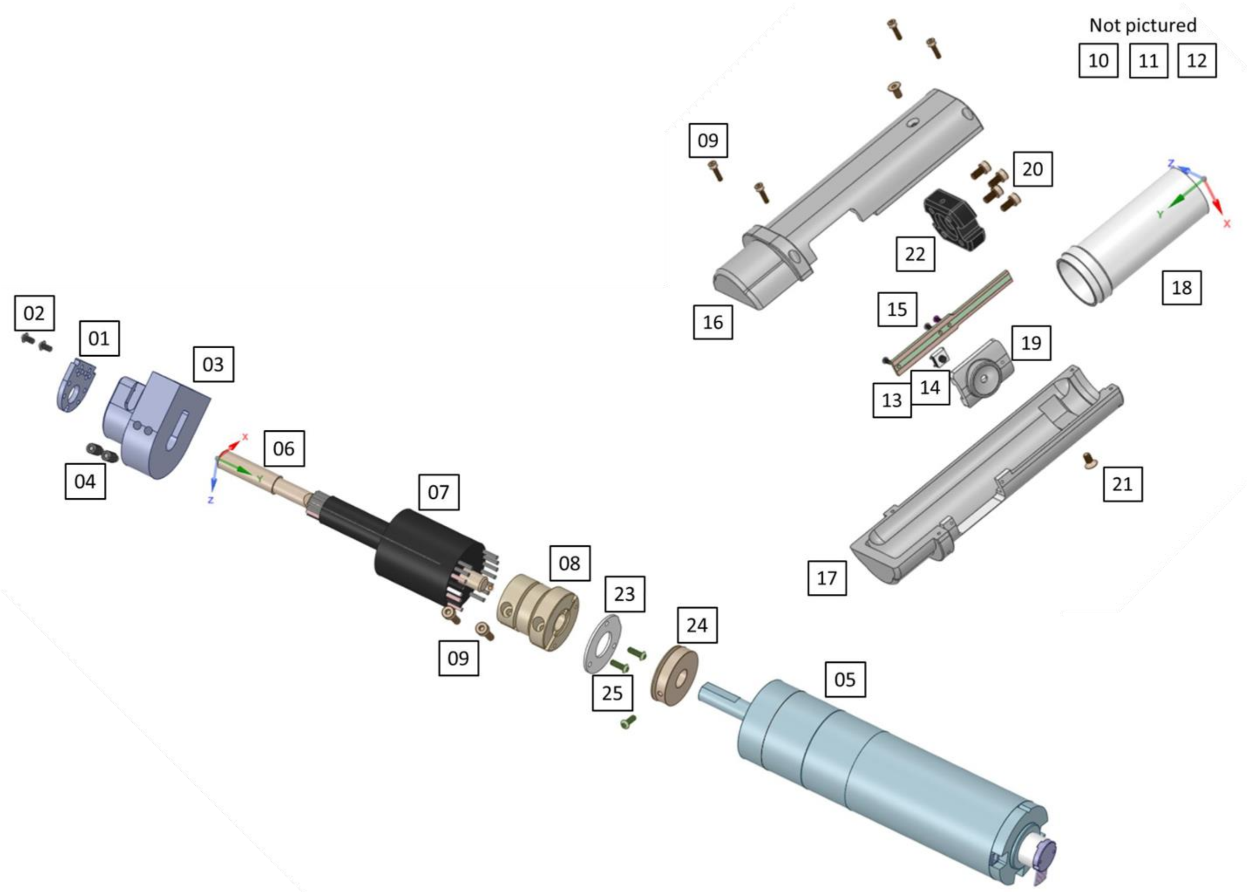

Figure I.1: Entire haptic torque handle assembly.

Table I.1: Haptic torque handle bill of materials (BOM).

Subassembly	BOM Number	Description	Supplier	Part Number	Material	Quantity
QRM Connection	1	PCB	JLPCB	N/A	N/A	1
	2	PCB Bolt	McMaster-Carr	90910A900	18-8 Stainless	2
	3	Male QRM Connection	Machined		6061 Aluminum	1
	4	Shaft Set Screw	McMaster-Carr	92905A056	Steel	2
Torque Generation	5	Motor, Gearbox, and Encoder Assembly	Maxon	N/A	N/A	1
	6	Shaft	Machined	N/A	6061 Aluminum	1
	7	Slipring	Moflon	MT0522-S12-VD		1
	8	Coupler	Machined	N/A	360 Brass	1
	9	M2 8 mm Socket Head Machine Screw	McMaster-Carr	91290A015	18-8 Stainless	2
	10	Filtering Resistors	Digi-Key	MFR-25FBF52-12K7	N/A	2
Button and ID	11	ID Resistor	Digi-Key	TBD	N/A	1
	12	Button Resistor	Digi-Key	TBD	N/A	1
	13	Button PCB	JLPCB	N/A	N/A	1
	14	Button	Digi-Key	B3FS-1050P	N/A	1
	15	M1.6 4 mm Button Head Machine Screw	McMaster-Carr	92095A322	18-8 Stainless	1
Housing	16	Cover 1	Machined	N/A	Delrin	1
	17	Cover 2	Machined	N/A	Delrin	1
	18	Cover 3	Machined	N/A	Delrin	1
	9	M2 8 mm Socket Head Machine Screw	McMaster-Carr	91290A015	Black-Oxide Steel	4
	19	Button Housing	Machined	N/A	Delrin	1
	15	M1.6 4 mm Button Head Machine Screw	McMaster-Carr	92095A322	18-8 Stainless	2
	20	M3 6 mm Socket Head Machine Screw	McMaster-Carr	92290A111	316 Stainless	4
	21	M3 6 mm Flat Head Machine Screw	McMaster-Carr	92125A126	18-8 Stainless	2
	22	Motor Attachment	Machined	N/A	Delrin	1
Load-Side Encoder (optional)	23	PCB	Entact Robotics	N/A	N/A	1
	24	Encoder Wheel	Entact Robotics	N/A	N/A	1
	25	M1.6 5 mm Button Head Machine Screw	McMaster-Carr	92095A323	18-8 Stainless	3

Table I.2: Wiring schematic for the haptic torque handle.

QRM Component (Explanation)	Slipring Color	Haptic Torque Handle Component
M+ (Motor Power Positive)	Red	Motor Power Positive
M- (Motor Power Negative)	Black	Motor Power Negative
5V (Power)	Purple	Motor Encoder Power
GND (Ground)	Gray	Motor Encoder Ground
	Green	ID Circuit Ground
LEA (Load Encoder Channel A)	White	*Motor Encoder Channel A Includes filtering resistor
LEB (Load Encoder Channel B)	Brown	*Motor Encoder Channel B Includes filtering resistor
ID (Identification circuit)	Yellow	Identification circuit Includes 2x 3kΩ R for identification and button
MEA (Motor Encoder Channel A)	N/A	*Not used
MEB (Motor Encoder Channel B)	N/A	*Not used

*The motor encoder was switched from the ME connections to the LE connections as detailed later in the manuscript

.

Appendix II

This appendix contains the ethical approvals all studies in this work. The cadaveric testing was done according to IRB A04-M13-18A. Figure II.1 shows the initial approval in 2018, and Figure II.2 to Figure II.5 show extension and revision approvals. The surgeon surveys were performed under IRB A03-M15-20A. Figure II.6 and Figure II.7 show the initial approval in 2020, and Figure II.8 shows the extension approval in 2021.

McGill

Faculty of Medicine
3655 Promenade Sir William Osler #633
Montreal, QC H3G 1Y6

Faculté de médecine
3655, Promenade Sir William Osler #633
Montréal, QC H3G 1Y6

Fax/Télécopieur: (514) 398-3870
Tél/Tel: (514) 398-3124

CERTIFICATION OF ETHICAL ACCEPTABILITY FOR RESEARCH INVOLVING HUMAN SUBJECTS

The Faculty of Medicine Institutional Review Board (IRB) is a registered University IRB working under the published guidelines of the Tri-Council Policy Statement, in compliance with the Plan d'action ministériel en éthique de la recherche et en intégrité scientifique (MSSS, 1998), and the Food and Drugs Act (17 June 2001); and acts in accordance with the U.S. Code of Federal Regulations that govern research on human subjects. The IRB working procedures are consistent with internationally accepted principles of Good Clinical Practices.

At a Board meeting on 14 May 2018, the Faculty of Medicine Institutional Review Board, consisting of:

Patricia Dobkin, PhD	Frank Elgar, PhD
Sylvie Lambert, PhD	Catherine Lecompte (non-voting)
Sally Mann, M.S.	Kathleen Montpetit, MSc
Roberta Palmour, PhD	Lucille Panet-Raymond, BA
Shahad Salman, LL.M.	Daniel Saumier, PhD
Blossom Shaffer, MBA	Margaret Swaine, BA

Examined the research project **A04-M13-18A** titled: *The development and evaluation of a novel surgical spine procedure into a physics driven virtual reality FEM training platform*

As proposed by: Dr. Mark Driscoll (Applicant) to ______ (Granting Agency, if any)

And consider the experimental procedures to be acceptable on ethical grounds for research involving human subjects.

14 May 2018 (Date) ______ (Chair, IRB) ______ (Dean of Faculty)

Institutional Review Board Assurance Number: FWA 00004545

Figure II.1: Initial ethical approval for the cadaveric studies.

McGill

Faculty of Medicine
3655 Promenade Sir William Osler #633
Montreal, QC H3G 1Y6

Faculté de médecine
3655, Promenade Sir William Osler #633
Montréal, QC H3G 1Y6

Fax/Télécopieur: (514) 398-3870
Tél/Tel: (514) 398-3124

April 12, 2018

Dr. Mark Driscoll
Department of Mechanical Engineering
Macdonald Engineering Bulding - Room 153
Montreal, Quebec H3A 0C3

RE: IRB Study Number A04-M13-18A
The development and evaluation of a novel surgical spine procedure into a physics driven virtual reality FEM training platform

Dear Dr. Driscoll,

Thank you for submitting the above-referenced study for an ethics review.

As this study involves no more than minimal risk, and in accordance with Articles 2.9 and 6.12 of the 2014 Edition of the Canadian Tri-Council Policy Statement of Ethical Conduct for Research Involving Humans (TCPS2 2014) and U.S. Title 45 CFR 46, Section 110 (b), paragraph (1), we are pleased to inform you that an expedited approval for the above-referenced study (March 29, 2018) was provided by the IRB Co-Chair on April 12, 2018. The ethics certificate is valid until **April 2019**.

The study proposal will be presented for corroborative approval at the next scheduled meeting of the Institutional Review Board, and a certification document will be issued to you at that time.

A review of all research involving human subjects is required on an annual basis in accord with the date of initial approval. The annual review should be submitted at least one month before **April 2019**. Please inform the IRB promptly of any modifications that may occur to the study over the next twelve months.

Sincerely,

Carolyn Ells

Carolyn Ells, PhD
Co-Chair
Institutional Review Board

cc: A04-M13-18A

Figure II.2: Ethical approval extension from 2018 to 2019.

McGill

Faculty of Medicine
3655 Promenade Sir William Osler #633
Montreal, QC H3G 1Y6

Faculté de médecine
3655, Promenade Sir William Osler #633
Montréal, QC H3G 1Y6

Fax/Télécopieur: (514) 398-3870
Tél/Tel: (514) 398-3124

April 16, 2019

Dr. Mark Driscoll
Department of Mechanical Engineering
Macdonald Engineering Bulding - Room 153
Montreal, Quebec H3A 0C3

RE: IRB Study Number A04-M13-18A
The development and evaluation of a novel surgical spine procedure into a physics driven virtual reality FEM training platform

Dear Dr. Driscoll,

Thank you for submitting an application for Continuing Ethics Review for the above-referenced study.

The study progress report was reviewed and Full Board re-approval was provided on April 15, 2019. The ethics certification renewal is valid until **April 13, 2020.**

The Investigator is reminded of the requirement to report all IRB approved protocol and consent form modifications to the Research Ethics Offices (REOs) for the participating hospital sites. Please contact the individual hospital REOs for instructions on how to proceed. Research funds may be withheld and / or the study's data may be revoked for failing to comply with this requirement.

Should any modification or unanticipated development occur prior to the next review, please notify the IRB promptly. Regulation does not permit the implementation of study modifications prior to IRB review and approval.

Sincerely,

Carolyn Ells

Carolyn Ells, PhD
Co-Chair
Institutional Review Board

cc: A04-M13-18A

Figure II.3: Ethical approval extension from 2019 to 2020.

McGill

Faculty of Medicine
3655 Promenade Sir William Osler #633
Montreal, QC H3G 1Y6

Faculté de médecine
3655, Promenade Sir William Osler #633
Montréal, QC H3G 1Y6

Fax/Télécopieur: (514) 398-3870
Tél/Tel: (514) 398-3124

March 26, 2020

Dr. Mark Driscoll
Department of Mechanical Engineering
Macdonald Engineering Bulding
817 Sherbrooke St. W. - Room 153
Montreal, Quebec H3A 0C3

RE: IRB Study Number A04-M13-18A
The development and evaluation of a novel surgical spine procedure into a physics driven virtual reality FEM training platform

Dear Dr. Driscoll,

Thank you for submitting an application for Continuing Ethics Review for the above-referenced study.

The study progress report was reviewed and an expedited re-approval was provided by the Chair on March 26, 2020 and will be reported at the next scheduled meeting of the IRB. The ethics certification renewal is valid from **April 13, 2020 to April 12, 2021.**

The Investigator is reminded of the requirement to report all IRB approved protocol and consent form modifications to the Research Ethics Offices (REOs) for the participating hospital sites. Please contact the individual hospital REOs for instructions on how to proceed. Research funds may be withheld and / or the study's data may be revoked for failing to comply with this requirement.

Should any modification or unanticipated development occur prior to the next review, please notify the IRB promptly. Regulation does not permit the implementation of study modifications prior to IRB review and approval.

Regards,

Roberta M. Palmour

Roberta Palmour, PhD
Chair
Institutional Review Board

cc: Sneha Patel
A04-M13-18A

Figure II.4: Ethical approval extension from 2020 to 2021.

McGill | Faculty of Medicine and Health Sciences | Faculté de médecine et des sciences de la santé

3655 Sir William Osler #633
Montreal, Quebec H3G 1Y6

3655, Promenade Sir William Osler #633
Montréal (Québec) H3G 1Y6

Tél/Tel: (514) 398-3124

April 13, 2021

Dr. Mark Driscoll
Department of Mechanical Engineering
Macdonald Engineering Bulding
817 Sherbrooke St. W. - Room 153
Montreal, Quebec H3A 0C3

RE: **IRB Study Number A04-M13-18A**
The development and evaluation of a novel surgical spine procedure into a physics driven virtual reality FEM training platform

Dear Dr. Driscoll,

Thank you for submitting an application for Continuing Ethics Review for the above-referenced study.

The study progress report was reviewed and full Board re-approval was provided on April 12, 2021. The ethics certification renewal is valid until **April 11, 2022**.

The Investigator is reminded of the requirement to report all IRB approved protocol and consent form modifications to the Research Ethics Offices (REOs) for the participating hospital sites. Please contact the individual hospital REOs for instructions on how to proceed. Research funds may be withheld and / or the study's data may be revoked for failing to comply with this requirement.

Should any modification or unanticipated development occur prior to the next review, please notify the IRB promptly. Regulation does not permit the implementation of study modifications prior to IRB review and approval.

Regards,

Roberta M. Palmour

Roberta M. Palmour, PhD
Chair
Institutional Review Board

cc: Sneha Patel
Frances Vera Spidle
A04-M13-18A

Figure II.5: Ethical approval extension from 2021 to 2022.

McGill
Faculty of Medicine
3655 Promenade Sir William Osler #633
Montreal, QC, H3G 1Y6
Faculté de médecine
3655, promenade Sir William Osler #633
Montréal, QC H3G 1Y6
Fax/Télécopieur:
(514) 398-3870
Tél/Tel: (514) 398-3124

March 6, 2020

Dr. Mark Driscoll
Mechanical Engineering
Macdonald Engineering Bldg
817 Sherbrooke West - # 153
Montreal, Quebec H3A 0C3

RE: IRB Review Number: A03-M15-20A / 20-03-019

The development and evaluation of a novel surgical spine procedure into a physics driven virtual reality FEM training platform

Dear Dr. Driscoll,

Thank you for submitting the above-referenced study for an ethics review.

As this study involves no more than minimal risk, and in accordance with Articles 2.9 and 6.12 of the 2nd Edition of the Canadian Tri-Council Policy Statement of Ethical Conduct for Research Involving Humans (TCPS 2 2018) and U.S. Title 45 CFR 46, Section 110 (b), paragraph (1), we are pleased to inform you that approval for the study and English and French consent forms (IRB dated February 2020) was provided by an expedited/delegated review on 06-Mar-2020, valid until **05-Mar-2021**. The study proposal will be presented for corroborative approval at the next meeting of the Committee.

The Faculty of Medicine Institutional Review Board (IRB) is a registered University IRB working under the published guidelines of the Tri-Council Policy Statement 2, in compliance with the Plan d'action ministériel en éthique de la recherche et en intégrité scientifique (MSSS, 1998), and the Food and Drugs Act (17 June 2001); and acts in accordance with the U.S. Code of Federal Regulations that govern research on human subjects (**FWA 00004545**). The IRB working procedures are consistent with internationally accepted principles of good clinical practice.

The Principal Investigator is required to immediately notify the Institutional Review Board Office, via amendment or progress report, of:

- Any significant changes to the research project and the reason for that change, including an indication of ethical implications (if any);
- Serious Adverse Effects experienced by participants and the action taken to address those effects;

Figure II.6: Ethical approval for the surgeon surveys and simulator testing (page 1).

- Any other unforeseen events or unanticipated developments that merit notification;
- The inability of the Principal Investigator to continue in her/his role, or any other change in research personnel involved in the project;
- A delay of more than 12 months in the commencement of the research project, and;
- Termination or closure of the research project.

The Principal Investigator is required to submit an annual progress report (continuing review application) on the anniversary of the date of the initial approval (or see the date of expiration).

The Faculty of Medicine IRB may conduct an audit of the research project at any time.

If the research project involves multiple study sites, the Principal Investigator is required to report all IRB approvals and approved study documents to the appropriate Research Ethics Office (REO) or delegated authority for the participating study sites. Appropriate authorization from each study site must be obtained before the study recruitment and/or testing can begin at that site. Research funds linked to this research project may be withheld and/or the study data may be revoked if the Principal Investigator fails to comply with this requirement. A copy of the study site authorization should be submitted the IRB Office.

It is the Principal Investigator's responsibility to ensure that all researchers associated with this project are aware of the conditions of approval and which documents have been approved.

The McGill IRB wishes you and your colleagues every success in your research.

Sincerely,

Carolyn Ells, PhD
Co-Chair
Institutional Review Board

cc: Dr. Sylvain Baillet, Associate Dean, Research
A03-M15-20A / 20-03-019

Figure II.7: Ethical approval for the surgeon surveys and simulator testing (page 2).

McGill | Faculty of Medicine and Health Sciences | Faculté de médecine et des sciences de la santé

3655 Sir William Osler #633
Montreal, Quebec H3G 1Y6

3655, Promenade Sir William Osler #633
Montréal (Québec) H3G 1Y6

Tél/Tel: (514) 398-3124

March 9, 2021

Dr. Mark Driscoll
Mechanical Engineering
Macdonald Engineering Bldg
817 Sherbrooke West - # 153
Montreal, QC H3A 0C3

RE: IRB Study Number A03-M15-20A (20-03-019)
The development and evaluation of a novel surgical spine procedure into a physics driven virtual reality FEM training platform

Dear Dr. Driscoll,

Thank you for submitting an application for Continuing Ethics Review for the above-referenced study.

The study progress report was reviewed and full Board re-approval was provided on March 8, 2021. The ethics certification renewal is valid from **March 5, 2021 to March 7, 2022**.

The Investigator is reminded of the requirement to report all IRB approved protocol and consent form modifications to the Research Ethics Offices (REOs) for the participating hospital sites. Please contact the individual hospital REOs for instructions on how to proceed. Research funds may be withheld and / or the study's data may be revoked for failing to comply with this requirement.

Should any modification or unanticipated development occur prior to the next review, please notify the IRB promptly. Regulation does not permit the implementation of study modifications prior to IRB review and approval.

Regards,

Roberta M. Palmour, PhD
Chair
Institutional Review Board

cc: Sam Alkadri
A03-M15-20A (20-03-019)

Figure II.8: Extension of ethical approval for the surgeon surveys and simulator testing from 2021 to 2022.

Appendix III

This appendix contains the part and software details for the freehand testing assembly. A drawing of all parts can be seen in Figure III.1 and the bill of materials (BOM) is in Table III.1. The Cap-Handle connection shown is of a previous design, and the weights are approximate.

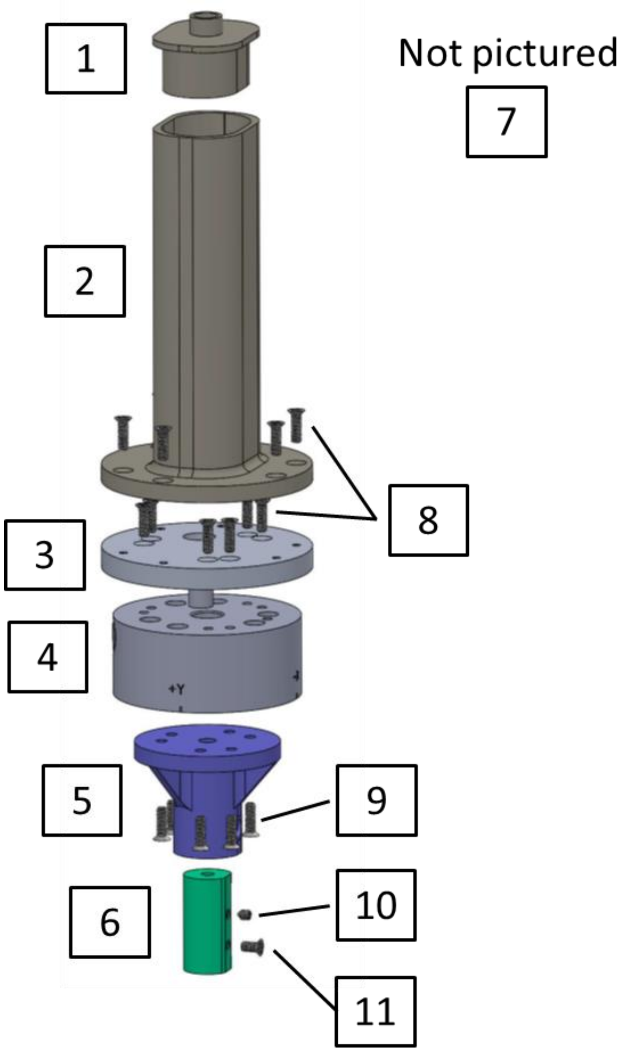

Figure III.1: Assembly of the freehand testing device.

Table III.1: Bill of materials (BOM) for the freehand testing device.

BOM Number	Description	Supplier	Supplier Part Number or Model	Material	Approximate Weight (g)	Quantity
1	Cap	N/A	N/A	Durable SLA Resin	50	1
2	Handle	N/A	N/A	Durable SLA Resin	6	1
3	Adapter Plate	Machined	N/A	6061 Aluminum	55	1
4	Load Cell	ATI Industrial Automation	Mini45	N/A	92	1
5	Receiver	Machined	N/A	6061 Aluminum	37	1
6	Insert	Machined	N/A	6061 Aluminum	12	1
7	CONCORDE® Clear Shaft	DePuy Synthes	N/A	N/A	10	1
8	M3x0.5 mm Flathead Screw, 10 mm Long	McMaster-Carr	93395A204	316 Stainless Steel	1	12
9	M3x0.5 mm Flathead Screw, 8 mm Long	McMaster-Carr	93395A201	316 Stainless Steel	1	6
10	M3x0.5 mm Cup-Point Set Screw, 4 mm long	McMaster-Carr	92029A101	316 Stainless Steel	1	1
11	M3x0.5 mm Flathead Screw, 6 mm Long	McMaster-Carr	93395A198	316 Stainless Steel	1	1

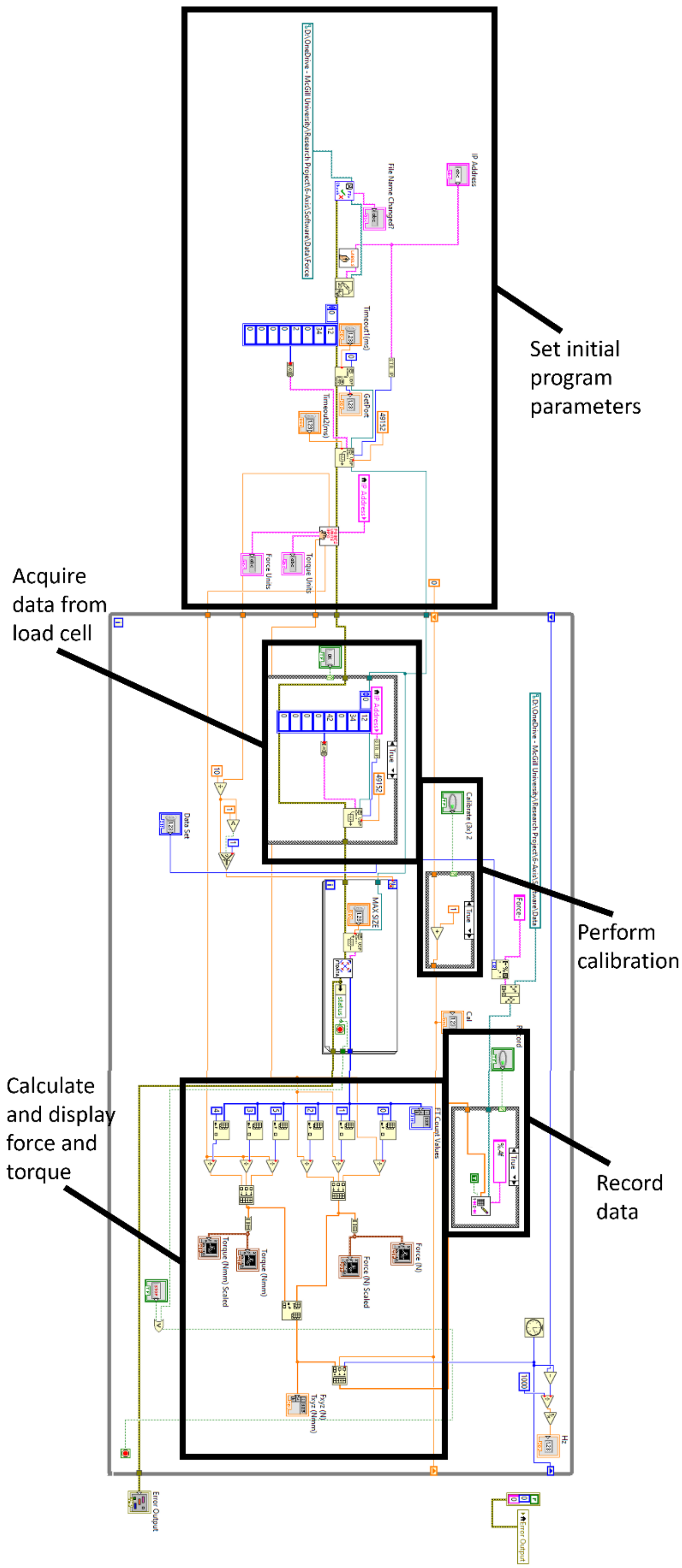

Figure III.2:Block diagram of the force and torque tracking software with section labels.

Appendix IV

This appendix contains the discectomy section of the post-simulator surgeon survey. Ethical approvals for the study are contained in Appendix II. Seven experienced spine surgeons performed a cadaveric procedure and then used the simulator to replicate the same procedure. They then filled out a 1-5 Likert scale questionnaire, the same one as viewed in Chapters 3, 4, and 6. Their feedback was used to update the simulator, and then 22 additional orthopedic and neurosurgeons used the simulator without cadaveric trials. All questions relevant to the discectomy steps and their results are shown in Table IV.1 to Table IV.4. Answers greater than 3 indicate satisfaction with a given aspect of the simulator.

Table IV.1: Surgeon questionnaire results for the facetectomy step.

Facetectomy Questions	Number of Responses	Results (1-5)
The orientation and angulation of the port in the physical world matches what is seen in the virtual world.	22	3.6±1.0
I am able to remove bone and soft tissue as needed to gain IVD access.	29	3.1±1.2
I can clear an adequate access area.	29	3.4±1.2
The physical Bur tool accurately resembles the real surgical tool	29	3.4±1.2
The virtual Bur tool accurately resembles the real surgical tool	29	2.9±1.0
I am able to maneuver the Bur tool similar to a real surgery.	29	2.7±1.1
The amount of bone removed using the Bur tool during each pass of the facetectomy step is similar to a real surgery.	22	2.5±1.1
The bone forces experienced using the Bur tool during the facetectomy step are similar to those experienced during a real surgery.	28	2.4±1.1
The soft tissue forces experienced using the Bur tool during the facetectomy step are similar to those experienced during a real surgery.	28	2.3±1.1
The physical REDACTED kerrison tool accurately resembles the real surgical tool.	5	2.0±1.0
The virtual REDACTED kerrison tool accurately resembles the real surgical tool.	5	2.4±1.3
I am able to maneuver the REDACTED tool similar to the kerrison tool in a real surgery.	4	2.8±1.0
The bone forces experienced using the REDACTED kerrison tool during the facetectomy step are similar to those usually experienced using the kerrison tool during a real surgery.	5	1.8±0.8
The soft tissue forces experienced using the REDACTED kerrison tool during the facetectomy step are similar to those usually experienced using the kerrison tool during a real surgery.	5	1.6±0.5

Table IV.2: Surgeon questionnaire results for the tissue retractor and annulotomy steps.

Tissue Retractor and Annulotomy Questions	Number of Responses	Results (1-5)
The physical Tissue Retractor tool accurately resembles the real surgical tool.	25	3.5±1.3
The virtual Tissue Retractor tool accurately resembles the real surgical tool.	25	3.1±1.2
I am able to use the Tissue Retractor tool to protect the nerve similarly to a real surgery.	21	3.0±1.3
The method of selecting annulotomy size is reasonable.	29	3.4±0.9
I am able to remove the amount of soft tissue that I want.	29	3.4±1.2

Table IV.3: Surgeon questionnaire results for the discectomy step.

Discectomy Questions	Number of Responses	Results (1-5)
The physical CONCORDE® Clear tool accurately resembles the real surgical tool.	29	3.9±1.0
The virtual CONCORDE® Clear tool accurately resembles the real surgical tool.	29	3.5±0.9
I am able to maneuver the CONCORDE® Clear tool similar to comparable curettes in a real surgery.	26	3.3±1.2
The forces experienced using the CONCORDE® Clear tool during the discectomy step are similar to those usually experienced using comparable curettes during a real surgery.	28	2.8±1.1
The torques experienced using the CONCORDE® Clear tool during the discectomy step are similar to those usually experienced using comparable curettes during a real surgery.	28	2.9±1.1
I am able to remove IVD similar to a real surgery.	29	3.2±0.9
I am able to scrape and prepare the endplates similar to a real surgery.	29	2.8±1.1
I am able to tell how far into the IVD I have penetrated.	29	3.4±1.2
The amount of disc removed as presented by the simulator metrics matches my expectations.	21	3.5±0.9

Table IV.4: Surgeon questionnaire results for the graphic user interface (GUI) and the simulator in general.

General and GUI Questions	Number of Responses	Results (1-5)
The visual guides shown during the simulation are similar to the ones used during a real surgery.	29	3.9±1.0
The simulator system setup - including the positioning of the screen, the haptic device, and the benchtop model - is similar to a real surgical setup.	29	3.3±0.9
The visual graphics shown REDACTED are similar to reality.	29	3.1±0.9
The internal impression of the tissue model shown REDACTED are similar to reality.	29	2.8±0.8
The external impression of the tissue model shown REDACTED are similar to reality.	29	3.0±1.0
The overall tasks and the associated skills required to complete the simulation run are similar to those required to complete a real surgery.	29	3.6±1.1
Would you recommend integrating this simulation training into a curriculum during surgical training programs as a mandatory block?	29	3.4±1.5
If not in its current form, does this simulator has the potential to substitute the cadaveric training experience?	21	3.4±1.6
Please rate the overall difficulty of the simulation procedure.	29	3.1±0.8
Please rate the overall usefulness of the metrics that are shown during the simulation.	22	3.8±1.1
Please rate your overall experience with the simulator	29	3.2±1.2